Heterogeneity in the Vascular Endothelium Enables Parallel Processing of Multiple Stimuli

A Thesis submitted to

Strathclyde Institute of Pharmacy & Biomedical Science

for the degree of

Doctor of Philosophy

by

Matthew David Lee

2019

Declaration of Author's Rights

This thesis is the result of the author's original research. It has been composed by the author and has not been previously submitted for examination which has led to the award of a degree.

Signed:  Date: 01/11/2019

Acknowledgements

When I began my PhD I knew it would be an arduous undertaking that would challenge my intellect, perseverance and patience. I can say with confidence it would have been difficult to complete without the help of a number of people and I hope those who have made my journey easier know the extent to which I am indebted to them.

First and foremost, I wish to express my immense gratitude to, respect for and admiration towards my primary supervisor Professor John McCarron. John's continued support and encouragement throughout my PhD is greatly appreciated and I could not have wished for a better supervisor. I have been fortunate to have shared many experiences with John over the past three years. Whether it be attending international conferences, hill walking or rock climbing, John's friendship and great sense of humour have made each experience much more enjoyable and fun. Our daily discussions, on all subject matters, have been both intriguing and greatly entertaining. It is not possible to describe the impact meeting John has had on both my academic and personal life, I hope he knows how much his help and guidance is appreciated. John, thank you for everything, I am forever grateful.

Secondly, I wish to thank my second supervisor Dr Calum Wilson. Calum has been a constant source of guidance and support throughout my PhD. I can safely say my PhD experience would have been nowhere near as fun or enjoyable if not for Calum. His fantastic sense of humour, keen interest in confectionery and above all his friendship have made the past 3 years nothing short of exceptional. I cannot express how thankful I am to have carried out my PhD under his supervision. Our conference trips will always be a highlight when I remember the past three years.

I also wish to extend my heartfelt gratitude to everyone in John's lab, both past and present. Helen Heathcote, Xun Zhang, Charlotte Buckley and Susan Chalmers, thanks for your continued support. Your guidance and encouragement has been invaluable and it has truly helped to improve my work. It has been great to be able to undertake

my PhD journey with you all. I also wish to thank Margaret MacDonald who helped with experimental preparation and was always available for a chat.

Finally, I could not have made it through my PhD without the overwhelming love and support from my family, especially my parents, David and Elizabeth, and my sister Sarah Jane. They are a constant source of encouragement and always showed interest in the work I was doing. I could not have asked to be surrounded by a more caring and supportive group of people. For that, I am truly grateful.

Publications

Wilson, C., Zhang, X., Buckley, C. Heathcote, H.R., Lee, M.D., and McCarron, J.G. (2019). Increased Vascular Contractility in Hypertension. Hypertension 74.

Heathcote, H.R., Lee, M.D., Zhang, X., Saunter, C.D., Wilson, C., and McCarron, J.G. (2019). Endothelial TRPV4 channels modulate vascular tone by Ca^{2+}-induced Ca^{2+} release at IP_3 receptors: endothelial TRPV4 activation induces IP_3-mediated Ca^{2+} release. Br. J. Pharmacol.

McCarron, J.G., Wilson, C., Heathcote, H.R., Zhang, X., Buckley, C., and Lee, M.D. (2019). Heterogeneity and emergent behaviour in the vascular endothelium. Curr. Opin. Pharmacol. 45, 23–32.

Lawton, P.F., Lee, M.D., Saunter, C.D., Girkin, J.M., McCarron, J.G., and Wilson, C. (2019). VasoTracker, a low-cost and open source pressure myograph system for vascular physiology. Front. Physiol. 10.

Lee, M.D., Wilson, C., Saunter, C.D., Kennedy, C., Girkin, J.M., and McCarron, J.G. (2018). Spatially structured cell populations process multiple sensory signals in parallel in intact vascular endothelium. Sci Signal 11.

Wilson, C., Lee, M.D., Heathcote, H., Zhang, X., Buckley, C., Girkin, J.M., Saunter, C.D., and McCarron, J.G. (2018). Mitochondrial ATP production provides long-range control of endothelial inositol trisphosphate–evoked calcium signaling. J. Biol. Chem.

McCarron, J.G., Lee, M.D., Wilson, C. (2017). The Endothelium Solves Problems That Endothelial Cells Do Not Know Exist. Trends in Pharmacological Sciences 38, 322–338.

Wilson, C., Lee, M. D., & McCarron, J. G. (2016). Acetylcholine released by endothelial cells facilitates flow-mediated dilatation. The Journal of Physiology, 594(24), 7267–7307.

Abstract

The endothelium is a complex network of cells that lines the entire vasculature and it controls virtually all cardiovascular functions. Changes in the behaviour of endothelial cells underly almost all cardiovascular disease. To regulate cardiovascular function, the endothelium integrates hundreds of signals that provide constant instructions. Signals arrive from as close as neighbouring endothelial cells and underlying smooth muscle cells to substances circulating from the most remote outpost of the body. These signals provide endless streams of information that must be integrated and decoded. How this is achieved is not understood. Therefore, the aim of this thesis is to investigate the mechanisms involved in endothelial Ca^{2+} signalling to muscarinic, purinergic and histaminergic activators and how the endothelium manages these extracellular signals when multiple agonists are present.

Using *en face* artery preparations we recorded the concurrent Ca^{2+} activity from hundreds of endothelial cells in intact resistance arteries. The results show that the endothelium is not a homogenous population of cells. Instead, spatially-distinct endothelial cells are primed to detect specific extracellular signals. These spatially-distinct cells are arranged in clusters and there is minimal overlap in agonist sensitivity between various clusters. By organising distinct subpopulations of cells to detect specific extracellular signals, the endothelium is able to carry out multiple, completely separate, functions in parallel.

In response to each type of extracellular signal, cells generate intracellular messages that have unique characteristics. When multiple extracellular signals are present together, messages are communicated across cells and computations carried out to generate new signals that are a composite of the inputs. These results suggest individual endothelial cells communicate with their neighbours and complex computations are carried out by combining the information from each source to generate a distinct output. These emergent properties of the endothelium generate a system in which the whole is not equal to the sum of the individual parts.

This thesis also describes an inexpensive and flexible pressure myograph system, VasoTracker, which permits the vascular activity of isolated, pressurized blood vessels to be monitored. The system includes all components that would be expected from a commercial pressure myograph system. VasoTracker is an open source system that makes use of existing hardware and software open source solutions.

Contents

List of Figures

List of Abbreviations and Symbols

2-APB: 2-aminoethoxydiphenyl borate
ACh: acetylcholine
ADP: adenosine diphosphate
ANOVA: analysis of variance
ATP: adenosine triphosphate
Ca^{2+}: calcium
cAMP: cyclic adenosine monophosphate
Cav: voltage-operated calcium channel
cGMP: cyclic guanosine monophosphate
CI: confidence Intervals
CICR: calcium-induced calcium release
CPA: cyclopiazonic acid
Cx: connexin
DAG: diacylglycerol
EC_{25}: effective concentration 25%
ECs: endothelial cells
EGTA: ethylene glycol tetraacetic acid
eNOS: endothelial nitric oxide synthase
ER: endoplasmic reticulum
F/F_0: baseline-corrected fluorescence intensity
F: fluorescence intensity
F_0: baseline fluorescence
FOV: field of view
G protein: guanine nucleotide-binding protein
GDP: guanosine 5'-diphosphate
GPCR: guanine nucleotide-binding protein-coupled receptor
GTP: guanosine-5'-triphosphate
I_{CRAC}: calcium release activated calcium current
IP: prostaglandin I_2 receptor
IP_1: inositol monophosphate
IP_2: inositol bisphosphate
IP_3: inositol 1,4,5-trisphosphate
IP_3R: inositol 1,4,5,-trisphosphate receptor
IP_4: inositol 1,3,4,5-tetrakisphosphate
IP_5: inositol pentakisphosphate
IP_6: inositol hexakisphosphate
K^+: potassium
M_3: muscarinic acetylcholine receptor, subfamily 3
MCU: mitochondrial calcium uniporter
$MgCl_2$: magnesium chloride
MLC: myosin light chain
MLCK: myosin light chain kinase
MLCP: myosin light chain phosphatase
mmHg: millimetres of mercury
NA: numerical aperture
Na^+: sodium

nAChR: nicotinic acetylcholine receptor
NCX: Na^{+}/Ca^{2+} exchanger
NO: nitric oxide
P2X: purinergic receptor cation channel
P2Y: purinergic G protein-coupled receptor
PGI_2: prostaglandin I_2/prostacyclin
PIP_2: phosphatidylinositol 4,5-bisphosphate
PKA: protein kinase A
PKC: protein kinase C
PLB: phospholamban
PLC: phospholipase C
PMCA: plasma membrane calcium ATPase
PSS: physiological saline solution
ROC: receptor-operated ion channel
ROI: region of interest
ROS: reactive oxygen species
RyR: ryanodine receptor
s: second
SEM: standard error of the mean
SERCA: sarco/endoplasmic reticulum calcium ATPase
SMC: smooth muscle cell
SMOC: second messenger-operated ion channel
SOC: store-operated ion channel
SOCE: store-operated calcium channel entry
SR: sarcoplasmic reticulum
STDev: standard deviation
STIM1: stromal interaction molecule 1
TRP: transient receptor potential cation channel
TRPV4: transient receptor potential cation channel, subfamily V, member 4
VGCC: voltage-gated calcium channel
$\Delta F/F_0$: change in baseline-corrected fluorescence intensity

Chapter 1. General Introduction

1.1 Anatomical Structure of Blood Vessels

It is the function of the vascular system to maintain cellular homeostasis and satisfy the metabolic demand of each tissue and organ (Pittman, 2011) by carrying blood through a complex network of blood vessels comprised of arteries, capillaries and veins. This system permits the exchange of nutrients from blood to tissue and removal of cellular metabolic waste from tissue to blood. The metabolic demand of tissues is dynamic and varies depending on cell type, location and local environmental factors (pH and temperature) (Reglin and Pries, 2014; Sokoloff and Kety, 1960). Extrinsic factors such as exercise may also influence the metabolic demand of tissue (Joyner and Casey, 2015).

In regulating cellular homeostasis, blood vessels (arteries, veins and capillaries) share some similarity in relation to structure and cellular composition. In general, the wall of arteries and veins comprise three distinct layers (Figure 1.1). The tunica adventitia is the outermost layer and is largely composed of connective tissue that helps to protect the vessel and anchor it to surrounding tissue. The tunica media is comprised of smooth muscle cells, that control vessel diameter, and the external elastic lamina that provides structural support. The tunica intima is the innermost part of the blood vessels and is composed of a single layer of endothelial cells and an internal elastic lamina, that provides flexibility and structure for the endothelial cells (Tennant and McGeachie, 1990).

1.1.1 Arteries, Capillaries and Veins

Differences in the composition of these layers allow blood vessels to perform diverse physiological roles. The largest arteries in the body are often found close to the heart and are referred to as ‘elastic’ arteries (Shirwany and Zou, 2010). The tunica media of these arteries contains a large number of collagen and elastin filaments which allow them to stretch during systole. These arteries give rise to smaller muscular arteries that contain multiple layers of smooth muscle cells that allow for involuntary control of blood vessel diameter and thus blood flow. Successive branches from

muscular arteries become increasingly smaller and eventually become arterioles. The tunica media of arterioles contains only one or two layers of smooth muscle cells. Arterioles are a major site of vascular resistance and reduce the velocity and pressure of blood flow to prevent damage to capillaries (Hu et al., 2012).

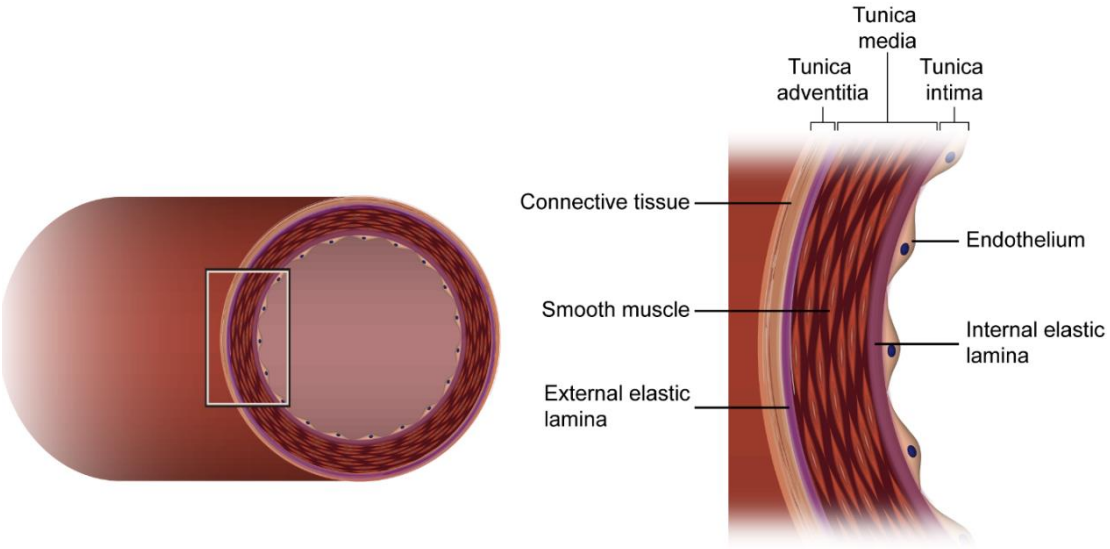

Figure 1.1 – Structure of the blood vessel wall.

Illustration of the structure of the blood vessel wall. Blood vessels are composed of three main layers: 1) the outermost layer is the tunica adventitia, composed predominantly of collagen and fibroblasts; 2) the middle layer is the tunica media, composed of the external elastic lamina and smooth muscle cells; 3) the innermost layer is the tunica intima, composed of the internal elastic lamina and a single layer of endothelial cells.

Capillaries differ in the usual structure of blood vessels and are marked by the complete absence of smooth muscle cells and consist of a single layer of endothelial cells, a basement membrane and pericytes. Capillaries are ~5-10 µm in diameter, just large enough for red blood cells to pass in the lumen, and they form large interwoven networks (Hudetz, 1997; Kornfield and Newman, 2014). These networks increase the total surface area of capillaries and it is here that the majority of nutrient and water exchange occurs by diffusion (Popel, 1980).

There are three main types of capillaries: continuous, fenestrated and discontinuous. Continuous capillaries have a tight uninterrupted layer of endothelial cells, allowing for the controlled passage of small molecules. Fenestrated capillaries, found mostly

at filtration sites, have pores in certain endothelial cells to allow the passage of larger molecules. Discontinuous capillaries, contain intercellular gaps and a fragmented basement membrane that facilitate delivery of macromolecules to highly metabolic cells such as hepatocytes (Griffin and Gao, 2017).

Upon leaving the capillaries, deoxygenated blood enters the venules. Venules are comprised of endothelial cells (intimal layer), smooth muscle cells (medial layer) and connective tissue (adventitial layer). However, there are fewer smooth muscle cells in the medial layer of venules when compared to arterioles. The network of venules converge to form a vein, where blood is returned to the heart, ready to be recirculated. Compared to arteries, veins have reduced smooth muscle content and therefore blood is moved through veins by the action of the skeletal-muscle pump. The directional movement is aided by the action of intraluminal one-way valves that, when closed, prevent the backflow of blood (Bazigou and Makinen, 2013).

The two major cell types present in most blood vessels are smooth muscle cells and endothelial cells and these are considered in the next two sections.

1.2 Smooth Muscle Cells

Regulation of blood flow and blood pressure throughout the body is achieved predominantly by the contraction and relaxation of vascular smooth muscle (vascular tone). Vascular tone is itself determined by competing vasoconstrictor and vasodilator influences. These vasoconstrictor and vasodilator mediators can originate from outside the organ or tissue in which the blood vessel is located (extrinsic) or originate from surrounding tissue or the vessel itself (intrinsic). Regardless of where the stimulus originated, smooth muscle cell contraction occurs in response to an increase in intracellular Ca^{2+} concentration.

The increase in intracellular Ca^{2+} concentration triggers contraction by first binding to calmodulin. Calmodulin is a multifunctional intracellular Ca^{2+}-binding protein. When Ca^{2+} is bound, the activated Ca^{2+}-calmodulin complex activates myosin light chain kinase (MLCK) resulting in phosphorylation of the light chain of myosin

(Kendrick-Jones et al., 1970; McCarron et al., 1992; Szent-Györgyi et al., 1973; Webb, 2003). Ca^{2+} regulation is vital to the control of smooth muscle contraction and relaxation and consequently blood vessel tone.

In smooth muscle, intracellular Ca^{2+} concentration is determined by the balance of influx and efflux of the ion from the extracellular space or Ca^{2+} release and uptake from the internal store. Ca^{2+} influx occurs through various Ca^{2+}-selective and non-selective cation channels found on the plasma membrane. The gating of these channels may be voltage-dependent (e.g. the voltage-dependent Ca^{2+} channel) or independent of voltage (e.g. store-operated Ca^{2+} channels). The major voltage-dependent Ca^{2+} channels (VDCCs) expressed in smooth muscle cells are T-type and L-type (Cav3.2 and Cav1.2) (McDonald et al., 1994). On depolarisation of the smooth muscle cell membrane, VDCC are activated and allow influx of Ca^{2+} ions into the cell. Ca^{2+} enters cells via the channels at rates of ~0.5 million ions per second to generate a steep gradient of Ca^{2+} concentration which lasts ~1 ms. The resulting Ca^{2+} concentration declines from ~10 μM to ~100 nM over a few hundred nanometers (McCarron et al., 2006).

Voltage-independent Ca^{2+} channels are often ligand-gated or store-operated channels that are activated by the binding of a ligand to the channel. An example is the P2X family of purinergic receptors. On binding of ATP the P2X channels permits the entry of Ca^{2+} into the cell. Although the P2X receptor is non-selective (also permitting potassium and sodium), the Ca^{2+} concentration gradient across the plasma membrane is such that substantial quantities of Ca^{2+} may enter the cell (Amberg and Navedo, 2013).

Ca^{2+} release from the internal store is also a major route for Ca^{2+} regulation in smooth muscle. Release of Ca^{2+} from the internal store may occur via inositol 1,4,5-trisphosphate (IP_3) receptors (IP_3R) or ryanodine receptors (RyR). The mechanisms of these receptors will be discussed further in sections below.

Following an increase in Ca^{2+}, removal of the ion from the cytoplasm has an important role in regulating vascular tone. Several mechanisms may contribute to the removal of Ca^{2+}. The plasma membrane Ca^{2+} ATPase (PMCA) and Na^{+}/Ca^{2+} exchanger (NCX) extrude Ca^{2+} from the cytosol to the extracellular space to lower the internal Ca^{2+} concentration. The sarcoplasmic reticular Ca^{2+} ATPase (SERCA) also reduces cytoplasmic Ca^{2+} concentration by permitting the uptake of Ca^{2+} into the lumen of the internal store. Importantly, these mechanisms of Ca^{2+} transport do not act independently of one another. Instead, the activation of one pathway can alter the effects of another. For example, depletion of SR Ca^{2+} can alter the plasma membrane potential and thus Ca^{2+} entry via voltage-dependent channels (Chalmers et al., 2007). Furthermore, Ca^{2+} release from the internal store via IP_3R and RyR may be inhibited by an increase in cytosolic Ca^{2+} concentration (Adkins and Taylor, 1999; Taylor, 1998).

1.3 The Endothelium

The endothelium is the innermost layer of cells lining the entire vascular system that play a central role in regulating virtually every cardiovascular function. Underlying the importance of the endothelium in controlling cardiovascular function is that it acts as a sophisticated sensory and signal processing centre that detects and integrates multiple cues on physiological status. This facility of the endothelium permits the cells to regulate blood perfusion, fluid and solute exchange, haemostasis and coagulation, inflammatory responses, vasculogenesis and angiogenesis (Michel, 2004; Muñoz-Chápuli et al., 2004; Tang and Conti, 2004; Yau et al., 2015).

Underlying the control of many of these functions is the endotheliums ability to detect and respond to hundreds of different stimuli. The endothelium receives and integrates information from hormones, neurotransmitters, endothelial cells, pericytes, smooth muscle cells, various blood cells, viral or bacterial infection, proinflammatory cytokines, and oxygen tension (Bhattacharya et al., 2008; Buonassisi and Venter, 1976; Duckles and Miller, 2010; Garland et al., 2017; Keller et al., 2003; Kusuma et al., 2014; Orozco et al., 2000). The endothelium is also sensitive

to several types of mechanical signals such as those derived from blood pressure and the flow of blood (Bagher et al., 2012; Wilson et al., 2015, 2016a).

1.4 Ca^{2+} Signalling in Endothelial Cells

Although the endothelium controls a myriad of functions, central to the communication relay system within endothelial cells, for many physiological pathways, is a single cation, Ca^{2+}. Chemical stimuli, that activate endothelial cells, are often transduced as changes in cytosolic Ca^{2+} concentration (Bagher et al., 2012; Borisova et al., 2009; Longden et al., 2017; Pantazaka et al., 2013), which may act alone or cooperate with other factors to elicit cellular responses (Stolwijk et al., 2016). Ca^{2+} links extracellular stimuli to physiological responses by regulating the synthesis and release of various vasoactive agents such as nitric oxide (NO), various peptides, and eicosanoids such as prostacyclin and thromboxane (discussed below). Through these Ca^{2+} -dependent mediators, the endothelium controls vascular tone, nutrient exchange, blood cell recruitment, blood clotting, and the formation of new blood vessels (Félétou, 2011).

Despite its ubiquity and importance, one aspect of Ca^{2+} ions in cellular signalling is reasonably unique; Ca^{2+} ions are neither made nor destroyed in the cell. Instead, Ca^{2+} is actively moved to change intracellular concentration. Therefore, a considerable amount of a cell's energy is devoted to the control of intracellular Ca^{2+} concentration. There are two main routes of entry for Ca^{2+} into the cytosolic space: 1) release from the intracellular store (endoplasmic reticulum, ER); and 2) influx across the plasma membrane from the extracellular space. These routes are considered in the sections below.

1.5 Ca^{2+} Release from the Intracellular Store

1.5.1 G Protein-Coupled Receptor Activation

Many signals to which endothelial cells respond are carried in the extracellular environment. This is true for the endogenous vasodilator acetylcholine (ACh). ACh

binds to and activates the muscarinic (M_3) G protein-coupled receptor (GPCR) (Wilson et al., 2016b). This heterotrimeric G protein has three subunits and in the inactive state, exists as a complex of three polypeptides (α, β and γ) (Kamato et al., 2015). A single guanosine diphosphate (GDP) group is bound to the G_α subunit however, upon agonist binding to the GPCR, GDP is replaced by guanosine triphosphate (GTP). This causes dissociation of the G protein complex into, G_α subunit, with bound GTP, and $G_{\beta\gamma}$ complex.

There are several subclasses of G-proteins. Of these, the G_q subclass of GPCRs is activated by this cascade and the $G_{q\alpha}$ subunit activates membrane bound phospholipase C (PLC) (Kamato et al., 2015; Wu et al., 1993). PLC hydrolyses phosphatidylinositol 4,5-bisphosphate (PIP_2), to produce diacylglycerol (DAG) and inositol 1,4,5-trisphosphate (IP_3) (Dennis et al., 1991; Harden et al., 2011; Nakamura and Nishizuka, 1994). After which, DAG remains in the membrane and IP_3 is free to diffuse through the cytosol. This pathway amplifies the original signal as a single PLC can produce many DAG and IP_3 molecules. However, there is also divergence of the signal as IP_3 and DAG activate separate distinct signalling pathways.

1.5.2 Inositol Phosphate

Inositol may contain a variable number of phosphate groups ranging from none, inositol, through to six the hexaphosphate form, IP_6. The inositol that has attracted most interest is IP_3. IP_3 is important in cell signalling and as a result of its middle number of phosphate groups, IP_3 can be broken down, by phosphodiesterases, to IP_1 or IP_2, or phosphorylated, by kinases, to produce IP_4, IP_5 or IP_6 (Irvine and Schell, 2001). Predominantly, it was thought that the primary role in converting IP_3 to another inositol phosphate analogue was to terminate the signalling cascade induced by IP_3. However, IP_2 and IP_4 are now appreciated to activate the same signalling pathway activated by IP_3, albeit at a reduced potency (Saleem et al., 2013). The precise role that inositol phosphate analogues (with the exception of IP_3) have on intracellular signalling is not fully understood. However, it seems unlikely that a cell

would devote energy to generate several specific phosphodiesterase and kinases to act on inositol phosphates if there was no further requirement for those molecules.

1.5.3 Role of Inositol Phosphate in Ca^{2+} Signalling

IP_3 receptors (IP_3R) are IP_3-gated, Ca^{2+}-permeable channels located on the endoplasmic reticulum in endothelial cells (Berridge and Irvine, 1984, 1989; Ehrlich and Watras, 1988; Prole and Taylor, 2019; Taylor and Laude, 2002). The ER is the main Ca^{2+} store in non-muscle cells and contains many Ca^{2+} binding proteins such as calreticulin and calsequestrin. The Ca^{2+} concentration in the ER may be as high as 3 mM and accounts for ~75% of the total intracellular Ca^{2+} reserve (Sambrook, 1990; Tran et al., 2000). When IP_3 binds to the IP_3R, Ca^{2+} is released from the ER to the cytosol. Although IP_3Rs are referred to as Ca^{2+} channels, they also permit the transfer of other cations. However, their *in vivo* 'selectivity' is due to the high accumulation of Ca^{2+} in the ER and high electrochemical gradient across the ER membrane (Taylor et al., 2004).

There are three IP_3R subtypes (IP_3R1, IP_3R2 & IP_3R3) with differing affinities for IP_3; IP_3R2 is more sensitive than IP_3R1 and both are considerably more sensitive than IP_3R3 (Iwai et al., 2007; Tu et al., 2005). IP_3R activity is modulated by Ca^{2+} itself in addition to IP_3. The effects of Ca^{2+} on IP_3Rs is dependent on the cytosolic Ca^{2+} concentration. At low concentrations of Ca^{2+} (e.g. <300 nM) IP_3Rs are sensitised to IP_3 to increase the release of Ca^{2+} from the ER. Conversely, at high concentrations (e.g. >300 nM) the release of Ca^{2+} through IP_3Rs is inhibited. Ca^{2+} thus acts as both a positive and negative feedback regulator of IP_3R activation.

1.5.4 Role of Ryanodine Receptors in Ca^{2+} Signalling

Another major route for Ca^{2+} release from the internal store is via RyR. The role of RyR in endothelial signalling is not resolved. Several studies have presented evidence for RyR expression in endothelial cells (Rusko et al., 1995; Wang et al., 1995; Ziegelstein et al., 1994). However, there is variation in the reported contribution of RyR to endothelial Ca^{2+} signalling as assessed by the effects of ryanodine. For

example, ryanodine evoked an increase in resting Ca^{2+} in various cultured endothelial cell lines such as human aorta ECs, human umbilical vein ECs and bovine pulmonary artery ECs suggesting that there are functional RyRs. However ryanodine did not alter basal Ca^{2+} in rat aorta ECs (Mozhayeva and Mozhayeva, 1996; Ziegelstein et al., 1994).

The functional role of RyRs in endothelial cells remains unclear as the RyR agonist caffeine does not evoke an increase in cytosolic Ca^{2+} in intact endothelium (Borisova et al., 2009; Wilson et al., 2018). Furthermore, the Ca^{2+} signals evoked by various physiological activators such as flow-induced autocrine/paracrine actions or carbachol-induced Ca^{2+} signalling were not altered by RyRs in endothelial cells of mesenteric arteries (Borisova et al., 2009; Wilson et al., 2016a). Although, these results suggest RyRs play a minimal role in endothelial Ca^{2+} signalling further study is required to determine the precise function of these channels.

1.6 Extracellular Ca^{2+}

The second major source of Ca^{2+} is the extracellular space. The plasma membrane is crucial for regulating the intracellular Ca^{2+} concentration by controlling both the influx and efflux of Ca^{2+} ions. Movement of Ca^{2+} ions into the cell is mediated mainly by ion channels that can be activated by either depolarisation of the plasma membrane (Voltage-gated Ca^{2+} channels; VDCC), agonists (agonist-operated channels) or environmental stimuli (transient receptor potential ion channels; TRP).

VGCC are the major Ca^{2+} influx route found in excitable cells like nerve and muscle but are largely excluded from non-excitable cells (Leung et al., 2008). Although, endothelial cells are generally considered to be a non-excitable cell type, they may express some voltage-operated Ca^{2+} (CaV) channels (Yakubu and Leffler, 2002). The physiological role of these VGCC in the endothelium remains unclear (Bkaily et al., 1993; Bossu et al., 1992). There is also evidence against a role of VGCC in the endothelium. For example, VGCC are gated by voltage changes across the plasma membrane; depolarisation of the membrane usually activates the channels and leads to a rapid influx of Ca^{2+}. However, depolarisation of the endothelial cell membrane

(with high K^+ solution) largely diminishes agonist induced Ca^{2+} entry rather than enhancing Ca^{2+} influx (Li et al., 1999). Furthermore, VGCC blockers (verapamil and diltiazem) have no effect on agonist-induced Ca^{2+} entry and application of the VGCC agonist BAY K8644 did not alter resting intracellular Ca^{2+} concentration (Li et al., 1999; Yamamoto et al., 1995). Together these experiments question the contribution of VGCC in regulating endothelial Ca^{2+} signalling.

Ligand-gated channels are another class of channel that permit ion transport across the plasma membrane. There are three distinct routes: receptor-operated channels (ROC), which are ionotropic channels that activate on ligand binding; second-messenger operated channels (SMOC): which active in response to intracellular generated mediators; and store-operated channels (SOC), which open in response to Ca^{2+} depletion in the intracellular store (Moccia et al., 2012).

At least two distinct ROCs are thought to be expressed in endothelial cells. These are the nicotinic ACh receptor (nAChR) and the purinergic P2X receptor (Hansen et al., 1999; Macklin et al., 1998; Ramirez and Kunze, 2002). nAChRs are non-selective cation channels, activated by the endogenous ligand ACh, that permit the transport of Ca^{2+}, Na^+ and K^+ ions across the plasma membrane. The expression of nAChRs does not appear to be uniform across the endothelium but, instead restricted to specific tissue (Moccia et al., 2004, 2012). Although, the function of nAChRs in the vascular endothelium remains unclear, the α7 subtype is thought to have an important role in angiogenesis (Cooke and Ghebremariam, 2008).

Like nAChRs, purinergic P2X receptors are a non-selective cation channel, activated by the endogenous ligand ATP. Seven subtypes of the P2X receptor ($P2X_{1-7}$) have been identified with reports of functional differences between the isoforms. Vascular endothelial cells have been reported to express all P2X subtypes in both arteries and veins although expression levels may vary between vascular beds (Pulvirenti et al., 2000; Ray et al., 2002). Although reported to be widely expressed in the endothelium, our previous studies find P2X receptors are not expressed on carotid artery endothelium (Lee et al., 2018). This conclusions arose from the observation that ATP

did not induce Ca^{2+} influx when the PLC-IP_3 pathway was blocked in intact rat carotid artery (Lee et al., 2018). Furthermore, when external Ca^{2+} was removed, the amplitude of the ATP-induced Ca^{2+} response due to the PLC-IP_3 pathway, was comparable to the response when external Ca^{2+} was present (Lee et al., 2018).

A second type of channel involved in Ca^{2+} influx are store-operated channels. SOCs are activated when the Ca^{2+} concentration of the internal store is reduced. Interestingly, the mechanism(s) underlying Ca^{2+} efflux from the internal store is not currently thought to play a role in SOC activation nor does an increase cytosolic Ca^{2+} (Hoth and Penner, 1992; Parekh and Penner, 1997; Parekh and Putney, 2005). Of several reported SOCs entry pathways, the best characterized is the Ca^{2+}-release-activated Ca^{2+} current (I_{CRAC}). I_{CRAC} was first recorded in rat basophilic leukemia mast cells, and later described in other cell types, including endothelial cells. Several components contribute to the I_{CRAC} system. One of these is STIM1, which resides in the ER and can bind Ca^{2+}. On activation by intracellular store depletion, STIM1 proteins translocate to close proximity of the plasma membrane (Abdullaev et al., 2008). A second protein ORAI1, also translocated to the site of STIM1, where it can form a pore in the plasma membrane and allow the influx of Ca^{2+}. However, further study is required to determine if other channels are also involved in store-operate Ca^{2+} entry and the role they have in mediating intracellular Ca^{2+} concentration.

Another proposed route of Ca^{2+} entry in endothelial cells is the transient receptor potential (TRP) class of ion channels. TRP channels are a family of non-selective cation channels that respond to various extracellular stimuli, including temperature, pH and mechanical forces as well as intracellular secondary messengers such as PIP_2 (Castillo et al., 2018; Harraz et al., 2018; Heathcote et al., 2019). More than 20 classes of Ca^{2+}-permeable TRP channels have been reported in cultured and native endothelial cells (Sullivan and Earley, 2013). TRPV4 activation caused vasorelaxation of preconstricted mesenteric arteries as a result of activation of the endothelium (Heathcote et al., 2019). However, TRP-induced vasodilation may be artery specific as Ca^{2+} influx and vasodilation following stimulation with cholinergic agonists in some, but not all

vessels, was reduced in TRPV4$^{-/-}$ mice. Store-operated Ca^{2+} entry via TRP channels has been also reported to produce endothelium-dependent vasodilation (Freichel et al., 2001). Further studies are required to determine the contribution of these channels in store-operated Ca^{2+} entry.

1.7 Removal of Cytosolic Ca^{2+}

Following an increase in intracellular Ca^{2+} concentration, Ca^{2+} must be restored back to resting levels. There are two main mechanisms for Ca^{2+} removal from the cytoplasm; efflux of Ca^{2+} from the cytosol across the plasma membrane to the extracellular space and re-uptake of the ion into the ER. Each mechanism plays a pivotal role in regulating intracellular Ca^{2+} concentration in endothelial cells.

1.7.1 Plasma Membrane Ca^{2+}-ATPase Pump & Na^{+}/Ca^{2+} Exchange

The plasma membrane contains at least two mechanisms that remove intracellular Ca^{2+}. One of these utilises ATP as an energy source while the other uses the electrochemical gradient that occurs across the plasma membrane (Hancock, 2016).

The plasma membrane Ca^{2+} ATPase (PMCA) pump is a P-type ATPase that drives the transport of one molecule of Ca^{2+} across the plasma membrane, using the energy provided by one ATP molecule. These pumps have a high affinity for Ca^{2+} (K_m = 100 to 200 nM) but relatively low transport capacity (Brini and Carafoli, 2009). This allows the PMCA pump to finely regulate cytosolic Ca^{2+} concentration at rest.

The second type of removal mechanism found on the plasma membrane, utilises the electrochemical gradient, is the Na^{+}/Ca^{2+} exchanger. The exchanger in most cell types, near the resting membrane potential, transports one Ca^{2+} ion out of the cell in exchange for three Na^{+} ions. Although they have a lower affinity for Ca^{2+}, than the PMCA pump, they extrude Ca^{2+} at a much higher rate (Brini and Carafoli, 2009). Therefore, after Ca^{2+} influx the Na^{+}/Ca^{2+} exchanger can transport a large amount of Ca^{2+} out of the cell, relatively quickly.

1.7.2 *SERCA*

ER Ca^{2+} depletion, activates the sacro/endoplasmic reticulum Ca^{2+}-ATPase (SERCA) pump. SERCA resides in the plasma membrane of the ER and transports Ca^{2+} into the ER at the expense of ATP hydrolysis. The uptake of Ca^{2+} by SERCA is regulated. For example, in cardiac cells, phospholamban (PLB) a phosphoprotein that is closely associated with the sarcoplasmic reticulum may restrict pumping rates (Moccia et al., 2012). Interestingly, nitric oxide production has also been shown to regulate SERCA by enhancing Ca^{2+} sequestration into the ER, working as an autoregulatory negative feedback system (Adachi et al., 2004).

1.7.3 *Mitochondria*

Although the ER is the major site of intracellular Ca^{2+} storage, other organelles are involved in actively regulating intracellular Ca^{2+} concentration. One such organelle is mitochondria. While classically viewed as the "battery" of the cell, that caters for the cellular energy demands by providing ATP (Ernster and Schatz, 1981), endothelial cells have been proposed to rely on glycolysis, rather than oxidative phosphorylation, to meet cellular energy requirements. Instead, of energy requirements, mitochondria may play a pivotal role in regulating intracellular Ca^{2+} signalling.

In native endothelial cells mitochondria are distributed widely throughout the cytoplasm and account for ~25% of the cells Ca^{2+} storage (Alevriadou et al., 2017; Wilson et al., 2018). Mitochondrial uptake of Ca^{2+} is driven by the proton gradient through the mitochondrial Ca^{2+} uniporter (MCU) channel. Although the affinity of the MCU is low, the channels have an important role in regulating cytosolic Ca^{2+}. We have previously shown that mitochondrial control of spontaneous Ca^{2+} release from the ER may be regulated by mitochondrial release of reactive oxygen species (ROS) and ATP (Wilson et al., 2018).

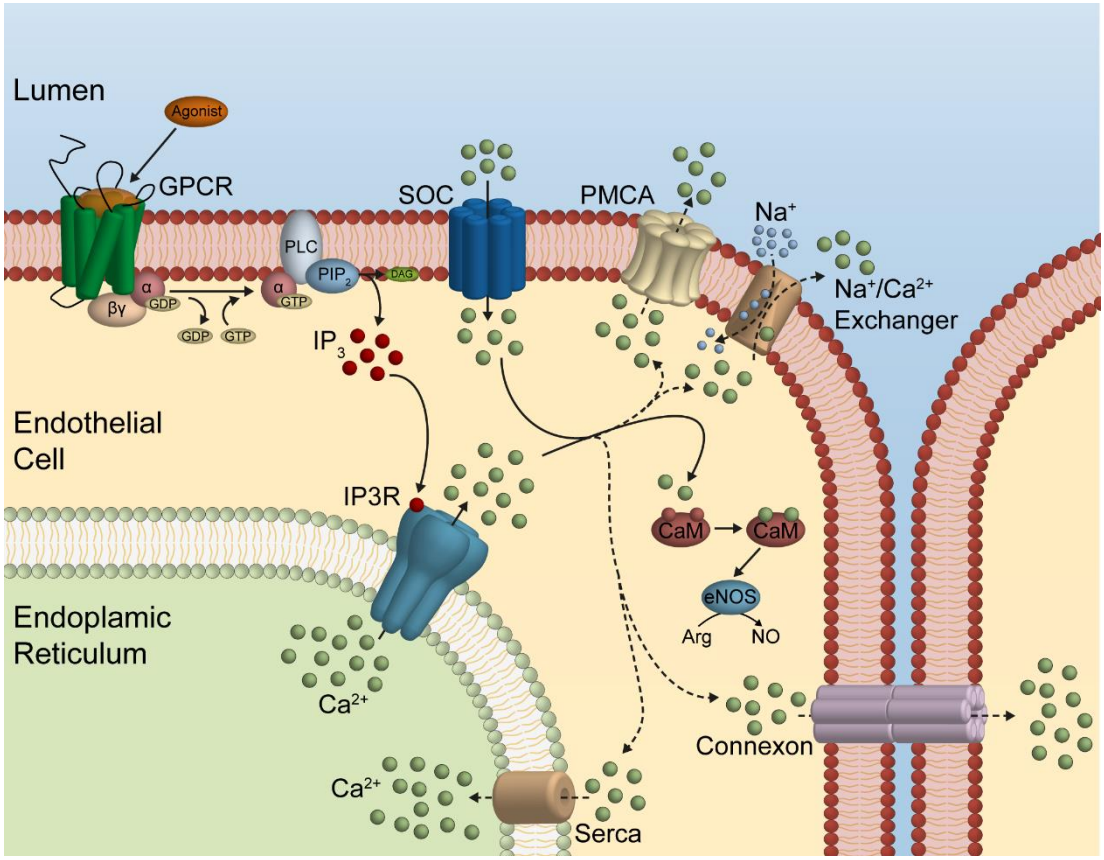

Figure 1.2 – GPCR Ca^{2+} signalling in endothelial cells.

Illustration of the GPCR Ca^{2+} signalling pathway in endothelial cells. Agonists bind to and activate the G-protein couple receptor (GPCR). A single guanosine diphosphate (GDP) group is bound to the Gα subunit however, upon activation, GDP is replaced by guanosine triphosphate (GTP). This causes dissociation of the G protein complex into, Gα subunit, with bound GTP, and Gβγ complex. Gqα activates membrane bound phospholipase C (PLC) which hydrolyses phosphatidylinositol 4,5-bisphosphate (PIP_2), to produce diacylglycerol (DAG) and inositol 1,4,5-trisphosphate (IP_3). DAG remains in the membrane and IP_3 (red spheres) is free to diffuse through the cytosol. IP_3 activates IP_3 receptors (IP_3R) on the endoplasmic reticulum (ER) to evoke Ca^{2+} (green spheres) release from the internal store. Depletion of Ca^{2+} within the ER leads to the activation of store-operated Ca^{2+} channels (SOC), located on the endothelial plasma membrane. This results in Ca^{2+} influx, to the cytoplasm. Intracellular Ca^{2+} binds to calmodulin to form the Ca^{2+}-calmodulin complex and subsequent activation of the endothelial nitric oxide synthase enzyme (eNOS). Activated eNOS converts L-arginine (Arg) to citrulline plus nitric oxide (NO). Removal of cytoplasmic Ca^{2+} may occur by several mechanisms (dashed lines): the plasma membrane Ca^{2+} ATPase (PMCA) pump drives the transport of one molecule of Ca^{2+} across the plasma membrane; the Na^+/Ca^{2+} exchanger utilises the electrochemical gradient and transports one Ca^{2+} ion out of the cell in exchange for three Na^+ ions (blue spheres); ER Ca^{2+} depletion, activates the ER plasma membrane residing sacro/endoplasmic reticulum Ca^{2+}-ATPase (SERCA) pump to transports Ca^{2+} into the ER at the expense of ATP hydrolysis. Ca^{2+} may also be transported to neighbouring endothelial cell via connexons. A connexon ring protrudes from the membrane of one endothelial cell and connects to the connexon from, a separate, neighbouring cell and allows the passage of Ca^{2+} ions between the cytoplasm of adjacent cells.

1.7.4 Lysosomes

Recently, there has been an increase in evidence suggesting that lysosomes may also play a role in regulating endothelial Ca^{2+} (Galione, 2015). Lysosomes are organelles that may act as an intracellular Ca^{2+} store (luminal concentration of ~0.4-0.6 mM) and like mitochondria they can sequester and release the ion (Garrity et al., 2016). However, much less is currently understood about their role in Ca^{2+} signalling and further study is required to determine the mechanisms involved in their activation and function. Lysosomes associate with IP_3R to sequester Ca^{2+} released from these channels. Disruption of lysosomes leads to an increase in cytosolic Ca^{2+} evoked by IP_3Rs (López-Sanjurjo et al., 2013). However, SOCs were unaffected, suggesting that lysosomes selectively sequester Ca^{2+} released through IP_3Rs while ignoring Ca^{2+} influx through SOCs (López-Sanjurjo et al., 2013).

By regulating the concentration of cytosolic Ca^{2+}, mitochondria and lysosomes may have a more prominent role in controlling Ca^{2+} mediated responses in the endothelium than previously thought. Furthermore, the ability of these organelles to control local Ca^{2+} concentrations may be vital in maintaining specificity of the Ca^{2+} signal, when relaying the information held in an extracellular stimulus to generate a physiological output. The importance of regulating local Ca^{2+} signals will thus be discussed.

1.8 Local Ca^{2+} Signals to Global Ca^{2+} Waves

Advances in endothelial Ca^{2+} imaging *in situ* has increased greatly over the past few decades and has allowed for evaluation of both spatially and temporally discrete subcellular Ca^{2+} signals as well as Ca^{2+} signals occurring throughout the cell (global signals) (Duza and Sarelius, 2004; Marie and Bény, 2002; Socha et al., 2012; Wilson et al., 2016b, 2018).

1.8.1 Ca^{2+} Puffs

Stimulated Xenopus oocytes revealed subcellular organization of IP_3-evoked Ca^{2+} signals (Parker et al., 1996). On IP_3R activation, Ca^{2+} release from the internal store occurred as a hierarchy of Ca^{2+} release events. Beginning with release from a single IP_3R ("blips"), progressing to activation of a single cluster of IP_3Rs ("puffs") and finally recruitment of successive sites, resulting in propagating Ca^{2+} waves across part or the entirety of the cell (Parker et al., 1996). It is thought that wave propagation occurs by Ca^{2+}-induced Ca^{2+} release (CICR) whereby, a Ca^{2+} puff sensitises neighbouring IP_3R to IP_3, increasing Ca^{2+} release from the ER (Figure 1.3).

1.8.2 Ca^{2+} Oscillations

The altered IP_3R sensitivity by Ca^{2+} may not be limited to 'local' signalling. Instead, Ca^{2+} may also sensitise IP_3Rs on completely separate internal stores. An increase in cytosolic Ca^{2+} concentration above a certain threshold will result in inhibition of IP_3Rs and cessation of Ca^{2+} release (Oancea and Meyer, 1996; Swatton et al., 1999). Cytosolic Ca^{2+} will be removed from the cytosol as described above. The resulting interplay of Ca^{2+} release/influx and Ca^{2+} re-uptake/extrusion will lead to oscillations in the intracellular Ca^{2+} concentration.

1.9 Decoding Intracellular Ca^{2+} Signals

Ca^{2+} ions are ubiquitous and versatile signalling ions capable of relaying a variety of extracellular stimuli into markedly different intracellular actions. However, it is not yet fully understood how changes in the concentration of a single cation can lead to multiple physiological outputs. Thus far, studies have indicated that extracellular stimuli rely mainly on variations in the spatiotemporal features of the Ca^{2+} signal to activate specific intracellular processes (Francis et al., 2016; Leybaert and Sanderson, 2012; McCarron et al., 2010; Parker and Smith, 2010).

1.9.1 *Decoding Ca^{2+} Oscillations*

Ca^{2+} oscillations are a common feature of most non-excitable cells (Zhu et al., 2008). How oscillation frequency regulates downstream events is not fully understood. Variations in the spatial and temporal properties of discrete Ca^{2+} events may allow the endothelium to selectively activate and coordinate various cellular responses (Taylor and Francis, 2014).

1.9.2 *Amplitude Modulation*

Downstream effectors can decode information contained in the amplitude of Ca^{2+} signals by variation in their affinity for Ca^{2+} (Dolmetsch et al., 1997). An effector with a high affinity binding site for Ca^{2+} will respond to small increases in intracellular Ca^{2+} concentration. Conversely, an effector with a low affinity binding site for Ca^{2+} will require a much larger increase in Ca^{2+} to respond. However, the specificity of the amplitude modulation system is limited as increasing the Ca^{2+} concentration to activate low affinity mediators may unavoidably recruit mediators with a high Ca^{2+} affinity. Two potential mechanisms to bypass this issue rely on the kinetics of the Ca^{2+} signal or a restricted location of the Ca^{2+} signal.

1.9.3 *Frequency Modulation*

One proposed mechanism to explain how changes in the frequency of the Ca^{2+} signal selectively relays information in the cell, relies on the Ca^{2+} binding kinetics of the effectors. For example, a Ca^{2+} spike may activate a small proportion of an enzyme and before the enzyme is 'turned off' the next Ca^{2+} spike occurs, recruiting more of the enzyme. However, if the frequency of the Ca^{2+} spikes become too low, then the enzymes will 'turn off' before the subsequent Ca^{2+} spike. In this way, the frequency of Ca^{2+} oscillations can mediate the downstream effects of the signalling cascade. Indeed, previous studies have shown that the frequency of the Ca^{2+} signal has an important role controlling the functional output of the cell (De Koninck and Schulman, 1998; Stojilković et al., 1992; Zhu et al., 2008).

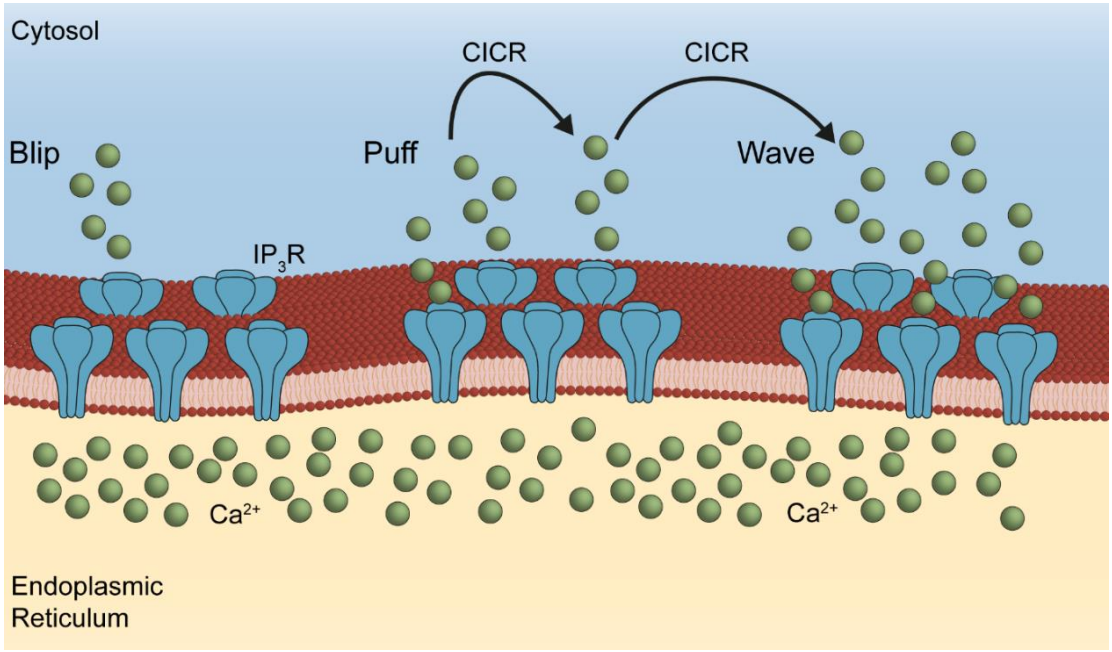

Figure 1.3 – Ca^{2+} blips, puffs and waves in endothelial cells.

Ca^{2+} release from a single IP_3 receptor (IP_3R) is termed a blip. Puffs are characterised by coordinated opening of multiple IP_3Rs within a cluster. Released Ca^{2+} may sensitize neighbouring IP_3Rs to IP_3 to generate a larger more sustained release in what is termed Ca^{2+}-induced Ca^{2+} release. Activation of successive clusters of IP_3Rs results in propagating Ca^{2+} waves across part or the entirety of the cell.

1.9.4 *Spatial Changes in the Ca^{2+} Signal*

The flux of Ca^{2+} via channels in either the internal store or across the plasma membrane leads to a local elevation in Ca^{2+} concentration. This build-up of Ca^{2+} in a microdomain near the ion channel decays rapidly with distance from tens of micromolar near the channel to a low nanomolar concentrations a few hundred nanometres away (McCarron et al., 2006; Neher, 1998; Parekh, 2008). The local increases in Ca^{2+} concentration at particular sites in the cell, allow specific cellular responses to be activated by co-localisation of the effector and subcellular Ca^{2+} microdomain (Dolmetsch et al., 2001; Leslie, 1997; Samanta and Parekh, 2017). Thus, the rise in Ca^{2+} at the microdomain leads to activation of a specific effector but rapid decay of the Ca^{2+} signal, with distance, would not be sufficient to recruit distant effectors. In support of this proposal, the slow Ca^{2+} chelator EGTA is inefficient in sequestering Ca^{2+} at the microdomain and activation of the Ca^{2+} effector persists. By contrast, the fast Ca^{2+} chelator BAPTA is able to reduce Ca^{2+} at the microdomain and inhibit the activation of the Ca^{2+} effector. Both chelators were equally efficient at inhibiting global increases in cytosolic Ca^{2+} concentration (Deisseroth et al., 1996; Di Capite et al., 2009; Neher, 1998).

Together these features of the Ca^{2+} signal *within an endothelial cell* allow for variations in Ca^{2+} oscillations at particular sites to highly regulate the recruitment of particular mediators in a specific signalling cascade. Changes to one aspect of the Ca^{2+} signal may be sufficient to effectively relay information. For example, Ca^{2+} signals with the same amplitude and frequency but located at separate microdomains could potentially recruit different mediators.

1.9.5 *Endothelial Cell to Cell Communication*

To coordinate the multitude of functions that are under its control, individual endothelial cells communicate with each other through specialized cell–cell junctions (gap junctions). Gap junctions are tubular structures, known as connexons, in the membrane that are formed by six connexin (Cx) proteins organised in a ring.

Numerous Cx isoforms have been identified, with expression varying between tissue. Endothelial cells predominantly express Cx37 and Cx40 (Cx43 has also been observed in ECs of the microvasculature and at branch points of arteries that experience turbulent blood flow) (Gabriels and Paul., 1998; Scheckenbach et al., 2011). The connexon ring protrudes from the membrane of one endothelial cell and connects to the connexon from a separate neighbouring cell. The linked connexons allow passage of ions and small molecules (<1200 Da), such as Ca^{2+} ions, cAMP and IP_3, between the cytoplasm of adjacent cells. Each gap junction may contain several hundred connexons (Sáez et al., 2003). However, connexons do not act as simple inert 'tunnels' but instead, through gating, regulate the movement of molecules between cells. Changes in Ca^{2+} concentration, pH, phosphorylation and cyclic nucleotides have been shown to control connexon opening (Oshima, 2014).

1.10 Physiological Effects of Intracellular Ca^{2+} in the Endothelium

Ca^{2+} controls a myriad of cellular functions including, generating new signals, phosphorylation events and even the regulation of intracellular Ca^{2+} concentration itself. These pathways can lead to many physiological outputs.

1.10.1 Effects of Nitric Oxide Release by Endothelial Cells

Henry Dale first showed that ACh was a vasodilator in 1914 (Dale, 1914). However, it wasn't until 1980 that the seminal work by Furchgott and Zawadzki, revealed that ACh-induced relaxation required an intact endothelium (Furchgott and Zawadzki, 1980). Several years later in 1987, Moncada reported that the action of nitric oxide, released by endothelial cells, acting on the underlying SMC was the mediator of ACh-induced endothelial dependent relaxation (Palmer et al., 1987).

Central to ACh-induced NO production in endothelial cells is Ca^{2+}. ACh activation of M_3 receptors leads to IP_3-mediated release of Ca^{2+} from the internal store and the subsequent activation of SOC. Intracellular Ca^{2+} binds to calmodulin to form the Ca^{2+}-calmodulin complex. This leads to the activation of the calmodulin-binding domain of endothelial nitric oxide synthase (eNOS) (Fleming et al., 2001). Activated eNOS

converts L-arginine to citrulline plus NO, in the presence of oxygen and NADPH (Palmer et al., 1988). Although the half-life of NO is relatively short (5-10 s) it can readily diffuse across the cell membrane and act on the underlying SMC.

NO converts the soluble guanylate cyclase enzyme to its active form to promote the production of 3,5-cyclic guanosine monophosphate (cGMP) from the guanosine-5'-triphosphate (GTP) substrate in vascular SMCs. cGMP activates protein kinase G, which promotes the re-uptake of Ca^{2+} into the sarcoplasmic reticulum. NO also inhibits voltage-gated Ca^{2+} channels and activates Ca^{2+}-dependent potassium channels in SMC (Bolotina et al., 1994). These mechanisms act to reduce the intracellular Ca^{2+} concentration, resulting in inhibition in the formation of the Ca^{2+}-calmodulin MLCK complex (Jin and Loscalzo, 2010). MLCK can no longer phosphorylate myosin and thus relaxation of SMC ensues.

In addition to being a potent vasodilator, NO is involved in several additional functions that maintain vascular homeostasis. NO inhibits platelet aggregation and adhesion to the surface of the endothelium by increasing intracellular cGMP to reduce platelet Ca^{2+} concentration and thus reduce platelet activation (Riddell and Owen, 1999; Wang et al., 1998). NO also has anti-inflammatory properties by inhibiting the synthesis and expression of cytokines and cell adhesion molecules that permit the recruitment of inflammatory cells to the cell surface, facilitating their entrance to the vessel wall (Bath et al., 1991; De Caterina et al., 1995).

The effects of NO are widespread and pivotal in maintaining vascular homeostasis. Indeed, dysfunction of the NO pathway (either synthesis or function) can lead to numerous diseases including atherosclerosis and hypertension (Cannon, 1998; Napoli and Ignarro, 2001). The role of Ca^{2+} in generating NO to mediate these functions cannot be understated. Ca^{2+} links the extracellular information stored in the ligand (ACh) to produce a functional output (NO-induced SMC relaxation).

1.10.2 Ca^{2+}-Induced Synthesis of Prostacyclin I_2

Increases in endothelial Ca^{2+} concentration also contributes to phospholipase A2-mediated production of the arachidonic acid metabolite, prostacyclin (PGI_2) (Balsinde et al., 2002). Once synthesised PGI_2 translocates to SMCs where it can bind to prostacyclin I_2 (IP) receptors, a Gs protein coupled receptor. IP activation leads to the release of the Gs complex which stimulates adenylyl cyclase, to increase intracellular levels of cyclic adenosine monophosphate (cAMP). This increase in cAMP causes activation of protein kinase A which subsequently mediates MLC phosphorylation. This is achieved by several downstream effects including 1) increased SERCA activity; 2) increased efflux of Ca^{2+} by PMCA; 3) inhibition of Ca^{2+} influx through voltage-operated Ca^{2+} channels due to K^+-channel activation; and 4) decreased Ca^{2+} sensitivity due to inhibition of MLCK.

1.10.3 Endothelial Permeability

As described above, the vascular endothelium forms a semipermeable barrier between blood plasma and interstitium. In order for plasma proteins and solutes to migrate from the blood to the underlying tissue they must be able to penetrate the vascular wall. This is achieved by two forms of transport, transcellular and paracellular. Transcellular transport occurs by caveolae-mediated vesicular transport through endothelial cells. Whereas, paracellular transport occurs through interendothelial cell junctions (Komarova and Malik, 2010).

1.10.4 Transcellular Transport

Transcellular transport or transcytosis selectively traffics macromolecules such as albumin and low-density lipoprotein across the endothelium by a vesicular transport mechanism (Armstrong et al., 2015; Ghitescu et al., 1986; Minshall et al., 2002). Transcytosis of macromolecules occurs by fission of the plasma membrane macrodomains enriched with caveolae. Caveolae then traverse the cytoplasm reaching the basolateral surface where they release their contents by exocytosis

(Komarova and Malik, 2010; Tuma and Hubbard, 2003). However, the role of endothelial Ca^{2+} signalling on this pathway is not fully understood.

Studies on transcytosis have remained relatively primitive when compared to other aspects of endothelial function. This is mainly due to technical limitations of studying transcytosis. Primary endothelial cells undergo significant phenotypic drift in cell culture, resulting in progressively fewer caveolae with each passage (Fung et al., 2018). Additionally, distinguishing between transcytosis and the contribution from artificial intercellular gaps or paracellular diffusion has proven difficult (Armstrong et al., 2012; Fung et al., 2018).

1.10.5 Paracellular Transport

Paracellular permeability of the endothelium is maintained by the interendothelial junctions that connect adjacent endothelial cells. These connections restrict the transport of plasma proteins. There are two types of interendothelial junctions present in the endothelium, tight junctions and adherens junctions, the expression of which varies between vascular beds. In the brain microcirculation strict control of endothelial permeability is exerted and therefore there is an increase in tight junctions (Dejana et al., 2009).

The paracellular permeability of the endothelium can be altered by external stimuli (Sukriti et al., 2014). Transmigration of leukocytes, formation of new blood vessel and blood vessel repair can all alter paracellular permeability. Furthermore, pathological processes such as inflammation and atherogenesis have been shown to increase paracellular permeability (Koenen et al., 2009; Sukriti et al., 2014; Tiruppathi et al., 2002).

The most common effect of these mediators in bringing about an increase in paracellular permeability is by adherens junction disruption. There are two independent mechanisms by which disruption of these junctions leads to increased endothelial permeability: disassembly of adherens junctions via phosphorylation and cytoskeletal reorganisation by acto-myosin contraction (Madara et al., 1987; Mehta

and Malik, 2006; Wojciak-Stothard and Ridley, 2002). The pathways regulating these two mechanisms are controlled by three interdependent signalling mechanisms c-Src kinase, RhoGTPase and Ca^{2+}. However, this thesis will focus on the role of changes in intracellular Ca^{2+}.

Inflammatory mediators, such as thrombin and histamine, have been shown to increase endothelial permeability by PLC-IP_3-induced increases in cytosolic Ca^{2+} concentration (Tiruppathi et al., 2002). A rise in intracellular Ca^{2+} causes activation of protein kinase Cα (PKCα). PKCα can also be activated by DAG.

Regulation of endothelial permeability by PKCα may be mediated by several possible mechanisms. PKCα may selectively phosphorylate p120-catenin, a protein directly involved in the stabilisation of cadherin expression at adherens junctions (Kourtidis et al., 2013). Phosphorylation of p120-catenin leads to dissociation of the protein from the cadherin complex resulting in endocytic internalization of cadherins (Komarova and Malik, 2010; Kourtidis et al., 2013). Thus, destabilisation of the adherens junctions and an increase in paracellular permeability.

PKCα also increases the production of RhoA GTPase by facilitating the exchange of GDP for GTP (Kozasa et al., 2011). This is achieved by phosphorylation of the GDP dissociation inhibitor (GDI-1), leading to a reduction in GDI-1 affinity for RhoA and resulting in the exchange of GDP for GTP (Knezevic et al., 2007; Mehta et al., 2001). RhoA GTPase activates Rho kinase to inhibit myosin light chain phosphatase (MLCP) (Barandier et al., 2003; Ming et al., 2004). This inhibition of MLCP with the concurring activation of MLCK by Ca^{2+}/calmodulin induces acto-myosin contraction. Therefore, activation of PKCα in conjunction with MLCK leads to a reorganisation of the actin cytoskeleton and hence an increase in endothelial permeability (Komarova and Malik, 2010).

Currently less is understood about the mechanisms governing endothelial permeability when compared to endothelial control of vasorelaxation. However, it is

clear that the role of Ca^{2+} is pivotal for controlling both of these physiological functions.

1.11 Measurement of Endothelial Ca^{2+}

Given the importance of Ca^{2+} as a secondary messenger it is critical that robust methods are available to measure intracellular Ca^{2+} concentration. The first reliable measurement of intracellular Ca^{2+} were performed by Ridgway and Ashley in 1967 by injecting the photoprotein aequorin into the giant muscle fibre of the barnacle (Ridgway and Ashley, 1967). Subsequently, a variety of fluorescent Ca^{2+} indicators have been produced to help elucidate the mechanisms involved in intracellular Ca^{2+} signalling (Grynkiewicz et al., 1985; Lock et al., 2015; Minta et al., 1989; Tsien, 1980, 1981; Williams et al., 1985). These indicators can be classified using several different criteria, the most common based on either their affinity for Ca^{2+} or whether they are ratiometric versus nonratiometric. These indicators allow for the analysis of Ca^{2+} levels not only at the cellular level but also subcellular level. Thus, they have elucidated many of the mechanisms underlying the spatiotemporal compartmentalisation of Ca^{2+} signalling within a cell. However, this thesis will focus mainly on the cellular level and discuss Ca^{2+} signalling across large field of endothelial cells.

Several techniques have been developed to study large scale Ca^{2+} signalling. Isolated endothelial tubes allow for the examination of endothelial Ca^{2+} signalling in the absence of confounding variables associated with surrounding smooth muscle cells and perivascular nerves (Socha and Segal, 2013). These studies allow for greater insight into the electrical dynamics of the endothelium and the communication that occurs between endothelial cells that is independent of smooth muscle cell interaction (Hakim et al., 2018).

In pressurised arteries the endothelium is monitored by focussing through the wall of artery that has been pressurised between two cannula. The endothelium is loaded with a Ca^{2+} indicator. Therefore, the mechanical response of pressurised artery can

be measured simultaneously with the Ca^{2+} response of individual endothelial cells (Falcone et al., 1993; Takano et al., 2004; Wagner et al., 1996; Yip and Marsh, 1996). These studies give a unique insight into how endothelial Ca^{2+} signals control vascular tone. Communication between endothelial cells has been shown to increases the spread of vasodilation over significant distances in mesenteric resistance arteries in response to local application of a vasodilator (Takano et al., 2004). Communication from the underlying smooth muscle cells to modulate the endothelial Ca^{2+} response have also been shown to occur in pressurised arteries (Dora et al., 2000).

The first *en face* artery preparation, where arteries are surgically opened and laid out flat for microscopic examination was first performed by Laskey et al in 1994 (Laskey et al., 1994). This technique allows for the measurement of changes in intracellular Ca^{2+} concentration in native endothelium. High-speed fluorescence imaging (wide-field and confocal) of open artery preparations permits large fields of endothelial networks to be visualised with high resolution. *En face* artery preparations have been utilised to determine the mechanisms involved in endothelial Ca^{2+} signalling at both cellular and subcellular level. For example, application of various agonists to the same field of endothelium have revealed variations in the response of individual endothelial cells (Huang et al., 2000; Lee et al., 2018; Marie and Bény, 2002; Wilson et al., 2016b). Several studies have also shown that signals from the underlying smooth muscle cells may modulate the Ca^{2+} response in endothelial cells (Garland et al., 2017). At the subcellular level, *en face* preparations have allowed for analysis of localised Ca^{2+} puffs and pulsars in native endothelial cells (Ledoux et al., 2008; Mumtaz, 2013; Nausch et al., 2012; Toussaint et al., 2015; Wilson et al., 2019). However, due to surgically opening the artery and pinning it flat the influence of the physiological structure of the artery is lost.

1.12 Summary

Given the acknowledged importance of Ca^{2+} in regulating endothelial function, and the uncertainty on how the ion regulates function-specific activities, the present project was undertaken. The main aim of this thesis is to determine how the

endothelium senses and responds to multiple stimuli that direct the vascular system to regulate various aspects of physiological status. To address this issue, we recorded the concurrent activity from hundreds of endothelial cells in intact resistance arteries. Small mesenteric arteries (second and third order) were used in this study as they, along with other resistance vessels, are crucial in the regulation of blood flow and control of blood pressure (Safar and Struijker-Boudier, 2010). Second and third order mesenteric arteries have the added benefit of being readily identified and dissected.

Chapter 3 describes the mechanisms underlying muscarinic-, purinergic- and histaminergic-evoked Ca^{2+} responses in the endothelium of intact resistance arteries. Chapter 4 describes the extent of heterogeneity and clustering of endothelial cells in response to various agonists. Furthermore, graph theory is utilised to analyse the signalling networks employed by the endothelium to detect and respond to different activators. Chapter 5 describes the features the Ca^{2+} signal evoked by muscarinic, purinergic and histaminergic receptor activation and the features of each signal when multiple agonists were present simultaneously. Chapter 6 presents a robust open source pressure myograph system, that can be readily adapted by other researchers and is comparable to other commercially available products. Finally, Chapter 7 presents a brief summary of the work contained within the preceding chapters and suggests areas for future work.

Given the acknowledged importance of Ca^{2+} in regulating endothelial function, and the uncertainty on how the ion regulates function-specific activities, the present project was undertaken. The objective of this thesis is to determine how the endothelium senses and responds to multiple stimuli that direct the vascular system to regulate various aspects of physiological status.

Chapter 2. Methods

2.1 Animal and Tissue Preparation

2.1.1 Animal Welfare

All animal care and experimental procedures were carried out with the approval of the University of Strathclyde Animal Welfare and Ethical Review Board [Schedule 1 procedure; Animals (Scientific Procedures) Act 1986, UK], under UK Home Office regulations. All experiments used tissue from male Sprague-Dawley rats (10 to 12 weeks old; 250 to 350 g). All rats were housed in pairs and maintained at a temperature of 21°C ± 2°C, 45-65% humidity, under a 12-hour light-dark cycle.

2.1.2 Mesenteric Artery Dissection

Rats were euthanized by intraperitoneal overdose of pentobarbital sodium (200 mg kg^{-1}; Pentaject; Merial Animal Health Ltd., UK) or CO_2 overdose. Subsequently, a midline laparotomy was performed to expose the mesentery. The mesentery was quickly removed and placed in chilled physiological saline solution (PSS; composition below). A section of the mesenteric arcade was isolated and pinned to the bottom of a Sylgard-coated (Dow-Corning Corp., USA) Petri dish, also filled with chilled PSS, using 0.2 mm stainless steel pins (26002-20, Fine Science Tools Inc., USA). Using a stereomicroscope (Nikon, UK), fine vannas micro-scissors and surgical forceps, adipose and connective tissue was removed to expose the superior mesenteric artery and first-order mesenteric branches. Removal of adipose and connective tissue along an arterial branch of the superior mesenteric artery exposed second and third order mesenteric arteries. Second- and third-order mesenteric arteries were then quickly dissected and pinned, to a custom flow chamber (800 µL volume) with a Sylgard bottom, containing chilled PSS. Arteries were then carefully cleaned of any remaining adipose or connective tissue.

2.2 En face Artery Preparation

Arteries were cut longitudinally, using microscissors and pinned flat, under a small amount of isometric tension, using 0.05 mm tungsten wire thread, lumen side facing

upward (Figure 2.1 A). Care was taken to ensure the artery was not damaged during stretching or wire insertion. Arteries were incubated in a loading solution containing a fluorescent Ca^{2+} indicator, Cal-520 acetoxymethyl ester (Cal-520/AM; 5 µM), 0.02% Pluronic F-127 and 0.35% dimethyl sulfoxide in PSS for 30 minutes at 37°C. Following incubation arteries were gently washed with PSS at room temperature and allowed to equilibrate for 30 minutes.

To image endothelial Ca^{2+} signalling on an upright microscope arteries were pinned to a custom bath chamber, the bottom of which was filled with Sylgard (Figure 2.1 B & C). Cal-520 was excited with 488 nm wide-field epifluorescence illumination provided by a LED illumination system (PE-300Ultra, CoolLED, Andover, UK) and imaged using an EMCCD camera (13-µm pixel size iXon Life 888; Andor), through a 16X (water immersion; numerical aperture of 0.8; Nikon CFI75) objective lens. Fluorescence emission was recorded at 10 Hz. Fluorescence illumination was controlled and images (16-bit depth) were captured by either WinFluor (University of Strathclyde, Glasgow, UK) or µManager (National Institutes of Health, Bethesda, MD, USA).

To enable visualisation of the endothelium, on an inverted microscope, arteries were dissected as described above. However, arteries were pinned to a Sylgard block rather than a custom chamber. This allowed the block to be inverted and placed in a custom flow chamber. The subsequent artery preparation and loading of the fluorescent Ca^{2+} indicator, was performed as described above. The bottom of the flow chamber was a 0-grade thickness coverslip, attached to the chamber with vacuum grease. The inverted Sylgard block was raised from the coverglass by two 200-micron pins. This served two purposes 1) to prevent contact of the glass and endothelium, 2) to allow solutions to be flowed between the artery and coverslip. Endothelial Ca^{2+} signalling on the inverted microscope was performed by exciting Cal-520 with a 488-nm wide-field epifluorescence illumination provided by a monochromator (Photon Technology International/Horiba UK Ltd.) and imaged using a back-illuminated electron-multiplying charge-coupled device (EMCCD) camera (13-µm pixel size;

iXon3, Andor) through a 40X (oil immersion; numerical aperture of 1.3; Nikon S Fluor) objective lens.

PSS and drugs were applied to the artery (for both the upright and inverted systems) using a syringe pump connected to the respective chamber, at a rate of 1.5 ml/min. All experiments were carried out at room temperature. Ca^{2+} responses were recorded over a 5-min period. This allowed for the recording of basal Ca^{2+} activity (no agonist; ~1 to 2 min) and the response to stimuli (~3 to 4 min). After pharmacological intervention arteries were washed for 5 minutes with PSS and allowed to rest for a further 5 minutes. This ensured a stable baseline was attained, before the subsequent addition of drugs.

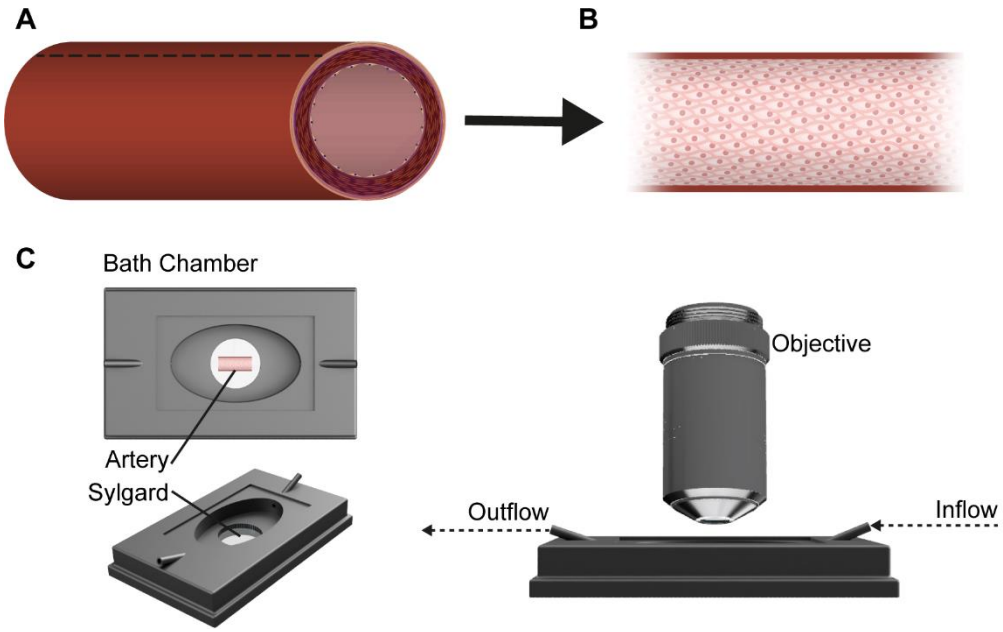

Figure 2.1 – Artery preparation for visualising endothelial Ca^{2+} responses.

(A) Illustration of a blood vessel. The dashed line indicates where the artery would be cut longitudinally. (B) Illustration of an artery that has been cut longitudinally and laid flat. The endothelium is facing upward. (C) A 3-dimensional rendering of a custom-made bath chamber. The chamber is fabricated from aluminium. A window, centred in the bottom of the chamber was filled with Sylgard and permitted light transmission. The Sylgard allowed the artery to be pinned to the chamber, lumen side facing upward, using 0.05 mm tungsten wire thread, under a small amount of isometric tension. The chamber was placed on an inverted fluorescence microscope and the endothelium was loaded with a fluorescent Ca^{2+} indicator, to enable visualisation.

2.3 Analysis of Endothelial Ca^{2+} Activity

Ca^{2+} signalling was recorded in large fields of endothelial cells (~200 cells; 40X objective or ~1000 cells; 16X objective) in intact arteries. We used these systems to assess the endothelial Ca^{2+} response to various agonists. To assess the concentration-dependence of agonist-evoked Ca^{2+} activity (Chapter 3), we stimulated endothelial cells with increasing concentrations of each agonist whilst Ca^{2+} activity was recorded, with a 10-minute wash/rest period between each agonist exposure. To identify the pathways involved in the Ca^{2+} response to agonist, we measured agonist-evoked (100 nM) activity before and after treatment with various pharmacological agents (30 minute incubation, concentrations described in the corresponding text/figure legends).

Traditionally, Ca^{2+} activity in endothelial cells has been analysed by averaging the fluorescence signal from several cells or across the whole of the imaged area. However, endothelial cells exhibit considerable heterogeneity in their response to Ca^{2+}-activating agonists (Kameritsch et al., 2012; Lee et al., 2018; Marie and Bény, 2002). As such heterogeneity cannot be accounted for by global measures of Ca^{2+} activity. Instead single-cell Ca^{2+} activity was assessed in all cells across the field-of-view (FOV) using a semi-automated analysis procedure.

2.3.1 Large Scale Ca^{2+} Signal Processing

Ca^{2+} imaging recordings were analysed using custom FIJI macros and custom analysis software written in the Python 2.7 programming language (Lee et al., 2018; Wilson et al., 2016b, 2018). This analysis consisted of four elements: 1) the generation of cellular regions-of-interest (ROIs) for each individual cell in the field-of-view; 2) the extraction of Ca^{2+} signals from each individual ROI and normalisation to its corresponding baseline; 3) the extraction of various Ca^{2+} signalling metrics (amplitude, frequency and percentage of active cells) from each cellular Ca^{2+} response; 4) the graphical representation of Ca^{2+} activity and statistical analysis. Each step is described below.

2.3.2 *ROI Generation and Alignment*

To allow a comparison (pairing) of the response of individual cells after various treatments, imaging datasets were grouped by experiment. In some experiments, a small percentage of cells moved outwith the field-of-view due to microscope drift. Only cells that remained within the field-of-view for each dataset within a group were used for analysis. This was achieved using a custom FIJI macro, which was used to identify the centre coordinates of each cell that remained within the field-of-view of all datasets in a group. First, for each group, an average intensity projection was created for each dataset. Then a virtual image was created that contained only the cells present in each of the individual datasets. This was achieved using an automated alignment plug-in in FIJI, to calculate the amount of drift between each consecutive dataset. The virtual image was then sharpened using a custom unsharp mask filter and individual cells identified using the Watershed Segmentation algorithm in FIJI. Centre coordinates of each cell were overlaid on the virtual image (using FIJI's multi-point selection tool) and were manually inspected to ensure each point corresponded to a single endothelial cell. After identifying individual endothelial cells, all Ca^{2+} signal extraction and processing was performed in Python 2.7.

2.3.3 *Automated Ca^{2+} Signal Extraction*

Cellular coordinates (obtained from virtual images) were projected across all other datasets within the corresponding imaging session using custom Python code. Single-cell Ca^{2+} traces were then automatically extracted from, non-background subtracted, Ca^{2+} imaging data by averaging the fluorescence intensity within circular ROIs (5 µm diameter) placed at the centre of each cell. Ca^{2+} traces were expressed as fractional change in fluorescence intensity (F/F_0), where F is fluorescence at time, t, and F_0 is baseline fluorescence intensity. F_0 was determined for each trace by averaging a 100-frame (10 s) baseline period before the application of a drug. F/F_0 traces were smoothed using 11-point (1.1 s), third-order polynomial Savitzky-Golay filter.

2.3.4 *Automated Ca^{2+} Signal Analysis*

Peaks in each Ca^{2+} signal were detected automatically using a zero-crossing detector on derivative F/F_0 traces. A threshold of five times the standard deviation of baseline noise was used to distinguish Ca^{2+} activity from noise. The discrete (first) derivative ($d(F/F_0)/dt$) of each Ca^{2+} signal (F/F_0) was calculated by convolving each F/F_0 trace with the first derivative of a Gaussian kernel (Wilson et al., 2015, 2016b). An increase in F/F_0 corresponds to a positive deflection in the discrete derivative, whilst a decrease in F/F_0 corresponds to a negative deflection in the discrete derivative. The zero-crossings associated with a positive deflection and a preceding negative deflection (one before, one between, and one after) in the derivative trace indicate, respectively, the start, peak, and end of an event in the corresponding Ca^{2+} trace. Thus, peaks in F/F_0 were identified by locating the times at which the discrete derivative changes from positive to negative. These times were used to extract various signal metrics from each individual cell (peak and steady-state amplitude) from the corresponding F/F_0 data. A cell was considered to be "active" if a peak was detected.

2.4 Graphical Representation of Ca^{2+} Activity

Ca^{2+} imaging recordings were represented graphically in two-dimensions by creating composite colour images. First, raw image stacks were temporally smoothed using a 20-frame running average filter. An average-intensity projection of the baseline period (30 seconds, 300 frames) was used to produce a greyscale "background" image of all endothelial cells. Background images were scaled to 8-bit format such that the minimum and maximum pixel intensities corresponded to a value of 0 and 255, respectively. Next, an image series highlighting changes in Ca^{2+} was created by performing a 10-frame (1 second) sequential subtraction. This was achieved by duplicating the temporally smoothed image stack twice and removing the first 10 frames from the first copy and the last 10 frames from the second. The first copy was then subtracted from the second, and the resulting image stack was spatially

smoothed by applying a low-pass Gaussian filter (2.0 pixel radius) to each frame. These images were then converted to a single image (STDev images) that showed all cells that exhibited Ca^{2+} activity. STDev images were created by taking the standard deviation of intensity of the sequential subtraction image stack. To prevent saturation, Ca^{2+} signal images were scaled by 50% and images were converted to 8-bit format. Finally, composite colour images were created by overlaying STDev Ca^{2+} images in colour onto the greyscale "background" image (showing all endothelial cells). Image processing was performed in FIJI (Schindelin et al., 2012).

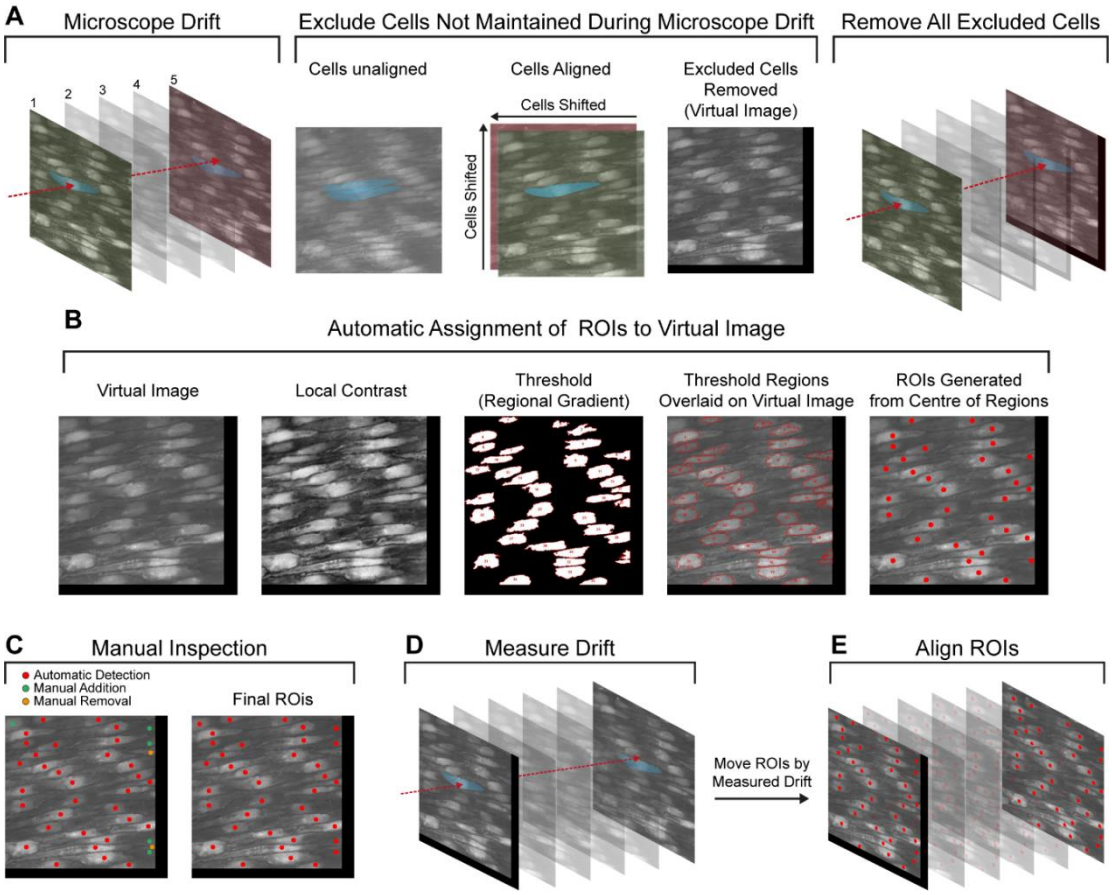

Figure 2.2 – ROI generation and alignment.

Occasionally movement occurred between recordings within an individual experiment. To allow direct comparisons of the response of individual cells, cellular ROIs were aligned across experiments. (A) The highlighted cell (blue) in the first experiment (green overlay) is the same cell highlighted in the 5th experiment (red overlay). The red line is maintained across all experiments and illustrates the drift of the highlighted cell from the original position (left). The Template Matching plug-in in FIJI was used to align the cells across all experiments (middle). A virtual image was created that excluded regions that were not maintained across all experiments. (B) ROIs were automatically generated for the virtual image using a threshold gradient. (C) ROIs were manually inspected to determine if all cells were included and if any ROIs overlapped multiple cells. (D) The drift from the virtual image for each recording was calculated. (E) ROIs were generated for each recording by shifting them the calculated distance from the virtual image.

2.5 Pressure Myography

2.5.1 Artery Preparation and Mounting

Second- and third-order mesenteric arteries were dissected and cleaned as described above and visually checked for the presence of side branches. Arteries with side branches were sealed by tying off the branch, using a single strand of silk suture thread, or discarded if the branches could not be tied. Arteries were then cannulated onto two heat-polished micropipettes using silk suture thread, in a self-heated single vessel chamber (Chapter 6). Arteries were gently heated to 37 °C by circulating PSS to the bath from a heated reservoir at 10 ml/min using a peristaltic pump. The distal end of each cannula (relative to artery attachment) was connected to a separate syringe containing PSS. The height of the two syringes was adjusted to alter arterial transmural pressure and pressure was increased in 10 mmHg increments followed by 10 minute equilibration, to a final pressure of 70 mmHg. Arteries were subsequently straightened and allowed to equilibrate for an additional 30 minutes. During this equilibration, arteries were tested for leaks (which may indicate branches in the vessel wall or insufficiently tied sutures) by stopping the flow of solution from the syringes to the arteries. Arteries that showed a reduction in pressure, indicative of leaks, were discarded. Intraluminal flow (~200 µl min^{-1}) was established by a hydrostatic pressure gradient (10 cm H_2O) across the artery.

Contraction data are represented as the percent reduction from resting diameter. Relaxation data (from constricted diameter) are represented as the percent of maximal relaxation (constricted diameter to resting diameter). Outer vessel diameter, intraluminal pressure, and bath temperature, were continuously monitored with a CMOS camera (diameter)**,** custom pressure/temperature monitors, and VasoTracker diameter tracking software (Chapter 6).

2.5.2 *Determination of Artery Viability*

Arteries were first contracted, to 80% of resting diameter, using phenylephrine (500 nM - 1 µM). Phenylephrine was applied to the outside of the artery by adding it to the superfusate, which was continuously recirculated throughout the myograph chamber. Once a stable contraction was attained, endothelium-dependent relaxation to ACh (1 µM) was examined. Only arteries that relaxed by more than 95% were considered to have a functional endothelium, all other arteries were discarded. The bath and reservoir were subsequently washed with PSS to remove phenylephrine and ACh.

2.5.3 *Assessment of Endothelial-Dependent Vasodilation*

Problems in assessing the effect of drugs on endothelial function may arise if drugs are applied to the outside of the artery. For example, the smooth muscle cells may also respond to the agonist (i.e. ATP), especially at high concentrations, or the molecule itself may be too large to diffuse freely through the arterial wall. Therefore, the preferred method to study the effects of agonist-induced endothelial activity in the present investigation, was to apply the drug intraluminally. Each activator was added to one of the height-adjustable reservoirs and flowed through the lumen of the artery. The direction of flow in each artery was the same as that *in vivo*. At 200 µl min^{-1}, drugs took 10 minutes to reach the artery. Therefore, drug perfusion occurred under gravitational flow for 20 minutes, before the subsequent addition of drug or wash with PSS. This allowed 10 minutes for the drug to reach the lumen and 10 minutes of application.

2.6 Reagents and Solutions

Cal-520/AM was obtained from Abcam. Pluronic F-127 was obtained from Invitrogen. AR-C118925XX, MRS 2179, U73122 and U73343 were obtained from Tocris Bioscience. All other drugs and chemicals were obtained from Sigma-Aldrich. PSS consisted of: 145 mM NaCl, 4.7 mM KCl, 2.0 mM MOPS, 1.2 mM NaH_2PO_4, 5.0 mM

glucose, 0.02 mM EDTA, 1.17 mM $MgCl_2$, and 2.0 mM $CaCl_2$, adjusted to pH 7.4 with NaOH. All solutions were freshly prepared daily.

Statistics are described in the Methods sections of the chapters that follow.

Chapter 3. Ca^{2+} Signalling in the Endothelium

3.1 Introduction

The endothelium is a complex sensory network that plays a critical role in regulating virtually every cardiovascular function (McCarron et al., 2017). The endothelium differs from most sensory systems in that each endothelial cell can potentially detect several different types of input and generate multiple different outputs; most sensory systems detect one input and generate one output. The endothelium can receive signals from circulating hormones, leukocytes, proinflammatory cytokines, neurotransmitters, pericytes, smooth muscle cells as well as endothelial cells themselves (Emerson and Segal, 2000; Kolka and Bergman, 2012; Longden et al., 2017; Socha et al., 2012). Furthermore, these signals can arrive from as close as neighbouring cells to the most remote outposts of the body. Endothelial cells must accurately relay the information held in the signals, many of which can arrive simultaneously, to generate specific outputs. These outputs include NO, prostacyclin, tissue contracting factors, plasminogen activator and endothelial-derived hyperpolarizing factor (Fleming et al., 1998; Furchgott and Zawadzki, 1980; Oliver et al., 2005; Sadowski and Badzynska, 2008). The generation of each of these signalling molecules is tightly regulated by changes in endothelial Ca^{2+} concentration (Endres et al., 2015). Through these Ca^{2+}-dependent mediators, the endothelium controls vascular tone, nutrient exchange, blood cell recruitment, blood clotting, and the formation of new blood vessels (Félétou, 2011; Heathcote et al., 2019; Kohn et al., 1995; Muñoz-Chápuli et al., 2004). Therefore, central to an understanding of endothelial function is an appreciation of the regulation of endothelial Ca^{2+} signalling.

Changes to intracellular Ca^{2+} concentration is achieved primarily by two distinct pathways; influx/efflux across the plasma membrane and release/re-uptake from the ER (Taylor and Francis, 2014). Several receptors regulate these pathways, to control changes in intracellular Ca^{2+} (discussed in Chapter 1). However, this thesis will primarily examine the role of signalling through G protein–coupled receptors of the $G\alpha_q$/11-subtype. Briefly, GPCR agonist binding leads to the activation of PLC, which hydrolyses PIP_2 to generate DAG and IP_3. IP_3 activation of IP_3Rs, on the ER, promotes

Ca^{2+} release from the internal store resulting in an increase in cytosolic Ca^{2+}. Depletion of Ca^{2+} from the ER results in SOCs activation and thus Ca^{2+} entry across the plasma membrane (Thillaiappan et al., 2017).

By utilising fluorescent Ca^{2+} indicators, various studies have demonstrated that the vasoactive endogenous ligands ACh, ADP, ATP and histamine evoke increases in endothelial Ca^{2+} (Avdonin et al., 2019a; Kameritsch et al., 2012; Marie and Bény, 2002). Predominantly, previous studies have investigated Ca^{2+} changes in either single cells or have taken the average response across primary cultures (Rotrosen and Gallin, 1986; Shen and DiCorleto, 2008; Viana et al., 1998; Yamamoto et al., 2000). However, the physiological characteristics of the Ca^{2+} signal or the response to the agonist may differ in single cells or cells in culture compared to the responses in intact blood vessels (Marie and Bény, 2002). Furthermore, examination of the global average of the Ca^{2+} signal across the entire endothelium may exclude important aspects of agonist-evoked Ca^{2+} signals.

To address the issue of co-ordination of signalling in the endothelium, we concurrently recorded the individual activity of hundreds of endothelial cells in intact blood vessels and examined the responses of individual cells to extracellular activators of muscarinic, purinergic and histaminergic receptors.

Each of these activators plays important physiological roles. Purinergic activation may occur by ATP released from activated platelets as part of the clotting cascade and may either increase or decrease endothelial permeability (Gündüz et al., 2003; Jacobson et al., 2006; Tanaka et al., 2003) and regulate vascular tone. ADP, also released by platelets, has been shown to promote endothelial cell migration (Abbracchio et al., 2006; Holmsen and Weiss, 1979; Shen and DiCorleto, 2008). This process may contribute to re-endothelialization and angiogenesis after vascular injury and ADP may also regulate vascular tone. Histaminergic activation of endothelial cells by histamine, primarily released from mast cells, has been shown to increase vascular permeability (Amin, 2012; Ashina et al., 2015; Kugelmann et al., 2018). Although, muscarinic activation of endothelial cells by ACh is used extensively

to determine endothelial viability, the precise physiological source of ACh and its role in the control of endothelial function has remained elusive. Recently, we have shown that the endothelium responds to flow by releasing ACh. Once free, ACh acts on endothelial cells (in an autocrine/paracrine manner) to generate a Ca^{2+} response, resulting in NO production and thus vasodilation (Wilson et al., 2016a).

The present study aimed to define the mechanisms of the muscarinic, purinergic and histaminergic Ca^{2+} signalling in large populations of endothelial cells in intact arteries. The results show that the increase in endothelial Ca^{2+} evoked by each agonist is concentration-dependent. The Ca^{2+} signals evoked by each agonist began in discrete cell clusters and propagated to neighbouring cells. As the concentration of agonist increased the number of cells and clusters increased. Interestingly, each agonist evoked a Ca^{2+} increase by activation of GPCRs, leading to IP_3 generation and Ca^{2+} release from the internal store to cause an increase in intracellular Ca^{2+} concentration and the subsequent influx of Ca^{2+} from the extracellular space. However, the sensitivity varied among different cells in the endothelium between different agonists. Collectively, these results suggest the endothelium utilises a sub-population of cells to detect several different activators, over various concentrations, to elicit an increase in intracellular Ca^{2+}. Ca^{2+} activity is not uniform across the endothelium with individual cells expressing variations in Ca^{2+} activity in a concentration-dependent manner.

3.2 Methods

3.2.1 Concentration Response

Artery dissection, preparation and endothelial Ca^{2+} signal analysis was performed as described in Chapter 2. Full non-cumulative concentration responses were obtained in *en face* preparations by applying agonists at various concentrations (ACh, 1nM – 10µM; ADP, 1 nM – 100 µM; ATP, 30 nM – 300 µM; histamine, 100 nM – 1 mM). A complete concentration-response curve, per agonist, was carried out in a single mesenteric artery preparation. After the application of an agonist at each concentration, arteries were washed with PSS for 5 minutes and allowed to rest until a stable baseline was attained, before the subsequent addition of agonist.

ROIs were generated for each individual endothelial cell, as described in Chapter 2. This allowed the concentration-dependent response of each cell and the average concentration response across the entire field of endothelium to be determined.

3.2.2 Muscarinic, Purinergic & Histaminergic Ca^{2+} Signalling Pathway

3.2.2.1 Receptor subtype involved in Agonist-induced Endothelial Ca^{2+} Signalling

In experiments designed to determine the receptor subtype involved in muscarinic, purinergic and histaminergic Ca^{2+} signalling, agonists were applied to the endothelium to generate a Ca^{2+} response. After 2 minutes of stimulus application, the inflow solution was changed to a combination of both activator and specific receptor blocker. Each experiment was recorded over a 10 minute period. This allowed for the recording of basal Ca^{2+} activity (no agonist, ~1 to 2 min), the response to stimuli (~2 to 3 min) and response to an activator in the presence of a specific blocker (~5 to 7 min). Arteries were then incubated in the antagonist for 10 minutes after which the agonist and blocker were reapplied (in combination) to endothelium.

3.2.2.2 *Phospholipase C*

To determine the involvement of PLC in agonist evoked Ca^{2+} signalling, the endothelium was activated by an agonist, washed in PSS and incubated with the selective PLC blocker U73122 (2 µM) for 20 minutes. The blocker remained present throughout all subsequent additions of agonist. U73433 (2 µM), the inactive analogue of U73122, was applied in the same way.

3.2.2.3 *Role of the Internal Store in Agonist-induced Ca^{2+} Signalling*

To assess the role of IP_3-mediated Ca^{2+} release from the internal store, 2-APB (100 µM) an IP_3 receptor blocker and ryanodine (30 µM) a specific ryanodine receptor modulator were used. Agonists were applied before (control) and after incubation (30 mins) with the blockers. Each blocker remained present throughout all subsequent additions of agonist.

In experiments designed to determine the role of the intracellular store in response to ACh, ADP, ATP and histamine the sarco/endoplasmic reticulum ATPase (SERCA) blocker, cyclopiazonic acid (CPA) (10 µM) was used to inhibit Ca^{2+} uptake from the cytosol to the endoplasmic reticulum. Agonists were applied before and after incubation (20 mins) with CPA.

Ionomycin (1 µM) was applied at the end of each experiment to ensure the endothelial cell viability (i.e. a Ca^{2+} response could be generated after pharmacological blocker intervention).

3.2.2.4 *Assessment of Ca^{2+} Influx During Agonist-Mediated Ca^{2+} Signalling*

To determine the contribution of Ca^{2+} influx in muscarinic, purinergic and histaminergic endothelial Ca^{2+} signalling, extracellular Ca^{2+} was removed. Two control Ca^{2+} responses were obtained in each preparation, for each agonist, as described above. This allowed for a comparison between repeatable agonist-evoked Ca^{2+} signals. Arteries were subsequently washed in Ca^{2+}-free PSS. After 60s of Ca^{2+}-free PSS, agonists were again applied to the endothelium. Arteries were washed in normal

PSS, after each application of Ca^{2+}-free PSS and agonist, to allow the store to refill before subsequent activations.

3.2.3 *Solutions and Drugs*

Solutions and drugs are described in Chapter 2. In experiments designed to determine the role of Ca^{2+} influx in agonist-induced Ca^{2+} signalling normal PSS was replaced with Ca^{2+}-free PSS. Ca^{2+}-free PSS consisted of: 145 mM NaCl, 4.7 mM KCl, 2.0 mM MOPS, 1.2 mM NaH_2PO_4, 5.0 mM glucose, 0.02 mM EDTA, 1.0 mM EGTA, and 2.34 mM $MgCl_2$, adjusted to pH 7.4 with NaOH. Ryanodine, 2-aminoethoxydiphenyl borate (2-APB), cyclopiazonic acid (CPA), were dissolved in DMSO.

3.2.4 *Statistics*

Summarised data are presented as means ± SEM values or geometric mean with 95% confidence intervals (95% CI) for EC_{50} values; n refers to the number of animals. For comparison of two groups, a Student's t test (paired data) or unpaired t test (unpaired data) was performed. For comparison of three or more groups a One-way ANOVA followed by Tukey's multiple comparisons test was used. Sigmoidal curves were fitted to concentration response data and the minima of the sigmoidal curves were constrained to zero. All statistical analyses and sigmoidal curve fitting were performed using GraphPad Prism, version 6.0 (GraphPad Software). $P < 0.05$ was considered statistically significant.

3.3 Results

3.3.1 Ca^{2+} Signal Propagation Within and Between Cells

Compartmentalisation of molecules and proteins, within a cell, is an important element in cellular signalling. Ca^{2+} signalling is also subject to compartmentalisation to facilitate selective activation of specific cell activities. The muscarinic agonist ACh (15 nM) evoked an increase in intracellular Ca^{2+} in the intact mesenteric artery endothelium (Figure 3.1 A). Ca^{2+} signals began in spatially discrete regions within a cell and propagated from there as waves through part or all of the cell (Figure 3.2). Additional cells were subsequently recruited either by direct activation by the agonist or propagation of the Ca^{2+} signal from the initial responding cells (Figure 3.1 B). Some cells were unresponsive or expressed minimal Ca^{2+} activity and others were highly active with repeating Ca^{2+} waves and oscillations (Figure 3.1 C-G). The amplitude and frequency of the Ca^{2+} signal varied between cells.

Due to the heterogeneous properties of the Ca^{2+} response, analysis of the average response across all cells may conceal, important, physiologically relevant, components of the Ca^{2+} signal. Therefore, each cell was analysed separately. A region of interested (ROI) was generated for each cell and the Ca^{2+} signal from each cell (ROI) was obtained separately (Figure 3.1 C and D).

3.3.2 Muscarinic Evoked Ca^{2+} Signals

We previously reported in large (carotid) arteries, muscarinic receptor activation evokes a concentration-dependent Ca^{2+} response in ECs. To investigate if similar responses are present in the endothelium of small arteries, we examined the concentration dependence of mesenteric resistance artery endothelium to the endogenous ligand ACh (1nM–10µM). Specifically, we extracted ACh-induced Ca^{2+} signals from each individual cell in the field-of-view. To directly compare single-cell Ca^{2+} signalling parameters (amplitude, duration, frequency) of individual cells, across all concentrations, full concentration response experiments (1nM–10µM) were carried out in the same preparation and field of endothelium.

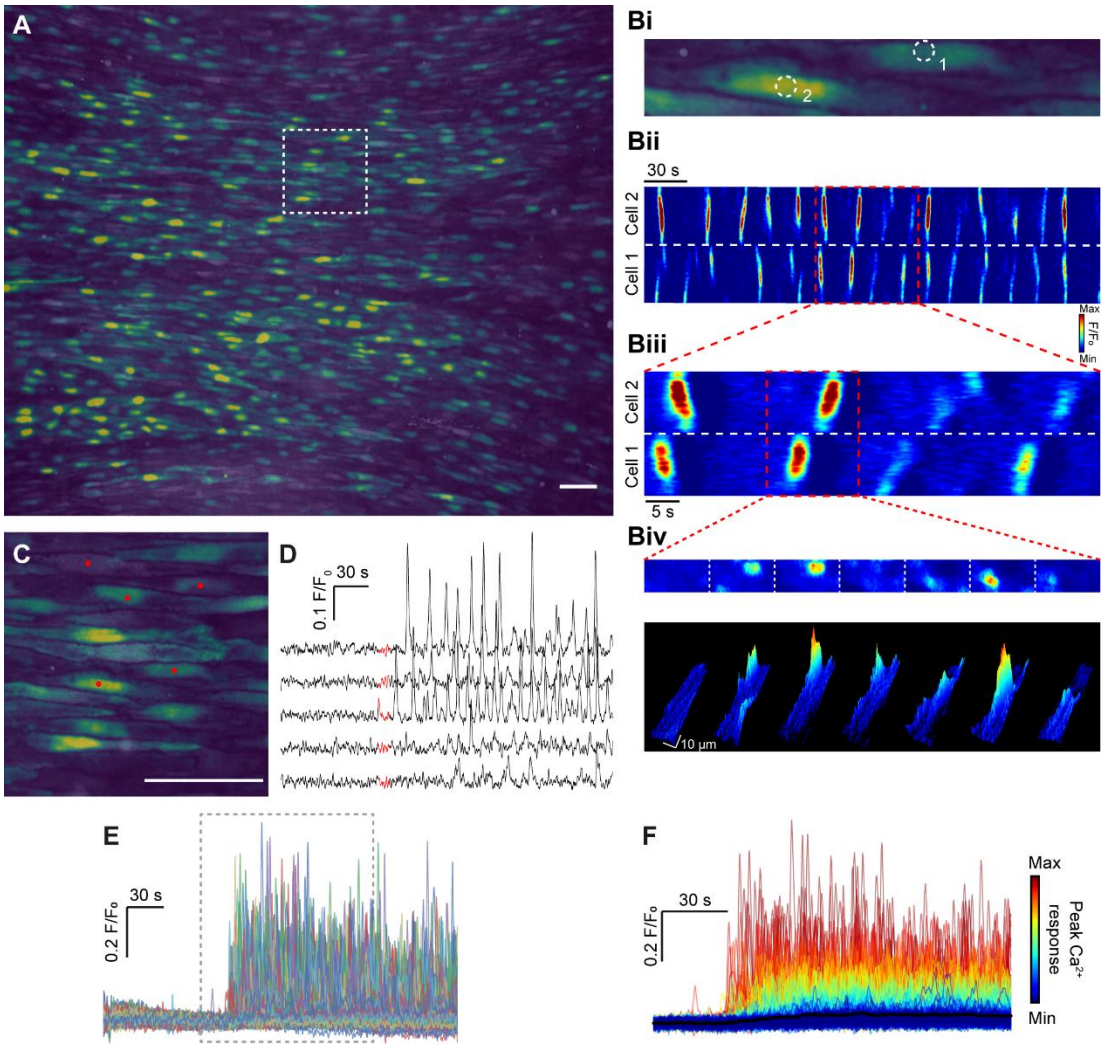

Figure 3.1 – Ca^{2+} signalling in intact mesenteric endothelium.

(A) Representative image showing ~1000 endothelial cells from an *en face* second order mesenteric artery. ACh-induced (15 nM) Ca^{2+} activity from a 5-minute recording superimposed. (Bi) Zoomed region taken from (A). (Bii and Biii) A 2D kymograph (linescan) showing the Ca^{2+} signal intensity (colour) plotted against time (x-axis) from the two cells labelled in (Bi) for the full 5-minute recording (Bii) and dashed region (Biii). (Biv) A 2D and 3D surface plot showing signal propagation between the two cells highlighted in (Biii). (C) Zoomed region from (A) as indicated by the dashed white box with superimposed ROIs (red dots). (D) Baseline corrected Ca^{2+} signals (F/F_0) obtained from the ROIs in (C). The highlighted section (red) on each individual Ca^{2+} signal indicates the software-determined baseline region. (E) Overlaid baseline corrected Ca^{2+} signals from each cell in (A). The signals were obtained using the same methods for signal extraction shown in (C-D). (F) Overlaid Ca^{2+} signals from region indicated in (E). The individual Ca^{2+} signals have been color-coded according to the amplitude of the initial rise in Ca^{2+}, red indicates the highest amplitude and blue the lowest amplitude. Scale bars, 50 µm.

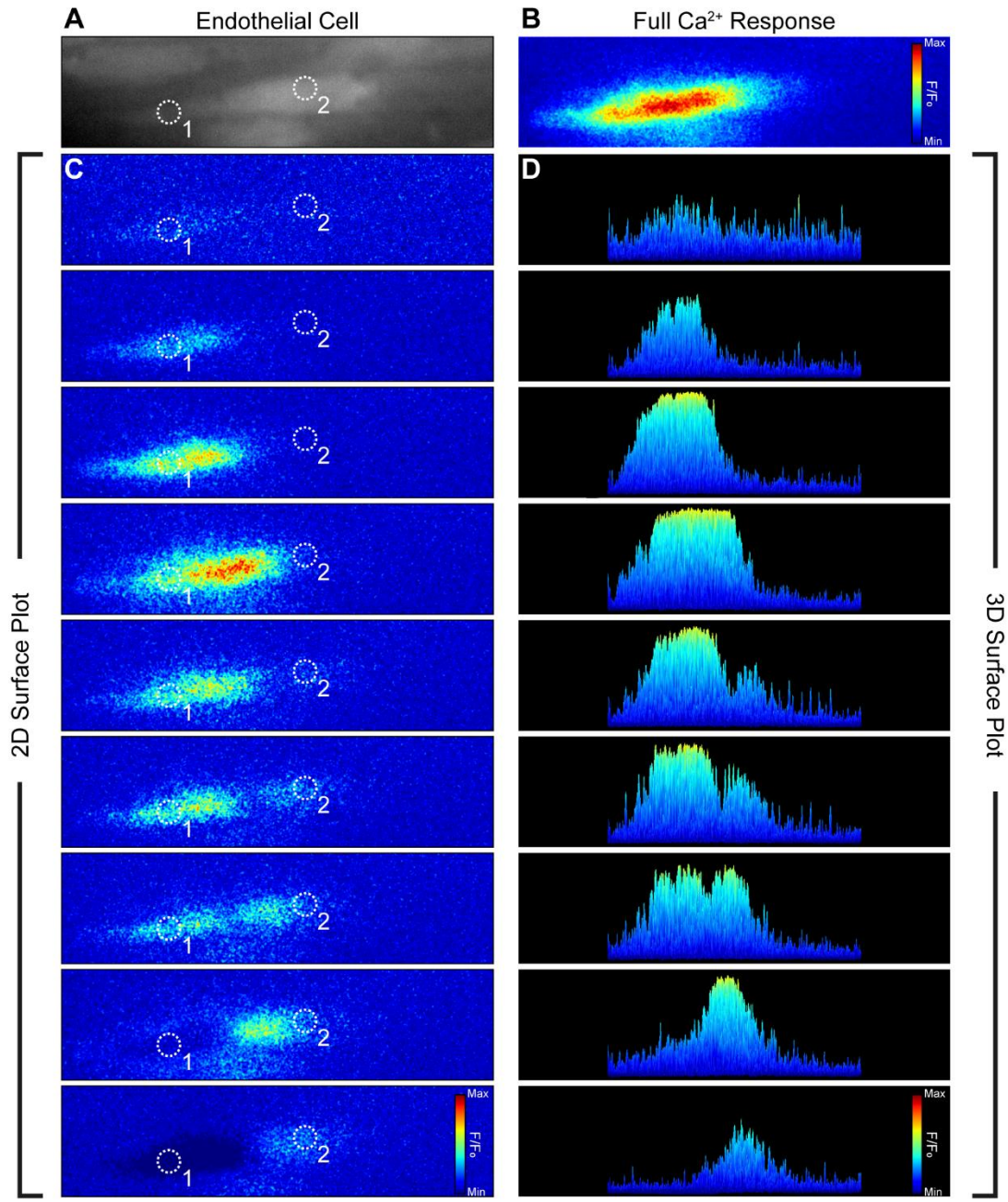

Figure 3.2 – Ca^{2+} signal propagation within an endothelial cell.

(A) Endothelial cell from an *en face* second order mesenteric artery. (B) A 2D surface plot showing the full Ca^{2+} response in a single endothelial cell after activation with ACh (15 nM). (C) A 2D surface plot showing Ca^{2+} signal propagation between two regions (dashed circles) in a single endothelial cell (B). (D) A 3D surface plot showing Ca^{2+} signal propagation in a single endothelial cell (B).

Notably, each concentration of ACh produced a heterogeneous response (Figure 3.3 A-C). The number of cells responding to ACh, and the amplitude of the Ca^{2+} signal in responding ECs, increased with ACh concentration (Figure 3.3 A-F). The concentration response relationship of the percentage of responding cells was significantly left shifted compared to that of Ca^{2+} activity within each cell (EC_{50} 13.5 nM, 95% CI = 10.5-17.5 nM vs 68.9 nM, 95% CI = 54.9-86.4 nM). Interestingly, all cells were activated (i.e. produced a Ca^{2+} response) before a maximal Ca^{2+} response was achieved. Thus, the differing concentration sensitivity of individual cells extended the overall sensitivity of the endothelium. Recruitment of neighbouring ECs likely occurs due to propagation of the Ca^{2+} signals through gap junctions or as a result of a direct but delayed activation by ACh or a combination of both.

Distinguishing between these possibilities has proved difficult. Pharmacological blockers of gap junctions, appear to exert effects beyond their target proteins in intact arteries. Previous studies have reported that the suppression of ACh-evoked endothelial Ca^{2+} signalling by the gap junction–blocking compounds carbenoxolone, glycyrrhetinic acid, and GAP-27, was independent of a direct effect on gap junctions (Wilson et al., 2016b).

Regardless of the mechanism of propagation among cells (Ca^{2+} or IP_3), the results demonstrate that there is cellular heterogeneity in the responses of endothelial cells, which is responsible for encoding information about extracellular stimuli. Coordination of Ca^{2+} signals is critical for a robust detection and communication system. While individual cells may occasionally generate Ca^{2+} signals as a result of stochastic noise, it is unlikely a cluster of cells will respond in unison to the same noise. If the concentration of the agonist exceeds the sensitivity range of the cluster, then a response will be generated that will propagate to neighbouring endothelial cells. Clustering may also limit interference from neighbouring cells that are responding to a different stimulus. For example, a single cell responding in isolation may easily be influenced by neighbouring cells and have its signal overridden

however, a cluster of cells each performing the same task may be much harder to override.

3.3.3 *Purinergic Evoked Ca^{2+} Signals*

To investigate whether or not cellular heterogeneity enables the endothelium to encode information from other agonists, we also examined the endothelial Ca^{2+} response to the purinergic agonists, ADP and ATP. For each purinergic agonist, full concentration-response relationships were carried out. Complete concentration responses for each agonist were carried out on the same preparation and the same field of endothelium (ADP: 1 nM–100 µM; ATP: 30 nM–300 µM).

Like the muscarinic (ACh) response, each purinergic activation (by ADP and ATP) also evoked heterogeneous Ca^{2+} responses across the endothelium (Figure 3.4 A-C and Figure 3.5 A-C). For each activator (ADP and ATP), the number of cells activated, and the amplitude of the Ca^{2+} signal in responding cells, increased with agonist concentration (Figure 3.4 A-F and Figure 3.5 A-F). The concentration-dependence of the percentage of responding cells was significantly left shifted when compared to the Ca^{2+} activity within each cell for both ADP (Figure 3.4 E-F; EC_{50} 111.0 nM, 95% CI = 87.8-140 nM vs 1.13 µM, 95% CI = 0.9-1.3 µM) and ATP (Figure 3.5 E-F; EC_{50} 1.08 µM, 95% CI = 0.8-1.4 µM vs 4.2 µM, 95% CI = 3.3-5.3 µM). Thus although there is only a narrow range of concentrations over which the endothelium as a whole responds to ADP and ATP, the concentration dependence of the response of individual cells to purinergic activation increased the overall sensitivity of the endothelium. Although both ADP and ATP could evoke Ca^{2+} activity in all mesenteric ECs the potency of ATP was significantly lower than ADP (EC_{50}; 111.0 nM for ADP vs 1.08 µM for ATP).

3.3.4 *Histaminergic Evoked Ca^{2+} Signals*

To further test the hypothesis that endothelial heterogeneity and clustering of cells with similar sensitivities, are features of endothelial information coding, we also examined histaminergic signalling. Histamine is a well-established regulator of vascular permeability and has also been reported to inhibit conducted vasodilation

(Payne et al., 2004). Histaminergic evoked Ca^{2+} signalling in cultured cells has been well documented (Avdonin et al., 2019b; Kameritsch et al., 2012; Worthen and Nollert, 2000; Zhou et al., 2014). However, there have been few studies on histamine-induced Ca^{2+} signalling in intact arteries. Previous studies on histamine-evoked Ca^{2+} signals have focussed primarily on the average histamine response across many cells and compared variations in the signal from regions of endothelium at either branch or non-branch sites (Huang et al., 2000). To our knowledge, no study has demonstrated how individual ECs in intact tissue respond to histamine.

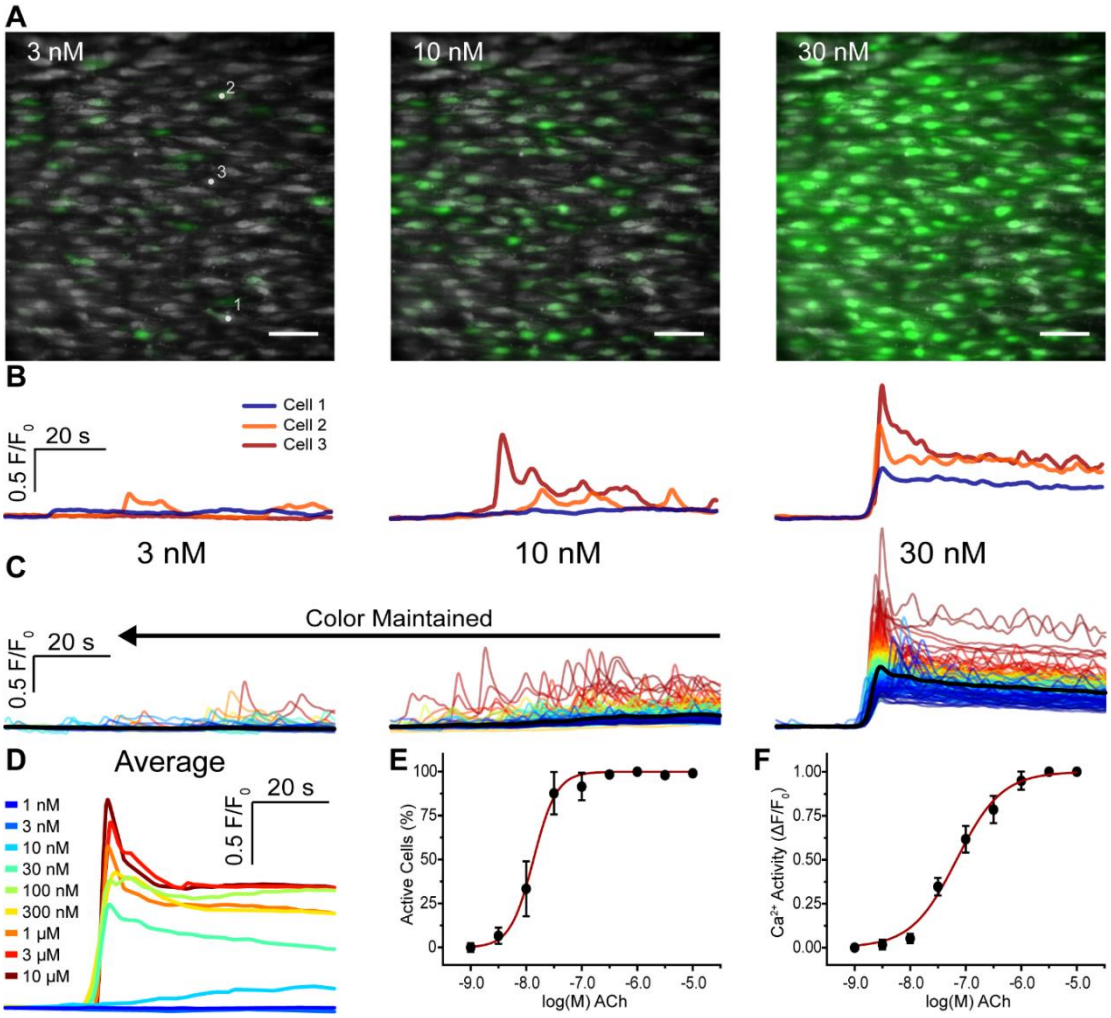

Figure 3.3 – Concentration-dependent ACh-induced Ca^{2+} signalling.

(A) Representative composite image of Ca^{2+} activity in *en face* second order mesenteric artery endothelium to increasing concentrations of ACh. (B) Ca^{2+} traces from individual cells indicated in (A). (C) Ca^{2+} signals from all individual cells in (A) Colours were assigned to the traces based on the amplitude of the initial response to ACh in each cell. Red indicated the highest amplitude and blue the lowest amplitude. Colours were assigned to the highest ACh concentration (far right) first and maintained across the previous concentrations. Thus allowing for direct comparison of the same cells between different ACh concentrations. (D) Average Ca^{2+} response (F/F_0) from all cells for each ACh concentration. (E) Percentage of all cells active at each concentration of ACh. (F) Average activity (F/F_0) of all cells for each concentration of ACh. Data are representative of n = 5 independent experiments from different artery preparations from different animals. Scale bars, 50 µm.

To determine the sensitivity of mesenteric ECs to histamine a full concentration response was carried out (Figure 3.6A-F; 100 nM – 1 mM). As with muscarinic and purinergic signalling, histamine evoked a Ca^{2+} rise in individual cells and the Ca^{2+} signal subsequently propagated to neighbouring endothelial cells.

The number of cells activated was concentration-dependent and the activity within each cell also increased with increasing concentration (Figure 3.6 A-F). Again, the activity of each cell (EC_{50} = 14.8 µM, 95% CI = 11.7-18.6 µM) was significantly right shifted when compared to the percentage of total cell activation (EC_{50} = 2.3 µM, 95% CI = 1.7-3.1 µM). Interestingly, histamine was the least potent activator of mesenteric EC Ca^{2+} signalling when compared to muscarinic and purinergic agonists (ACh EC_{50} = 13.5 nM; ADP EC_{50} = 111.0 nM; ATP EC_{50} = 1.08 µM; Histamine EC_{50} = 2.3 µM).

3.3.5 Detection and Transduction of Agonist-Induced Ca^{2+} Signals

The pathway involved in the transmission of extracellular signals to generate a physiological output involves multiple signalling components (Chapter 1). Briefly, G_q protein-coupled receptors stimulate phospholipase C (PLC) to produce IP_3, which subsequently activates IP_3Rs to evoke Ca^{2+} release from the endoplasmic reticulum. This decrease in ER Ca^{2+} leads to an influx of extracellular Ca^{2+} across the plasma membrane via SOCE (Chapter 1) to cause an increase in intracellular Ca^{2+}. To determine the Ca^{2+} signalling pathway activated by muscarinic, purinergic, and histaminergic agonists, we tested the effects of inhibiting/ blocking specific components of the signalling cascade.

The first step in many cell signalling mechanisms is the detection of a signal, by a specific receptor, at the plasma membrane. Therefore, we sought to determine the receptor subtype involved in the detection of extracellular stimuli for muscarinic, purinergic and histaminergic signalling.

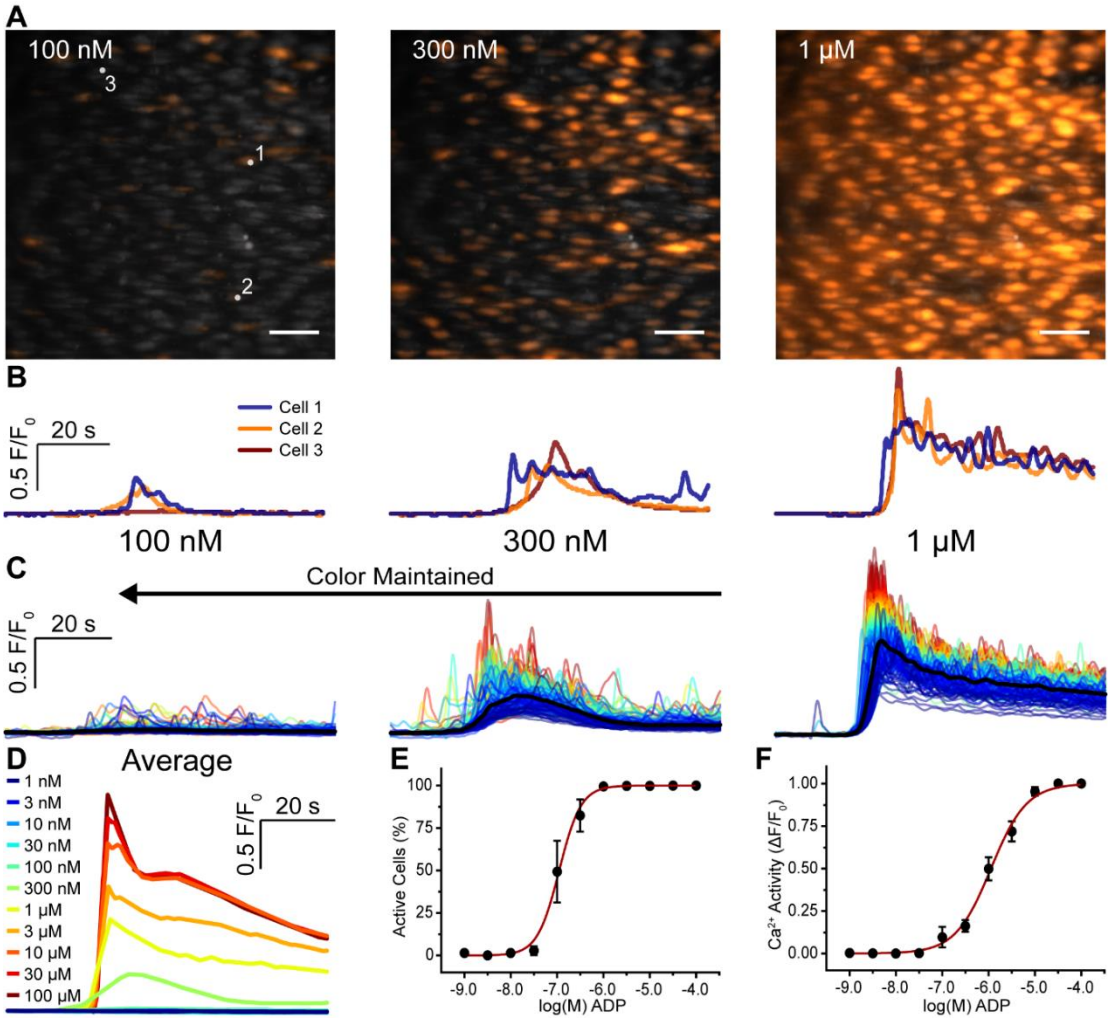

Figure 3.4 – Concentration-dependent ADP-induced Ca^{2+} signalling.

(A) Representative composite image of Ca^{2+} activity in *en face* second order mesenteric artery endothelium to increasing concentrations of ADP. (B) Ca^{2+} traces from individual cells indicated in (A). (C) Ca^{2+} signals from all individual cells in (A) Colours were assigned to the traces based on the amplitude of the initial response to ADP in each cell. Red indicated the highest amplitude and blue the lowest amplitude. Colours were assigned to the highest ADP concentration (far right) first and maintained across the previous concentrations. Thus allowing for direct comparison of the same cells between different ADP concentrations. (D) Average Ca^{2+} response (F/F_0) from all cells for each ADP concentration. (E) Percentage of all cells active at each concentration of ADP. (F) Average activity (F/F_0) of all cells for each concentration of ADP. Data are representative of n = 5 independent experiments from different artery preparations from different animals. Scale bars, 50 µm.

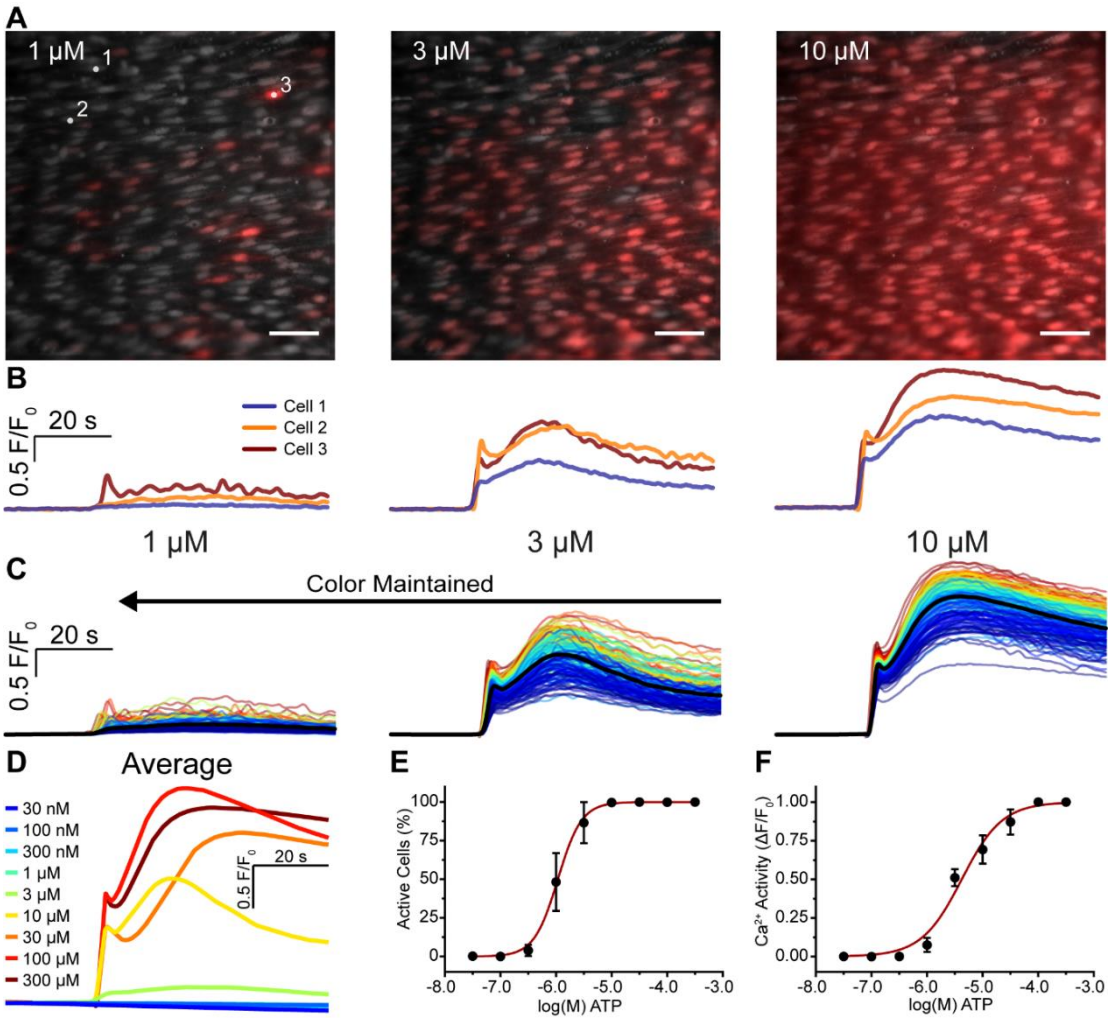

Figure 3.5 – Concentration-dependent ATP-induced Ca^{2+} signalling.

(A) Representative composite image of Ca^{2+} activity in *en face* second order mesenteric artery endothelium to increasing concentrations of ATP. (B) Ca^{2+} traces from individual cells indicated in (A). (C) Ca^{2+} signals from all individual cells in (A) Colours were assigned to the traces based on the amplitude of the initial response to ATP in each cell. Red indicated the highest amplitude and blue the lowest amplitude. Colours were assigned to the highest ATP concentration (far right) first and maintained across the previous concentrations. Thus allowing for direct comparison of the same cells between different ATP concentrations. (D) Average Ca^{2+} response (F/F_0) from all cells for each ATP concentration. (E) Percentage of all cells active at each concentration of ATP. (F) Average activity (F/F_0) of all cells for each concentration of ATP. Data are representative of n = 5 independent experiments from different artery preparations from different animals. Scale Bars, 50 µm

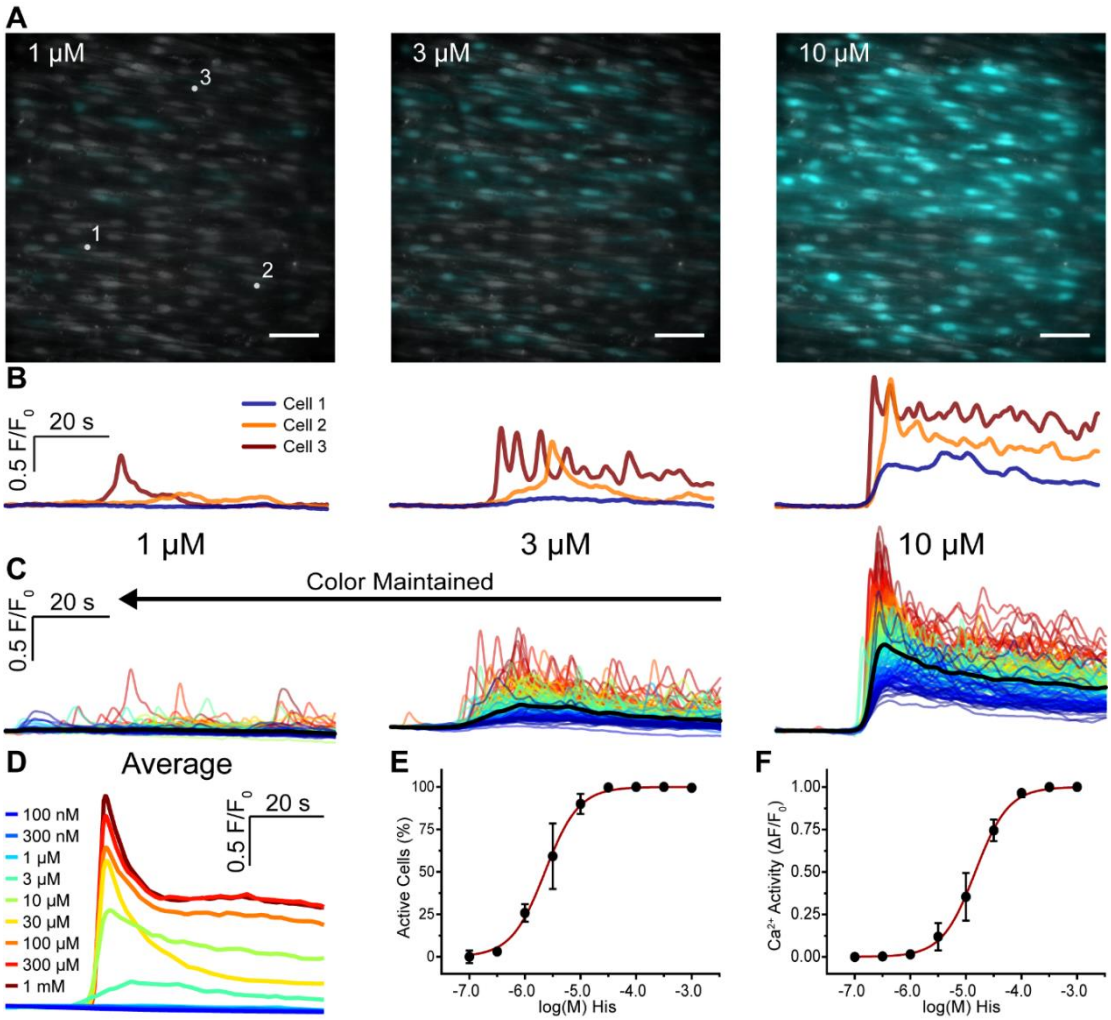

Figure 3.6 – Concentration-dependent histamine-induced Ca^{2+} signalling.

(A) Representative composite image of Ca^{2+} activity in *en face* second order mesenteric artery endothelium to increasing concentrations of histamine. (B) Ca^{2+} traces from individual cells indicated in (A). (C) Ca^{2+} signals from all individual cells in (A) Colours were assigned to the traces based on the amplitude of the initial response to histamine in each cell. Red indicated the highest amplitude and blue the lowest amplitude. Colours were assigned to the highest histamine concentration (far right) first and maintained across the previous concentrations. Thus allowing for direct comparison of the same cells between different histamine concentrations. (D) Average Ca^{2+} response (F/F_0) from all cells for each histamine concentration. (E) Percentage of all cells active at each concentration of histamine. (F) Average activity (F/F_0) of all cells for each concentration of histamine. Data are representative of n = 5 independent experiments from different artery preparations from different animals. Scale bars, 50 µm

ACh-induced Ca^{2+} signals were completely abolished by the selective M_3 receptor blocker 4-DAMP (1,1-dimethyl4-diphenylacetoxypiperidinium iodide). Therefore, endothelial response to ACh arises via M_3 receptor activation (Figure 3.7 A-C).

ATP-induced Ca^{2+} responses were inhibited by the P2Y2-selective antagonist AR-C118925XX, but unaffected by the selective P2Y1 antagonist, MRS2179 (Figure 3.7 A-C). Conversely, ADP-induced Ca^{2+} responses were unaffected by incubation with AR-C118925XX, but were abolished by MRS2179 (Figure 3.7 A-C). Taken together, these results show that ADP and ATP mediated Ca^{2+} signalling in mesenteric ECs occurs through two separate purinergic receptor subtypes – P2Y2 for ATP and P2Y1 for ADP.

Histamine induced Ca^{2+} signalling was abolished by the H_1 selective blocker, triprolidine, but unaffected by the H_2 selective blocker cimetidine. Therefore, histamine-induced Ca^{2+} signalling is evoked by activation of the H_1 receptor subtype (Figure 3.7 A-C).

Following G_q protein activation, the $G_q\alpha$ subunit (and also $G_q\beta\gamma$ subunit) activates PLC. This leads to the formation of intracellular IP_3. In support of a role of PLC in the Ca^{2+} increases, the PLC inhibitor, U73122 (2 μM), but not its inactive analogue, U73343 (2 μM), inhibited Ca^{2+} signals evoked by each of the four agonists (Figure 3.8 A-C).

Ca^{2+} release from the internal store may occur via IP_3 receptor (IP_3R) or ryanodine receptor (RyR) activation or both. To directly test the contribution of IP_3R or RyR activation on Ca^{2+} release from the internal store, during agonist stimulation, we examined the effects of the IP_3R antagonist, 2-aminoethoxydiphenyl borate (2-APB) and the selective RyR modulator, ryanodine. 2-APB abolished the Ca^{2+} response to all four agonists. Ryanodine had no significant effect on the Ca^{2+} signals (Figure 3.9 A-C). These results suggest that Ca^{2+} release in response to each of the agonists occurs via IP_3R.

To assess the involvement of Ca^{2+} release from the internal store the sarcoendoplasmic reticulum ATPase (SERCA) blocker, cyclopiazonic acid (CPA; 10 μM), was used to inhibit Ca^{2+} uptake from the cytosol to the endoplasmic reticulum. Depletion of the internal store by CPA significantly reduced the amplitude of the Ca^{2+} signal evoked by each agonist (Figure 3.10). Collectively these observations indicate that in mesenteric ECs, ACh, ADP, ATP and histamine-induced Ca^{2+} release from the internal store occurs via IP_3R activation and the endothelial response to each of the agonists is mediated by the G_q -PLC-IP_3R pathway.

In the absence of external Ca^{2+} (Ca^{2+}-free PSS that contained 1 mM EGTA), each of the four agonists produced an initial increase in intracellular Ca^{2+} that was comparable to the initial increase observed under normal conditions. However, the maintained response (observed with normal PSS) returned to baseline levels in the absence of extracellular Ca^{2+} (Figure 3.11 A-C). These observations suggest that the initial response to each agonist arises via Ca^{2+} release from internal stores, as described above, whilst the maintained response is due to Ca^{2+} influx across the plasma membrane. Although other signalling molecules (such as DAG and IP_4) play an important role in the regulation of Ca^{2+} activity within the cell, the pathway examined here is the primary mechanism for muscarinic, purinergic and histaminergic control of intracellular Ca^{2+}.

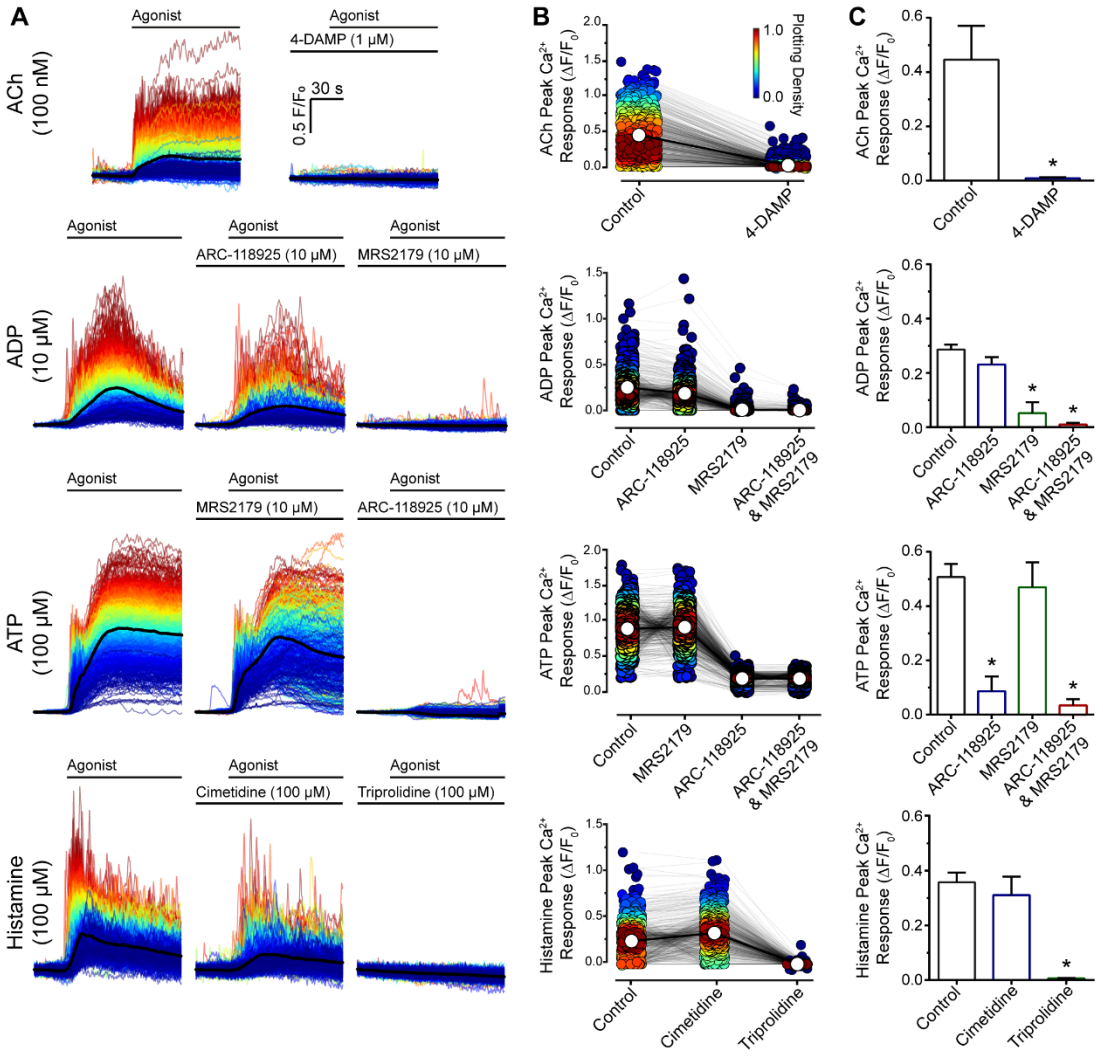

Figure 3.7 – Receptor subtypes involved in muscarinic, purinergic and histaminergic Ca^{2+} signalling in the mesenteric artery.

(A) Ca^{2+} signals from all individual cells (~1000 cells), before (left) and after incubation (5 min) with the indicated antagonist. All traces from individual cells are overlaid and coloured based on the amplitude of the initial peak (highest amplitude in red, through to lowest in blue) and the black line represents the average. (B) Paired peak Ca^{2+} response ($\Delta F/F_0$) from individual cells before and after indicated treatment. Each circle represents an individual cell and these are matched for each treatment (grey lines) from a single experiment. The average response is marked by white circles and matched across treatments by a solid black line. The plotting density colour coding indicates the distribution of peak $\Delta F/F_0$ values. Red indicates a higher frequency of occurrence of a particular peak $\Delta F/F_0$ value, and blue indicates a low frequency of occurrence of a peak $\Delta F/F_0$ value. (C) Summary data illustrating average peak response to ACh, ADP, ATP and histamine in control (black) and after incubation with the indicated antagonist. Data are representative of n = 5 independent experiments, from artery preparations, from different animals; *P < 0.05, either paired student t test or One-way ANOVA followed by Dunnett's multiple comparisons test.

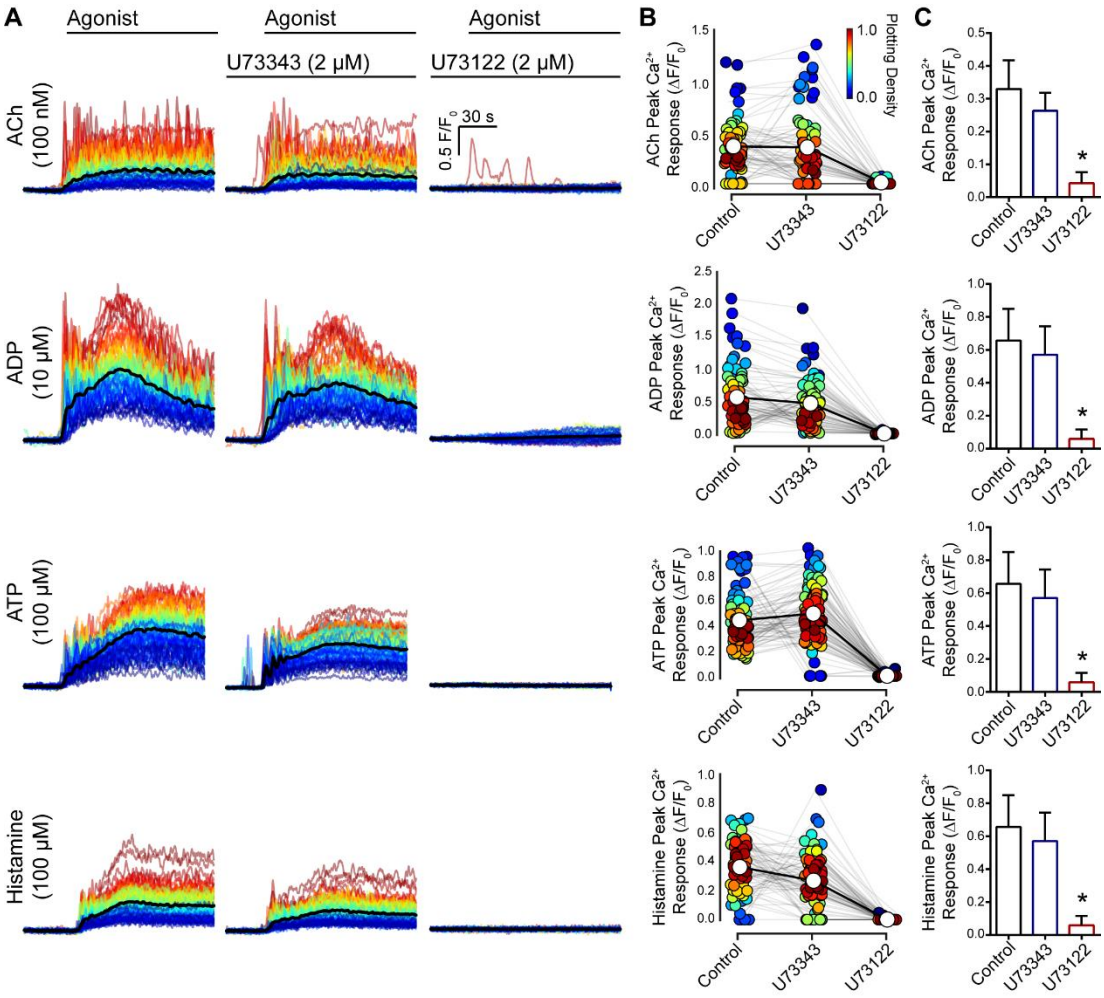

Figure 3.8 – PLC regulation of muscarinic, purinergic and histaminergic Ca^{2+} responses.

(A) Ca^{2+} signals from all individual cells (~100 cells), before (left) and after incubation with the Phospholipase C (PLC) inactive analogue, U73343 (middle; 2 µM, 10 min) and the active form, U73122 (right; 2 µM, 10 min). All traces from individual cells are overlaid and coloured based on amplitude of initial peak (highest amplitude in red, through to lowest in blue) and the black line represents the average. (B) Paired peak Ca^{2+} response ($\Delta F/F_0$) from individual cells before and after treatment with U73343 and U73122. Each circle represents an individual cell and these are matched for each treatment (grey lines) from a single experiment. The average response is marked by white circles and matched across treatments by a solid black line. The plotting density colour coding indicates the distribution of peak $\Delta F/F_0$ values. Red indicates a higher frequency of occurrence of a particular peak $\Delta F/F_0$ value, and blue indicates a low frequency of occurrence of a peak $\Delta F/F_0$ value. (C) Summary data illustrating average peak response to ACh, ADP, ATP and histamine in control (black) and after incubation with U73343 and U73122 (red). Data are representative of n = 5 independent experiments, from artery preparations, from different animals; *P < 0.05, One-way ANOVA followed by Tukey's multiple comparisons test.

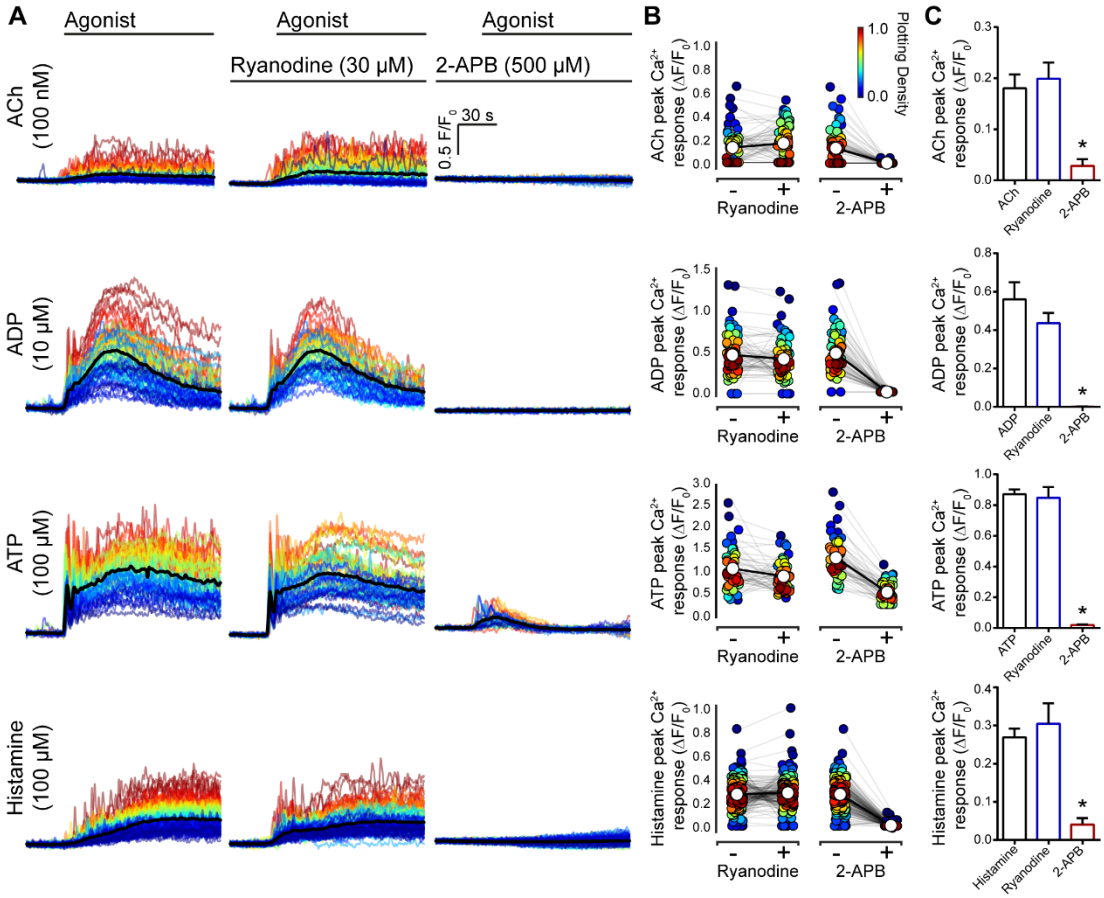

Figure 3.9 – IP_3 controls muscarinic, purinergic and histaminergic-mediated Ca^{2+} release from mesenteric endothelial cells.

(A) Ca^{2+} signals from all individual cells (~100 cells), before (left) and after incubation with the ryanodine receptor blocker, ryanodine (middle; 30 µM, 20 min) and the IP_3 receptor antagonist 2-aminoethoxydiphenyl borate (2-APB; right; 500 µM, 20 min). All traces from individual cells are overlaid and coloured based on amplitude of initial peak (highest amplitude in red, through to lowest in blue) and the black line represents the average. (B) Paired peak Ca^{2+} response ($\Delta F/F_0$) from individual cells before and after treatment with ryanodine (left) and 2-APB (right). Each circle represents an individual cell and these are matched for each treatment (grey lines) from a single experiment. The average response is marked by white circles and matched across treatments by a solid black line. The plotting density colour coding indicates the distribution of peak $\Delta F/F_0$ values. Red indicates a higher frequency of occurrence of a particular peak $\Delta F/F_0$ value, and blue indicates a low frequency of occurrence of a peak $\Delta F/F_0$ value. (C) Summary data illustrating average peak response to ACh, ADP, ATP and histamine in control (black) and after incubation with ryanodine (blue) and 2-APB (red). Data are representative of n = 5 independent experiments, from artery preparations, from different animals; *P < 0.05, One-way ANOVA followed by Dunnett's multiple comparisons test.

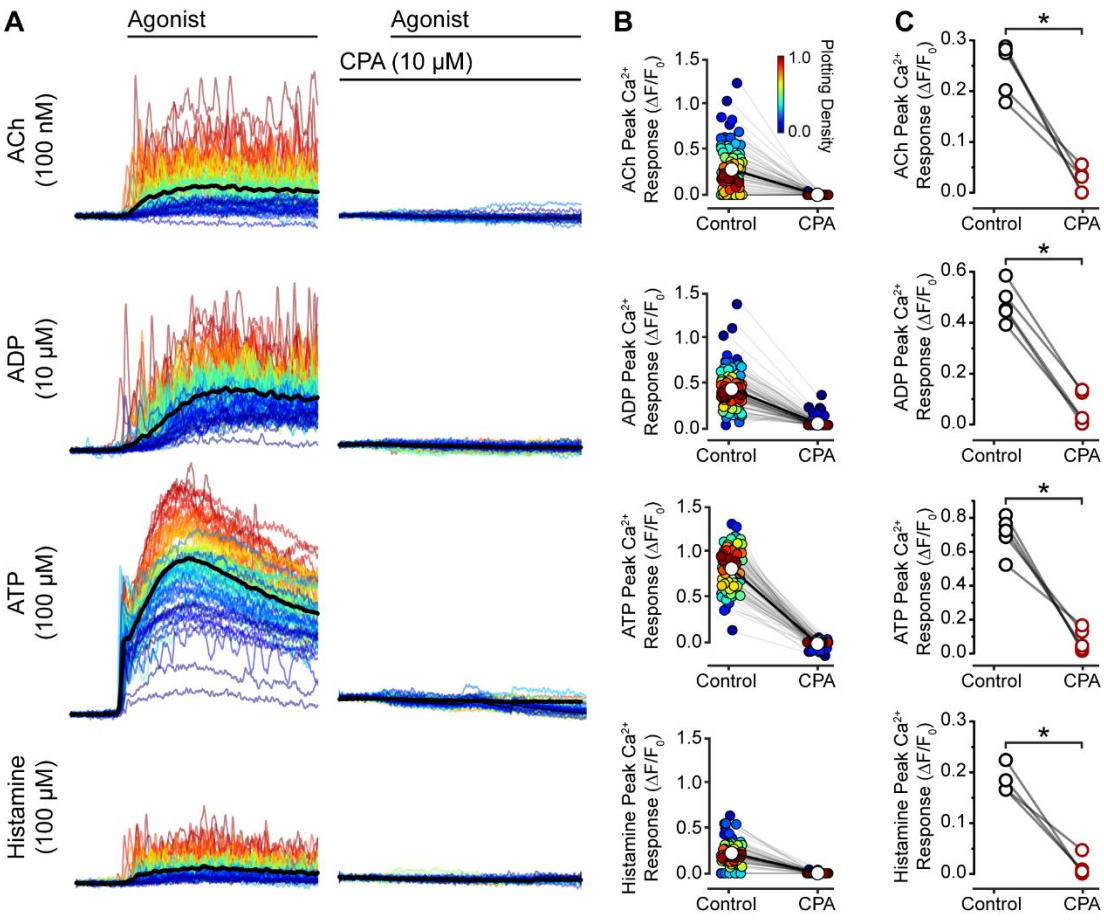

Figure 3.10 – Effect of internal store depletion on muscarinic, purinergic and histaminergic Ca^{2+} signalling.

(A) Ca^{2+} signals from all individual cells (~100 cells), before (left) and after (right) incubation with cyclopiazonic acid (CPA; 10 µM, 5 min). All traces from individual cells are overlaid and coloured based on amplitude of initial peak (highest amplitude in red, through to lowest in blue) and the black line represents the average. (B) Paired peak Ca^{2+} response ($\Delta F/F_0$) from individual cells before and after treatment with CPA. Each circle represents an individual cell and these are matched for each treatment (grey lines) from a single experiment. The average response is marked by white circles and matched across treatments by a solid black line. The plotting density colour coding indicates the distribution of peak $\Delta F/F_0$ values. Red indicates a higher frequency of occurrence of a particular peak $\Delta F/F_0$ value, and blue indicates a low frequency of occurrence of a peak $\Delta F/F_0$ value. (C) Summary data illustrating average peak response to ACh, ADP, ATP and histamine in control (black) and after incubation in CPA (red). Data are representative of n = 5 independent experiments, from artery preparations, from different animals; *P < 0.05, paired Student t test.

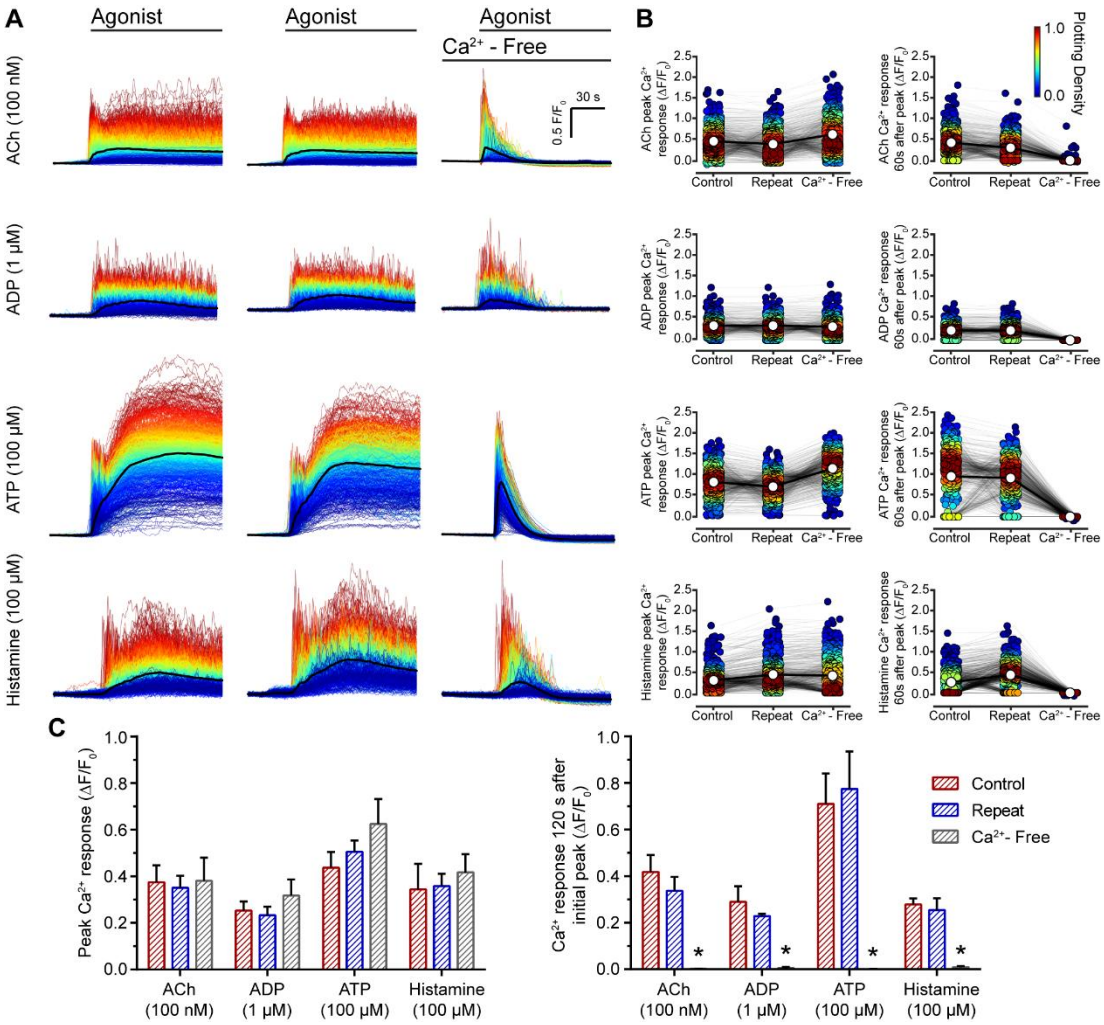

Figure 3.11 – Effect of Ca^{2+} influx on muscarinic, purinergic and histaminergic Ca^{2+} signalling.

(A) Ca^{2+} signals from all individual cells (~1000 cells), including 30 s of baseline and 120 s of activation. All traces from individual cells are overlaid and coloured based on amplitude of initial peak (highest amplitude in red, through to lowest in blue) and the black line represents the average. Agonist and concentration are shown on the left of each trace and time of activation is shown above. (B) Paired peak (left) Ca^{2+} response ($\Delta F/F_0$) and steady state (right) Ca^{2+} response ($\Delta F/F_0$; measured at 60 s after the initial peak) from individual cells. Each circle represents an individual cell and these are matched for each treatment (grey lines) from a single experiment. The average response is marked by white circles and matched across treatments by a solid black line. The plotting density colour coding indicates the distribution of peak $\Delta F/F_0$ values. Red indicates a higher frequency of occurrence of a particular peak $\Delta F/F_0$ value, and blue indicates a low frequency of occurrence of a peak $\Delta F/F_0$ value. (C) Summary data illustrating average peak and steady-state responses to ACh, ADP, ATP and histamine in control (red), repeat (blue) and after removal of external Ca^{2+} (grey). Data are representative of n = 5 independent experiments, from artery preparations, from different animals; *P < 0.05, One-way ANOVA followed by Dunnett's multiple comparisons test.

3.4 Discussion

A major challenge faced by the endothelium is the need to process an enormous quantity of information held in the complex chemical environment to which the vascular system is exposed. From this information decisions on physiological outputs are made. The endothelium uses a multitude of receptors to continuously monitor vanishingly small changes in the concentration of extracellular signals that each provides cues to the ever-changing physiological state (Civciristov and Halls, 2019). Extracellular signals must be accurately detected and correctly relayed via intracellular Ca^{2+} signals so that information is not lost. Precisely how the endothelium processes the entire chemical composition to which it is exposed and transduces multiple extracellular signals, to specific cell activities is not understood. Here how muscarinic, purinergic and histaminergic signalling occurs in the intact mesenteric endothelium has been investigated. The results show that each agonist evokes Ca^{2+} signals that are concentration-dependent but not homogenous across the endothelium. Ca^{2+} signals begin in individual endothelial cells that propagate to neighbouring cells. This increase in endothelial Ca^{2+} is mediated by activation of GPCRs to generate IP_3 leading to Ca^{2+} release from the internal store by IP_3R activation.

In this study, the Ca^{2+} responses to muscarinic, purinergic and histaminergic activators in large numbers of endothelial cells in intact blood vessel were analysed. Each agonist evoked concentration-dependent increases in endothelial Ca^{2+}. Low concentrations of each agonist evoked rapid localised increases in Ca^{2+} that led to Ca^{2+} propagation across the whole-cell. The concentration-dependence of the endothelium to each agonist was not uniform across the entire endothelium. Instead, low concentrations of agonist activated small, spatially distinct regions of endothelial cells with some cells being highly responsive, while other cells responded weakly or not at all. Higher concentration recruited additional cells. Furthermore, each agonist evoked a concentration-dependent response in each individual endothelial cell. Thus, increasing concentration of agonist recruited an increasing number of cells and an

increasing amplitude of Ca^{2+} signal in each activated cell. This configuration may act to increase the dynamic range and sensitivity of endothelium to each activator. Different cells respond to various changes in concentration. This ensures the entire system does not become saturated at low concentrations of agonist (and can detect changes at higher concentrations) while ensuring small changes at low concentrations are detected. Intriguingly, all cells were active before a maximal Ca^{2+} response was achieved, as expected from a population of cells with various sensitivities i.e. the Ca^{2+} activity within each cell continued to rise with increasing agonist concentration. Collectively, these results demonstrate that the concentration dependence of the response of individual cells increased the overall sensitivity of the endothelium.

Increasing the concentration of agonist caused the additional recruitment of endothelial cells, to generate a Ca^{2+} response. This recruitment may occur due to the propagation of a Ca^{2+} wave from one cell to another via gap junction or the effects of the agonist directly activating neighbouring cells (Kameritsch et al., 2012; Kansui et al., 2008). Although gap junction blockers are available to study this mechanism our previous study has shown that these blockers may have off-target effects that alter the Ca^{2+} response independently of an effect on gap junctions (Wilson et al., 2016a). Therefore, further study is required to determine the role of gap junctions in mediating the propagation of Ca^{2+} signals. The propagation of Ca^{2+} waves may be fundamental in coordinating various vascular responses. Previous studies have shown that localised application of ACh causes upstream dilation via Ca^{2+} signal propagation (Bagher et al., 2011; Socha et al., 2012).

In line with the work of Kameritsch et al., our results show heterogenous endothelial Ca^{2+} signalling in response to agonist stimulation (Kameritsch et al., 2012). In contrast to these results, others have reported homogenous Ca^{2+} responses to agonist activation (Berra-Romani et al., 2004; Boittin et al., 2013). This discrepancy may be due to differences in concentrations used to stimulate endothelial cells as our results also show that a high concentration of agonist elicits a response in all endothelial

cells. A heterogeneous distribution of receptors and other surface molecules has been described in cultured EC by several studies (Hong et al., 2006; Kirchhofer et al., 1994; Ko et al., 2009) While one might argue that, in cell culture, proliferation and different cell cycle phases may contribute to such an inhomogeneous distribution or expression, our results confirm that such inhomogeneities also occur in intact tissue (Kameritsch et al., 2012). Heterogeneities between ECs seem not to be restricted to receptor expression. The distribution of the endothelial markers vWf and CD34 in the human pulmonary capillary endothelium have also been shown (Müller et al., 2002). In these vessels, different subpopulations of EC expressed CD34 or vWf and only a limited fraction of cells co-expressed both markers. However, the underlying mechanisms giving rise to variations in protein expression between neighbouring cells is not yet fully understood (Aird, 2007).

ACh-induced vasodilation is used extensively to determine endothelial functionality. However, the physiological role of muscarinic receptors on the endothelium has remained elusive. We have previously shown that flow-evoked endothelial dependent vasodilation is dependent on ACh-induced Ca^{2+} signals evoked by muscarinic receptor activation (Wilson et al., 2016a). However, the expression of all five subtypes of muscarinic receptor has been shown across various vascular beds (Gericke et al., 2011, 2014; Radu et al., 2017). mRNA expression analysis has shown that the M_3 receptor subtype is the prevailing muscarinic subtype expressed in the vascular endothelium (Gericke et al., 2014; Radu et al., 2017). Our results show that ACh evoked Ca^{2+} signals in the intact mesenteric endothelium occurs by activation of the M_3 receptor subtype.

The expression and physiological role of purinergic receptor subtypes in the vasculature is incompletely characterised. Studies to identify purinergic receptor expression on the endothelium are made more complex as both metabotropic P2Y receptors and ionotropic P2X receptors are expressed (Ray et al., 2002). Currently, there is a lack of specific antagonists for the majority of P2 receptors with many blockers exerting significant off target effects (Burnstock, 2017). In this study we used

two antagonists that have been shown to selectively block $P2Y_1$ and $P2Y_2$ receptors (Burnstock, 2017; Liu et al., 2015; Muoboghare et al., 2019). The results suggest that the endogenous purinergic ligands ADP and ATP induce an increase in endothelial Ca^{2+} by activation of completely separate P2Y receptor subtypes. The highly selective $P2Y_1$ antagonist MRS2179, inhibited ADP-induced Ca^{2+} responses whereas the selective $P2Y_2$ blocker AR-C118925XX had no effect on ADP-induced Ca^{2+} activity. Conversely, MRS 2179 did not reduce ATP evoked Ca^{2+} responses but the Ca^{2+} response was inhibited by blocking of the $P2Y_2$ receptor with AR-C118925XX. Significantly, removal of external Ca^{2+} had no effect on the initial increase in Ca^{2+} evoked by either ADP or ATP suggesting that endothelial P2X receptor activation by ADP or ATP was not a significant contributor to the response as blocking Ca^{2+} influx across the plasma did not alter the initial peak. Interestingly, it has been reported that $P2X_4$ receptor knockout mice have increased blood pressure (Craigie et al., 2018; Stokes Leanne et al., 2011; Yamamoto et al., 2006). However, this may be due to the expression of $P2X_4$ on vascular SMC rather than ECs. Collectively, these results suggest that the endogenous purinergic ligands ATP and ADP may increase endothelial cell Ca^{2+} by utilising separate P2Y receptor subtypes. However, further study is required to determine the exact physiological role of both P2Y and P2X receptors in the vasculature.

Histaminergic receptor activation may evoke an increase in endothelial permeability and vasodilation (Kawai and Ohhashi, 1995; Satoh and Inui, 1984; Tiruppathi et al., 2002; van Nieuw Amerongen et al., 1998). Histamine exerts its effects by binding to its four receptors, H_1, H_2, H_3, and H_4, on target cells in various tissues (Otani et al., 2016). Previous studies have shown that in cultured endothelial cells H_1 and H_2 receptors are predominantly expressed (Hekimian et al., 1992; Heltianu et al., 1982; Kameritsch et al., 2012; Lu et al., 2010; Otani et al., 2016). However, studies examining histamine evoked endothelial Ca^{2+} responses in intact tissue have rarely been carried out (Huang et al., 2000; Ying Xiaoyou et al., 1996). Our study is the first to report histamine-induced Ca^{2+} responses in the endothelium of intact mesenteric arteries. We found that Ca^{2+} signals evoked by histamine occur by activation of the

H_1 receptor as the H_1 blocker triprolidine abolished the histamine-induced Ca^{2+} response while the selective H_2 blocker cimetidine had no effect.

The Ca^{2+} response evoked by each of the agonists, irrespective of the receptor subtype, was dependent on Ca^{2+} influx across the plasma membrane. Removal of external Ca^{2+} did not alter the initial increase in intracellular Ca^{2+}. However, after this initial rise the intracellular Ca^{2+} concentration rapidly decreased to basal levels. Collectively, these results suggest that Ca^{2+} influx across the plasma membrane is required to maintain muscarinic, purinergic and histaminergic Ca^{2+} responses in the endothelium but is not responsible for the initial increase. However, Ca^{2+} influx may have a pivotal role in controlling vascular tone as Ca^{2+} influx through TRPV4 channels have been reported to cause maximal dilation of resistance arteries (Sonkusare et al., 2012).

This study demonstrates that the initial increase in Ca^{2+} evoked by ACh, ADP, ATP and histamine in the intact endothelium occurs by Ca^{2+} release from the internal store. Although the drugs used to determine the role of Ca^{2+} release from the internal store have off target effects, our conclusion was supported by several interventions (Bootman et al., 2002; Klein et al., 2011). GPCR binding caused the activation of PLC to generate IP_3. The PLC inhibitor, U73122, completely abolished the Ca^{2+} response evoked by the different agonists by blocking the action of the enzyme in generating IP_3 from PIP_2. Blocking the action of IP_3 on IP_3Rs with 2-APB also completely abolished the Ca^{2+} response as did depletion of the internal store with CPA. Thus, in order for each agonist to evoke a Ca^{2+} response in the endothelium, activation of the GPCR/PLC/IP_3R signalling cascade is required.

The results described in this chapter may have important consequences on studies examining endothelial cell responses. Here we have shown that each cell, that is presumably exposed to the same microenvironment, does not respond uniformly to an activator. Therefore, analysis of the response of only one cell from a population may hide properties of the system that are present when the entire population is examined. For example, a single cell may not respond to histamine (or only at high

concentrations) but is activated by low concentrations of ACh. However, examination of a separate cell from the same population may show the reverse. As a collective, the endothelium has properties that exceed the capabilities of single cells. This feature is not unique to the endothelium. Biological systems are recognised increasingly as having properties that are distinct from the individual components of the system (Kesić, 2016; Regenmortel, 2004). New distinct features often arise from interactions and give rise to behaviours that are absent when cells are examined in isolation (McCarron et al., 2019).

The repertoire of functional GPCRs in the endothelium are incompletely characterised. The variation of receptor expression between vascular beds has made characterisation even more complex. In the present study we show that muscarinic, purinergic and histaminergic receptor activation causes an increase in endothelial Ca^{2+}. This increase in Ca^{2+} is dependent on the concentration of agonist. At low agonist concentrations, Ca^{2+} responses occur in spatially distinct cells. Additionally, we characterise the mechanisms involved in generating a Ca^{2+} response to ACh, ADP, ATP and histamine. Interestingly, each activator elicits its response by the same mechanisms. Although this may be expected, it could lead to complications in the detection and relaying of the information stored in each activator if more than one is present at any time, which would presumably occur *in vivo*.

Chapter 4. Ca^{2+} Signalling Network in the Vascular Endothelium

4.1 Introduction

Vascular heterogeneity is normally described as terms of variations in the structure of the endothelium between different vessel types or different organs. For example, endothelial cells align in the direction of blood flow at straight artery segments but not at branch points (Poduri et al., 2017). There are also variations in endothelial structure between artery beds whereby, the endothelium can be non-fenestrated (cerebral circulation), fenestrated (small intestine, endocrine glands) or discontinuous (liver, spleen) (Chapter 1). These structural variations arise due to differences in the microenvironment (chemical or shear stress) to which the endothelium is exposed and permit the endothelium to control the extent of fluid exchange in tissues. However, the structure of endothelial cells is not irreversibly fixed and can adjust if the microenvironment alters. When canine arterial segments were excised and reimplanted, at 90° rotation, endothelial cells realigned to the direction of blood flow (Flaherty et al., 1972). Furthermore, when endothelial cells from different regions are isolated and grown in tissue culture, they become uncoupled from extracellular cues, that they would experience *in* vivo and undergo a phenotypic drift (Aird, 2007; Durr et al., 2004). Therefore, feedback from the extracellular environment is vital in controlling the structural heterogeneity observed in the endothelium. While structural heterogeneity is widely accepted to occur, understanding of functional heterogeneity in the endothelium is poorly developed.

Indeed, most studies on sensing and activation, treat the endothelium as lacking functional heterogeneity and as a homogeneous population of cells that respond uniformly to each activator. This belief is probably derived from the nature of the experimental approach (e.g. organ bath pharmacology) and the assumption that biological systems maximize the tissues ability to respond to perturbations through the coordinated uniform responses in populations of cells.

Notwithstanding the view that endothelial cells within a region of a blood vessel are largely identical, different endothelial cell phenotypes occur within neighbouring regions of the same blood vessels - even between neighbouring endothelial cells.

These cells are presumably exposed to an identical extracellular environment, so the stimuli for protein expression must be similar (Aird, 2005). This local variation in phenotype is largely unexplained (Yuan et al., 2016). For example, a mosaic pattern of microdomains of von Willebrand factor-positive and -negative endothelial cells occurs in the capillaries of many vascular beds and in the aorta (Aird, 2005; Tomlinson et al., 1991). There is also heterogeneity in the distribution of angiotensin II immunostaining in neighbouring endothelial cells of the femoral artery (Tomlinson et al., 1991). Acetylcholine (ACh)-evoked Ca^{2+} responses are larger at branches in the rat thoracic aorta than at nearby non-branch regions. The reverse was true for histamine (Huang et al., 2000). The sensitivity to histamine and ACh was not distributed evenly among neighbouring cells but arranged in 'belts' of high sensitivity that varied by ∼100-fold along the flow lines. In studies of murine thoracic aorta endothelial cells, while most cells (82%) responded to ATP, large fractions of cells did not respond to ACh, bradykinin, or substance P (Marie and Bény, 2002). Our previous studies have also shown that the distribution of receptors is not uniform across the endothelium. Instead, muscarinic and purinergic receptors were distributed in different cells in the endothelium of the carotid artery (Lee et al., 2018). Together these studies suggest that neighbouring regions of the endothelium appear to be specialised to detect particular chemical activators.

Recent advances in single cell analysis has also revealed heterogeneity in gene expression (Kalluri et al., 2019; Vanlandewijck et al., 2018). These variations have been shown to occur between different blood vessels, artery beds and perhaps most interestingly even between neighbouring endothelial cells (Chi et al., 2003). However, the underlying reason and mechanisms giving rise to localised heterogeneity remains unclear. The physiological role of cells that are just a few microns apart, and that are presumably exposed to virtually identical microenvironments, being endowed with different functions as determined by protein expression remains unresolved.

The endothelium is constantly bombarded by tens of different, simultaneously arriving extracellular activators, that each provides cues to the physiological state.

The endothelium must manage its response to each of these extracellular signals to maintain cardiovascular homeostasis. This requires selective detection, processing, and ultimately, integration of each of the separate inputs. We propose below that endothelial heterogeneity provides the endothelium with an ability to solve complex sensory problems and process multiple simultaneously arriving signals in parallel. We show that the endothelium is organized into spatially structured clusters of agonist-sensitive cells and there is minimal overlap in agonist sensitivity between clusters. This arrangement allows the endothelium to selectively detect specific activators and due to the limited overlap of agonist specific sensing cells, multiple activators can be processed at the same time.

To control vascular homeostasis, the endothelium must ensure that the information held in each extracellular stimulus is accurately relayed within the cell, in order to generate the correct response. Individual endothelial cells are thought to respond and relay the information held in a wide range of distinct inputs by changes in amplitudes, duration, and oscillation frequency of the Ca^{2+} signal (Chapter 1). However, how a large population of intact endothelial cells sense multiple stimuli, that each activate the same pathway to converge on intracellular Ca^{2+} signalling, is not fully understood. Here we propose an additional feature that allows the endothelium to generate stimulus-specific responses via Ca^{2+} signalling. Separate clusters of cells selectively and separately detect different activators. This spatial segregation of detection may allow the endothelium to simultaneously and sensitively process various elements of the chemical environment in parallel.

In this chapter to assess and quantify the extent of heterogeneity and clustering of endothelial cells, a system wiring diagram is used. The system wiring diagram graphically depicts how components of a system are physically and logically connected to identify relationships in a network. The mathematical foundation of the system wiring diagram is graph theory. A graph in this context is not a diagram of x versus y but a collection of elements (nodes), which may be connected structurally or functionally with each other via ‘edges’. Thus, a graph of a multicellular Ca^{2+}

signalling network may be depicted as signalling links (edges or components; e.g. gap junctions) between interacting cells (nodes). The number of edges associated with each node is a property called node degree and the degree distribution is used to quantify the diversity of the entire network. Using these graphs, the topology or architecture of the network may be characterised to determine various measures of connectivity. Here, the number of components (isolated responding cells and responding clusters), the total number of isolated cells and clusters of cells, the total number of clusters, the number of cells per cluster, the mean degree, the average number of active neighbours for each agonist-sensitive cell is determined.

4.2 Methods

4.2.1 Endothelial Ca^{2+} Signal Analysis

Endothelial Ca^{2+} signalling was imaged as described in Chapter 2. Endothelial viability was assessed by application of maximum concentration of ACh (100 nM) at the start of each experiment to ensure a Ca^{2+} response could be evoked in every cell. To investigate the spatial distribution of agonist-sensitive endothelial cells, low concentrations (EC_{25}, from full concentration response data, in Chapter 3, showing the 'percentage of active cells') of multiple agonists (ACh, ADP, ATP, and histamine) were sequentially applied to the same endothelial preparation. During each of these experiments, agonist-evoked Ca^{2+} activity in a single field of endothelial cells was recorded.

4.2.2 Cell Clustering and Neighbour Analysis

To quantitatively study endothelial cell connectivity, we constructed theoretical representations of the endothelial network using graph theory in Python 2.7. To do this, we first placed cell markers (lines) along the length of each individual endothelial cell using the ROI manager in FIJI (Figure 4.1 A). We then used the "dilate no merge" plugin in FIJI to dilate each of these lines simultaneously until it touched another (dilating) line or the perimeter of the field-of-view (Randell et al., 2017). In this way, we were able to generate accurate ROIs for each cell in the field-of-view (Figure 4.1 B). Cells at the boundary of the field-of-view have unknown connectivity therefore we excluded these cells from any analysis. To do this, we created a set of coordinates containing the centre point of each line (through the cell) and calculated the corresponding concave hull (alpha shape) (Moreira and Santos, 2019). The concave hull is the envelope that encompasses all ROIs (Figure 4.1 B). Any ROIs with a vertex that extended beyond this envelope was considered to be a cell at the boundary of the field-of-view (boundary cell) (Figure 4.1 B).

Cellular ROIs were used to determine connectivity between endothelial cells. To achieve this, the minimum distance between each ROI and every other ROI was

measured. Cell pairs with a separation of zero were classified as neighbours. We represented these structural networks as graphs using the NetworkX library in Python 2.7 (Hagberg et al., 2008). The graphs allowed Ca^{2+} responses from individual cells to be compared with the Ca^{2+} response evoked in neighbouring endothelial cells. Boundary cells were excluded from the analysis as they lacked a full complement of neighbours.

4.2.3 Assessment of Clustering of Agonist Specific Sensing Cells

To determine the degree, if any, of clustering of agonist-sensitive endothelial cells we created graphs of responding cells for each agonist. To create these graphs, we identified the 25% most sensitive cells and excluded all other cells. We then computed the following standard graph theoretic measures to assess cell clustering: number of components, the total number of isolated cells and clusters of cells; the total number of clusters; the number of cells per cluster and the mean degree, the average number of active neighbours for each agonist-sensitive cell.

To determine whether the extent of endothelial clustering of agonist specific sensing cells was greater (or less) than would be expected if agonist specific sensing cells were randomly positioned throughout the endothelium, we used a permutation analysis (Fitzmaurice et al., 2007; Pesarin, 2016). The permutation analysis is a statistical test in which the distribution of the measured data is compared to random rearrangements of the measured data. First, the EC_{25} agonist-evoked Ca^{2+} response data was used to generate a random distribution of cell activity. The Ca^{2+} response from each active cell was randomly assigned to any other cell (excluding boundary cells) to generate a new graph of active cells. Once a cell was assigned a Ca^{2+} response, in the random model, it was removed from the list of cells to which a Ca^{2+} response could be allocated. This ensured an equivalent number of active cells were present in the random model as the EC_{25} agonist evoked Ca^{2+} response data. Cell clustering was then calculated as described above (number of components, number of clusters, number of cells per cluster and mean degree). This process was repeated

1000 times for each dataset and the mean number of components, number of clusters, number of cells per cluster and mean degree then calculated.

4.2.4 Statistics

Summarised data are presented as means ± SEM values; n is the number independent experimental replicates (number of animals). For statistical comparison of two groups, a two-tailed Student's t test (paired data) was performed. Two-tailed one-way ANOVA with Tukey's multiple comparisons test, as appropriate, was used for statistical comparison of three or more groups. All statistical analyses were performed using GraphPad Prism, version 6.0 (GraphPad Software). $P < 0.05$ was considered statistically significant.

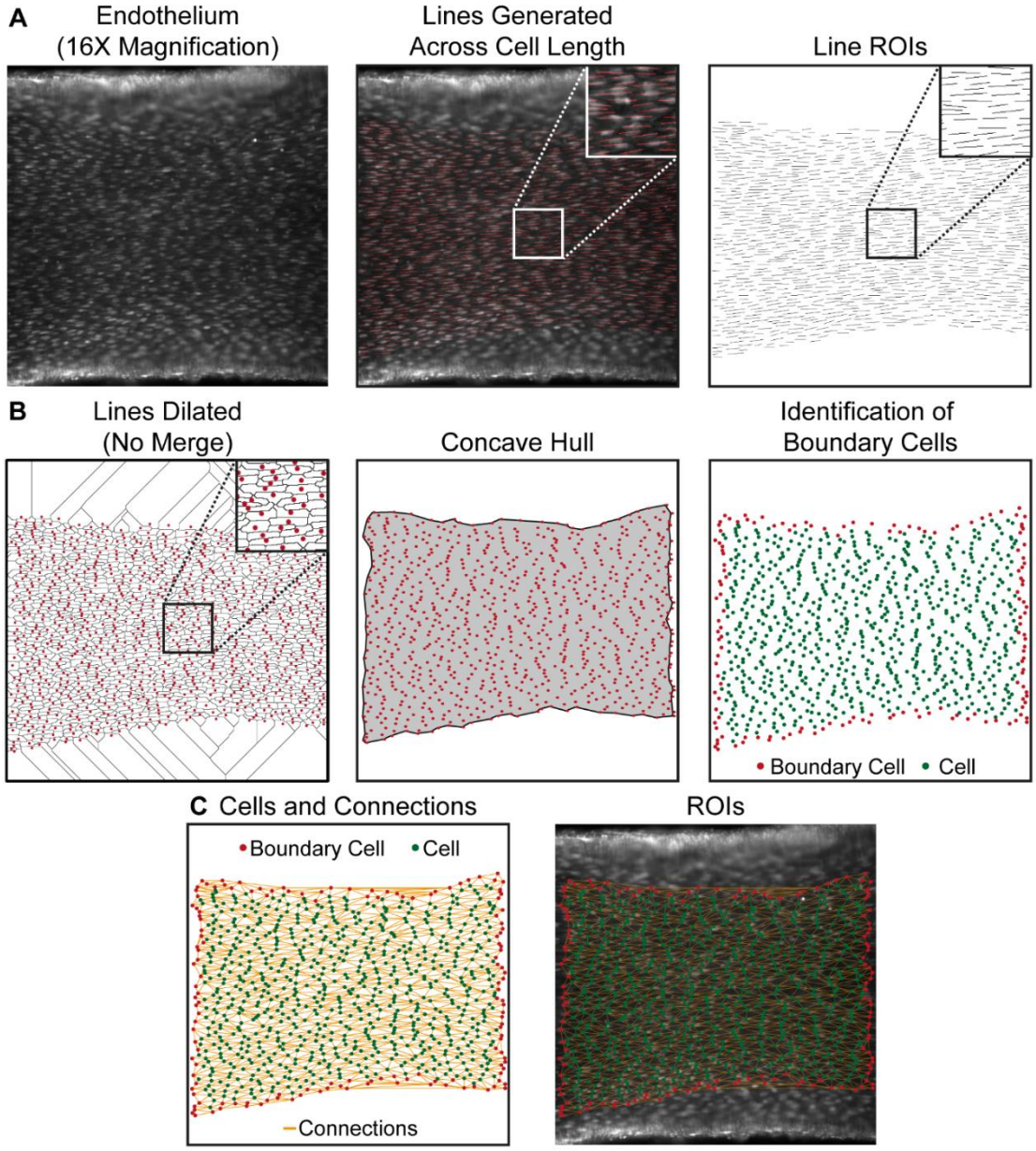

Figure 4.1 – Reconstructing endothelial network connectivity from Ca^{2+} imaging recordings.

(A) Representative Ca^{2+} image (left), showing ~1000 endothelial cells, of an *en face* second-order mesenteric artery. Line ROIs drawn along the length of each individual cell (middle and right) used to create cell outlines. (B) Cellular ROIs (left) generated using the "dilate no merge" plugin in FIJI. (Middle panel) A concave hull was applied to determine the boundary of the preparation, encompassing all cells. The concave hull was used to identify cells at the boundary of the network (or field-of-view; right). (C) Reconstructed endothelial network (left) overlaid on Ca^{2+} image (right) showing cell locations (green/red dots) and connections between neighbouring endothelial cells (orange dots). Scale bars, 50 µm.

4.3 Results

4.3.1 Clustering of Agonist-Selective Endothelial Cells

Critical to an understanding of endothelial function, is a determination of how the endothelium senses and processes information held in the multitude of activators that act on the endothelium. To investigate how the endothelium detects multiple stimuli, we examined the patterns of endothelial Ca^{2+} activity evoked by four distinct agonists (ACh, ADP, ATP and histamine). To achieve this, we identified each endothelial cell in large fields of native endothelia, and constructed graph theoretical representations of the underlying structural network. In these graphs (Figure 4.2 A-B), each endothelial cell is represented by a node and connections between neighbouring endothelial cells are represented by edges (lines connecting nodes). Endothelial cells formed a regular lattice network, with each cell in contact with an average of six neighbours (Figure 4.2 E).

We examined the spatial distribution of endothelial cell sensitivity by activating the endothelium with low concentrations of each of the four agonists. To do this, we applied each agonist at an EC_{25} (determined from full concentration-response studies, Chapter 2). Activation of 25% of cells with the EC_{25} was not always achieved due to variations in the sensitivity between preparations. Occasionally, the EC_{25} failed to activate 25% of cells. When fewer than 25% of cells responded, the concentration was increased to ensure that at least 25% of cells responded. When more than 25% of cells responded (which was only apparent in later analysis) the analysis was restricted to the first 25% of cells to respond (Figure 4.2 C and D). Additionally, cells at the boundary of the field-of-view were not included in the analysis to ensure only cells with a full complement of neighbours were considered (Figure 4.2 D).

We first sought to determine if the cells activated by the EC_{25} of each agonist were reproducible and if these responding cells were altered if the sequence of agonist application changed. First, ACh (EC_{25}) was applied to the artery, followed by ADP (EC_{25}) after the cells were washed and allowed to recover as described in Chapter 2.

After another round of wash and recovery ADP (EC_{25}) was applied, followed another wsh and recovery before the final application of ACh (EC_{25}). The cells activated by each agonist were highly reproducible, and the same pattern of cell activity for each agonist occurred regardless of the sequence of agonist application (Figure 4.3 A-C). The Ca^{2+} response evoked by the EC_{25} of ACh (0.10 ± 0.02 $\Delta F/F_0$) was significantly less than the Ca^{2+} response evoked by 1 µM ionomycin (1.29 ± 0.18 $\Delta F/F_0$; Figure 4.3 D and E).

Next the number of components were considered. Components consist of cells that were positioned in a cluster (i.e. an active cell and an active neighbour) and cells that responded in isolation (i.e. no responding neighbour). When compared to a random model, in which active cells were randomly re-positioned 1000 times, there were significantly more components per 100 cells in randomly re-positioned data than in the real measured data (control) (ACh: 6.3 ± 0.11 in control vs 8.5 ± 0.20 in random, Figure 4.4 A-C; ADP: 6.9 ± 0.13 in control vs 8.4 ± 0.08 in random, Figure 4.5 A-C; ATP: 7.1 ± 0.51 in control vs 8.5 ± 0.06 in random, Figure 4.6 A-C; Histamine: 7.1 ± 0.31 in control vs 8.62 ± 0.05 in random, Figure 4.7 A-C). The results suggest that there is an increased cell clustering in the real measured data than would be predicted from a random arrangement of responding cells.

In support of this conclusion, the number of clusters per 100 cells (i.e. cells that responded with a neighbour also responding) was also significantly increased in the random model for ACh and histamine when compared to measured data (control) (ACh: 3.5 ± 0.09 in control vs 4.1 ± 0.07 in random model; Histamine: 3.6 ± 0.12 in control vs 4.0 ± 0.10). However, there was no significant difference between the number of clusters when compared to the random model for ADP or ATP. The latter result suggests that ADP and ATP sensing is more distributed across the endothelium when compared to ACh and histamine.

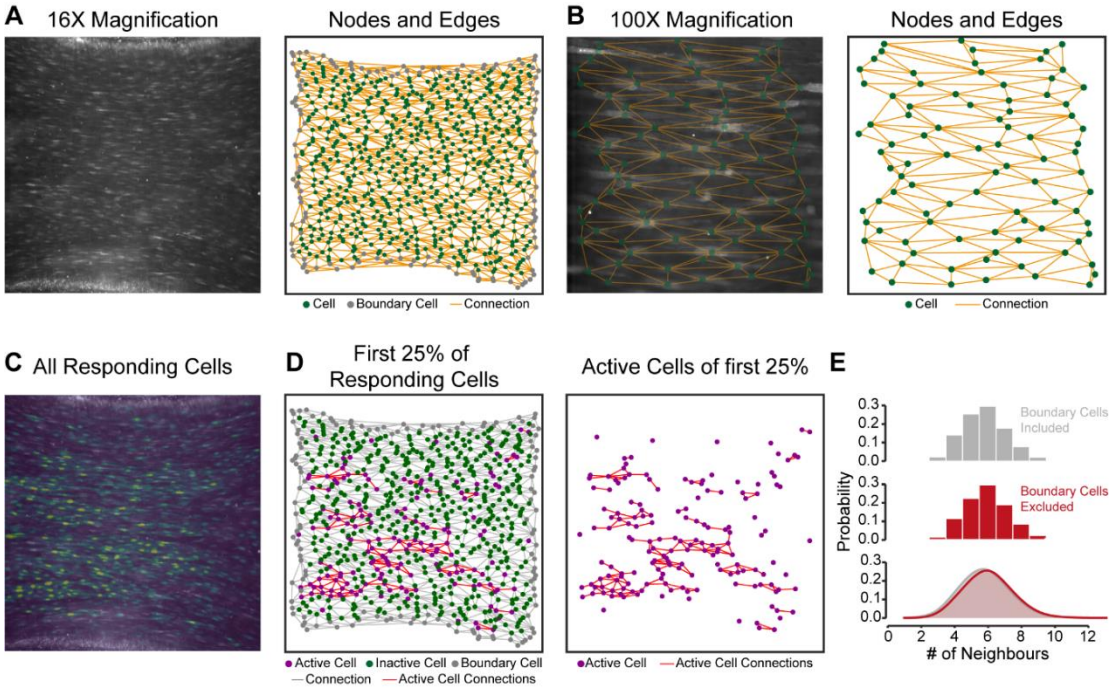

Figure 4.2 – Neighbour analysis of endothelial cell activity.(A) High-resolution, low-magnification Ca^{2+} image (Cal-520 fluorescence, left) and corresponding structural network (right) of a large section of the endothelium of an intact second-order mesenteric artery. In the right panel, the centre of each cell is indicated by green ROIs, and connections between neighbouring cells are shown as orange lines. Cells positioned at the boundary of the field-of-view are coloured grey. (B) High-resolution, high-magnification image (left) of a region of endothelial cells from the same field of endothelial cells shown in A, and corresponding structural network (right). (C) Pseudo-coloured Ca^{2+} image illustrating ACh-evoked (15 nM) Ca^{2+} activity throughout a 5-minute recording. (D) Location of ACh-responsive cells (first 25% of cells to respond, purple) shown with (left) and without (right) ACh-insensitive cells (green). (E) Probability density distributions showing the number of neighbours for each cell in A with boundary cells included (grey) or excluded (red). Scale bars, 50 µm.

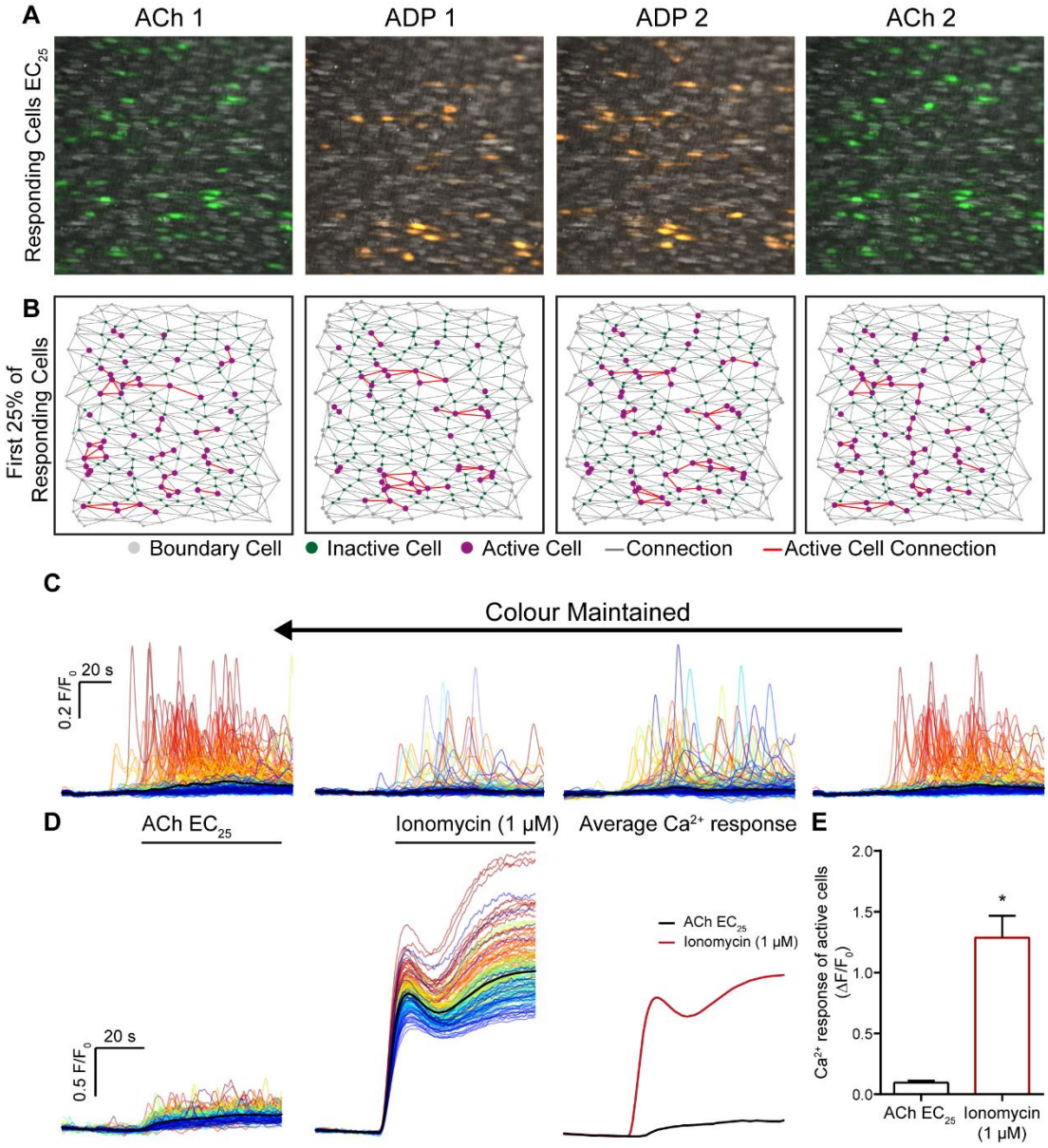

Figure 4.3 – Reproducibility of endothelial cell Ca^{2+} response.

(A) Representative composite image of Ca^{2+} activity in *en face* second order mesenteric artery endothelium to the EC_{25} of ACh (green) and ADP (orange). (B) Reconstructed endothelial network showing locations of active cells (purple dots), inactive cells (green dots) and boundary cells (grey dots). Lines connect responding cells to their nearest responding neighbours (red) or non-responding neighbours (grey). (C) Ca^{2+} signals from all individual cells in (A) Colours were assigned to the traces based on the amplitude of the response to ACh in each cell. Red indicated the highest amplitude and blue the lowest amplitude. Colours were assigned to the last ACh application first and maintained across the previous applications of ADP and ACh. Thus, allowing for direct comparison of the same cells between each agonist application. (D) Ca^{2+} signals after the application of ACh (EC_{25}) and ionomycin (1 µM). (E) Summary data illustrating the Ca^{2+} responses to ACh (EC_{25}) and ionomycin (1 µM). Data are representative of n = 5 independent experiments, from artery preparations, from different animals; *P < 0.05 compared to ACh response, paired Student t test.

For each of the four agonists, the mean number of cells in each cluster was significantly higher than would be expected from a random distribution (5.2 ± 0.09 for ACh measured, 3.8 ± 0.06 for ACh random, Figure 4.4 A-C;4.8 ± 0.22 for ADP measured, 3.8 ± 0.13 for ADP random, Figure 4.5 A-C; 5.5 ± 0.68 for ATP measured, 3.9 ± 0.14 for ATP random, Figure 4.6 A-C; 4.7 ± 0.36 for histamine measured, 3.8 ± 0.12 for histamine random, Figure 4.7 A-C). Similarly, irrespective of agonist, the mean degree (i.e. number of active neighbours) of active cells was higher than would be expected if responsive cells were distributed randomly throughout the endothelial cell network (1.7 ± 0.01 for ACh measured, 1.3 ± 0.01 for ACh random; ADP: 1.5 ± 0.04 measured vs 1.3 ± 0.05 in random; ATP: 1.7 ± 0.11 measured vs 1.3 ± 0.06 in random; Histamine; 1.6 ± 0.09 measured vs 1.3 ± 0.05 in random). The mean degree is the average number of active neighbours of each agonist-activated cell. Collectively, these results suggest that agonist-sensitive endothelial cells are positioned in spatially distinct clusters throughout the endothelium.

There was no significant difference in the number of components per 100 cells, number of clusters per 100 cells, number of cells per cluster or degree distribution between the agonists (Figure 4.8 A-D). This suggests that the endothelium does not vary the distribution of clusters or the properties of each cluster in detecting a specific agonist.

4.3.2 Spatial Separation of Agonist-Sensitive Endothelial Cell Clusters

Close visual inspection of Ca^{2+} activity evoked by the four agonists in the same preparation revealed variations in the cells that were sensitive to each activator (Figure 4.9 A-C). For example, cells that responded with a high amplitude Ca^{2+} response to ATP did not respond with the same intensity (or at all) to the other agonists (Figure 4.9 B). Indeed, initial observations revealed insufficient overlap of cells that responded to one agonist when compared to the cells that responded to other treatments (Figure 4.9 A-C).

Therefore, we sought to determine if there was any overlap between the subpopulation of cells that were sensitive to one agonist when compared to those that were sensitive to a separate agonist. A low concentration of ACh (EC_{25}) evoked a response in 23.78 ± 3.87% of all cells. Of these ACh-activated cells, 30.14 ± 8.15% responded to ADP, 33.75 ± 5.67% responded to ATP and 33.85 ± 2.84% responded to histamine (Figure 4.10 A and B). Of those cells that responded to the EC_{25} of ADP, (27.07 ± 5.99% of entire population), 25.18 ± 4.36% responded to ACh, 44.8 ± 8.84% responded to ATP and 41.72 ± 2.66% responded to histamine (Figure 4.10 A and B). For those cells responding to the EC_{25} of ATP (30.84 ± 5.85% of entire population), 26.01 ± 4.23% responded to ACh, 39.51 ± 8.35% responded to ADP and 39.61 ± 4.29% responded to histamine (Figure 4.10 A and B). Finally, of the cells responding to the EC_{25} of histamine (29.19 ± 2.96% of entire population), 28.81 ± 6.27% responded to ACh, 39.18 ± 9.47% responded to ADP, and 41.3 ± 7.63% responded to ATP (Figure 4.10 A and B). There was no significant overlap between the subpopulation of cells that responded to one agonist when compared to the subpopulation that responded to any of the other agonists.

The majority of cells (33.2 ± 1.4%) responded to one agonist. However, there is a subpopulation of cells that responded to two (22.9 ± 2.3%) or three agonists (10.8 ± 2.6%). Interestingly, a small subpopulation of cells responded to all four agonists (2.8 ± 1.0%) (Figure 4.10 C). One possibility to explain this observation is that cells that respond to three or more agonists arise from propagation of the Ca^{2+} signal from a neighbouring agonist sensitive cell rather than the cell expressing all four receptor subtypes. However, further study is required to determine the expression of receptors in endothelial cells. Some 30% (30.3 ± 4.4%) of cells did not respond to any of the four agonists, at the EC_{25} concentration. This observation suggests these cells may be primed to detect other agonists not studied here.

Together, these observations indicate, the endothelium utilises spatially distinct clusters of cells that are primed to detect a specific agonist, with little overlap with cells that are more sensitive to another agonist.

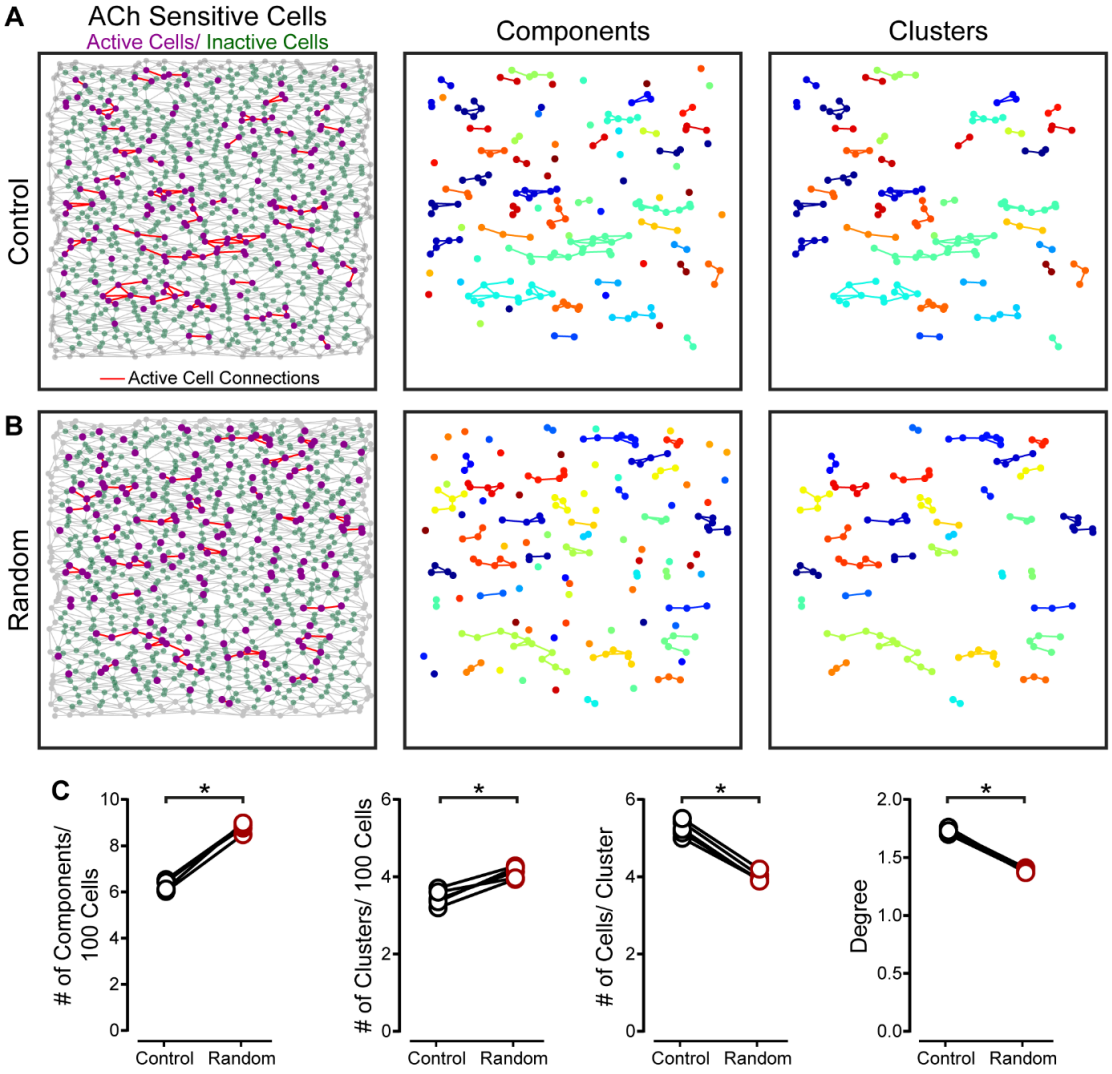

Figure 4.4 – Clustering of ACh-sensitive endothelial cells.

The first 25% of responding cells to ACh (EC_{25}) and their spatial relationships were calculated from neighbour analysis. (A) Reconstructed endothelial network (left) showing locations of active cells (purple dots), inactive cells (green dots) and boundary cells (grey dots). Lines connect responding cells to their nearest responding neighbours (red) or non-responding neighbours (grey). The middle panel, shows the separate components of the active cells and the right panels, shows the individual clusters. Components are cells that respond in isolation or together with a neighbour. Clusters are cells that respond with an active neighbour. (B) Random model of the endothelial network shown in A, showing the active cells (left), components (middle) and clusters (right). (C) Summary data illustrating the distribution of ACh sensitive cells across the endothelium compared to a random distribution. Data are representative of n = 5 independent experiments, from artery preparations, from different animals; *P < 0.05, paired Student t test.

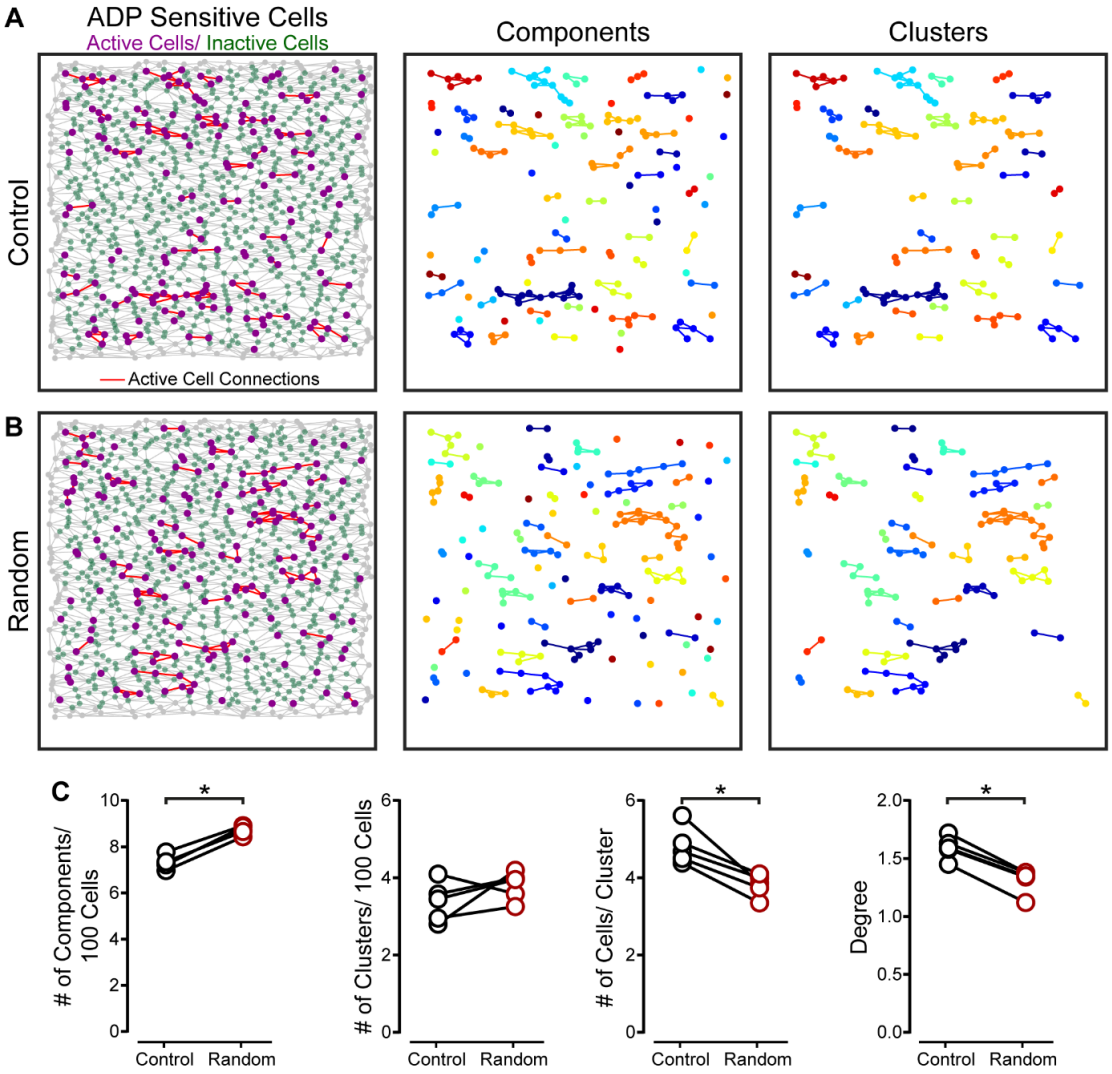

Figure 4.5 – Clustering of ADP-sensitive endothelial cells.

The first 25% of responding cells to ADP (EC_{25}) and their spatial relationships were calculated from neighbour analysis. (A) Reconstructed endothelial network (left) showing locations of active cells (purple dots), inactive cells (green dots) and boundary cells (grey dots). Lines connect responding cells to their nearest responding neighbours (red) or non-responding neighbours (grey). The middle panel, shows the separate components of the active cells and the right panels, shows the individual clusters. Components are cells that respond in isolation or with a neighbour. Clusters are defined as cells that respond with an active neighbour. (B) Random model of the endothelial network shown in A, showing the active cells (left), components (middle) and clusters (right). (C) Summary data illustrating the distribution of ADP sensitive cells across the endothelium compared to a random distribution. Data are representative of n = 5 independent experiments, from artery preparations, from different animals; *P < 0.05, paired Student t test.

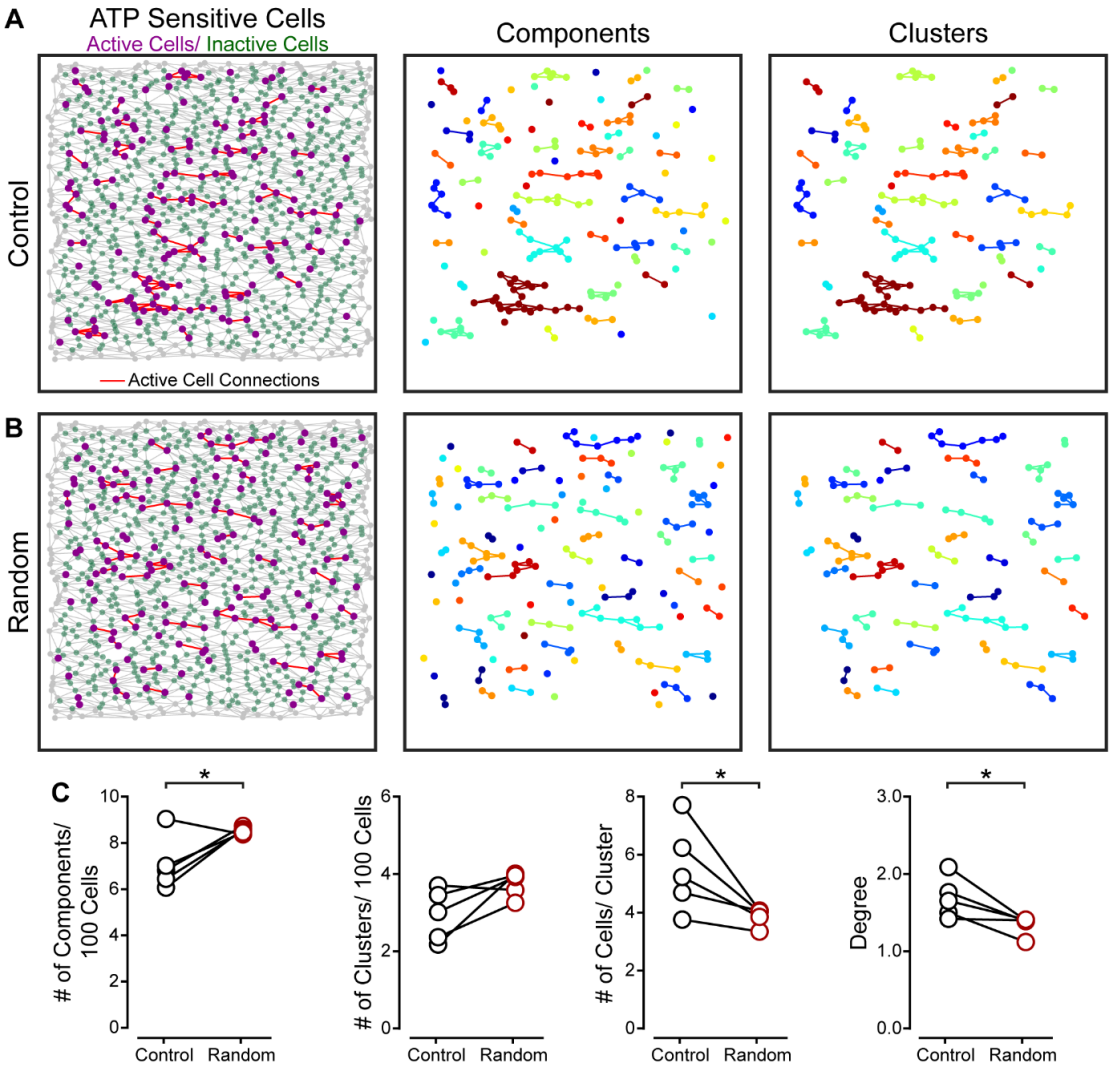

Figure 4.6 – Clustering of ATP-sensitive endothelial cells.

The first 25% of responding cells to ATP (EC_{25}) and their spatial relationships were calculated from neighbour analysis. (A) Reconstructed endothelial network (left) showing locations of active cells (purple dots), inactive cells (green dots) and boundary cells (grey dots). Lines connect responding cells to their nearest responding neighbours (red) or non-responding neighbours (grey). The middle panel, shows the separate components of the active cells and the right panels, shows the individual clusters. Components are cells that respond in isolation or with a neighbour. Clusters are defined as cells that respond with an active neighbour. (B) Random model of the endothelial network shown in A, showing the active cells (left), components (middle) and clusters (right). (C) Summary data illustrating the distribution of ATP sensitive cells across the endothelium compared to a random distribution. Data are representative of n = 5 independent experiments, from artery preparations, from different animals; *P < 0.05, paired Student t test.

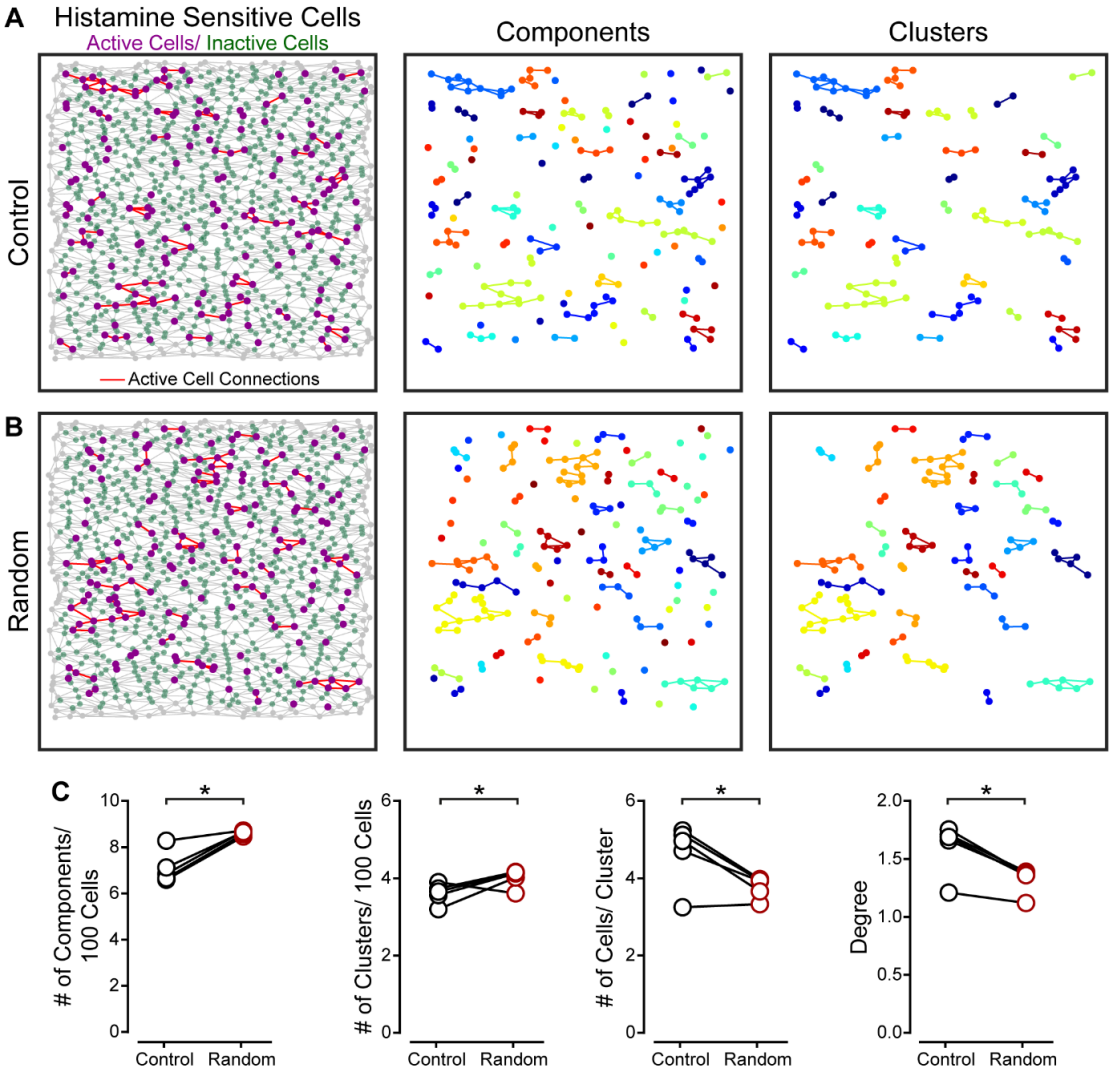

Figure 4.7 – Clustering of histamine-sensitive endothelial cells.

The first 25% of responding cells to histamine (EC_{25}) and their spatial relationships were calculated from neighbour analysis. (A) Reconstructed endothelial network (left) showing locations of active cells (purple dots), inactive cells (green dots) and boundary cells (grey dots). Lines connect responding cells to their nearest responding neighbours (red) or non-responding neighbours (grey). The middle panel, shows the separate components of the active cells and the right panels, shows the individual clusters. Components are defined as cells that respond in isolation or with an active neighbour. Clusters are defined as cells that respond with a neighbour. (B) Random model of the endothelial network shown in A, showing the active cells (left), components (middle) and clusters (right). (C) Summary data illustrating the distribution of histamine sensitive cells across the endothelium compared to a random distribution. Data are representative of n = 5 independent experiments, from artery preparations, from different animals; *P < 0.05, paired Student t test.

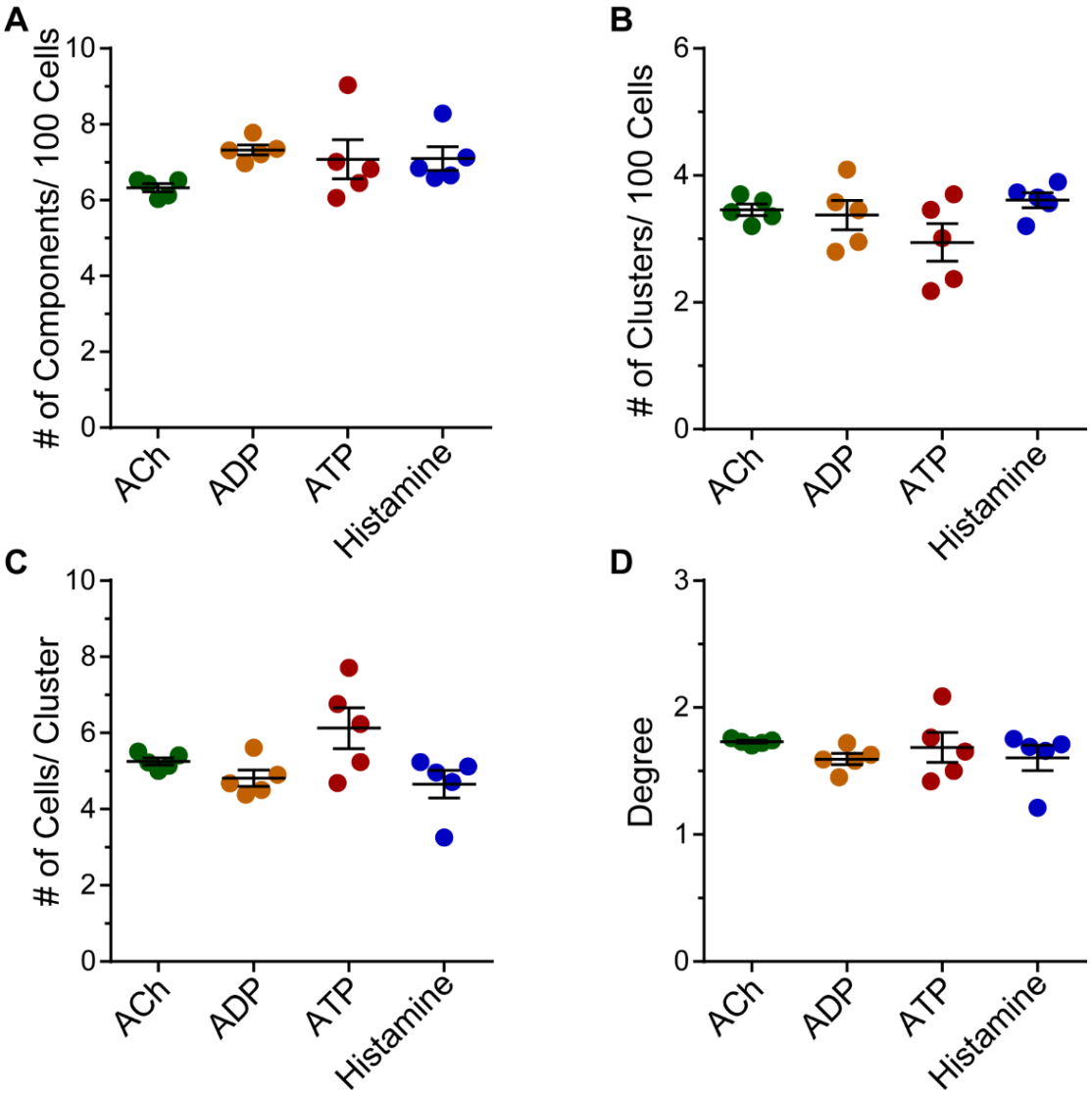

Figure 4.8 – Comparison of ACh-, ADP-, ATP- and histamine-sensitive endothelial cell clustering.

Summary data showing the effects of the different agonists (ACh, green; ADP, orange; ATP, red; histamine, blue) on the mean number of components per 100 cells (A), the mean number of clusters per 100 cells (B), the mean number of cells in a cluster (C), and the mean degree (D). The number of components is the number of isolated groups (single cells or clusters) of responding cells. The number of clusters is the number of components with at least two connected cells. The degree is the number of active neighbours of each responding cell. Data are shown as mean values for each independent experimental replicate (dots) with grand mean ± SEM indicated. Each experimental replicate was stimulated with each of the indicated agonists (n = 5).

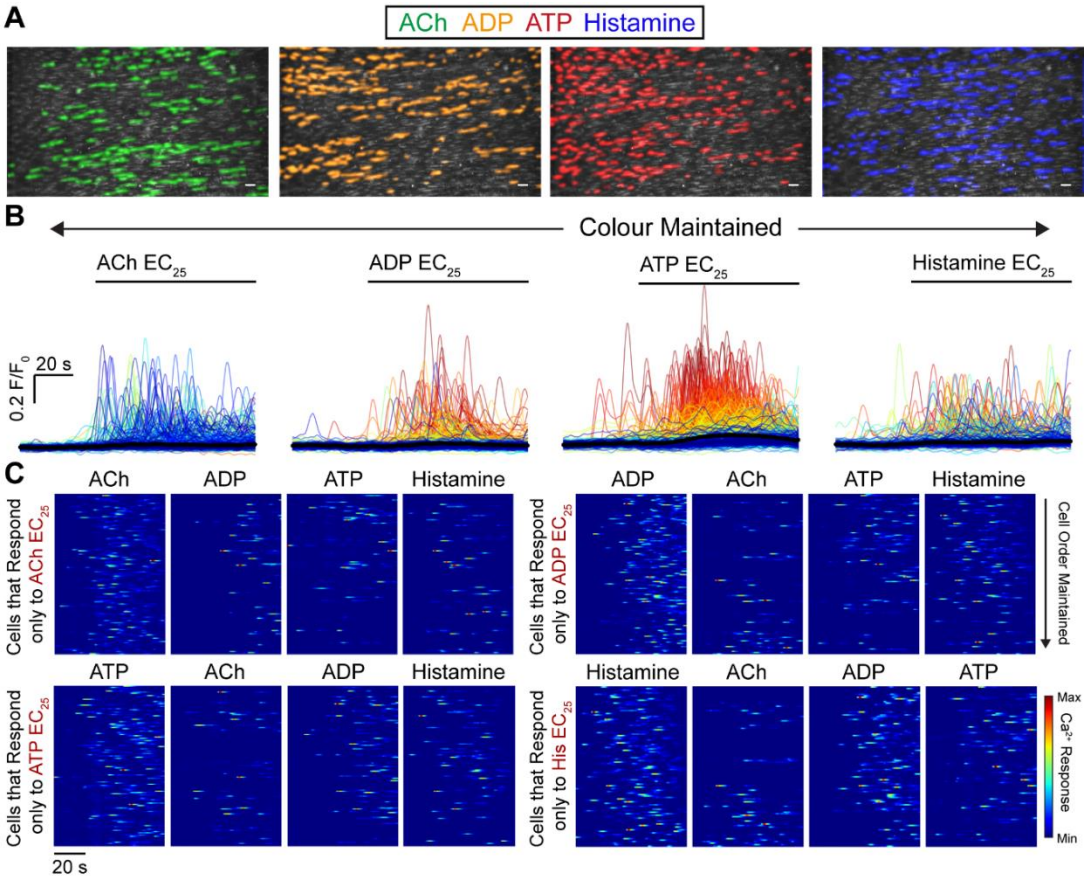

Figure 4.9 – Ca^{2+} activity evoked by ACh, ADP, ATP and histamine occur in spatially discrete cells.

(A) Composite endothelial Ca^{2+} image (second-order mesenteric artery, ~ 1000 cells) with activity evoked by the EC_{25} of ACh (green), ADP (orange), ATP (red) and histamine (blue) overlaid. Each image shows the response to the indicated agonist and it is the same field of endothelium throughout. (B) Cellular Ca^{2+} signals from each dataset shown in A. Ca^{2+} signals have been coloured according to the magnitude of the response to ATP (red, highest, to blue, lowest), and the colour (identity) of each trace has been maintained across the other datasets (i.e. if a cells trace is coloured red for ATP then it is also coloured red for ACh, ADP and histamine). (C) Heatmap representation of Ca^{2+} signals, of the active signals, shown in B. Each line represents the Ca^{2+} response from a separate endothelial cell. Scale bars, 50 µm.

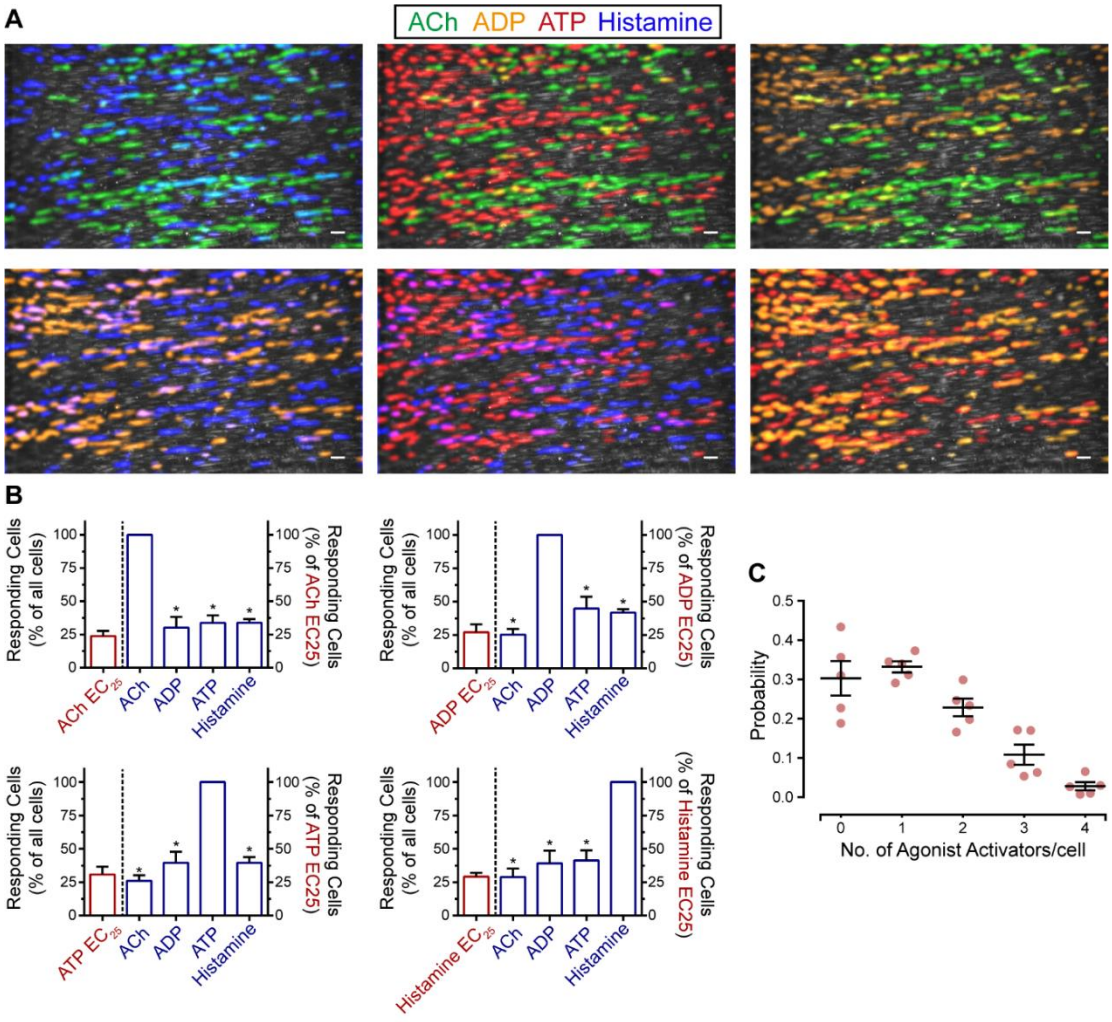

Figure 4.10 – Different agonists activate spatially distinct clusters of cells.

(A) Composite Ca^{2+} images illustrating the overlap of agonist-specific Ca^{2+} activity for pairs of agonists in the same field of endothelium. Agonists (EC_{25} of ACh (green), ADP (orange), ATP (red) and histamine (blue)) were sequentially applied (5-minute washout, 5-minute rest) to the same artery. (B) Summary data showing the percentage of the total population of cells activated at the EC_{25} (red), and the percentage of these same cells (active; red bar) that are activated by each of the other agonists (blue). Data is mean ± SEM (n = 5). (C) Proportion of the number of activators an individual cell detects. Data shown as mean values for each independent experimental replicate (dots) with grand mean ± SEM indicated (n=5) *P < 0.05, one-way ANOVA followed by Tukey's multiple comparisons test. Scale bars, 50 µm.

4.4 Discussion

In this study, whether or not the endothelium utilises specific cells to detect different stimuli was addressed. The Ca^{2+} response to ACh, ADP, ATP and histamine were analysed in large numbers of endothelial cells in intact blood vessels. The results show that low concentrations of each agonist evoked responses in discrete clusters of cells and these clusters were spatially unique for each agonist. There was minimal overlap between the cluster of cells activated by one agonist and those activated by a different agonist.

4.4.1 Heterogeneity in the Endothelium

Most studies examining sensing and activation treat the endothelium as being a homogenous population of cells that respond uniformly to each activator. The assumption that endothelial cells behave uniformly is implicit in most experimental approaches used to study the endothelium. In pressure or wire myograph studies, the mechanical response of arteries or veins is used as an indirect measurement of endothelial function (Yuill et al., 2011). Although these experiments have yielded many important insights into endothelial function (e.g. discovery of nitric oxide) they treat the response of thousands of endothelial cells as an average and assume each cell responds uniformly (Furchgott and Zawadzki, 1980). Conversely, studies examining single endothelial cells also treat the population of cells to be homogenous and that the response of the single cell is representative of the entire population. Many current interpretations of gene expression, protein levels or metabolic signalling that are derived from immunoblots, PCR or microarrays also assume that all cells of a population are comparable in receptor complement and signalling processes (Navarro et al., 2013). Nevertheless, studies using these experimental approaches have revealed many of the mechanisms utilised by the endothelium to control vascular function.

When individual cells in a population have been examined, differences in the time course of responses or expression of proteins have been almost universally reported.

For example, there is variation in the expression of von Willebrand factor in different vascular beds (Aird et al., 1997; Vanlandewijck et al., 2018). There is an increase in ACh evoked Ca^{2+} responses at branches in rat aorta when compared to neighbouring cells away from the branch points (Huang et al., 2000). The reverse was true for histamine. Agonist-evoked (ACh, ADP, ATP, histamine) endothelial dependent Ca^{2+} signals also generated heterogeneous responses at low concentrations (Chapter 4). However, analysis of the clusters evoked by agonists in the endothelium of intact resistance arteries has not been characterised.

To address this, we analysed the Ca^{2+} response evoked by low concentrations of ACh, ADP, ATP and histamine in large populations of endothelial cells in resistance arteries. Our results show that the endothelium does not respond uniformly to each activator. Instead, sub-populations of cells are activated by each agonist. On average only ~30% of those cells that responded to the EC_{25} concentration of one agonist also responded to another agonist. Interestingly ~30% of the cells in the population did not respond to any of the four agonist examined suggesting they may be more sensitive to another activator not examined here.

The mechanisms that give rise to endothelial heterogeneity are not yet clear. Heterogeneity may occur by two distinct routes, nurture (microenvironment) and nature (epigenetics). It is clear that receptor and protein expression varies not only amongst different organs but also within the same tissue (Chi et al., 2003; Kalluri et al., 2019; Vanlandewijck et al., 2018). This presumably occurs due to variations in the microenvironment to which the endothelium is exposed (Aird, 2007; Durr et al., 2004). However, if each endothelial cell was intrinsically identical then cells exposed to the same microenvironment should be the same. In the present study, we have shown that this is not the case. Instead, endothelial cells positioned one to two cells apart do not respond uniformly to an activator. Therefore, changes may occur during embryonic development or changes, in protein expression, may occur over time (Acar et al., 2008; Aird, 2005; Yuan et al., 2016). Further study is required to understand

the mechanisms underlying endothelial heterogeneity and the role changes to these mechanisms play in disease.

4.4.2 Clustering of Agonist Specific Sensing Cells

ACh, ADP, ATP and histamine evoked Ca^{2+} responses revealed that cells with comparable sensitives to an agonist were positioned in discrete clusters and the number of cells within a cluster is significantly greater than those expected to occur in random model. Furthermore, the number of neighbours an active cell has is also increased when compared to a random distribution.

Clustering of cells creates properties of the system that are absent in single cells and generates a mechanism to help reject noise. For example, clustering may enable a co-incidence detection system (Chapter 3) (Lee et al., 2018; Wilson et al., 2016b). When single endothelial cells are activated (as occurs due to stochastic noise), there is little propagation of signals to neighbouring cells (Wilson et al., 2016b). However, when two or more neighbouring cells are activated together, signal propagation occurs. By rejecting noise, signal detection improves and randomly occurring events are unlikely to be propagated. These observations again show that the endothelium as a whole has properties that are quite distinct from those of individual cells. Furthermore, clustering ensures that the endothelium is not overwhelmed when several activators are present simultaneously; each individual cluster can carry out a separate process. This system is valuable when the number of inputs the endothelium will receive at any given time is difficult to predict. Clustering may offer other advantages by allowing the uptake and breakdown mechanisms for diffusible messengers (e.g. nitric oxide, prostaglandin) to be overwhelmed, providing increased spillover of signals. Clustering may also limit interference from neighbouring cells that are responding to a different stimulus. A single cell responding in isolation may easily be influenced by neighbouring cells and have its signal overridden. However, a cluster of cells each performing the same task may be much harder to override. Collectively, these features of endothelial clustering provide greater scalability and may allow the endothelium to adapt to changing demands (during disease e.g. hypertension).

We have previously shown that receptor distribution varies between endothelial cells and clustering of cells with specific receptor expression occurs (Lee et al., 2018; Wilson et al., 2016b). However, the mechanisms underlying variations in receptor regulation and cellular clustering remain poorly understood. Self-replication during development or changes at different developmental ages and cellular renewal may lead to clustering (McCarron et al., 2019). Alternatively, receptor expression may be influenced by a feedback mechanism from neighbouring endothelial cells. Further study is required to determine how a subpopulation of cells that are primed to detect a specific agonist are grouped together in clusters.

4.4.3 Efficient Relay of Information in the Endothelium

Despite the diverse functional activities of the endothelium, the anatomy and connectivity of the cells and network are largely fixed, with each cell having six neighbours on average. The question of how a large functional signalling repertoire arises from a fixed anatomy and connectivity using predominantly a single communication signal (Ca^{2+}) both within and between cells is unresolved.

Current dogma suggests that variations in amplitude, frequency and spatial distributions of the Ca^{2+} response within a single endothelial cell allows the endothelium to relay information held in an external stimuli, to generate a specific physiological output (Chapter 1). This may permit Ca^{2+} to specifically regulate various activities in a single endothelial cell. Here we have shown that the endothelium also utilises spatially discrete clusters of cells to efficiently detect and relay the information held in the external media to generate a specific response. Although each agonist generates a Ca^{2+} response by the GPCR/PLC/IP_3 pathway there is no significant overlap in the cells that responds to one agonist when compared to the cells that respond to another. Interestingly, cells that responded to purinergic receptor (P2Y) activation, albeit different subtypes, did not show any significant overlap.

The endothelium is exposed to an ever changing and perhaps unpredictable environment. Therefore, the endothelium may benefit by maintaining a diversity of cellular phenotypes to ensure that any changes in the environment can be detected. Unlike a strategy where individual cells sense and respond uniformly to the environment, maintenance of a standing diversity may be preferred when a rapid response of at least a subpopulation is advantageous (Dueck et al., 2016). This has been studied extensively in single cell organisms (Beaumont et al., 2009; Martins and Locke, 2015; Mineta et al., 2015). For example, a small sub-population of bacterial cells growing in rich media display a phenotype that is not optimal for that particular environment. However, due to "bet hedging" these cells can, survive an unpredictable stress (e.g., antibiotic exposure) (Martins and Locke, 2015). Therefore, by utilising sub-populations of cells to detect future events, that may not necessarily occur often, if at all (i.e. plaque rupture during atherosclerosis) the endothelium may exhibit "bet-hedging" behaviour.

Collectively, our results suggest that specific cells are primed to detect certain agonists. These cells are positioned in discrete clusters and are spatially distinct from cells that are primed to detect a different activator. We suggest this sensing system allows the endothelium to detect and separately process the instructions held in multiple separate agonists simultaneously. For example, if one cluster of cells responds to an agonist (ACh) a separate cluster of cells can detect and respond to another agonist (histamine). This allows the endothelium to process multiple, completely separate, functions in parallel.

Chapter 5. Emergent Behaviour in the Vascular Endothelium

5.1 Introduction

To maintain vascular homeostasis, the endothelium co-ordinates the response to numerous activators across many cells. To carry out these activities the endothelium senses and responds to numerous signals held in the extracellular environment and releases various vasoactive agents. However, the extracellular environment to which the endothelium is exposed is complex and dynamic. Signals can arrive from neighbouring endothelial cells, underlying smooth muscle cells, neurotransmitters, circulating blood cells and inflammatory mediators (Bhattacharya et al., 2008; Duckles and Miller, 2010; Garland et al., 2017; Keller et al., 2003; Orozco et al., 2000). To add to the complexity in signal detection, many of these signals arrive simultaneously and may be fluctuating constantly around baseline levels. We have shown that the endothelium detects these signals by using clusters of cells that are primed for a specific activator (Chapter 4). However, it is not yet fully understood how these distinct clusters seamlessly integrate information across cells to mediate endothelial function when multiple agonists are present simultaneously.

To co-ordinate the myriad of functions under its control, endothelial communication occurs. Each endothelial cell is connected to approximately six neighbouring cells Communication occurs via gap junctions (Chapter 1 and 4) and the low electrical resistance of the endothelium (~5–70 MΩ) demonstrates a high extent of connectivity between cells (Carter and Ogden, 1994; Marchenko and Sage, 1993; Yamamoto et al., 2001). However, the challenge faced by the endothelium in coordinating function cannot be understated. In adults there are approximately 10 trillion endothelial cells that form a single connective layer throughout the entire body (Galley and Webster, 2004). This number is 100 times greater than the number of neurons in the brain and illustrates the extent of the task in coordinating activities (Azevedo et al., 2009). Even on a local scale the problem faced by the endothelium in coordinating vascular function is complex. There are approximately 2000 endothelial cells per square millimetre in rat arteries and the processes governed by each cell must be coordinated to regulate local output.

What makes endothelial control of vascular function most remarkable is that there is no master control that regulates the combined output of all cells. Endothelial cells do not report back to a central hub that gathers the available information to generate an output. Instead, each individual endothelial cell monitors the local microenvironment to detect any changes and from this information makes a decision on output.

Since, as shown in Chapters 3 & 4, endothelial cells are sensitive detectors of limited specific pieces of information, each individual endothelial cell receives only a small element of the overall information available. As a consequence, some cells may appear to be 'oblivious' to changes occurring in the microenvironment. For example, we have shown that only a sub-population of cells can detect a specific agonist at low concentrations to generate a Ca^{2+} response (Chapter 4). Presumably, the other cells in the population do not initiate a Ca^{2+} response because they cannot detect the change in concentration of the activator. Other cells will respond to different activators. Therefore, each endothelial cell receives only a small element of the overall information and cannot itself resolve the complexity of all information presented. While each cell receives only a small element of the overall information available, cells share information by communicating with neighbours. From the collective information sharing an organised behaviour in the endothelium emerges.

This organised behaviour of the endothelium shares many features with emergent or 'swarm' intelligence. Swarm intelligence is the organised behaviour of large communities that occurs without a global organiser (Camazine et al., 2003; Garnier et al., 2007). Primarily, this concept was born from the study of social insects and how large colonies are organised to solve complex problems without a centralised control. Each individual within these social communities has limited abilities but the exchange of information permits individuals to be both influenced by, and influence, their neighbours (Ioannou, 2017). This provides a problem-solving capacity that arises from the interactions of individual components with the environment and the

interaction between individual components (i.e. the whole is greater than the sum of its parts).

Swarm intelligent systems have the following typical properties: the system comprises many individuals that belong to only a few phenotypes; the overall behaviour of the system results from the interactions of individuals with each other and with their environment; and the interactions among the individuals are based on simple rules that use only local information that the individuals exchange directly (McCarron et al., 2017).

A vital characteristic of swarm intelligence is that the individual components (endothelial cells) must be able to co-operate with one another. This imposes the requirement that there is a common communication pathway/mechanism between components (Dorigo et al., 2013). Cell-to-cell communication networks have critical roles in coordinating diverse organismal processes, such as tissue development or immune cell response. However, compared with intracellular signal transduction networks, the function and engineering principles of cell-to-cell communication networks are poorly understood. In endothelial cells, communication is thought to occur via gap junctions (Chapter 1).

In this chapter, we sought to determine the features of the Ca^{2+} signal evoked by muscarinic, purinergic and histaminergic receptor activation and if the features of each signal interact and are altered when multiple agonists were present simultaneously. Our approach makes use of graph theory (Chapter 4) to determine the distribution of cells sensitive to a single agonist and to compare signals arising from these cells when agonists, which activate other separate cells, were applied in duplicate, triplicate and quadruplicate. Here we show that the Ca^{2+} signal evoked by each agonist (ACh, ADP, ATP and histamine) is unique to each agonist. However, despite separate cells being activated by each agonist, the Ca^{2+} signals arising from each cell is altered when multiple agonists were present. Indeed, the steady state response (Ca^{2+} influx across the plasma membrane) was greater than either the average or the summation of responses, when the agonists were applied separately.

Since this change occurred in cells that were sensitive to only one agonist, there is communication between endothelial cells (i.e. the Ca^{2+} response in cells that respond to only one agonist have their Ca^{2+} response altered by cells responding to a separate agonist). Significantly the signals that appear when more than one agonist is present differ from any of the individual responses and exceed the average or summation of the responses.

New features that appear in a system and which differ from the expectations of the sum of the components are called 'emergent properties' (Kesić, 2016; Regenmortel, 2004). Emergent properties differ significantly from those observed in linear (resultant) systems. Unlike linear systems where the whole is equal to the sum of the parts, emergent systems arise from non-linear interactions and create new collective behaviours that make the whole much greater than the sum of the parts. Emergent properties cannot be reduced to properties of the constituent parts of the system and resist attempts at being inferred or predicted by calculation. In this chapter, the emergent properties of the endothelium that arise when multiple agonists are present is examined.

5.2 Methods

5.2.1 *Endothelial Ca^{2+} Signal Analysis*

Endothelial Ca^{2+} signalling was imaged as described in Chapter 2. Endothelial cell viability was assessed by application of ACh (100 nM) at the start of each experiment to ensure a Ca^{2+} response was evoked in every cell. To investigate the spatial distribution of agonist-sensitive endothelial cells, low concentrations (EC_{25}, from full concentration-response data, in Chapter 3, showing the 'percentage of active cells') of multiple agonists (ACh, ADP, ATP, and histamine) were sequentially applied to endothelial cell preparations. To determine the cells that responded when multiple agonists were present, agonists were applied simultaneously in pairwise, triplicate or quadruplicate at the respective EC_{25}. After each agonist application (singular or combination), arteries were washed with PSS for 5 minutes and allowed to rest for an additional 5 minutes before the subsequent addition of agonists. During each experiment, agonist-evoked Ca^{2+} activity in a single field of endothelial cells, from the same preparation, was recorded.

5.2.2 *Cell Clustering and Neighbour Analysis*

To quantitatively study endothelial cell connectivity, we constructed graph theoretical representations of the endothelial network using Python 2.7 as described in Chapter 4.

5.2.3 *Analysis of the Features of the Ca^{2+} Signal*

To determine whether or not the characteristics of the Ca^{2+} signal can be predicted when multiple agonist are present, we first analysed the features of the Ca^{2+} response when agonists were applied individually. Due to the temporal variations in the Ca^{2+} response across the endothelium, the Ca^{2+} signal in all active cells were aligned based on the initial peak. This ensured the features of the Ca^{2+} signal was dependent on the agonist activation and not an average response of asynchronously responding cells at a given time.

Using the measured Ca^{2+} response, when agonists were applied in isolation, predicted average and summed responses were calculated for all of the possible agonist combinations.

5.2.4 Statistics

Summarised data are presented as means ± SEM values; n is the number of independent experimental replicates (number of animals). For statistical comparison of two groups, a two-tailed Student's t test (paired data) was performed. Two-tailed one-way ANOVA with Tukey's multiple comparisons test or two-tailed two-way ANOVA with Dunnett's multiple comparisons test, as appropriate, was used for statistical comparison of three or more groups. All statistical analyses were performed using GraphPad Prism, version 6.0 (GraphPad Software). $P < 0.05$ was considered statistically significant.

5.3 Results

5.3.1 Spatiotemporal Features of Agonist-Evoked Ca^{2+} Responses

The endothelium receives signals from a multitude of different activators, many of which arrive simultaneously *in vivo*. However, few studies examine how the endothelium integrates these signals to coordinate vascular function. Therefore, we sought to investigate how the endothelium manages multiple, simultaneously arriving, stimuli that converge on Ca^{2+} signalling. To achieve this, we first identified each endothelial cell in large fields of native endothelia and measured the characteristics of the Ca^{2+} response evoked by low concentrations (EC_{25}) of four distinct agonists (ACh, ADP, ATP and histamine). As shown previously (Chapters 3 & 4), the endothelium does not respond uniformly to each agonist, instead discrete subpopulations are more sensitive to a specific activator (Chapter 4). Additionally, there are differences between cells in the amplitude of responses and in the time of activation (Chapter 4). To overcome the issue of temporal variations, the Ca^{2+} responses from individual cells were aligned in time with respect to the initial peak of the Ca^{2+} response. This synchronized the Ca^{2+} response in each cell, allowing for the features of the Ca^{2+} response, evoked by each agonist, to be analysed.

The features of the spatiotemporal Ca^{2+} signal evoked by ACh, ADP, ATP and histamine differed substantially. ACh evoked repetitive oscillations on an elevated baseline, ADP and ATP a large initial peak which declined towards baseline. ADP had an increased number of oscillations when compared to ATP. Histamine evoked repetitive oscillations that were similar in amplitude.

To determine the spatial distribution of endothelial cell sensitivity when multiple agonists are present, we applied low concentrations (EC_{25}) of each agonist simultaneously in various combinations. Analysis was limited to only the first 25% of cells to respond. Cells that were present at the boundary of the field-of-view were ignored from any analysis (Chapter 4) to ensure only cells with a full complement of neighbours were analysed. When the agonists were applied in combination, analysis

of the endothelial cell network revealed that of the first 25% of responding cells, some cells responded to only one activator, whilst another subpopulation responded two or three different agonists (Figure 5.1 A, Figure 5.2 A, Figure 5.3 A, Figure 5.4 A, Figure 5.5 A). A small number of cells (1 or 2) responded to four agonists (Figure 5.5 A). Interestingly, some cells did not respond when the agonists were applied individually and only responded when multiple agonists were present.

The additional recruitment of cells that occurred when multiple agonists were present (but not when applied individually) may have arisen from a limited expression of these receptors on the cell. Although a cell may express multiple receptor subtypes, a low concentration of an agonist (when applied individually) may be insufficient to initiate a Ca^{2+} response. Only when multiple agonists are applied simultaneously is the threshold for initiating a Ca^{2+} response reached. An alternative explanation may be that the Ca^{2+} response generated in neighbouring cells may be communicated to facilitate the initiation of a Ca^{2+} response. For example, a cell that expresses muscarinic and not purinergic receptors, that does not respond to low concentrations of ACh, may have its activity altered if it's neighbouring cells respond to ATP. Indeed, our previous studies have shown that cells that are highly unresponsive to one agonist (even at high concentrations) have their response altered, when neighbouring cells (that do respond to the agonist) are activated (Lee et al., 2018). However, further study is required to determine how additional cells that do not respond when agonists are applied individually are subsequently recruited when a combination of agonists are present.

We next sought to determine if the Ca^{2+} response evoked by each agonist was altered when additional agonists were also present (duplicate, triplicate or quadruplicate) at all possible variations. We restricted the analyses of the combination response to only those cells that responded when an agonist was applied individually. This ensured any variation of the Ca^{2+} response was due to the action of the additional agonists and not a consequence of averaging responses across all active cells (i.e. to study the action of ATP on ACh evoked Ca^{2+} response, only ACh-sensitive cells were

analysed. Therefore, ATP-sensitive cells were excluded from the analysis – unless they also responded to ACh).

5.3.2 *Pairwise Agonist-Evoked Ca^{2+} Responses*

When compared to ACh alone (0.23 ± 0.02 $\Delta F/F_0$), there was a significant increase in the peak Ca^{2+} response in the paired application of ACh and ADP (0.30 ± 0.04 $\Delta F/F_0$) or ACh and ATP (0.32 ± 0.03 $\Delta F/F_0$). However, the paired application of ACh and histamine (0.25 ± 0.03 $\Delta F/F_0$) did not significantly increase the peak Ca^{2+} response when compared to ACh alone. The steady state response was significantly increased when the agonists were applied in combination, when compared to ACh alone (0.05 ± 0.01 $\Delta F/F_0$ for ACh; 0.15 ± 0.03 $\Delta F/F_0$ for ACh and ADP; 0.18 ± 0.03 $\Delta F/F_0$ for ACh and ATP; 0.13 ± 0.03 $\Delta F/F_0$ for ACh and histamine; Figure 5.1 B and C).

For ADP-sensitive cells, only ATP in the paired application significantly increased the peak Ca^{2+} response (0.20 ± 0.007 $\Delta F/F_0$ for ADP; 0.22 ± 0.02 $\Delta F/F_0$ for ADP and ACh; 0.34 ± 0.02 $\Delta F/F_0$ for ADP and ATP; 0.24 ± 0.03 $\Delta F/F_0$ for ADP and histamine). However, the amplitude of the pairwise steady state response, for all agonist combinations, was significantly increased when compared to ADP alone (0.02 ± 0.007 $\Delta F/F_0$ for ADP; 0.12 ± 0.03 $\Delta F/F_0$ for ADP and ACh; 0.16 ± 0.01 $\Delta F/F_0$ for ADP and ATP; 0.13 ± 0.03 $\Delta F/F_0$ for ADP and histamine; Figure 5.2 B and C).

Only the combination of ATP and ADP increased the peak Ca^{2+} response in ATP-sensitive cells, when compared to ATP alone (0.28 ± 0.03 $\Delta F/F_0$ for ATP; 0.29 ± 0.03 $\Delta F/F_0$ for ATP and ACh; 0.37 ± 0.02 $\Delta F/F_0$ for ATP and ADP; 0.26 ± 0.02 $\Delta F/F_0$ for ATP and histamine). However, the amplitude of the steady state response was significantly increased by each of the pairwise agonist applications (0.05 ± 0.008 $\Delta F/F_0$ for ATP; 0.15 ± 0.03 $\Delta F/F_0$ for ATP and ACh; 0.17 ± 0.01 $\Delta F/F_0$ for ATP and ADP; 0.14 ± 0.01 $\Delta F/F_0$ for ATP and histamine; Figure 5.3 B and C).

For histamine-sensitive cells, the pairwise application of the agonists significantly increased both the peak (0.19 ± 0.02 $\Delta F/F_0$ for histamine; 0.24 ± 0.03 $\Delta F/F_0$ for histamine and ACh; 0.25 ± 0.03 $\Delta F/F_0$ for histamine and ADP; 0.25 ± 0.01 $\Delta F/F_0$ for

histamine and ATP) and steady state response (0.03 ± 0.01 $\Delta F/F_0$ for histamine; 0.09 ± 0.02 $\Delta F/F_0$ for histamine and ACh; 0.13 ± 0.02 $\Delta F/F_0$ for histamine and ADP; 0.13 ± 0.01 $\Delta F/F_0$ for histamine and ATP; Figure 5.4 B and C). Collectively, these results show that the Ca^{2+} response in agonist specific sensing cells is altered when an additional agonist is present.

5.3.3 Pairwise Ca^{2+} Responses Differ from Individual Agonist Evoked Signals

We next sought to determine if a pairwise Ca^{2+} response could be predicted from the Ca^{2+} response generated by the individual agonists. The mean peak of the pairwise Ca^{2+} response was not significantly different than the calculated mean peak of the agonists when applied individually (Figure 5.1 D, Figure 5.2 D, Figure 5.3 D, Figure 5.4 D). However, the summation of the peak amplitude (i.e. the addition of the peak response of the agonists when applied individually) was significantly greater than the pairwise peak Ca^{2+} response. Therefore, the amplitude of the pairwise peak Ca^{2+} response is an average of the peak response, when the agonists were applied separately.

Conversely, the measured pairwise steady state Ca^{2+} response was significantly larger than either the calculated mean or the summed steady state response of the individual agonists (Figure 5.1 D, Figure 5.2 D, Figure 5.3 D, Figure 5.4 D). Thus, the intercellular computation that integrates these responses appears to be nonlinear and synergistic for the steady-state response, in that the combined response exceeds a linear summation of each input.

5.3.4 Triplicate and Quadruplicate Agonist-Evoked Ca^{2+} Responses

We next explored the effects of simultaneous application of triplicate and quadruplicate agonists (at their respective EC_{25}) on the features of ACh, ADP, ATP and histamine evoked Ca^{2+} responses. There was a significant increase in the peak (0.30 ± 0.02 $\Delta F/F_0$ for the combination of ACh, ADP and ATP; 0.31 ± 0.01 $\Delta F/F_0$ for the combination of ACh, ADP and histamine; 0.33 ± 0.04 $\Delta F/F_0$ for the combination of

ACh, ATP and histamine; 0.34 ± 0.02 $\Delta F/F_0$ for all four agonists) and steady-state responses (0.16 ± 0.01 $\Delta F/F_0$ for the combination of ACh, ADP and ATP; 0.16 ± 0.02 $\Delta F/F_0$ for the combination of ACh, ADP and histamine; 0.17 ± 0.02 $\Delta F/F_0$ for the combination of ACh, ATP and histamine; 0.18 ± 0.02 $\Delta F/F_0$ for all four agonists) of ACh sensitive cells when agonists were applied in triplicate and quadruplicate (at all various combinations) compared to ACh alone (0.23 ± 0.02 $\Delta F/F_0$ for peak; 0.05 ± 0.01 $\Delta F/F_0$ for steady-state).

There was no significant increase in the peak response of ADP-sensitive cells, at the various triplicate and quadruplicate conditions, when compared to single agonist application (0.29 ± 0.04 $\Delta F/F_0$ for ADP; 0.33 ± 0.03 $\Delta F/F_0$ for the combination of ADP, ACh and ATP; 0.28 ± 0.01 $\Delta F/F_0$ for the combination of ADP, ACh and histamine; 0.33 ± 0.02 $\Delta F/F_0$ for the combination of ADP, ATP and histamine; 0.29 ± 0.01 $\Delta F/F_0$ for all four agonists; Figure 5.5 B and C). However, there was a significant increase in the steady-state response for ADP sensitive cells, at the various triplicate and quadruplicate conditions, when compared to single agonist application (0.02 ± 0.001 $\Delta F/F_0$ for ADP; 0.17 ± 0.01 $\Delta F/F_0$ for the combination of ADP, ACh and ATP; 0.15 ± 0.01 $\Delta F/F_0$ for the combination of ADP, ACh and histamine; 0.18 ± 0.02 $\Delta F/F_0$ for the combination of ADP, ATP and histamine; 0.19 ± 0.02 $\Delta F/F_0$ for all four agonists; Figure 5.5 B and C)

Like for ADP sensitive cells, there was no significant increase in the peak response of ATP-sensitive cells at the various combination when compared to ATP alone (0.31 ± 0.03 $\Delta F/F_0$ for ATP; 0.36 ± 0.04 $\Delta F/F_0$ for the combination of ATP, ACh and ADP; 0.29 ± 0.05 $\Delta F/F_0$ for the combination of ATP, ACh and histamine; 0.32 ± 0.02 $\Delta F/F_0$ for the combination of ATP, ADP and histamine; 0.33 ± 0.02 $\Delta F/F_0$ for all four agonists; Figure 5.5 B and C). However, there was a significant increase in steady-state response of ATP sensitive cells at the various agonist combinations when compared to ATP alone (0.05 ± 0.01 $\Delta F/F_0$ for ATP; 0.18 ± 0.01 $\Delta F/F_0$ for the combination of ATP, ACh and ADP; 0.17 ± 0.02 $\Delta F/F_0$ for the combination of ATP, ACh and histamine; 0.18 ± 0.01

$\Delta F/F_0$ for the combination of ATP, ADP and histamine; 0.19 ± 0.01 $\Delta F/F_0$ for all four agonists; Figure 5.5 B and C).

Like for purinergic agonist sensitive cells, there was no significant increase in the peak response of histamine-sensitive cells at the various combination when compared to histamine alone (0.25 ± 0.03 $\Delta F/F_0$ for histamine; 0.28 ± 0.02 $\Delta F/F_0$ for the combination of histamine, ACh and ADP; 0.28 ± 0.01 $\Delta F/F_0$ for the combination of histamine, ACh and ATP; 0.27 ± 0.02 $\Delta F/F_0$ for the combination of histamine, ADP and ATP; 0.27 ± 0.02 $\Delta F/F_0$ for all four agonists; Figure 5.5 B and C). However, there was a significant increase in steady-state response of histamine sensitive cells at the various agonist combinations when compared to histamine alone (0.03 ± 0.01 $\Delta F/F_0$ for histamine; 0.15 ± 0.02 $\Delta F/F_0$ for the combination of histamine, ACh and ADP; 0.15 ± 0.02 $\Delta F/F_0$ for the combination of histamine, ACh and ATP; 0.16 ± 0.02 $\Delta F/F_0$ for the combination of histamine, ADP and ATP; 0.17 ± 0.02 $\Delta F/F_0$ for all four agonists; Figure 5.5 B and C).

Interestingly, there was no significant difference in the peak or steady state response between each of the combinatorial responses (i.e. the different triplicate or quadruplicate combinations).

To determine if the Ca^{2+} response generated by triplicate or quadruplicate application of the agonists could be predicted from the Ca^{2+} response generated by the individual agonists, we calculated the average and summed response of the various agonist combinations. The measured triplicate and quadruplicate peak Ca^{2+} responses were not significantly different from the average peak response (Figure 5.6). However, the peak response was significantly less than the summation. Intriguingly, the steady state response was significantly greater in endothelial cells tuned to detect a specific agonist compared to both the predicted average and summation (Figure 5.6).

Collectively, these results suggest that when multiple agonists are present the peak Ca^{2+} response does not alter significantly from when an agonist is applied in isolation.

However, the steady state response is not a linear summation but instead exceeds the sum of the individual parts.

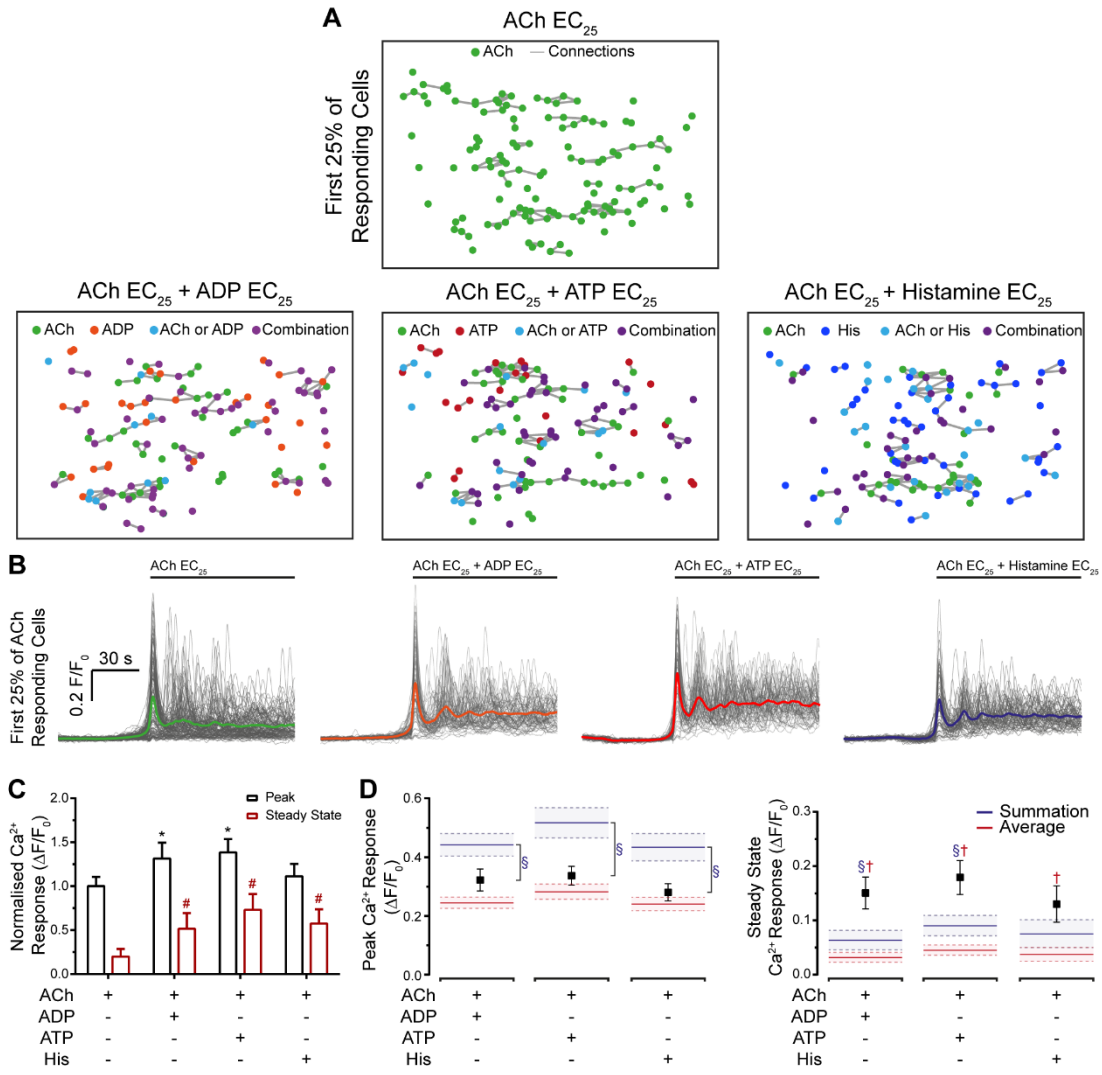

Figure 5.1 – A comparison of ACh-sensitive cells during pairwise agonist application.

(A) Spatial maps of endothelial responsivity to ACh (left, EC_{25}) or the combination of ACh (EC_{25}) and the additional agonist (EC_{25}) shown above the boxes. Coloured circles indicate activated cells, whilst lines show functional connections between neighbouring cells. Some ECs were responsive to a single activator (ACh, green; ADP, orange; ATP, red; histamine, blue), Other cells were responsive to more than one activator (light blue). Yet other cells responded only when more than one activator (combinatorial stimuli) was present (purple). (B) Peak-aligned Ca^{2+} responses from ACh-sensitive cells (to ACh, left, EC_{25}) or the combination of ACh (EC_{25}) and the additional agonist (EC_{25}) shown above the trace. Grey lines show the Ca^{2+} responses of individual cells, and the average response is the overlaid coloured line. (C) Summary data illustrating the effect of various agonists on the mean peak and steady state responses to ACh. The steady state response is taken as the signal 60 s after the initial peak. (D) Comparison of peak (left) or steady state (right) Ca^{2+} responses to combinatorial stimuli with predicted summation (blue) or predicted average (red); *$P < 0.05$ compared to control peak, $^{\#}P < 0.05$ compared to control steady state, $^{\S}P < 0.05$ compared to predicted summation, $^{\dagger}P < 0.05$ compared to predicted average, (n = 5 independent experiments), using TWO-way ANOVA followed by Dunnett's multiple comparisons test.

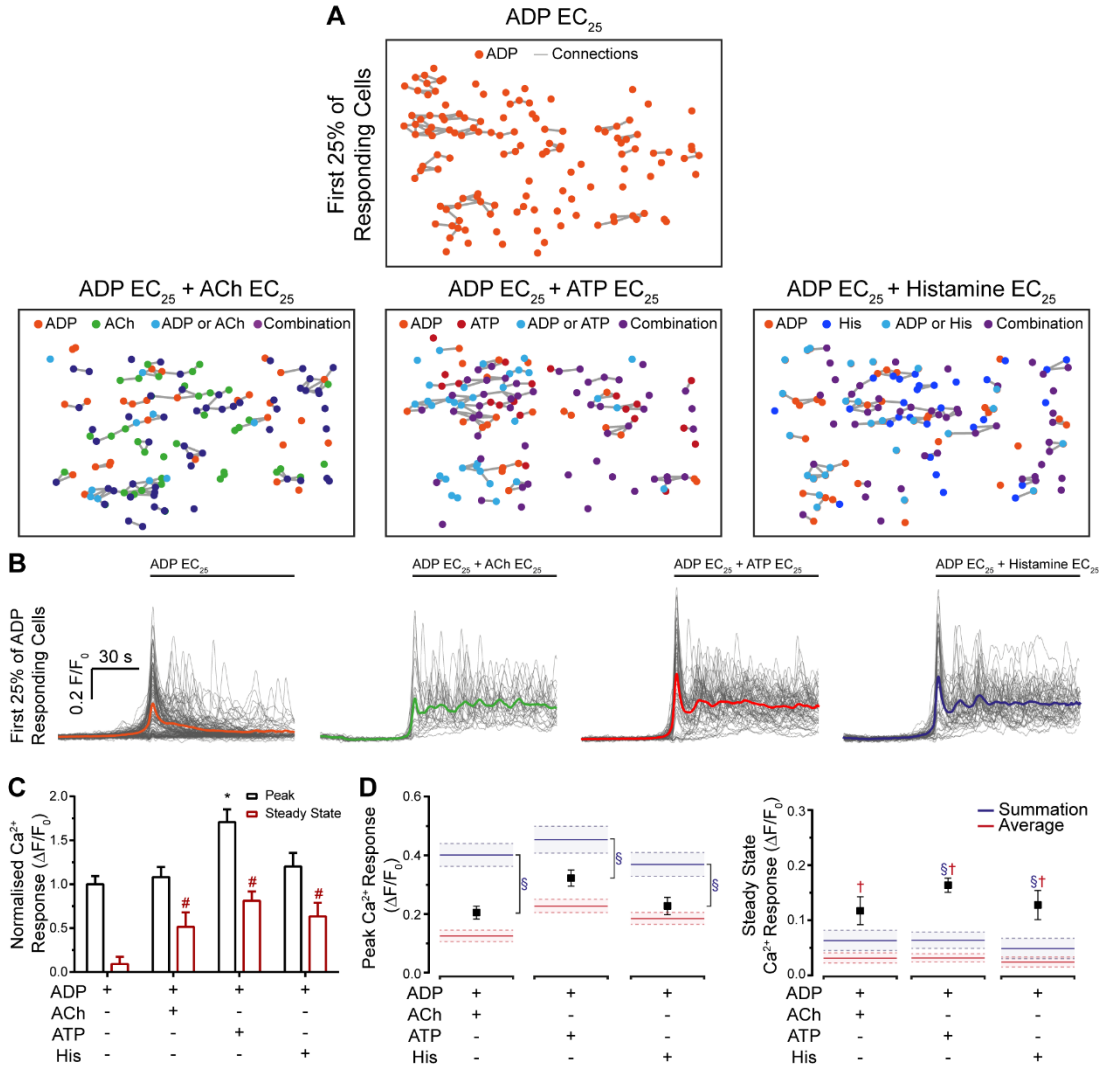

Figure 5.2 – A comparison of ADP-sensitive cells during pairwise agonist application.

(A) Spatial maps of endothelial responsivity to ADP (left, EC_{25}) or the combination of ADP (EC_{25}) and the additional agonist (EC_{25}) shown above the boxes. Coloured circles indicate activated cells, whilst lines show functional connections between neighbouring cells. Some ECs were responsive to a single activator (ACh, green; ADP, orange; ATP, red; histamine, blue), Other cells were responsive to more than one activator (light blue). Yet other cells responded only when more than one activator (combinatorial stimuli) was present (purple). (B) Peak-aligned Ca^{2+} responses from ADP-sensitive cells (to ADP, left, EC_{25}) or the combination of ADP (EC_{25}) and the additional agonist (EC_{25}) shown above the trace. Grey lines show the Ca^{2+} responses of individual cells, and the average response is the overlaid coloured line. (C) Summary data illustrating the effect of various agonists on the mean peak and steady state responses to ADP. The steady state response is taken as the signal 60 s after the initial peak. (D) Comparison of peak (left) or steady state (right) Ca^{2+} responses to combinatorial stimuli with predicted summation (blue) or predicted average (red); *$P < 0.05$ compared to control peak, $^{\#}P < 0.05$ compared to control steady state, $^{\S}P < 0.05$ compared to predicted summation, $^{\dagger}P < 0.05$ compared to predicted average, (n = 5 independent experiments), using TWO-way ANOVA followed by Dunnett's multiple comparisons test.

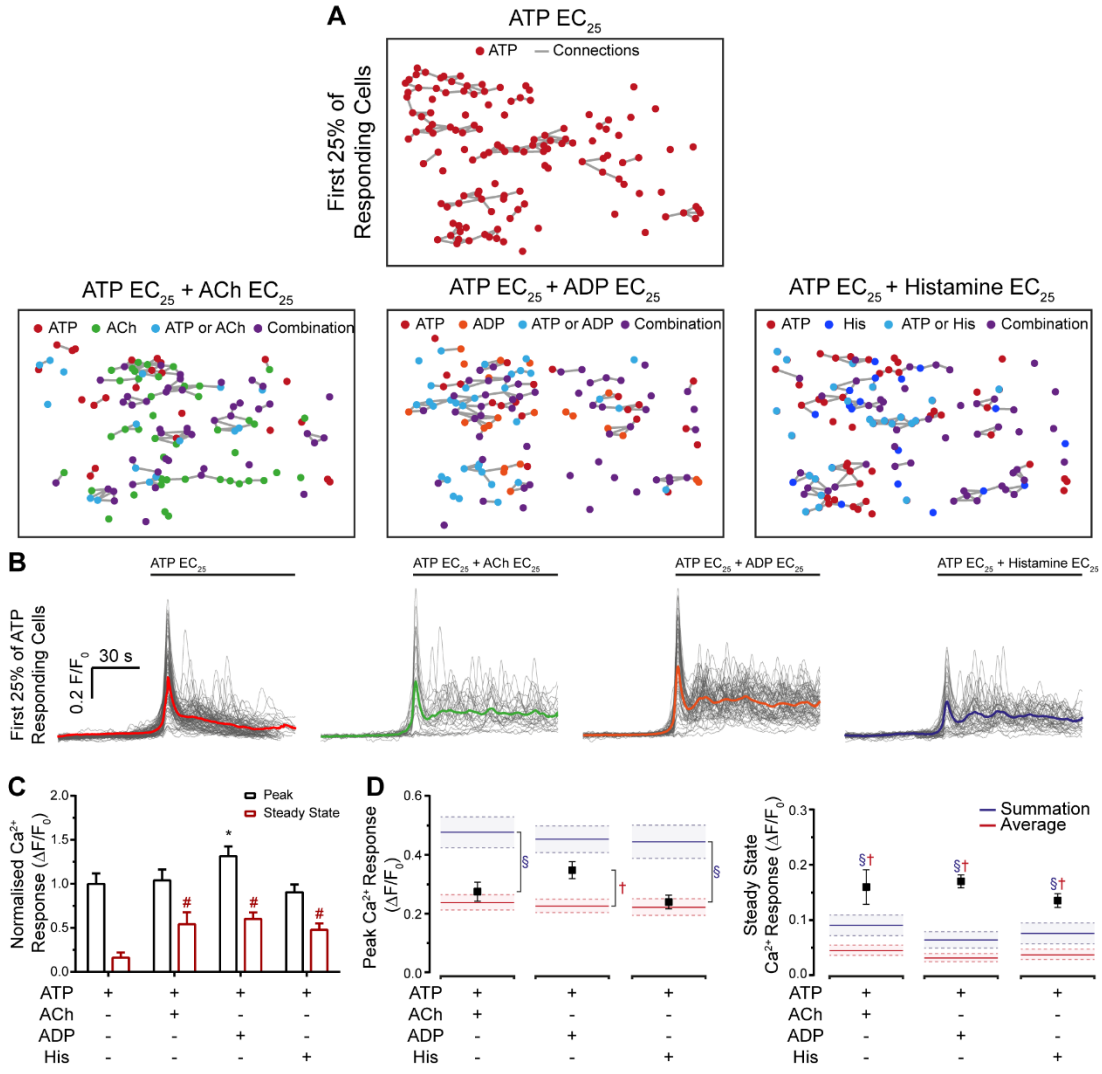

Figure 5.3 – A comparison of ATP-sensitive cells during pairwise agonist application.

(A) Spatial maps of endothelial responsivity to ATP (left, EC_{25}) or the combination of ATP (EC_{25}) and the additional agonist (EC_{25}) shown above the boxes. Coloured circles indicate activated cells, whilst lines show functional connections between neighbouring cells. Some ECs were responsive to a single activator (ACh, green; ADP, orange; ATP, red; histamine, blue), Other cells were responsive to more than one activator (light blue). Yet other cells responded only when more than one activator (combinatorial stimuli) was present (purple). (B) Peak-aligned Ca^{2+} responses from ATP-sensitive cells (to ATP, left, EC_{25}) or the combination of ATP (EC_{25}) and the additional agonist (EC_{25}) shown above the trace. Grey lines show the Ca^{2+} responses of individual cells, and the average response is the overlaid coloured line. (C) Summary data illustrating the effect of various agonists on the mean peak and steady state responses to ATP. The steady state response is taken as the signal 60 s after the initial peak. (D) Comparison of peak (left) or steady state (right) Ca^{2+} responses to combinatorial stimuli with predicted summation (blue) or predicted average (red); *$P < 0.05$ compared to control peak, $^{\#}P < 0.05$ compared to control steady state, $^{\S}P < 0.05$ compared to predicted summation, $^{\dagger}P < 0.05$ compared to predicted average, (n = 5 independent experiments), using TWO-way ANOVA followed by Dunnett's multiple comparisons test.

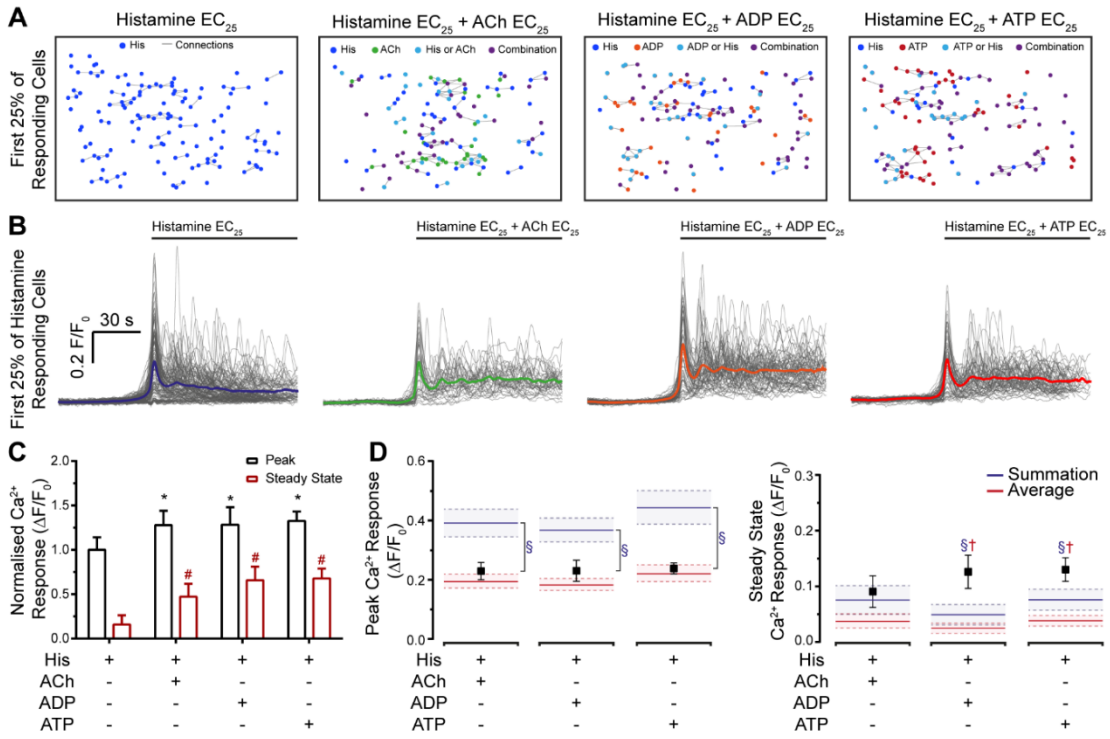

Figure 5.4 – A comparison of histamine-sensitive cells during pairwise agonist application.

(A) Spatial maps of endothelial responsivity to histamine (left, EC_{25}) or the combination of histamine (EC_{25}) and the additional agonist (EC_{25}) shown above the boxes. Coloured circles indicate activated cells, whilst lines show functional connections between neighbouring cells. Some ECs were responsive to a single activator (ACh, green; ADP, orange; ATP, red; histamine, blue), Other cells were responsive to more than one activator (light blue). Yet other cells responded only when more than one activator (combinatorial stimuli) was present (purple). (B) Peak-aligned Ca^{2+} responses from histamine-sensitive cells (to histamine, left, EC_{25}) or the combination of histamine (EC_{25}) and the additional agonist (EC_{25}) shown above the trace. Grey lines show the Ca^{2+} responses of individual cells, and the average response is the overlaid coloured line. (C) Summary data illustrating the effect of various agonists on the mean peak and steady state responses to histamine. The steady state response is taken as the signal 60 s after the initial peak. (D) Comparison of peak (left) or steady state (right) Ca^{2+} responses to combinatorial stimuli with predicted summation (blue) or predicted average (red); $^{*}P < 0.05$ compared to control peak, $^{\#}P < 0.05$ compared to control steady state, $^{\S}P < 0.05$ compared to predicted summation, $^{\dagger}P < 0.05$ compared to predicted average, (n = 5 independent experiments), using TWO-way ANOVA followed by Dunnett's multiple comparisons test.

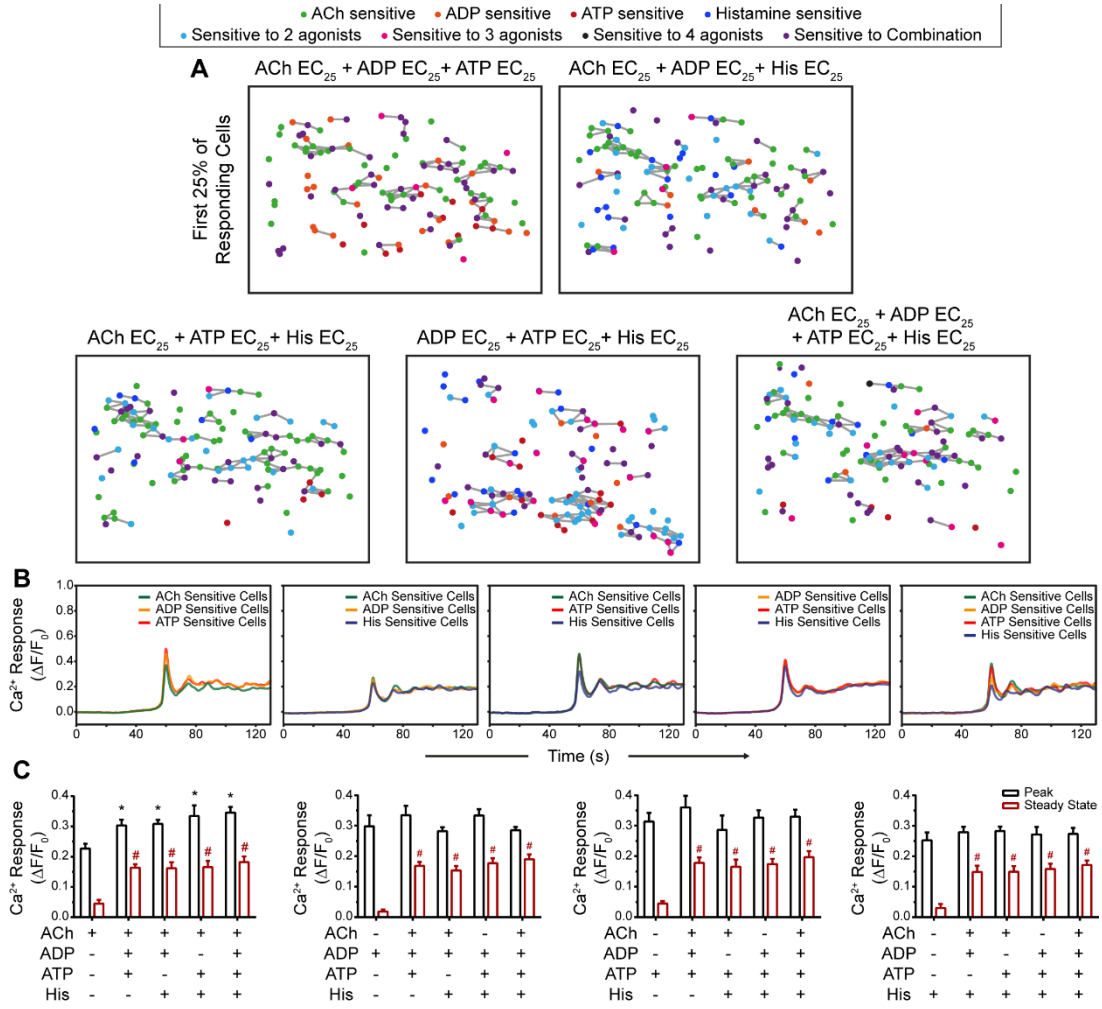

Figure 5.5 – Comparison of triplicate and quadruple agonist application.

(A) Spatial maps of endothelial responsivity to indicated combinations (EC_{25}) of agonist. Coloured circles indicate activated cells coloured circles and lines show functional connections between neighbouring active cells. Some ECs were responsive to a single activator (ACh, green; ADP, orange; ATP, red; histamine, blue) whilst other cells responded to two (light blue), three (pink) or four (black) activators. Some cells responded only when more than one agonist was present (combinatorial stimuli; purple). (B) Peak-aligned average Ca^{2+} responses from ACh (green), ADP (orange), ATP (red), histamine (blue)-sensitive cells at various combinations (EC_{25}) of agonist. Thus allowing for a direct comparison agonist sensitive cells between different combinations. (C) Summary data illustrating the effect of various agonists combinations on the mean peak and steady state (mean response 60 s after initial peak) responses compared to single agonist application. *P < 0.05 compared to single agonist peak, $^{\#}$P < 0.05 compared to single agonist steady state, (n = 5 independent experiments), using One-way ANOVA followed by Dunnett's multiple comparisons test.

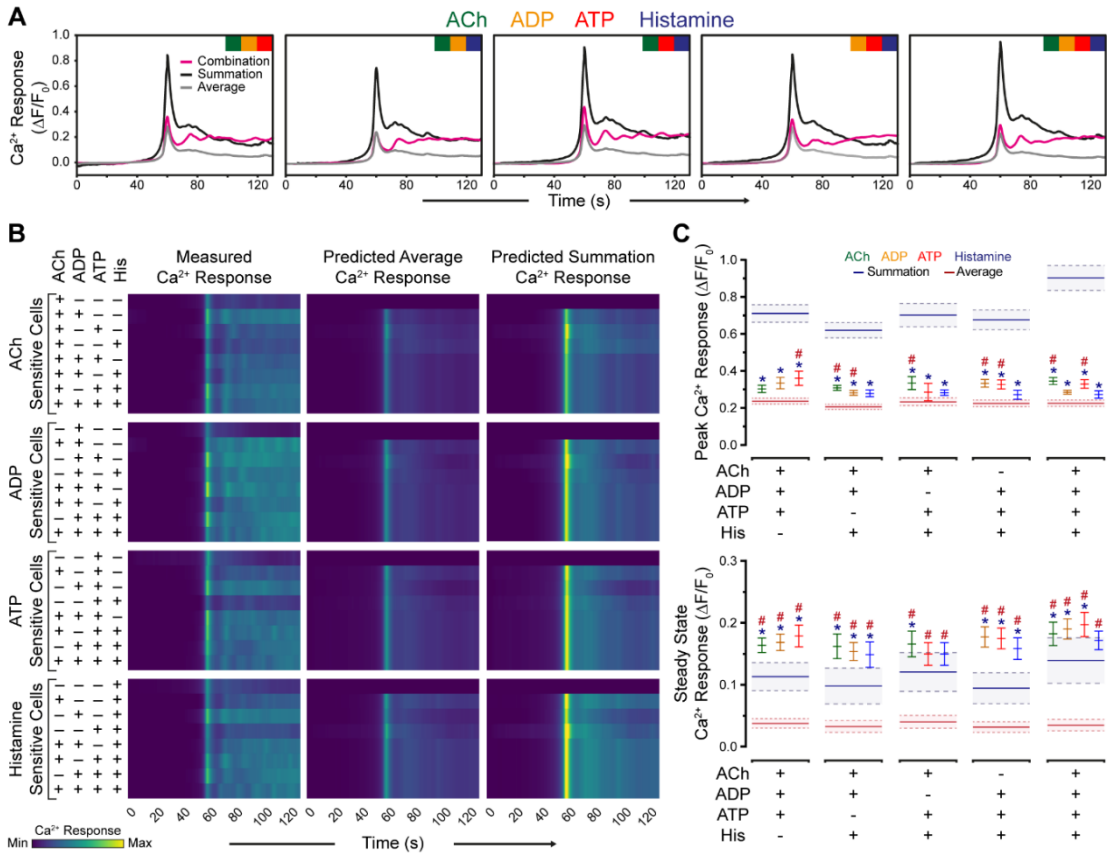

Figure 5.6 – Prediction of summation & average.

(A) Peak-aligned average Ca^{2+} responses to various agonist combinations (pink). The predicted summation (black) and predicted average (grey) of the combination, calculated from the individual agonist (EC_{25}) Ca^{2+} responses are shown. (B) Heatmap representation of measured and predicted Ca^{2+} response, of ACh, ADP, ATP and histamine sensitive cells at various agonist combinations. (C) Comparison of peak (top) or steady state (bottom) Ca^{2+} responses to combinatorial stimuli with predicted summation (blue) or average (red) models. *P < 0.05 compared to predicted summation, #P < 0.05 compared to predicted average, (n = 5 independent experiments), using TWO-way ANOVA followed by Dunnett's multiple comparisons test.

5.4 Discussion

To control cardiovascular function, the endothelium must process an enormous quantity of information, held in the chemical environment to which it is exposed. In this study it has been shown that different agonists evoke distinct Ca^{2+} signals and the Ca^{2+} signals are shared amongst cells. When more than one stimulus is present new distinct Ca^{2+} signals are generated, which are composites of the individual signals. Thus, cells in the vascular endothelium collaborate with network partners and carry out computations on the input signals to integrate the entire information held in extracellular stimuli.

The endothelium controls virtually all cardiovascular activity and must, as a consequence, sense and respond to numerous signals that direct physiological output (Aird, 2012). Many (Dora et al., 1997; Noren et al., 2016; Tran et al., 2000) though not all (Stolwijk et al., 2016) extracellular activators are transduced to changes in intracellular Ca^{2+} concentration to evoke specific cell activities. In most studies examining endothelial Ca^{2+} signalling, activators are applied separately, one at a time. Although this approach has revealed many of the mechanisms utilised by the endothelium to detect and relay the information held in the extracellular stimuli, it may not represent the complexity of activator action on the endothelium that occurs *in vivo*. Few studies have examined how the endothelium responds when multiple agonists are simultaneously applied. Our results show that when multiple agonists are applied in combination some cells were sensitive to only one agonist (*unimodal* cells), whilst others were sensitive to two, three or four agonists (*multimodal* cells). When agonists were applied separately, the Ca^{2+} response in multimodal cells were distinctive for each agonist. This observation suggests that the signals evoked by each agonist are a feature of the agonist acting on the cells, rather than a feature of the cell itself.

While Ca^{2+} responses were distinctive for each agonist when applied singly, when multiple agonists were present, new signals were generated that were distinct from

the individual responses. This observation suggests that cells perform computations by combining information from each signal to generate a new output. Presumably in multimodal cells these new signals, that were generated when multiple agonists were present, occur due to the expression of different receptors. However, changes to the Ca^{2+} response when multiple agonists were present, also occurred in unimodal cells (i.e. cells that respond to only one agonist). We have previously shown that cells that responded to only one activator and did not respond to a second agonist (even at high concentrations) showed modification of the Ca^{2+} response when both agonists were present at the EC_{25} (Lee et al., 2018). Therefore, it seems likely that cells receive signals (Ca^{2+} or IP_3) from neighbouring cells to alter responses when multiple agonists are present.

Taken together these results suggest that different stimuli evoke distinctive signals in endothelial cells, that the input/output relationship for a given cell and agonist is not fixed and that cells act as computational elements when more than one signal is present. The precise nature of the computation is not clear but it appears that it is not a simple summation or averaging of each separate signal. In the case of the steady-state response, the computation appears to be non-linear and expansive in that the combined response exceeds linear summation of each input. The computation is a feature emerging from the collective dynamics of the endothelial network and provides a mechanism for the endothelium to interactively monitor external environments via sensing that is distributed across separate cells. This arrangement may give rise to the diverse function in the endothelium arising from a fixed network structure that communicates using a single signalling molecule (Ca^{2+}).

As a collective, the endothelium has properties that exceed the capabilities of single cells. This feature is not unique to the endothelium. Biological systems are recognised increasingly as having properties that are distinct from the individual components of the system (Carmichael, 2016; He et al., 2014; Londono et al., 2014; Parrish et al., 2002). New distinct features often arise from interactions and give rise to behaviours that are absent when cells are examined in isolation. New features that arise when

components interact are referred to as emergent features (Carmichael, 2016; Kesić, 2016). The emergent properties of the endothelium generate a system in which the whole is not equal to the sum of the individual parts. The difference between the behaviour of individual cells and the population average result in the endothelium being capable of processing more information, more precisely, than cells acting alone. These features have important implications for basic investigations on endothelial function and on drug discovery (see below).

Intriguingly, the initial peak Ca^{2+} response did not alter significantly between single and multiple agonist application (with the exception of ACh-sensitive cells). However, the steady state response increased significantly at the various agonist combinations. This may suggest that the peak (initial Ca^{2+} release from the ER, Chapter 3) plays less of a role in the mediating the response during prolonged exposure to a stimulus. Instead, the interplay between ER Ca^{2+} release, influx of Ca^{2+} across the plasma membrane and re-uptake of Ca^{2+} to the ER (steady state) may have a more prominent role. Examination of the subcellular regions of the initial Ca^{2+} response to combinatorial agonist application in multimodal cells, may reveal the mechanisms involved in maintaining a constant, invariable peak response.

Key to understanding the interactions that occur in the endothelium is one defining principal – the endothelium exists in a complex steady-state. The system resists changes and will continuously work back towards the steady-state value to maintain cardiovascular function. The steady-state condition is maintained by numerous interactions and feedback in the system (Kotas and Medzhitov, 2015). In cardiovascular disease, alterations of key components (enzymes, ion channels) may trigger a change which forces the entire system into a new steady-state, albeit one that is dysfunctional. However, the new dysfunctional condition will once again be maintained in a steady-state by multiple altered interactions and feedbacks occurring among enzymes, metabolic processes and ion channels. As a result, there are multiple changes in the function of the components of the system (e.g. enzymes, ion channels). However, most of the changes will be consequences rather than causes of

cardiovascular disease. Indeed most are, in fact, beneficial changes acting to stabilise the system and halt or limit the progression of the disease (Figure 5.7). Amongst the numerous changes that occur, the triggering, initiating, event may not be easy to identify. Therefore, targeting pathways blindly, as is done through reductionism (e.g. identified with proteomics), may have adverse effects as stabilising 'beneficial' changes will almost certainly be targeted. Pharmacologically altering the behaviour of a biomarker/protein may not restore the system. Instead, these pharmacological agents may cause additional changes in overall function of the system and yet another new steady-state could arise. The interactions and feedbacks that occur in complex systems may explain why the development of successful drugs in treating cardiovascular disease has remained minimal. A successful approach for rational therapeutic development in any system with emergent properties will require an understanding of the multiple interactions among vital components that support the entire network's structure and function, and how the interactions change in cardiovascular disease.

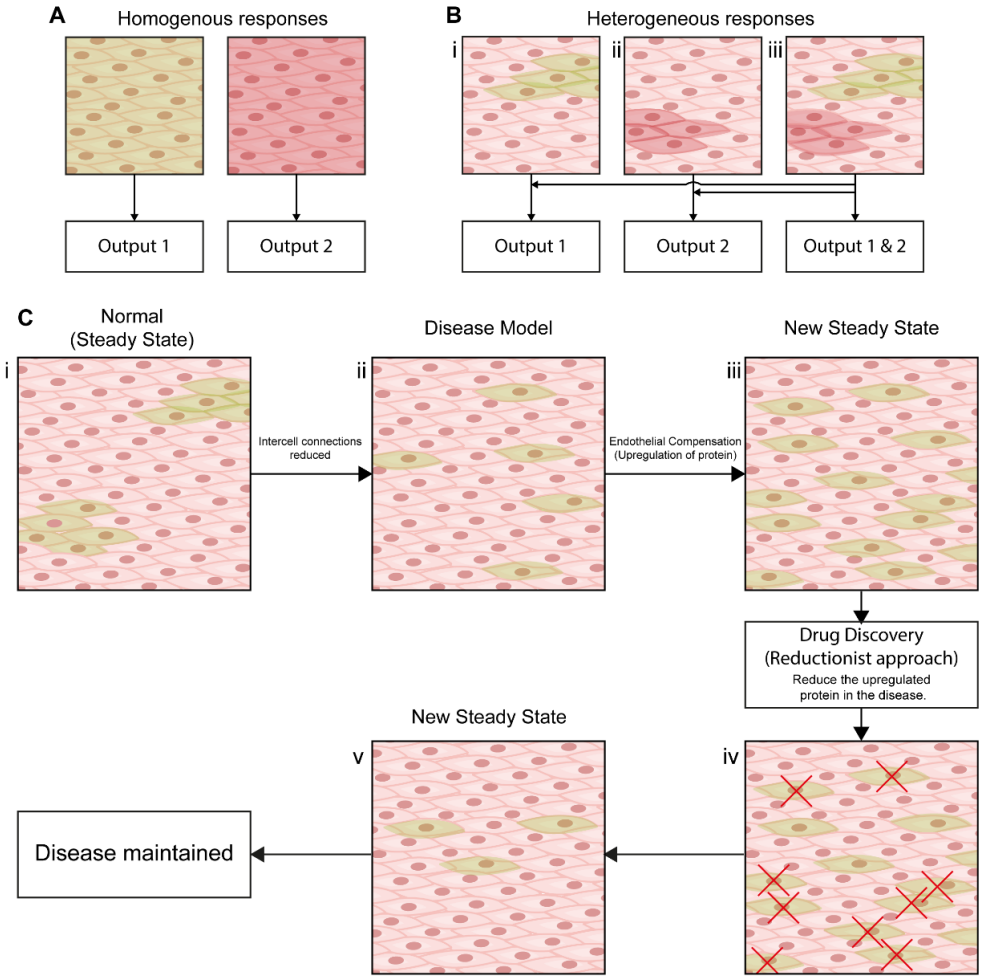

Figure 5.7 – Uniformity, heterogeneity and reductionism.

(A) Illustration of a homogenous population of endothelial cells responding to a single stimulus. The response is uniform across the endothelium to either stimulus (red or green) and a single output is generated for each stimulus. (B) Illustration of a heterogeneous population of cells responding to one (Bi and ii) and two (Biii) different stimuli. Separate spatially distinct clusters of cells process and respond to each activator to generate specific outputs. When both agonists are present multiple outputs can be generated. (C) Illustration showing a reductionist approach to drug discovery. The normal, steady-state behaviour present in health (Ci) may be disrupted in disease (Cii). The endothelium may compensate for this alteration by upregulating proteins in other cells to restore a near normal steady-state in disease (Ciii). A reductionist approach to drug discovery, that measures the individual components, may attribute this upregulation to the dysfunction in disease rather than the compensatory mechanism employed by the endothelium to overcome the disease. Targeting this upregulated protein may force the endothelium into another new steady-state that is not beneficial (Civ) which lacks the compensatory mechanism (Cv) present before pharmacological intervention.

Chapter 6. VasoTracker

6.1 Introduction

Blood vessel diameter is a critical regulator of the flow of blood. Cardiovascular disease conditions associated with diabetes, obesity and hypertension are frequently associated with altered blood flow regulation as a result of changes in blood vessel diameter (Durante et al., 1988; Li and Bukoski, 1993; Mulvany et al., 1978; Touyz et al., 1995). As such, the measurement of vessel diameter is often used to assess vascular function (Angelsen and Brubakk, 1976; Lee et al., 2009; Qamar et al., 1986). Conceptually, the relationship between blood flow and vessel diameter is simple. An increase in vessel diameter results in an increase in blood flow due to a decrease in the forces that oppose the flow of blood (e.g. friction). Conversely, a decrease in vessel diameter results in a decrease in blood flow. However, despite the simple relationship between flow and diameter, there are complex interactions between endothelial cells, smooth muscle cells and pericytes that govern blood vessel diameter and thus blood flow.

One methodology to measure artery diameter in isolated, *ex vivo*, artery preparations is pressure myography. In pressure myography there is minimal manipulation of the artery and many of the physiological responses that occur in vivo are retained (e.g. development of spontaneous basal tone and myogenic activity) (Buus et al., 1994). Pressurized arterial preparations allow the study of microvascular function in near-physiological conditions (Jadeja et al., 2015). In pressure myography blood vessels are cannulated and connected to a perfusion system than can alter the intraluminal pressure of the blood vessel and maintains the normal *in vivo* configuration of the artery.

The simplicity, practicality, and fidelity of the pressure myograph for assessing artery function *ex vivo* is evidenced by its widespread adoption in vascular research labs. The majority of pressure myographs used in vascular research are commercial systems that are available from two principal suppliers (Danish Myo Technology, Denmark, and Living Systems Instrumentation, United States). While these systems are robust and accurately monitor vessel diameter and pressure, their flexibility and

adaptability are limited. Moreover, the systems themselves are rather costly. Here, we describe the construction and use of a complete pressure myograph system, VasoTracker, with heated myograph chamber, temperature controller, pressure head and pressure monitor, microscope, computer, and diameter analysis software. The design of the system is open source and, as such, we make available a complete component list, design files, software, and instructions for building and operating the system/software. This approach follows the route taken by the OpenSPIM project, where the release of microscope blueprints has spurred on an entire community of researchers to build their own instruments (Girkin and Carvalho, 2018; Pitrone et al., 2013).

VasoTracker (Figure 6.1) provides measurement of outer diameter, lumen diameter, wall thickness, control and measurement of intraluminal pressure and temperature in a range of blood vessel sizes. In designing VasoTracker, we wanted to produce a system that might lower the cost of pressure myography and help expand the use of the technique in both research and teaching laboratories, whilst also increasing the flexibility of the method and enabling easier integration with other experimental approaches (e.g., other imaging techniques). To achieve this, we have, as much as possible, built VasoTracker using existing open source hardware and software solutions. Control electronics are based on open source Arduino microcontrollers and associated open source expansion boards (called “shields”) that extend the Arduino’s capabilities. The VasoTracker software is written in the open source programming language, Python, using libraries from the open source software for microscope imaging, μManager (Stuurman et al., 2010). The analysis of vessel diameter using VasoTracker is comparable to other commercially available products with the added benefit of being readily adaptable by other researchers.

6.2 Methods

6.2.1 VasoTracker Hardware Overview

In order to study vascular function blood vessels were mounted in a bath chamber between two cannulae. Each cannula is connected to one of two height-adjustable reservoirs. An increase in the height of both reservoirs will result in an increase in intraluminal pressure. However, when the heights of the reservoirs are offset solution will flow from the higher of the two reservoirs to the lower resulting in flow through the lumen of the artery. Therefore, experiments may be conducted with, or without, flow through the lumen of the vessel. Pressure is monitored by inline pressure transducers and an Arduino-based data acquisition system. The vessel chamber itself contains heating elements that enable experiments to be performed at physiological temperatures, avoiding the need for superfusion. Temperature is measured and controlled by an additional Arduino-based temperature controller. Blood vessels are imaged using a CCD camera attached to the microscope camera port (Figure 6.1). The VasoTracker software, displays images of the mounted blood vessel and permits real time traces of vessel diameter (inner and outer), temperature and transmural pressure.

6.2.2 Vessel Chamber

The VasoTracker vessel chamber is constructed from two components; a metal (aluminium) insert and an acrylic base (holder), which are held together by two thumb screws (Figure 6.2). The materials were chosen to provide efficient heat transfer to the bath solution via two resistive heating elements. Mounted on each end of the chamber base are cannula holders (MSC-1 M, Siskiyou, OR, United States). The cannula holders are held in place by 3-axis translation stages (DT12XYZ/M, Thorlabs, Newton, NJ, United States) that enable simple and precise axial alignment of the cannula and positioning of the blood vessel. A window, centred in the bottom of the chamber and sealed with a circular coverslip, permits light transmission and allows the chamber to be mounted on either upright or inverted microscopes. The

base of the chamber is studded with neodymium magnets that allow plumbing to be held in place with magnetic holders for perfusion (of drugs) or oxygenation.

6.2.3 *Temperature Controller*

VasoTracker utilizes a built-in heating system to maintain the chamber temperature that allows experiments to be carried out at physiological temperatures (37°C). Two resistive heating elements (Kool-Pak 0.2Ω, Caddock, Riverside, CA, United States) are mounted on the imaging chamber base together with a temperature sensor (10k NTC Thermistor, Adafruit, New York City, NY, United States). A low-cost Arduino data acquisition system consisting of an Arduino Uno, a Wheatstone bridge shield (RB-Onl-38, RobotShop, Mirabel, QC, Canada) and an LCD display shield (LCD 1602, iTead Studio, Shenzen, China) was used to set (by the user) and display the temperature. The temperature controller (Arduino) uses a simple "bang-bang" control method that switches the heaters on/off when the bath temperature is below/above this desired temperature, as appropriate (Figure 6.3). This method of heating control achieves stability of better than ± 1°C. The temperature controller and the temperature acquisition software were designed and written by Dr Calum Wilson.

6.2.4 *Pressure Controller*

To enable pressure to be applied to cannulated blood vessels, each cannula is connected to an independent reservoir (20 ml syringe). Magnets attached to the syringe allow the height of the reservoir to be easily adjusted by changing the position on a magnetic rail, thus setting the hydrostatic pressure at the level of the artery in the chamber. The pressure set by column height is monitored by flow through pressure transducers (26PCDFG5G, Honeywell, Morris Plains, NJ, United States) and a low-cost Arduino data acquisition system consisting of an Arduino Uno, a Wheatstone bridge shield (RB-Onl-38, RobotShop, Mirabel, QC, Canada) and an LCD display shield (LCD 1602, iTead Studio, Shenzen, China). The pressure is recorded and displayed on the VasoTracker software via the Arduino serial port.

6.2.5 *VasoTracker Software*

The VasoTracker software allows the acquisition, display and recording of images of pressurized blood vessels as well as the acquisition and recording temperature and pressure from the Arduino control systems. Furthermore, VasoTracker permits the real time calculation, graphing, and recording of blood vessel diameter.

6.2.6 *Blood Vessel Diameter Analysis Algorithm*

The VasoTracker system measures artery outer and inner diameter by taking advantage of variations in intensity that are present in images of pressurized blood vessels. These variations arise because the artery is held orthogonal to the z-axis of the microscope system such that only the mid-plane of the artery is in focus. When imaged in this way, alterations in the optical density of the vessel, which manifest as changes in the intensity profile, permit the wall of the artery to be easily identified (Figure 6.4). Edges of the blood vessel correspond to rapid changes in light intensity profiles that are measured perpendicular to the long axis of the blood vessel (scan lines). VasoTracker identifies these rapid changes by detecting peaks in the derivative of the intensity profile (integrated across 25 pixels). Vessel diameter is calculated for a default number, 20 (which can be changed), of equally spaced scan lines along the width of the artery, and averaged to give a reliable measure of outer and inner diameter. For each of the scan lines, outer and inner diameters are indicated on the real-time image feed by a blue or red line, respectively (Figure 6.5).

In cases where the presence of side-branches, adherent fat/connective tissue, or debris cannot be avoided, the tracking algorithm may fail to accurately track the vessel wall. VasoTracker has two features that minimize errors in these circumstances. First, the modified z-score test can be used to identify and exclude outliers from the average diameter calculation and these are indicated on the live image feed by black lines (Iglewicz and Hoaglin, 1993). Second, a region of interest may be added to the live image recording that avoids side-branches or adherent

fat/connective tissue. VasoTracker will then use this ROI to track diameter (Figure 6.5 A).

6.2.7 Solutions and Drugs

Solutions and drugs are described in Chapter 2. In experiments designed to determine the role of passive properties of the vascular wall normal PSS was replaced with Ca^{2+}-free PSS. Ca^{2+}-Free PSS consisted of: 145 mM NaCl, 4.7 mM KCl, 2.0 mM MOPS, 1.2 mM NaH_2PO_4, 5.0 mM glucose, 0.02 mM EDTA, 1.0 mM EGTA, and 2.34 mM $MgCl_2$, adjusted to pH 7.4 with NaOH.

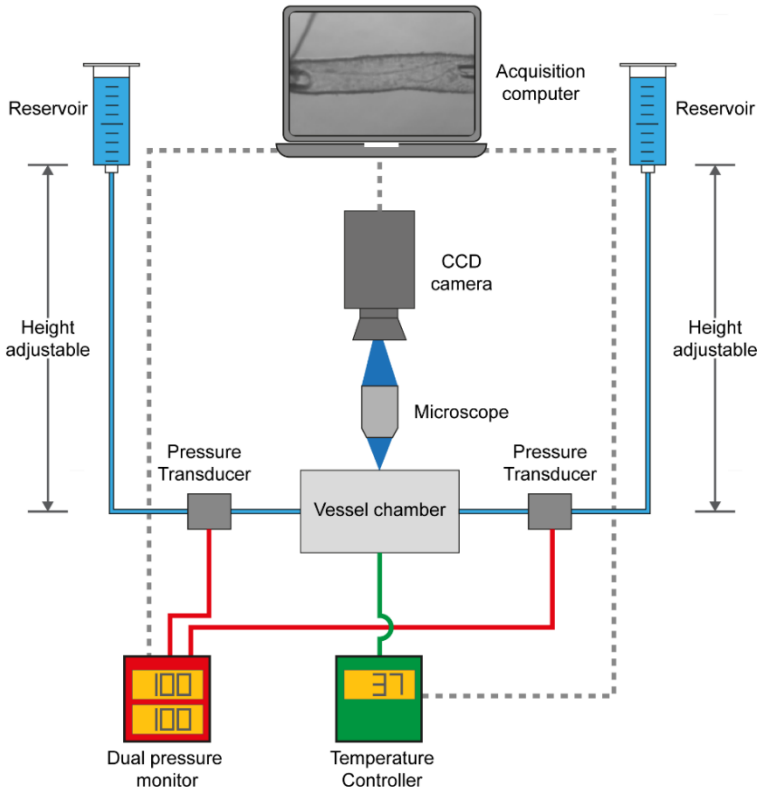

Figure 6.1 – Schematic diagram of the VasoTracker components.

Schematic diagram showing the core components of the VasoTracker system. Arteries are mounted in a custom vessel imaging chamber and imaged by a large-format CCD camera mounted on a microscope. Intraluminal pressure and flow are controlled via two height-adjustable reservoirs. Pressure is monitored by an Arduino pressure monitor. The imaging chamber temperature is controlled by a second Arduino. Image, pressure, and temperature data is acquired, stored and displayed by the acquisition software that automatically determines outer and inner blood vessel diameter.

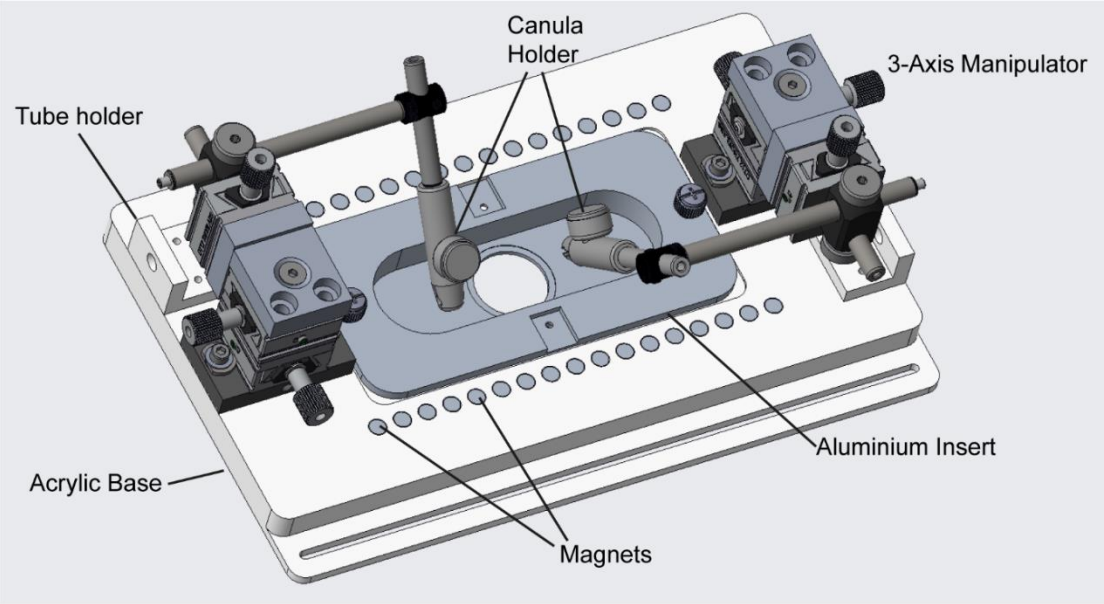

Figure 6.2 – VasoTracker chamber.

3-dimensional rendering of the VasoTracker Chamber. An aluminium insert sits within the acrylic base, held together by two thumb screws. The base of the chamber is studded with magnets to allow perfusion or oxygenation plumbing to be held in place. Mounted on each end of the chamber base are cannula which are held in place by 3-axis translation stages that enable simple and precise axial alignment of the cannula and positioning of the blood vessel. A window, centred in the bottom of the chamber and sealed with a circular coverslip, permits light transmission and allows the chamber to be mounted on either upright or inverted microscopes.

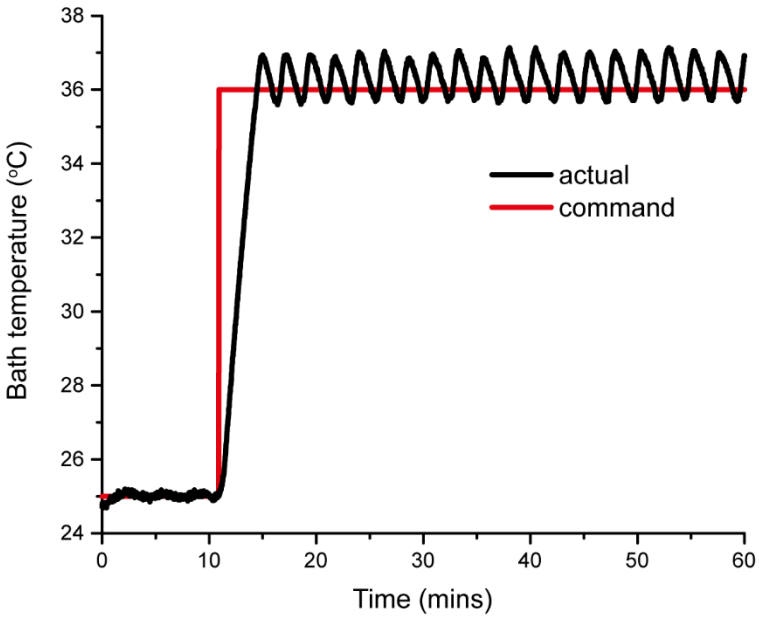

Figure 6.3 – VasoTracker temperature controller response curve.

The curves show the actual response (black line) to a step command from 25 to 37°C. The bath temperature reaches the set point in approximately 5 min and maintains this temperature with a stability better than ± 1°C.

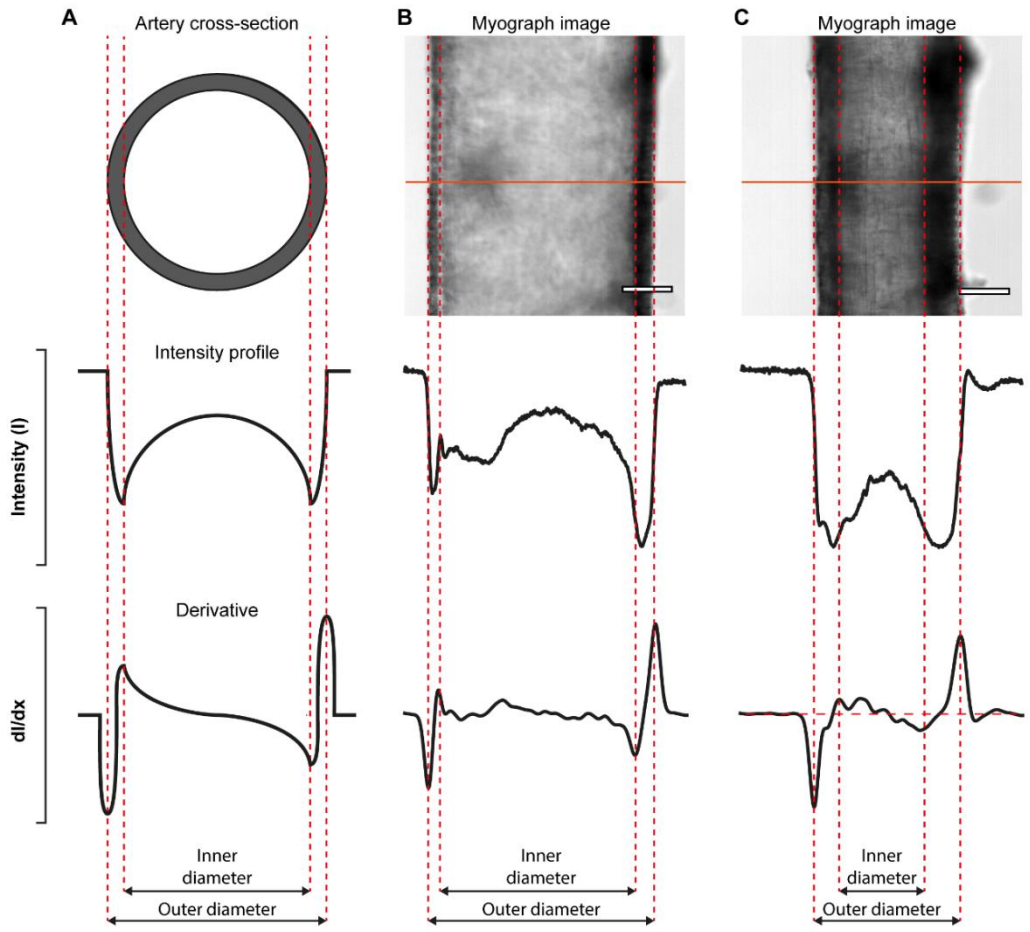

Figure 6.4 – Analysis of the inner and outer diameter of pressurized blood vessels.

(A) Schematic diagram (cross-sectional view, top) of an artery, idealized intensity profile (middle), and the first derivative of the idealized intensity profile (bottom) illustrating how peaks in the derivative profile may be used to identify the edges of an artery. (B and C) Real-data examples illustrating the algorithm. The top panels show a first-order mesenteric artery, pressurized to 80 mmHg, in the absence (B) and presence (C) of phenylephrine (1 µM). Scale bars, 100 µm.

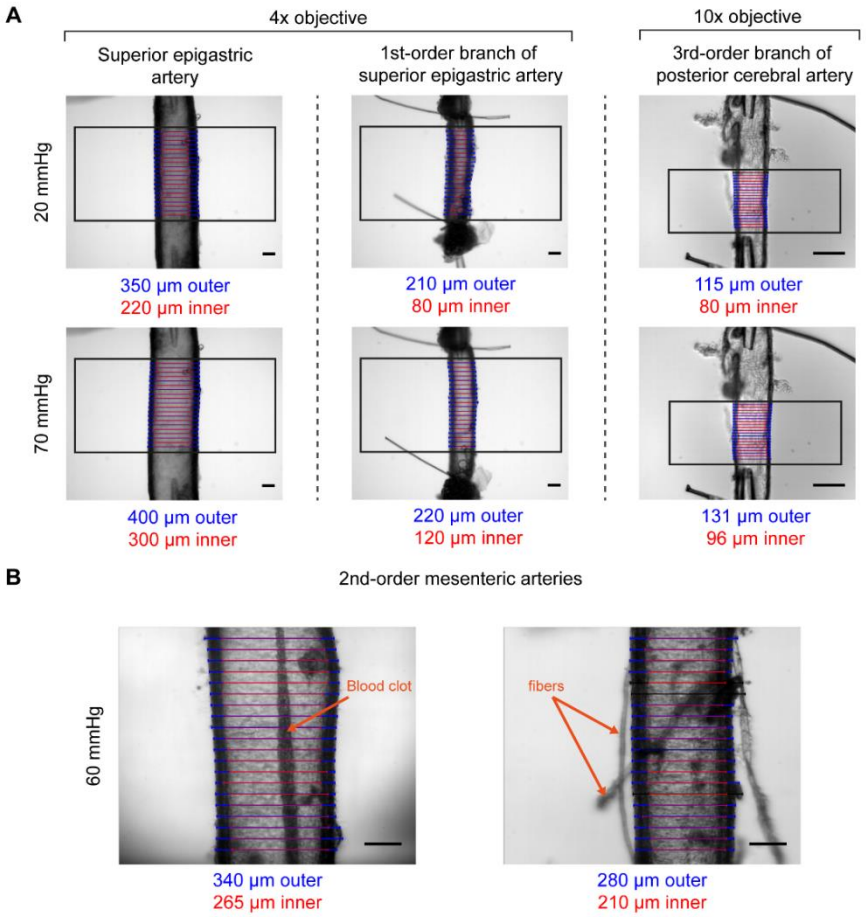

Figure 6.5 – Vessel diameter of various blood vessels.

(A) Example images showing outer and inner diameter tracking in the superior epigastric artery, a first-order branch of the superior epigastric artery, and a third-order branch of the posterior cerebral artery. Each artery was exposed to 20 mmHg and 70 mmHg intraluminal pressure, and the diameter tracking algorithm was confined to a region of interest (black box). Blue/red scan lines indicate outer and inner diameter measurements, respectively. Outliers are coloured black. (B) Example images showing diameter tracking in second-order mesenteric arteries pressurized to 60 mmHg imaged under sub-optimal conditions. The artery shown on the left has a blood clot in the middle of the lumen which could not be flushed out. The artery on the right has numerous fibres and other debris attached to the adventitia. Despite the condition of these arteries, in both examples VasoTracker was capable of accurately tracking the vessel wall. Scale bars, 100 µm.

6.3 Results

6.3.1 Pressure Myograph Experiment Verification

Pressure myography has been used extensively to elucidate the mechanisms involved in regulating vascular function. Studies using pressure myography have revealed variations in blood vessel functions between arteries from different vascular beds. Adaptations to the system have also revealed differences in vascular permeability. Here we show the records of several experiments to demonstrate the effectiveness and versatility of VasoTracker.

6.3.2 Passive Properties of Blood Vessels

Mechanical stimuli may evoke responses in both the active and passive properties of the vascular wall. To study the passive properties of the vascular wall, third order mesenteric arteries were placed in a Ca^{2+}-free bath solution to prevent SMC contraction. A cumulative increase in intraluminal pressure (0-160 mmHg), provided by increasing the height of the syringes, resulted in an increase in vessel diameter. During this recording, average inner and outer diameters were calculated for the default number of line-scans (20). Both the outer and inner diameter increased with increasing pressure until maximal diameter was achieved (Figure 6.6). The results of the tracking algorithm are shown overlaid on the original images and it is evident from these that VasoTracker is able to accurately track both the inner and outer artery wall. Studies examining the passive properties of the vascular wall are often used to assess arterial remodelling.

6.3.3 Myogenic Reactivity

A myogenic response occurs when an increase in transmural pressure or stretch results in vasoconstriction or a pressure decrease results in vasodilation. Myogenic responses are intrinsic properties of SMCs in an intact blood vessel and are independent of outside influences such as neurotransmitter, hormones or autacoids (Johansson, 1989). Myogenic responses occur predominantly in small arteries and

arterioles and may be critical to the establishment of basal vascular resistance and the regulation of blood flow. Here we show the myogenic response of the posterior cerebral artery. A small side branch of the artery was tied off (using a single strand of thread) to prevent intraluminal flow. VasoTracker was able to accurately monitor the inner and outer diameter of the blood vessel and ignore the thread in the FOV. A stepwise increase in the intraluminal pressure from 40 to 60 mmHg resulted in vasoconstriction of the artery (from 288 µm to 164 µm, outer diameter) (Figure 6.7). Conversely, a decrease in pressure (60 mmHg to 40 mmHg) relaxed the vessel back to its initial diameter.

6.3.4 Agonist Evoked Contraction and Dilation

Smooth muscle is frequently assessed by measuring blood vessel contraction and relaxation to various agonists Ca^{2+}-mobilizing agonists. Here we show that 5-HT (1 µM) applied to the vessel chamber results in vasoconstriction of the posterior cerebral artery (initial outer diameter = 185 µm), pressurised to 60 mmHg. The initial contraction was followed by the subsequent development of vasomotion (Figure 6.8 A).

The function of the endothelium can also be assessed by pressure myography. Agonists may stimulate the endothelium to release nitric oxide or endothelial-derived hyperpolarising factors to initiate vasorelaxation (Chapter 1). Damage to the endothelium may impair or even abolish these responses (Furchgott and Zawadzki, 1980). Here we show that intraluminal application of the endothelial-dependent vasodilator ACh (1 µM) induced complete relaxation in a pre-contracted second-order mesenteric artery (phenylephrine, 1 µM), pressurised to 60 mmHg (Figure 6.8 B).

6.3.5 Propagated Vasodilation

Previous studies have shown the critical role of vasodilation in regulating arterial tone. VasoTracker allows for the analysis of the diameter (outer and inner) at each individual scan line. This enables the propagation of vasodilation to be determined.

Here we show flow-induced vasodilation in a third-order mesenteric artery pre-contracted with phenylephrine (1 µM). A stepwise increase in the flow gradient (i.e. increase the height of one syringe to offset the pressure across the artery and thus induce flow) from 0 to 10 cm H_2O resulted in vasodilation at the proximal end of the artery with respect to the highest syringe (Figure 6.9). Subsequently, dilation propagated to the distal end of the artery (Figure 6.9).

6.3.6 Comparison of VasoTracker with Commercial Software

To verify the tracking capability of VasoTracker, we performed experiments using a commercial pressure myograph system (Model 110P; Danish Myo Technology) and compared the results with those of the VasoTracker algorithm. In these experiments, arteries were mounted in the Danish Myo Technology myograph chamber and visualized at 10× magnification on an inverted Nikon Diaphot microscope. Images of the arteries were obtained by a CCD video camera (Watec, WAT-902A) and relayed to a computer for online diameter measurement and graphing (performed by the vessel tracking software, MyoView). MyoView software does not record the image feed. Thus, to enable a comparison with VasoTracker to be made, the camera feed was split and fed to a USB frame grabber (Dazzle DVC 100, Pinnacle Systems, Mountain View, CA, United States) and recorded on a separate computer system by µManager software. Images were recorded for subsequent off-line analysis by the VasoTracker algorithm. VasoTracker measurements matched those obtained by the MyoView algorithm (Figure 6.10).

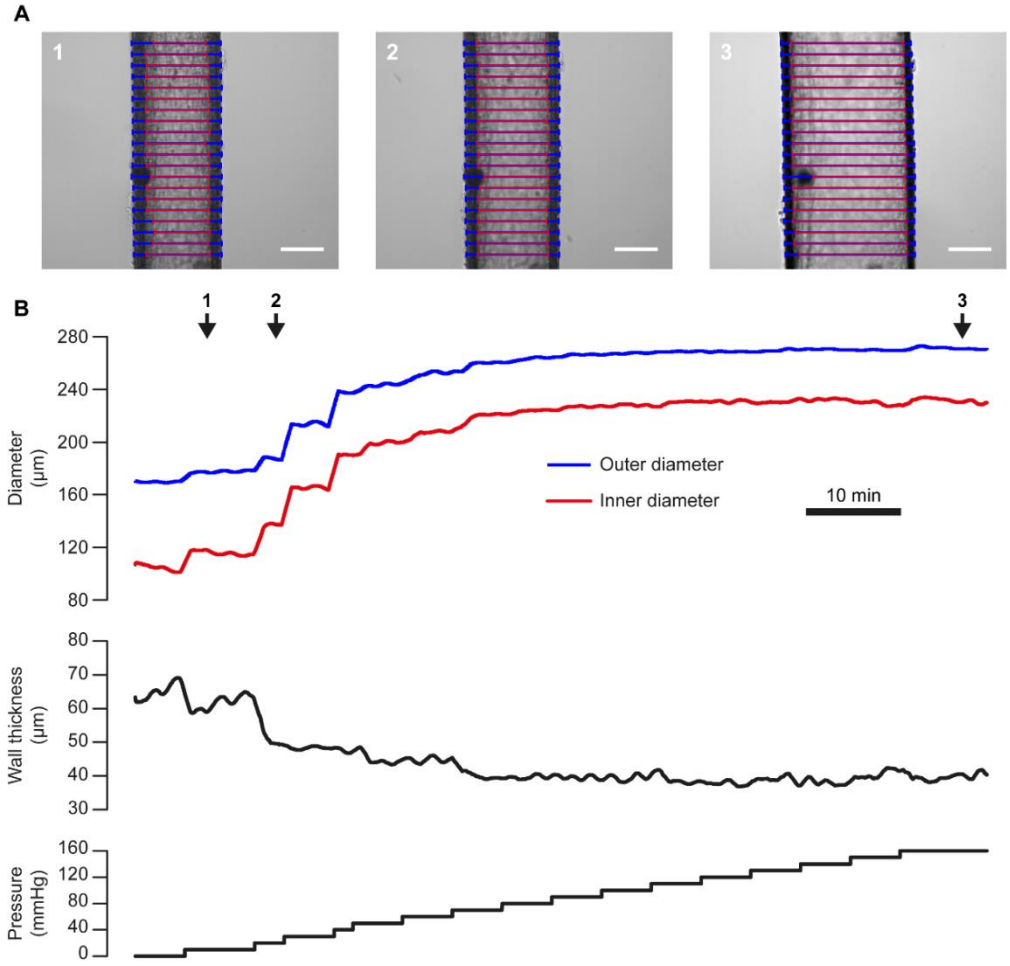

Figure 6.6 – Pressure diameter relationship.

(A) Images of a third-order mesenteric artery at three time points during an experiment in which the vessel was subject to a step-wise increases in pressure from 0 to 160 mmHg (in a Ca^{2+}-free bath solution). Blue and red lines indicate VasoTracker measurements of outer and inner vessel diameter, respectively. (B) Traces showing the full time-course of outer and inner diameter (top), wall thickness (middle), and pressure (bottom) for the experiment shown in (A). Numbered arrows indicate the time corresponding to the images in (A). Scale bars, 100 µm.

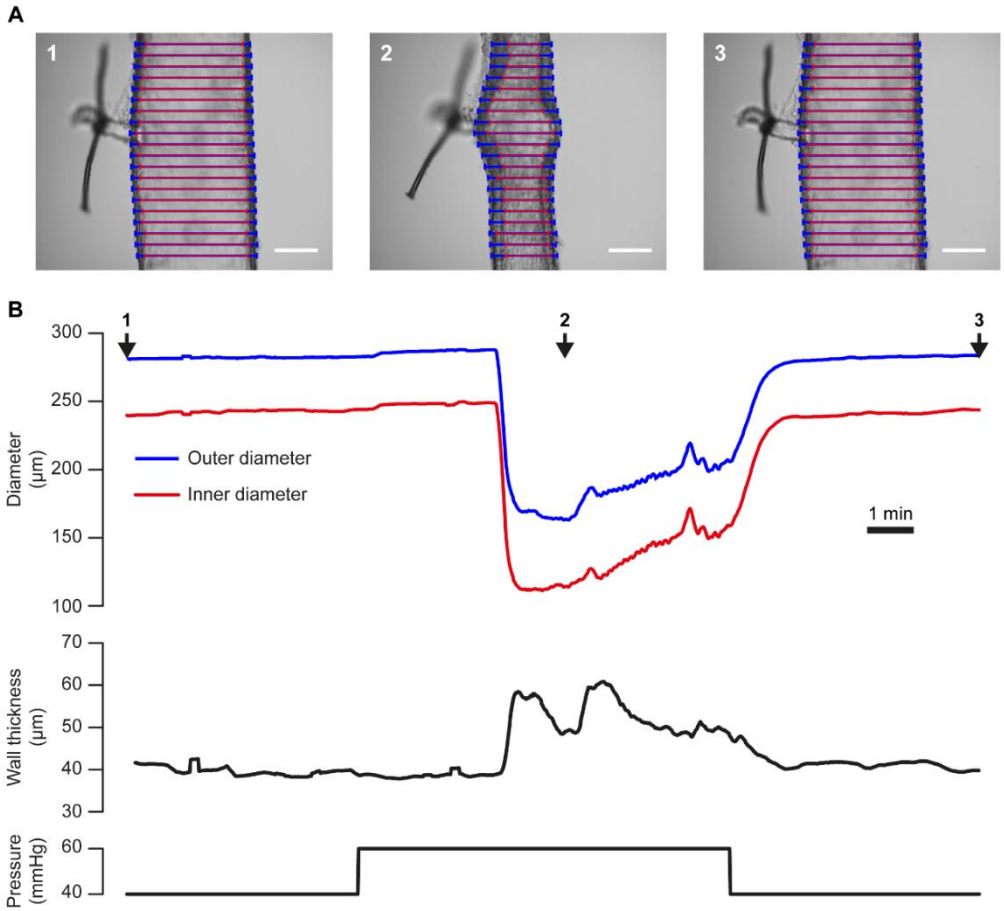

Figure 6.7 – Myogenic tone.

(A) Images of a single posterior cerebral artery during an experiment in which the vessel was subject to a step-wise increase from 40 mmHg (1), to 60 mmHg (2), and then a decrease to 40 mmHg (3), in pressure. A ~20 µm diameter side branch, which was tied off with a single strand of thread, can be seen protruding from the vessel. Blue and red lines indicate VasoTracker measurements of outer and inner vessel diameter, respectively. (B) Traces showing the full time-course of outer and inner diameter (top), wall thickness (middle), and pressure (bottom) for the experiment shown in (A). Numbered arrows indicate the time corresponding to the images in (A). Scale bars, 100 µm.

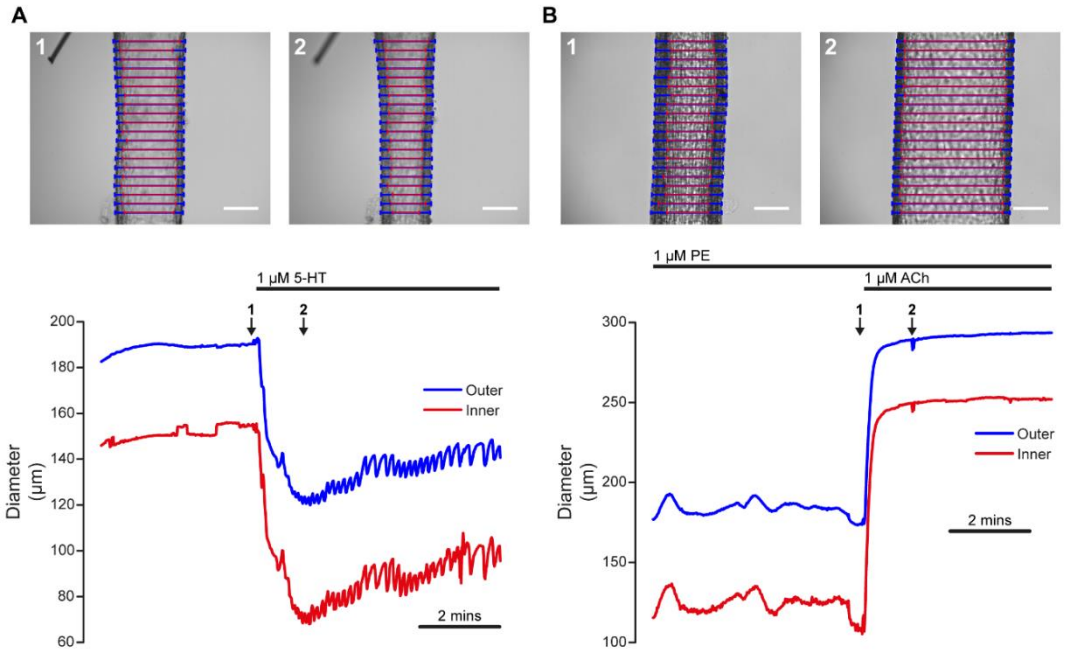

Figure 6.8 – Agonist-evoked contraction and relaxation.

(A) Time-course of contraction of a posterior cerebral artery (60 mmHg) in response to 5-HT (1 µM). The top panels show the artery before (1) and after (2) the application of 5-HT. The lower panel shows the diameter measured by VasoTracker (average of 20 line-scans). Outer (blue) and inner (red) diameter are shown. The time points corresponding to the images shown in the upper panel are indicated by the numbered arrows. (B) Time-course of dilation of a pre-contracted (Phenylephrine, 1 µM) second-order mesenteric artery (60 mmHg) to ACh (1 µM). Images show the artery before (top, 1) and after (top, 2) the application of ACh (1 µM). Again, the bottom panel shows average artery diameters (outer and inner, 20 line-scans) measured by VasoTracker for the full experiment. Scale bars, 100 µm.

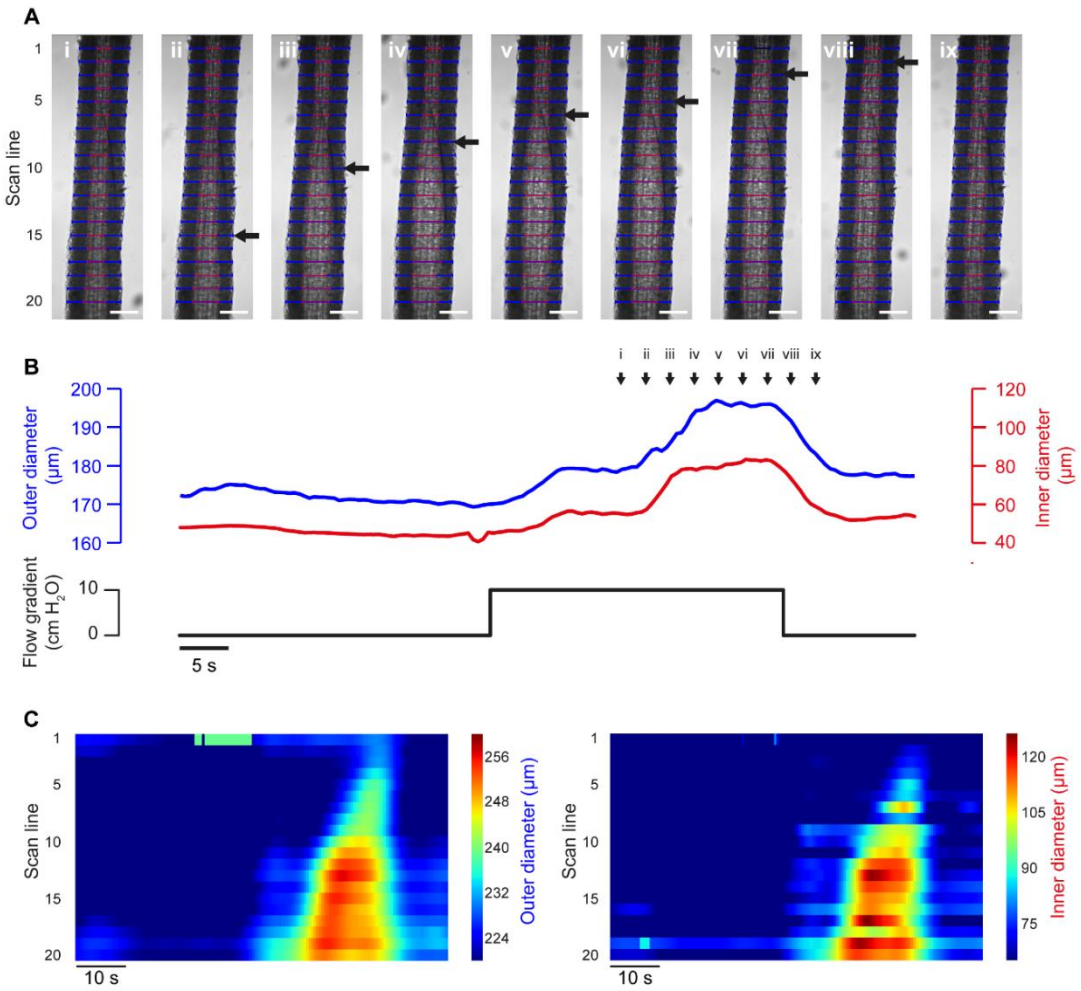

Figure 6.9 – Flow-induced propagated vasodilation.

(A) Images of a pre-contracted (Phenylephrine, 500 nM) third-order rat mesenteric artery at nine time points during an experiment in which dilation was initiated by intraluminal flow (~100 µl/min, established by a 10 cm H_2O flow gradient across the vessel). The black arrow indicates the wave front of the propagated dilation. Blue and red lines indicate VasoTracker measurements of outer and inner vessel diameter, respectively. (B) Traces showing average outer and inner diameter measurements (top) and the flow gradient (bottom) for the experiment shown in (A). (C) Heat plots showing diameter (colour) plotted against time (x-axis) for each of the scan lines (y-axis) shown in (A). Scale bars, 100 µm.

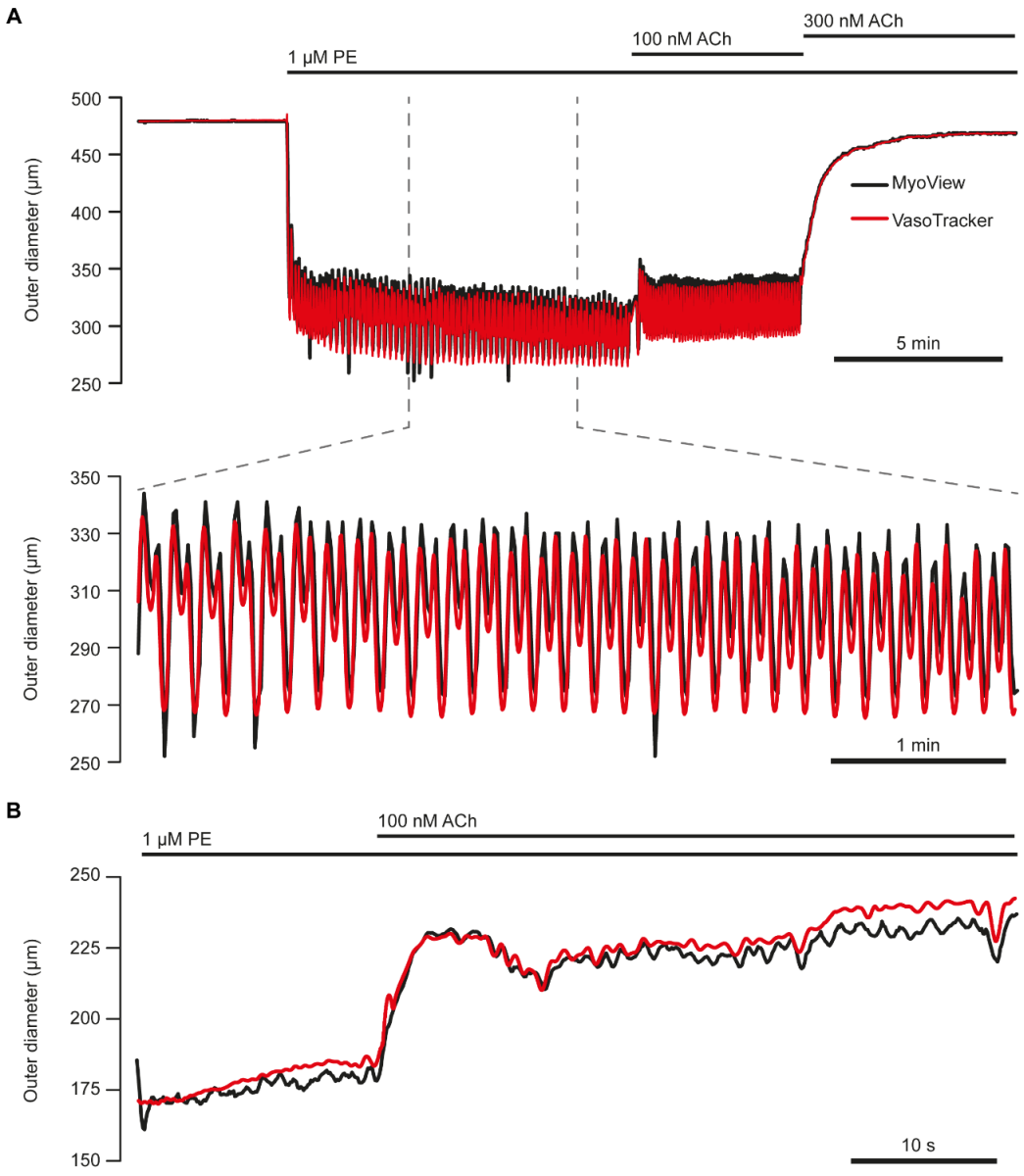

Figure 6.10 – Comparison of VasoTracker diameter tracking with commercial software.

(A) Top: full time course of an experiment in which the outer diameter of a first-order mesenteric artery (60 mmHg) was tracked by both VasoTracker (red) and MyoView (black, Danish Myo Technology). Upon the addition of phenylephrine (1 µM) to the bath, the artery contracted and developed vasomotion (shown on expanded time course in bottom panel of (A). ACh (100 nM) resulted in a slight dilation, whilst a slightly higher concentration of ACh (300 nM) abolished vasomotion and fully reversed the phenylephrine-induced contraction. (B) Example trace (VasoTracker, red; MyoView, black) showing the relaxation of a pre-contracted (phenylephrine, 300 nM) third-order mesenteric artery in response to ACh (100 nM).

6.4 Discussion

Pressure myography has enabled vascular function to be studied in controlled environments that closely resemble many *in vivo* parameters. Studies utilising pressure myography have revealed many of the features that regulate vascular function. Modifications of the original design of pressure myography have been established as new questions arose on vascular function. For example, in some myographs, one end of an artery is mounted on a cannula with the other end occluded (Halpern et al., 1984). In others, the artery is mounted on two cannula (Halpern and Osol, 1986). In another variation of the mounting technique, special double-barreled cannula are used (VanBavel et al., 1990). Transmural pressure may be established by one of two techniques: either by a pressure head where reservoirs of physiological saline are set at a height to create a pressure column and so set the hydrostatic pressure, or by a servo-controlled pump system. Together, the many myograph variants permit the study of arteries across a range of sizes and under a range of conditions and, for example, permit the effects of flow at constant pressure be studied. The capabilities of the pressure myograph has been extended further by combining it with fluorescence techniques to assess arterial diameter (Falcone et al., 1993; Garland et al., 2017; VanBavel et al., 1990). The technique has even been adapted to enable visualization of leukocyte adhesion to the endothelium and, more recently, to permit drugs to be applied to only half of the length of a single artery, allowing conducted responses to be assessed in the other half (Michell et al., 2011; Palao et al., 2018). There is a growing requirement for a pressure myograph systems that can accurately and monitor blood vessel function whilst regulating the environment to which the blood vessel is exposed and that can be easily adapted to every changing research demands.

Here we describe an inexpensive and flexible pressure myograph system, VasoTracker, which permits the vascular activity of isolated, pressurized blood vessels to be monitored. The system includes all components that would be expected from a commercial pressure myograph system: a vessel chamber for mounting

arteries; pressure columns and a pressure monitor for establishing and monitoring intraluminal pressure; heaters and a temperature controller for controlling the chamber temperature; a microscope and CCD camera for imaging; and software for acquiring images and calculating blood vessel diameter. VasoTracker is an open source system that makes use of existing hardware and software open source solutions. For example, both the pressure monitor and the temperature controller are built using Arduino electronics boards and the software was written entirely in Python.

The open source principle has created numerous system and software designs, which can be readily modified, to assist researchers in their scientific endeavours (e.g. open source syringe pumps, pulse generators, pressure ejection systems, and even microscopes) (Forman et al., 2017; Holm et al., 2014; Sanders and Kepecs, 2014; Wijnen et al., 2014). Open source technologies offer the benefit of being easy to modify and so can often be adapted to meet particular specifications better than commercial alternatives. Additionally, open source software is available at no cost, and open source instrumentation may be obtained significantly cheaper (as designs are made freely available) than commercial alternatives. In the field of vascular physiology, there are numerous examples of open source software packages making an impact: µManager Open Source Microscopy Software (Edelstein et al., 2014; Stuurman et al., 2010), is used routinely by vascular physiologists for image acquisition; as are ImageJ and FIJI for image processing applications (Francis et al., 2012; Rueden et al., 2017; Schindelin et al., 2012). However, there are limited open source hardware options available to study vascular function.

Here we have shown that VasoTracker is able to accurately monitor the inner and outer diameter and intraluminal pressure of a blood vessel, whilst simultaneously regulating the temperature in the chamber. VasoTracker provides the ability to measure diameter at up to 50 separate scan lines, and uses a statistical filtering process to minimize the contribution of such inaccurate measurements to the overall (average) diameter measurement. In addition, an ROI may also be used to limit

readings to specific areas of a blood vessel. Due to being open source there is the potential for future developments and considerable potential for researchers to expand and enhance myography with tailored vascular reactivity experiments.

Chapter 7. General Discussion

7.1 Summary of Principle Findings

The work presented in this thesis describes how individual endothelial cells form a sophisticated network that can detect multiple stimuli simultaneously. By analysing the Ca^{2+} responses in each individual cell from a large population of endothelial cells in an intact artery, we have shown that the endothelium does not respond uniformly to agonists. Instead, cells are positioned in clusters with comparable sensitivity to a specific activator. The results have also shown that the endothelium does not simply relay the information held in the extracellular activator but instead may interact with the inputs to generate new distinctive signals that differ in a non-linear way from the inputs. This thesis also describes a new robust hardware and software system to study arterial function using pressure myography. VasoTracker is freely available and the open source properties of the system allow for more flexibility and adaptation than commercially available products.

Here, we demonstrate that ACh, ADP, ATP and histamine activate different subtypes of GPCRs on the vascular endothelium. Canonical GPCR signalling involves PLC activation and subsequent PIP_2 breakdown into IP_3 and DAG (Dennis et al., 1991; Harden et al., 2011; Nakamura and Nishizuka, 1994). IP_3 readily diffuses to the ER where it elicits its effects via IP_3Rs to cause release of Ca^{2+} from the internal store into the cytoplasm. This resulting decrease in store Ca^{2+} content activates store-operated Ca^{2+} channels on the plasma membrane and subsequent Ca^{2+} influx from the extracellular space into the endothelial cell (Thillaiappan et al., 2017) (Chapter 3). Several studies have shown heterogeneity in cultured endothelial cells to ACh, ADP, ATP and histamine (as well as various proteins) (Hong et al., 2006; Kameritsch et al., 2012; Kirchhofer et al., 1994; Ko et al., 2009; Müller et al., 2002). However, few have examined the concentration-dependence of the endothelium to each agonist. Here we show, an increase in intracellular Ca^{2+} is not simply a binary mechanism whereby a cell is either active or not. Instead, the Ca^{2+} response evoked by ACh, ADP, ATP and histamine are concentration-dependent in small resistance arteries.

Unique properties of individual cells may be lost if the response of the entire population is averaged (Socha et al., 2012). Therefore, we analysed the response of all cells, from a large population in the intact mesenteric endothelium. The Ca^{2+} response evoked by each agonist began in discrete clusters of cells and additional cells were recruited in a concentration-dependent manner, either by direct activation by the agonist or propagation of the Ca^{2+} response to neighbouring cells. Clustering creates domains of sensitivity. This clustering behaviour was previously reported in other studies although the underlying physiological reason was unclear (Marie and Bény, 2002; Senis et al., 1996; Tomlinson et al., 1991; Yuan et al., 2016). Clustering may provide a signal-coincidence detection system (Wilson et al., 2016b). Studies have shown that when one cell alone was activated (as would occur in stochastic noise events), there was limited communication to neighbouring cells. However, when two or more adjacent cells were activated simultaneously pronounced communication occurred and propagating Ca^{2+} waves were transmitted to neighbouring cells (Wilson et al., 2016b). The propagation provides secondary amplification and a means of communicating over distance. Spontaneous, randomly occurring events (i.e., not agonist evoked) that occur in single cells are rarely transmitted to neighbouring cells (Kansui et al., 2008; Ledoux et al., 2008). Thus, the endothelium recognises the spontaneous events as noise and does not generate a transmitted response. By rejecting noise, signal detection will improve and randomly occurring events are unlikely to be propagated (Peterson et al., 1954). Detecting signals that are around basal values is a critical element in biological systems in complex environments. These signals will appear as small increases in concentration on a noisy baseline value (Assunção-Miranda et al., 2005; Civciristov and Halls, 2019; Civciristov et al., 2018). The mechanisms by which endothelial cells process small signals in noisy environments are not well understood. We propose that coincidence detection derived from the interactive behaviour of neighbouring cells improves the reliability and the precision of signal detection.

The amplitude of the Ca^{2+} response within each cell was also concentration-dependent. Interestingly, at agonist concentrations that just activated all cells, the

amplitude of the Ca^{2+} response in each cell was still submaximal. Further increases in agonist concentration increased the amplitude of the Ca^{2+} response. These results suggest that endothelial cells within activator ensembles are primed with a small range of activation thresholds, perhaps due to differential receptor expression (Lee et al., 2018). The combination of various activation thresholds, responses of variable amplitude, and plasticity in cell recruitment presumably maximises sensitivity to various agonists over a wide concentration range whilst enabling signals to be relayed over a large dynamic range. The complex interaction of bioactive molecules with spatially distinct domains of effector cells, and the ability of cells to communicate with each over the whole endothelial surface suggests that non-excitable endothelial cells function cooperatively as an artery-lining, macroscopic excitable network (McCarron et al., 2017).

Together, the observations suggest several interesting sensing properties of the endothelium. (i) Sensing and control are fully distributed among numerous cells. (ii) Communication among the cells occurs in a highly localised way. (iii) System-level sensing is substantially greater than the sensing repertoire of any single individual cell. Each cell follows its own simple sensing rules based on sensitivity and the activity of its neighbours. These simple rules appear to be: (i) remain quiescent in the absence of an activator; (ii) respond when the concentration is in the correct range for the cells sensitivity; and (iii) respond when two or more neighbouring cells respond. These simple features constitute a sophisticated, wide-ranging detector in which the endothelium as a collective solves complex sensory problems that no single cell is aware exists (McCarron et al., 2017, 2019).

Coordinated arterial function requires vascular cells to produce a concerted output (Socha et al., 2012; Yashiro and Duling, 2000). In the intact artery, coordinated endothelial signalling occurs because endothelial cells, which are in direct contact with each other, are interconnected. Each may be in contact with several other endothelial cells (Socha et al., 2012), such that they form a complex network lining the inner surface of the blood vessel. However, an interesting question arises in how

do cells distinguish the agonist activating them as each agonist elicits its effects through the same mechanism?

Our results show that low concentrations of each agonist evoked a Ca^{2+} response in only distinct subpopulations of cells; i.e. the endothelium utilises subpopulations of cells to detect specific agonists. (Chapter 4). Those cells primed to detect an agonist form clusters which are spatially distinct and have minimal overlap with cells that are primed to detect other different activators. This clustering of cells that are primed to detect a specific agonist may offer several advantages (Altschuler and Wu, 2010). Clustering may allow the uptake and breakdown mechanisms for diffusible messengers (e.g. nitric oxide, prostaglandin) to be overwhelmed, providing increased spillover of signals. Clustering may also limit interference from neighbouring cells that are responding to a different stimulus, that is, a single cell responding in isolation may easily be influenced by neighbouring cells and have its signal overridden. A cluster of cells each performing the same task may be much harder to override. By organising cells that are primed to detect specific agonists into distinct subpopulations, the endothelium is able to carry out multiple, completely separate, functions in parallel. This may offer additional benefits that allow the endothelium to adapt to an ever-changing environment.

Here we have shown that, even though separate cells are activated by muscarinic and purinergic and histaminergic agonists, when the agonists were present together in various combinations, the resulting Ca^{2+} signal is distinct from those signals generated by the agonists in isolation (Chapter 5). The precise nature of the computation carried out on the signals and the underlying mechanisms are not yet clear. Nonetheless, the computation is important in that it is a feature that emerges from the collective dynamics of the endothelial network. This feature may allow the endothelium to interactively monitor external environments via distributed sensing across separate cells. Examining the endothelial system as a whole reveals properties that differ substantially from those of individual cells and is an example of ‘the whole being greater than the sum of its parts’.

Here, we also report a full open source system that can be used to study vascular function (Chapter 6). All hardware and software is freely available and is capable of integration into microscopes already in use in many laboratories. The low entry barrier and the potential for future developments opens considerable potential for researchers to expand and enhance myography with tailored vascular reactivity experiments.

7.2 Future Work

Although the present work has shown that the endothelium is not a homogenous population of cells and responds heterogeneously to different activators, the mechanisms underlying the variations between neighbouring cells is unclear (Aird, 2007). Part of the answer may be in the distribution of receptors. We have previously shown that the distribution of muscarinic and purinergic receptors is heterogeneous across the carotid endothelium (Lee et al., 2018). This arrangement may also occur in the mesenteric artery and gives rise to the variation in Ca^{2+} response, to different agonists, between cells. However, even if true, the uneven expression of receptors in different cells is not random across the endothelium. Instead, cells with comparable sensitivity (and presumably receptor expression) to an agonist form clusters. The mechanisms giving rise to the organisation of cells into clusters are not yet clear. Perhaps there is feedback control of function and receptor expression based on location or a result of a self-organisation process at the cellular level. The ability to monitor the Ca^{2+} response of endothelial cells during angiogenesis or during vascular repair would give significant insight into the regulatory mechanism governing receptor expression and hence endothelial heterogeneity. Migration assays have recently been developed that allow for the tracking of endothelial cells (Feng et al., 2017; Oubaha et al., 2012). However, these studies are normally carried out in cultured cells and they may not necessarily reflect the true *in vivo* action of endothelial cells (i.e. the effects of the underlying SMCs on migration).

Presumably, cells that respond to a specific activator have the proteins required to initiate a physiological response (e.g. cells that detect ACh are equipped with the

proteins and substrates to produce nitric oxide). Further study may reveal that there is also functional heterogeneity in the endothelium and only specific cells have the ability to generate the desired physiological output.

The network arrangement of endothelial cells may be critical to vascular function. Endothelial cells are fixed in physical space and the physical connections between cells are invariant; the arrangement is a mesh (with each EC having on average 6 neighbouring ECs). Despite this fixed anatomy, the number of functional communication routes in the endothelium is large and gives rise to multiple possible outputs (Wilson et al., 2016a). Previously it has been shown that communication across the endothelium shows the complex varying paths on agonist activation (Heathcote et al., 2019; Wilson et al., 2016a). The dynamic, changing paths of communication may arise in part from the refractory time each cell has after the Ca^{2+} increase, which forces signals to take alternative routes or terminate. To identify the nature of the functional network properties and features of signal propagation spatiotemporal cross-correlation analysis may be used to assess cross-level interdependence of Ca^{2+} signals in cell networks (Jing et al., 2013).

The sensing and control systems that we propose operate in the endothelium are inherently stable and fault tolerant. However, things do go wrong in cardiovascular disease. Most studies examining the cellular problems in cardiovascular disease are population studies based on either large numbers of cultured cells or contraction/relaxation investigations in intact tissue. Implicit in these approaches is that the endothelium is a uniform population of cells that respond uniformly to an activator. When changes in response are measured in cardiovascular disease with these approaches, the cells are usually considered to be uniformly affected. However, the ensemble behaviours of a population may not represent the behaviours of any individual cell (Altschuler and Wu, 2010). Here we have shown that cells are not uniform in function and as a result the problems in cardiovascular disease may be much more difficult to resolve than has been previously considered.

In cardiovascular disease, altered sensitivity to agonists may arise not because the sensitivity of all cells in the population has changed or even because the sensitivity of any cell has changed. Rather, altered sensitivity may arise because of a change in the distribution of cells that are otherwise completely normal. This change in distribution may significantly depress or enhance the function of the endothelium while the behaviour of each cell is unchanged. Alternatively, the communication between cells may be changed in cardiovascular disease. Further study is required to understand the importance of the structural and functional network properties of the endothelium and how the network is altered in cardiovascular disease.

An additional area worthy of investigation is in the mechanisms that generate emergent signals in the endothelium. In particular, what is the nature of the feedback operating between cells when multiple agonists are present? How does communication between cells take place? What are the mechanisms underlying the modified 'emergent' Ca^{2+} signals? What is the nature of the computation carried out by the cells? What is the message carried in the modified signal? How does emergent signalling change in cardiovascular disease? The answers to these questions will provide new insights into how the endothelium is able to play a central role in regulating virtually every cardiovascular function.

.

References

Abbracchio, M.P., Burnstock, G., Boeynaems, J.-M., Barnard, E.A., Boyer, J.L., Kennedy, C., Knight, G.E., Fumagalli, M., Gachet, C., Jacobson, K.A., et al. (2006). International Union of Pharmacology LVIII: update on the P2Y G protein-coupled nucleotide receptors: from molecular mechanisms and pathophysiology to therapy. Pharmacol. Rev. *58*, 281–341.

Abdullaev, I.F., Bisaillon, J.M., Potier, M., Gonzalez, J.C., Motiani, R.K., and Trebak, M. (2008). Stim1 and Orai1 mediate CRAC currents and store-operated calcium entry important for endothelial cell proliferation. Circ. Res. *103*, 1289–1299.

Acar, M., Mettetal, J.T., and van Oudenaarden, A. (2008). Stochastic switching as a survival strategy in fluctuating environments. Nat. Genet. *40*, 471–475.

Adachi, T., Weisbrod, R.M., Pimentel, D.R., Ying, J., Sharov, V.S., Schöneich, C., and Cohen, R.A. (2004). S-Glutathiolation by peroxynitrite activates SERCA during arterial relaxation by nitric oxide. Nat. Med. *10*, 1200–1207.

Adkins, C.E., and Taylor, C.W. (1999). Lateral inhibition of inositol 1,4,5-trisphosphate receptors by cytosolic Ca^{2+}. Curr. Biol. *9*, 1115–1118.

Aird, W.C. (2005). Spatial and temporal dynamics of the endothelium. J. Thromb. Haemost. *3*, 1392–1406.

Aird, W.C. (2007). Phenotypic Heterogeneity of the Endothelium. Circulation Research *100*, 158–173.

Aird, W.C. (2012). Endothelial Cell Heterogeneity. Cold Spring Harb Perspect Med *2*.

Aird, W.C., Edelberg, J.M., Weiler-Guettler, H., Simmons, W.W., Smith, T.W., and Rosenberg, R.D. (1997). Vascular Bed–specific Expression of an Endothelial Cell Gene Is Programmed by the Tissue Microenvironment. J Cell Biol *138*, 1117–1124.

Alevriadou, B.R., Shanmughapriya, S., Patel, A., Stathopulos, P.B., and Madesh, M. (2017). Mitochondrial Ca^{2+} transport in the endothelium: regulation by ions, redox signalling and mechanical forces. J R Soc Interface *14*.

Altschuler, S.J., and Wu, L.F. (2010). Cellular heterogeneity: when do differences make a difference? Cell *141*, 559–563.

Amberg, G.C., and Navedo, M.F. (2013). Calcium dynamics in vascular smooth muscle. Microcirculation *20*, 281–289.

Amin, K. (2012). The role of mast cells in allergic inflammation. Respiratory Medicine *106*, 9–14.

Angelsen, B.A., and Brubakk, A.O. (1976). Transcutaneous measurement of blood flow velocity in the human aorta. Cardiovasc. Res. *10*, 368–379.

Armstrong, S.M., Khajoee, V., Wang, C., Wang, T., Tigdi, J., Yin, J., Kuebler, W.M., Gillrie, M., Davis, S.P., Ho, M., et al. (2012). Co-regulation of transcellular and paracellular leak across microvascular endothelium by dynamin and Rac. Am. J. Pathol. *180*, 1308–1323.

Armstrong, S.M., Sugiyama, M.G., Fung, K.Y.Y., Gao, Y., Wang, C., Levy, A.S., Azizi, P., Roufaiel, M., Zhu, S.-N., Neculai, D., et al. (2015). A novel assay uncovers an unexpected role for SR-BI in LDL transcytosis. Cardiovasc. Res. *108*, 268–277.

Ashina, K., Tsubosaka, Y., Nakamura, T., Omori, K., Kobayashi, K., Hori, M., Ozaki, H., and Murata, T. (2015). Histamine Induces Vascular Hyperpermeability by Increasing Blood Flow and Endothelial Barrier Disruption In Vivo. PLoS One *10*.

Assunção-Miranda, I., Guilherme, A.L., Reis-Silva, C., Costa-Sarmento, G., Oliveira, M.M., and Vieyra, A. (2005). Protein kinase C-mediated inhibition of renal Ca^{2+} ATPase by physiological concentrations of angiotensin II is reversed by AT1- and AT2-receptor antagonists. Regul. Pept. *127*, 151–157.

Avdonin, P.V., Nadeev, A.D., Mironova, G.Y., Zharkikh, I.L., Avdonin, P.P., and Goncharov, N.V. (2019a). Enhancement by Hydrogen Peroxide of Calcium Signals in Endothelial Cells Induced by 5-HT1B and 5-HT2B Receptor Agonists.

Avdonin, P.V., Rybakova, E.Yu., Avdonin, P.P., Trufanov, S.K., Mironova, G.Yu., Tsitrina, A.A., and Goncharov, N.V. (2019b). VAS2870 Inhibits Histamine-Induced Calcium Signaling and vWF Secretion in Human Umbilical Vein Endothelial Cells. Cells *8*.

Azevedo, F.A.C., Carvalho, L.R.B., Grinberg, L.T., Farfel, J.M., Ferretti, R.E.L., Leite, R.E.P., Jacob Filho, W., Lent, R., and Herculano-Houzel, S. (2009). Equal numbers of neuronal and nonneuronal cells make the human brain an isometrically scaled-up primate brain. J. Comp. Neurol. *513*, 532–541.

Bagher, P., Davis, M.J., and Segal, S.S. (2011). Visualizing calcium responses to acetylcholine convection along endothelium of arteriolar networks in Cx40BAC-GCaMP2 transgenic mice. Am J Physiol Heart Circ Physiol *301*, H794–H802.

Bagher, P., Beleznai, T., Kansui, Y., Mitchell, R., Garland, C.J., and Dora, K.A. (2012). Low intravascular pressure activates endothelial cell TRPV4 channels, local Ca^{2+} events, and IK_{Ca} channels, reducing arteriolar tone. PNAS *109*, 18174–18179.

Balsinde, J., Winstead, M.V., and Dennis, E.A. (2002). Phospholipase A2 regulation of arachidonic acid mobilization. FEBS Letters *531*, 2–6.

Barandier, C., Ming, X.-F., Rusconi, S., and Yang, Z. (2003). PKC is required for activation of ROCK by RhoA in human endothelial cells. Biochem. Biophys. Res. Commun. *304*, 714–719.

Bath, P.M., Hassall, D.G., Gladwin, A.M., Palmer, R.M., and Martin, J.F. (1991). Nitric oxide and prostacyclin. Divergence of inhibitory effects on monocyte chemotaxis and adhesion to endothelium in vitro. Arterioscler. Thromb. *11*, 254–260.

Bazigou, E., and Makinen, T. (2013). Flow control in our vessels: vascular valves make sure there is no way back. Cell Mol Life Sci *70*, 1055–1066.

Beaumont, H.J.E., Gallie, J., Kost, C., Ferguson, G.C., and Rainey, P.B. (2009). Experimental evolution of bet hedging. Nature *462*, 90–93.

Berra-Romani, R., Rinaldi, C., Raqeeb, A., Castelli, L., Magistretti, J., Taglietti, V., and Tanzi, F. (2004). The duration and amplitude of the plateau phase of ATP- and ADP-evoked Ca^{2+} signals are modulated by ectonucleotidases in in situ endothelial cells of rat aorta. J. Vasc. Res. *41*, 166–173.

Berridge, M.J., and Irvine, R.F. (1984). Inositol trisphosphate, a novel second messenger in cellular signal transduction. Nature *312*, 315.

Berridge, M.J., and Irvine, R.F. (1989). Inositol phosphates and cell signalling. Nature *341*, 197.

Bhattacharya, R., Sinha, S., Yang, S.-P., Patra, C., Dutta, S., Wang, E., and Mukhopadhyay, D. (2008). The neurotransmitter dopamine modulates vascular permeability in the endothelium. Journal of Molecular Signaling *3*, Art. 14.

Bkaily, G., d'OrlÃ©ans-Juste, P., Naik, R., PÃ©rodin, J., Stankova, J., Abdulnour, E., and Rola-Pleszczynski, M. (1993). PAF activation of a voltage-gated R-type Ca^{2+} channel in human and canine aortic endothelial cells. Br J Pharmacol *110*, 519–520.

Boittin, F.-X., Alonso, F., Le Gal, L., Allagnat, F., Bény, J.-L., and Haefliger, J.-A. (2013). Connexins and M3 muscarinic receptors contribute to heterogeneous Ca^{2+} signaling in mouse aortic endothelium. Cell. Physiol. Biochem. *31*, 166–178.

Bolotina, V.M., Najibi, S., Palacino, J.J., Pagano, P.J., and Cohen, R.A. (1994). Nitric oxide directly activates calcium-dependent potassium channels in vascular smooth muscle. Nature *368*, 850–853.

Bootman, M.D., Collins, T.J., Mackenzie, L., Roderick, H.L., Berridge, M.J., and Peppiatt, C.M. (2002). 2-aminoethoxydiphenyl borate (2-APB) is a reliable blocker of store-operated Ca^{2+} entry but an inconsistent inhibitor of InsP3-induced Ca2+ release. FASEB J. *16*, 1145–1150.

Borisova, L., Wray, S., Eisner, D.A., and Burdyga, T. (2009). How structure, Ca^{2+} signals, and cellular communications underlie function in precapillary arterioles. Circ. Res. *105*, 803–810.

Bossu, J.L., Elhamdani, A., and Feltz, A. (1992). Voltage-dependent calcium entry in confluent bovine capillary endothelial cells. FEBS Letters *299*, 239–242.

Brini, M., and Carafoli, E. (2009). Calcium Pumps in Health and Disease. Physiological Reviews *89*, 1341–1378.

Buonassisi, V., and Venter, J.C. (1976). Hormone and neurotransmitter receptors in an established vascular endothelial cell line. Proc. Natl. Acad. Sci. U.S.A. *73*, 1612–1616.

Burnstock, G. (2017). Purinergic Signalling: Therapeutic Developments. Front Pharmacol *8*.

Buus, N.H., VanBavel, E., and Mulvany, M.J. (1994). Differences in sensitivity of rat mesenteric small arteries to agonists when studied as ring preparations or as cannulated preparations. Br. J. Pharmacol. *112*, 579–587.

Camazine, S., Deneubourg, J.-L., Franks, N.R., Sneyd, J., Bonabeau, E., and Theraula, G. (2003). Self-organization in Biological Systems (Princeton University Press).

Cannon, R.O. (1998). Role of nitric oxide in cardiovascular disease: focus on the endothelium. Clinical Chemistry *44*, 1809–1819.

Carmichael, S.T. (2016). Emergent properties of neural repair: elemental biology to therapeutic concepts. Annals of Neurology *79*, 895–906.

Carter, T.D., and Ogden, D. (1994). Acetylcholine-stimulated changes of membrane potential and intracellular Ca^{2+} concentration recorded in endothelial cells in situ in the isolated rat aorta. Pflugers Arch. *428*, 476–484.

Castillo, K., Diaz-Franulic, I., Canan, J., Gonzalez-Nilo, F., and Latorre, R. (2018). Thermally activated TRP channels: molecular sensors for temperature detection. Phys Biol *15*, 021001.

Chalmers, S., Olson, M.L., MacMillan, D., Rainbow, R.D., and McCarron, J.G. (2007). Ion channels in smooth muscle: Regulation by the sarcoplasmic reticulum and mitochondria. Cell Calcium *42*, 447–466.

Chi, J.-T., Chang, H.Y., Haraldsen, G., Jahnsen, F.L., Troyanskaya, O.G., Chang, D.S., Wang, Z., Rockson, S.G., van de Rijn, M., Botstein, D., et al. (2003). Endothelial cell diversity revealed by global expression profiling. Proc Natl Acad Sci U S A *100*, 10623–10628.

Civciristov, S., and Halls, M.L. (2019). Signalling in response to sub-picomolar concentrations of active compounds: Pushing the boundaries of GPCR sensitivity. British Journal of Pharmacology *176*, 2382–2401.

Civciristov, S., Ellisdon, A.M., Suderman, R., Pon, C.K., Evans, B.A., Kleifeld, O., Charlton, S.J., Hlavacek, W.S., Canals, M., and Halls, M.L. (2018). Preassembled GPCR signaling complexes mediate distinct cellular responses to ultralow ligand concentrations. Sci. Signal. *11*.

Cooke, J.P., and Ghebremariam, Y.T. (2008). Endothelial Nicotinic Acetylcholine Receptors and Angiogenesis. Trends Cardiovasc Med *18*, 247–253.

Craigie, E., Menzies, R.I., Larsen, C.K., Jacquillet, G., Carrel, M., Wildman, S.S., Loffing, J., Leipziger, J., Shirley, D.G., Bailey, M.A., et al. (2018). The renal and blood pressure response to low sodium diet in P2X4 receptor knockout mice. Physiol Rep *6*, e13899.

Dale, H.H. (1914). The Action of Certain Esters and Ethers of Choline, and Their Relation to Muscarine. J Pharmacol Exp Ther *6*, 147–190.

De Caterina, R., Libby, P., Peng, H.B., Thannickal, V.J., Rajavashisth, T.B., Gimbrone, M.A., Shin, W.S., and Liao, J.K. (1995). Nitric oxide decreases cytokine-induced endothelial activation. Nitric oxide selectively reduces endothelial expression of adhesion molecules and proinflammatory cytokines. J Clin Invest *96*, 60–68.

De Koninck, P., and Schulman, H. (1998). Sensitivity of CaM kinase II to the frequency of Ca^{2+} oscillations. Science *279*, 227–230.

Deisseroth, K., Bito, H., and Tsien, R.W. (1996). Signaling from Synapse to Nucleus: Postsynaptic CREB Phosphorylation during Multiple Forms of Hippocampal Synaptic Plasticity. Neuron *16*, 89–101.

Dejana, E., Orsenigo, F., Molendini, C., Baluk, P., and McDonald, D.M. (2009). Organization and signaling of endothelial cell-to-cell junctions in various regions of the blood and lymphatic vascular trees. Cell Tissue Res *335*, 17–25.

Dennis, E.A., Rhee, S.G., Billah, M.M., and Hannun, Y.A. (1991). Role of phospholipase in generating lipid second messengers in signal transduction. FASEB J. *5*, 2068–2077.

Di Capite, J., Ng, S.W., and Parekh, A.B. (2009). Decoding of cytoplasmic Ca^{2+} oscillations through the spatial signature drives gene expression. Curr. Biol. *19*, 853–858.

Dolmetsch, R.E., Lewis, R.S., Goodnow, C.C., and Healy, J.I. (1997). Differential activation of transcription factors induced by Ca^{2+} response amplitude and duration. Nature *386*, 855–858.

Dolmetsch, R.E., Pajvani, U., Fife, K., Spotts, J.M., and Greenberg, M.E. (2001). Signaling to the Nucleus by an L-type Calcium Channel-Calmodulin Complex Through the MAP Kinase Pathway. Science *294*, 333–339.

Dora, K.A., Doyle, M.P., and Duling, B.R. (1997). Elevation of intracellular calcium in smooth muscle causes endothelial cell generation of NO in arterioles. Proc. Natl. Acad. Sci. U.S.A. *94*, 6529–6534.

Dora, K.A., Hinton, J.M., Walker, S.D., and Garland, C.J. (2000). An indirect influence of phenylephrine on the release of endothelium-derived vasodilators in rat small mesenteric artery. Br J Pharmacol *129*, 381–387.

Dorigo, M., Floreano, D., Gambardella, L.M., Mondada, F., Nolfi, S., Baaboura, T., Birattari, M., Bonani, M., Brambilla, M., Brutschy, A., et al. (2013). Swarmanoid: A Novel Concept for the Study of Heterogeneous Robotic Swarms. IEEE Robotics Automation Magazine *20*, 60–71.

Duckles, S.P., and Miller, V.M. (2010). Hormonal modulation of endothelial NO production. Pflugers Arch *459*, 841–851.

Dueck, H., Eberwine, J., and Kim, J. (2016). Variation is function: Are single cell differences functionally important?: Testing the hypothesis that single cell variation is required for aggregate function. Bioessays *38*, 172–180.

Durante, W., Sen, A.K., and Sunahara, F.A. (1988). Impairment of endothelium-dependent relaxation in aortae from spontaneously diabetic rats. Br J Pharmacol *94*, 463–468.

Durr, E., Yu, J., Krasinska, K.M., Carver, L.A., Yates, J.R., Testa, J.E., Oh, P., and Schnitzer, J.E. (2004). Direct proteomic mapping of the lung microvascular endothelial cell surface in vivo and in cell culture. Nat. Biotechnol. *22*, 985–992.

Duza, T., and Sarelius, I.H. (2004). Localized transient increases in endothelial cell Ca^{2+} in arterioles in situ: implications for coordination of vascular function. American Journal of Physiology-Heart and Circulatory Physiology *286*, H2322–H2331.

Edelstein, A.D., Tsuchida, M.A., Amodaj, N., Pinkard, H., Vale, R.D., and Stuurman, N. (2014). Advanced methods of microscope control using μManager software. J Biol Methods *1*.

Ehrlich, B.E., and Watras, J. (1988). Inositol 1,4,5-trisphosphate activates a channel from smooth muscle sarcoplasmic reticulum. Nature *336*, 583.

Emerson, G.G., and Segal, S.S. (2000). Electrical Coupling Between Endothelial Cells and Smooth Muscle Cells in Hamster Feed Arteries Role in Vasomotor Control. Circulation Research *87*, 474–479.

Endres, B.T., Staruschenko, A., Schulte, M., Geurts, A.M., and Palygin, O. (2015). Two-photon Imaging of Intracellular Ca^{2+} Handling and Nitric Oxide Production in Endothelial and Smooth Muscle Cells of an Isolated Rat Aorta. JoVE (Journal of Visualized Experiments) e52734.

Ernster, L., and Schatz, G. (1981). Mitochondria: a historical review. J. Cell Biol. *91*, 227s–255s.

Falcone, J.C., Kuo, L., and Meininger, G.A. (1993). Endothelial cell calcium increases during flow-induced dilation in isolated arterioles. American Journal of Physiology-Heart and Circulatory Physiology *264*, H653–H659.

Félétou, M. (2011). The Endothelium, Part I: Multiple Functions of the Endothelial Cells -- Focus on Endothelium-Derived Vasoactive Mediators. Colloquium Series on Integrated Systems Physiology: From Molecule to Function *3*, 1–306.

Feng, T., Yu, H., Xia, Q., Ma, Y., Yin, H., Shen, Y., and Liu, X. (2017). Cross-talk mechanism between endothelial cells and hepatocellular carcinoma cells via growth factors and integrin pathway promotes tumor angiogenesis and cell migration. Oncotarget *8*, 69577–69593.

Fitzmaurice, G.M., Lipsitz, S.R., and Ibrahim, J.G. (2007). A note on permutation tests for variance components in multilevel generalized linear mixed models. Biometrics *63*, 942–946.

Flaherty, J.T., Pierce, J.E., Ferrans, V.J., Patel, D.J., Tucker, W.K., and Fry, D.L. (1972). Endothelial nuclear patterns in the canine arterial tree with particular reference to hemodynamic events. Circ. Res. *30*, 23–33.

Fleming, I., Bauersachs, J., Fisslthaler, B., and Busse, R. (1998). Ca^{2+}-Independent Activation of the Endothelial Nitric Oxide Synthase in Response to Tyrosine Phosphatase Inhibitors and Fluid Shear Stress. Circulation Research *82*, 686–695.

Fleming Ingrid, Fisslthaler Beate, Dimmeler Stefanie, Kemp Bruce E., and Busse Rudi (2001). Phosphorylation of Thr495 Regulates Ca^{2+}/Calmodulin-Dependent Endothelial Nitric Oxide Synthase Activity. Circulation Research *88*, e68–e75.

Forman, C.J., Tomes, H., Mbobo, B., Burman, R.J., Jacobs, M., Baden, T., and Raimondo, J.V. (2017). Openspritzer: an open hardware pressure ejection system for reliably delivering picolitre volumes. Scientific Reports *7*.

Francis, M., Qian, X., Charbel, C., Ledoux, J., Parker, J.C., and Taylor, M.S. (2012). Automated region of interest analysis of dynamic Ca^{2+} signals in image sequences. Am. J. Physiol., Cell Physiol. *303*, C236-243.

Francis, M., Waldrup, J.R., Qian, X., Solodushko, V., Meriwether, J., and Taylor, M.S. (2016). Functional Tuning of Intrinsic Endothelial Ca^{2+} Dynamics in Swine Coronary Arteries. Circ. Res. *118*, 1078–1090.

Freichel, M., Suh, S.H., Pfeifer, A., Schweig, U., Trost, C., Weißgerber, P., Biel, M., Philipp, S., Freise, D., Droogmans, G., et al. (2001). Lack of an endothelial store-operated Ca^{2+} current impairs agonist-dependent vasorelaxation in TRP4 −/− mice. Nat Cell Biol *3*, 121–127.

Fung, K.Y.Y., Fairn, G.D., and Lee, W.L. (2018). Transcellular vesicular transport in epithelial and endothelial cells: Challenges and opportunities. Traffic *19*, 5–18.

Furchgott, R.F., and Zawadzki, J.V. (1980). The obligatory role of endothelial cells in the relaxation of arterial smooth muscle by acetylcholine. Nature *288*, 373–376.

Gabriels Joseph E., and Paul David L. (1998). Connexin43 Is Highly Localized to Sites of Disturbed Flow in Rat Aortic Endothelium but Connexin37 and Connexin40 Are More Uniformly Distributed. Circulation Research *83*, 636–643.

Galione, A. (2015). A primer of NAADP-mediated Ca^{2+} signalling: From sea urchin eggs to mammalian cells. Cell Calcium *58*, 27–47.

Galley, H.F., and Webster, N.R. (2004). Physiology of the endothelium. Br. J. Anaesth. *93*, 105–113.

Garland, C.J., Bagher, P., Powell, C., Ye, X., Lemmey, H.A.L., Borysova, L., and Dora, K.A. (2017). Voltage-dependent Ca^{2+} entry into smooth muscle during contraction promotes endothelium-mediated feedback vasodilation in arterioles. Sci Signal *10*.

Garnier, S., Gautrais, J., and Theraulaz, G. (2007). The biological principles of swarm intelligence. Swarm Intell *1*, 3–31.

Garrity, A.G., Wang, W., Collier, C.M., Levey, S.A., Gao, Q., and Xu, H. (2016). The endoplasmic reticulum, not the pH gradient, drives calcium refilling of lysosomes. Elife *5*.

Gericke, A., Sniatecki, J.J., Mayer, V.G.A., Goloborodko, E., Patzak, A., Wess, J., and Pfeiffer, N. (2011). Role of M1, M3, and M5 muscarinic acetylcholine receptors in cholinergic dilation of small arteries studied with gene-targeted mice. American Journal of Physiology - Heart and Circulatory Physiology *300*, H1602–H1608.

Gericke, A., Steege, A., Manicam, C., Böhmer, T., Wess, J., and Pfeiffer, N. (2014). Role of the M3 Muscarinic Acetylcholine Receptor Subtype in Murine Ophthalmic Arteries After Endothelial Removal. Invest Ophthalmol Vis Sci *55*, 625–631.

Ghitescu, L., Fixman, A., Simionescu, M., and Simionescu, N. (1986). Specific binding sites for albumin restricted to plasmalemmal vesicles of continuous capillary endothelium: receptor-mediated transcytosis. J. Cell Biol. *102*, 1304–1311.

Girkin, J.M., and Carvalho, M.T. (2018). The light-sheet microscopy revolution. J. Opt. *20*, 053002.

Griffin, C.T., and Gao, S. (2017). Building discontinuous liver sinusoidal vessels. J. Clin. Invest. *127*, 790–792.

Grynkiewicz, G., Poenie, M., and Tsien, R.Y. (1985). A new generation of Ca^{2+} indicators with greatly improved fluorescence properties. J. Biol. Chem. *260*, 3440–3450.

Gündüz, D., Hirche, F., Härtel, F.V., Rodewald, C.W., Schäfer, M., Pfitzer, G., Piper, H.M., and Noll, T. (2003). ATP antagonism of thrombin-induced endothelial barrier permeability. Cardiovasc Res *59*, 470–478.

Hagberg, A.A., Schult, D.A., and Swart, P.J. (2008). Exploring Network Structure, Dynamics, and Function using NetworkX. In Proceedings of the 7th Python in Science Conference, G. Varoquaux, T. Vaught, and J. Millman, eds. (Pasadena, CA USA), pp. 11–15.

Hakim, M.A., Buchholz, J.N., and Behringer, E.J. (2018). Electrical dynamics of isolated cerebral and skeletal muscle endothelial tubes: Differential roles of G-protein-coupled receptors and K^+ channels. Pharmacology Research & Perspectives *6*, e00391.

Halpern, W., and Osol, G. (1986). Resistance vessels in hypertension. Prog. Clin. Biol. Res. *219*, 211–223.

Halpern, W., Osol, G., and Coy, G.S. (1984). Mechanical behavior of pressurized in vitro prearteriolar vessels determined with a video system. Ann Biomed Eng *12*, 463–479.

Hancock, J.T. (2016). Cell Signalling (Oxford, New York: Oxford University Press).

Hansen, M.A., Dutton, J.L., Balcar, V.J., Barden, J.A., and Bennett, M.R. (1999). P2X (purinergic) receptor distributions in rat blood vessels. J. Auton. Nerv. Syst. *75*, 147–155.

Harden, T.K., Waldo, G.L., Hicks, S.N., and Sondek, J. (2011). Mechanism of Activation and Inactivation of Gq/Phospholipase C-β Signaling Nodes. Chem Rev *111*, 6120–6129.

Harraz, O.F., Longden, T.A., Hill-Eubanks, D., and Nelson, M.T. (2018). PIP_2 depletion promotes TRPV4 channel activity in mouse brain capillary endothelial cells. Elife *7*.

He, Y., Kulasiri, D., and Samarasinghe, S. (2014). Systems biology of synaptic plasticity: a review on N-methyl-D-aspartate receptor mediated biochemical pathways and related mathematical models. BioSystems *122*, 7–18.

Heathcote, H.R., Lee, M.D., Zhang, X., Saunter, C.D., Wilson, C., and McCarron, J.G. (2019). Endothelial TRPV4 channels modulate vascular tone by Ca^{2+}-induced Ca^{2+} release at IP_3 receptors: endothelial TRPV4 activation induces IP_3-mediated Ca^{2+} release. British Journal of Pharmacology.

Hekimian, G., Côte, S., Van Sande, J., and Boeynaems, J.M. (1992). H_2 receptor-mediated responses of aortic endothelial cells to histamine. Am. J. Physiol. *262*, H220-224.

Heltianu, C., Simionescu, M., and Simionescu, N. (1982). Histamine receptors of the microvascular endothelium revealed in situ with a histamine-ferritin conjugate: characteristic high-affinity binding sites in venules. J. Cell Biol. *93*, 357–364.

Holm, T., Klein, T., Löschberger, A., Klamp, T., Wiebusch, G., Linde, S. van de, and Sauer, M. (2014). A Blueprint for Cost-Efficient Localization Microscopy. ChemPhysChem *15*, 651–654.

Holmsen, H., and Weiss, H.J. (1979). Secretable storage pools in platelets. Annu. Rev. Med. *30*, 119–134.

Hong, D., Jaron, D., Buerk, D.G., and Barbee, K.A. (2006). Heterogeneous response of microvascular endothelial cells to shear stress. American Journal of Physiology - Heart and Circulatory Physiology *290*, H2498–H2508.

Hoth, M., and Penner, R. (1992). Depletion of intracellular calcium stores activates a calcium current in mast cells. Nature *355*, 353–356.

Hu, D., Cai, D., and Rangan, A.V. (2012). Blood Vessel Adaptation with Fluctuations in Capillary Flow Distribution. PLoS One *7*.

Huang, T.Y., Chu, T.F., Chen, H.I., and Jen, C.J. (2000). Heterogeneity of [Ca^{2+}](i) signaling in intact rat aortic endothelium. FASEB J. *14*, 797–804.

Hudetz, A.G. (1997). Blood flow in the cerebral capillary network: a review emphasizing observations with intravital microscopy. Microcirculation *4*, 233–252.

Iglewicz, B., and Hoaglin, D.C. (1993). How to Detect and Handle Outliers (ASQC Quality Press).

Ioannou, C.C. (2017). Swarm intelligence in fish? The difficulty in demonstrating distributed and self-organised collective intelligence in (some) animal groups. Behavioural Processes *141*, 141–151.

Irvine, R.F., and Schell, M.J. (2001). Back in the water: the return of the inositol phosphates. Nature Reviews Molecular Cell Biology *2*, 327.

Iwai, M., Michikawa, T., Bosanac, I., Ikura, M., and Mikoshiba, K. (2007). Molecular Basis of the Isoform-specific Ligand-binding Affinity of Inositol 1,4,5-Trisphosphate Receptors. J. Biol. Chem. *282*, 12755–12764.

Jacobson, J.R., Dudek, S.M., Singleton, P.A., Kolosova, I.A., Verin, A.D., and Garcia, J.G.N. (2006). Endothelial cell barrier enhancement by ATP is mediated by the small GTPase Rac and cortactin. American Journal of Physiology-Lung Cellular and Molecular Physiology *291*, L289–L295.

Jadeja, R.N., Rachakonda, V., Bagi, Z., and Khurana, S. (2015). Assessing Myogenic Response and Vasoactivity In Resistance Mesenteric Arteries Using Pressure Myography. J Vis Exp e50997.

Jin, R.C., and Loscalzo, J. (2010). Vascular nitric oxide: formation and function. J Blood Med *1*, 147–162.

Jing, D., Lu, X.L., Luo, E., Sajda, P., Leong, P.L., and Guo, X.E. (2013). Spatiotemporal properties of intracellular calcium signaling in osteocytic and osteoblastic cell networks under fluid flow. Bone *53*, 531–540.

Johansson, B. (1989). Myogenic tone and reactivity: definitions based on muscle physiology. J Hypertens Suppl *7*, S5-8; discussion S9.

Joyner, M.J., and Casey, D.P. (2015). Regulation of Increased Blood Flow (Hyperemia) to Muscles During Exercise: A Hierarchy of Competing Physiological Needs. Physiol Rev *95*, 549–601.

Kalluri Aditya S., Vellarikkal Shamsudheen K., Edelman Elazer R., Nguyen Lan, Subramanian Ayshwarya, Ellinor Patrick T., Regev Aviv, Kathiresan Sekar, and Gupta Rajat M. (2019). Single-Cell Analysis of the Normal Mouse Aorta Reveals Functionally Distinct Endothelial Cell Populations. Circulation *140*, 147–163.

Kamato, D., Thach, L., Bernard, R., Chan, V., Zheng, W., Kaur, H., Brimble, M., Osman, N., and Little, P.J. (2015). Structure, Function, Pharmacology, and Therapeutic Potential of the G Protein, Gα/q,11. Front. Cardiovasc. Med. *2*.

Kameritsch, P., Pogoda, K., Ritter, A., Münzing, S., and Pohl, U. (2012). Gap junctional communication controls the overall endothelial calcium response to vasoactive agonists. Cardiovasc. Res. *93*, 508–515.

Kansui, Y., Garland, C.J., and Dora, K.A. (2008). Enhanced spontaneous Ca^{2+} events in endothelial cells reflect signalling through myoendothelial gap junctions in pressurized mesenteric arteries. Cell Calcium *44*, 135–146.

Kawai, Y., and Ohhashi, T. (1995). Histamine H_2 receptor-mediated endothelium-dependent relaxation in canine spinal artery. Jpn. J. Physiol. *45*, 607–618.

Keller, T.T., Mairuhu, A.T.A., de Kruif, M.D., Klein, S.K., Gerdes, V.E.A., ten Cate, H., Brandjes, D.P.M., Levi, M., and van Gorp, E.C.M. (2003). Infections and endothelial cells. Cardiovasc Res *60*, 40–48.

Kendrick-Jones, J., Lehman, W., and Szent-Györgyi, A.G. (1970). Regulation in molluscan muscles. J. Mol. Biol. *54*, 313–326.

Kesić, S. (2016). Systems biology, emergence and antireductionism. Saudi Journal of Biological Sciences *23*, 584–591.

Kirchhofer, D., Tschopp, T.B., Hadváry, P., and Baumgartner, H.R. (1994). Endothelial cells stimulated with tumor necrosis factor-alpha express varying amounts of tissue factor resulting in inhomogenous fibrin deposition in a native blood flow system. Effects of thrombin inhibitors. J. Clin. Invest. *93*, 2073–2083.

Klein, R.R., Bourdon, D.M., Costales, C.L., Wagner, C.D., White, W.L., Williams, J.D., Hicks, S.N., Sondek, J., and Thakker, D.R. (2011). Direct Activation of Human

Phospholipase C by Its Well Known Inhibitor U73122. J. Biol. Chem. *286*, 12407–12416.

Knezevic, N., Roy, A., Timblin, B., Konstantoulaki, M., Sharma, T., Malik, A.B., and Mehta, D. (2007). GDI-1 Phosphorylation Switch at Serine 96 Induces RhoA Activation and Increased Endothelial Permeability. Molecular and Cellular Biology *27*, 6323–6333.

Ko, Y.-C., Chien, H.-F., Jiang-Shieh, Y.-F., Chang, C.-Y., Pai, M.-H., Huang, J.-P., Chen, H.-M., and Wu, C.-H. (2009). Endothelial CD200 is heterogeneously distributed, regulated and involved in immune cell-endothelium interactions. J. Anat. *214*, 183–195.

Koenen, R.R., Pruessmeyer, J., Soehnlein, O., Fraemohs, L., Zernecke, A., Schwarz, N., Reiss, K., Sarabi, A., Lindbom, L., Hackeng, T.M., et al. (2009). Regulated release and functional modulation of junctional adhesion molecule A by disintegrin metalloproteinases. Blood *113*, 4799–4809.

Kohn, E.C., Alessandro, R., Spoonster, J., Wersto, R.P., and Liotta, L.A. (1995). Angiogenesis: role of calcium-mediated signal transduction. Proc Natl Acad Sci U S A *92*, 1307–1311.

Kolka, C.M., and Bergman, R.N. (2012). The Barrier Within: Endothelial Transport of Hormones. Physiology (Bethesda) *27*, 237–247.

Komarova, Y., and Malik, A.B. (2010). Regulation of Endothelial Permeability via Paracellular and Transcellular Transport Pathways. Annual Review of Physiology *72*, 463–493.

Kornfield, T.E., and Newman, E.A. (2014). Regulation of Blood Flow in the Retinal Trilaminar Vascular Network. J Neurosci *34*, 11504–11513.

Kotas, M.E., and Medzhitov, R. (2015). Homeostasis, Inflammation, and Disease Susceptibility. Cell *160*, 816–827.

Kourtidis, A., Ngok, S.P., and Anastasiadis, P.Z. (2013). p120 catenin: an essential regulator of cadherin stability, adhesion-induced signaling, and cancer progression. Prog Mol Biol Transl Sci *116*, 409–432.

Kozasa, T., Hajicek, N., Chow, C.R., and Suzuki, N. (2011). Signalling mechanisms of RhoGTPase regulation by the heterotrimeric G proteins G12 and G13. J Biochem *150*, 357–369.

Kugelmann, D., Rotkopf, L.T., Radeva, M.Y., Garcia-Ponce, A., Walter, E., and Waschke, J. (2018). Histamine causes endothelial barrier disruption via Ca^{2+} -mediated RhoA activation and tension at adherens junctions. Sci Rep *8*, 1–14.

Kusuma, S., Peijnenburg, E., Patel, P., and Gerecht, S. (2014). Low oxygen tension enhances endothelial fate of human pluripotent stem cells. Arterioscler. Thromb. Vasc. Biol. *34*, 913–920.

Laskey, R.E., Adams, D.J., and van Breemen, C. (1994). Cytosolic [Ca^{2+}] measurements in endothelium of rabbit cardiac valves using imaging fluorescence microscopy. Am. J. Physiol. *266*, H2130-2135.

Ledoux, J., Taylor, M.S., Bonev, A.D., Hannah, R.M., Solodushko, V., Shui, B., Tallini, Y., Kotlikoff, M.I., and Nelson, M.T. (2008). Functional architecture of inositol 1,4,5-trisphosphate signaling in restricted spaces of myoendothelial projections. PNAS *105*, 9627–9632.

Lee, J., Jirapatnakul, A.C., Reeves, A.P., Crowe, W.E., and Sarelius, I.H. (2009). Vessel diameter measurement from intravital microscopy. Ann Biomed Eng *37*, 913–926.

Lee, M.D., Wilson, C., Saunter, C.D., Kennedy, C., Girkin, J.M., and McCarron, J.G. (2018). Spatially structured cell populations process multiple sensory signals in parallel in intact vascular endothelium. Sci. Signal. *11*, eaar4411.

Leslie, C.C. (1997). Properties and regulation of cytosolic phospholipase A2. J. Biol. Chem. *272*, 16709–16712.

Leung, F.P., Yung, L.M., Yao, X., Laher, I., and Huang, Y. (2008). Store-operated calcium entry in vascular smooth muscle. Br J Pharmacol *153*, 846–857.

Leybaert, L., and Sanderson, M.J. (2012). Intercellular Ca^{2+} Waves: Mechanisms and Function. Physiol Rev *92*, 1359–1392.

Li, J., and Bukoski, R.D. (1993). Endothelium-dependent relaxation of hypertensive resistance arteries is not impaired under all conditions. Circ. Res. *72*, 290–296.

Li, L., Bressler, B., Prameya, R., Dorovini-Zis, K., and Van Breemen, C. (1999). Agonist-stimulated calcium entry in primary cultures of human cerebral microvascular endothelial cells. Microvasc. Res. *57*, 211–226.

Liu, R., Ma, S., Lu, Z., Shen, H., Sun, L., and Wei, M. (2015). The ADP antagonist MRS2179 regulates the phenotype of smooth muscle cells to limit intimal hyperplasia. Cardiovasc Drugs Ther *29*, 23–29.

Lock, J.T., Parker, I., and Smith, I.F. (2015). A comparison of fluorescent Ca^{2+} indicators for imaging local Ca^{2+} signals in cultured cells. Cell Calcium *58*, 638–648.

Londono, C., Loureiro, M.J., Slater, B., Lücker, P.B., Soleas, J., Sathananthan, S., Aitchison, J.S., Kabla, A.J., and McGuigan, A.P. (2014). Nonautonomous contact guidance signaling during collective cell migration. Proc. Natl. Acad. Sci. U.S.A. *111*, 1807–1812.

Longden, T.A., Dabertrand, F., Koide, M., Gonzales, A.L., Tykocki, N.R., Brayden, J.E., Hill-Eubanks, D., and Nelson, M.T. (2017). Capillary K^+-sensing initiates retrograde hyperpolarization to increase local cerebral blood flow. Nature Neuroscience *20*, 717–726.

López-Sanjurjo, C.I., Tovey, S.C., Prole, D.L., and Taylor, C.W. (2013). Lysosomes shape Ins(1,4,5)P_3-evoked Ca^{2+} signals by selectively sequestering Ca^{2+} released from the endoplasmic reticulum. J Cell Sci *126*, 289–300.

Lu, C., Diehl, S.A., Noubade, R., Ledoux, J., Nelson, M.T., Spach, K., Zachary, J.F., Blankenhorn, E.P., and Teuscher, C. (2010). Endothelial histamine H_1 receptor signaling reduces blood–brain barrier permeability and susceptibility to autoimmune encephalomyelitis. PNAS *107*, 18967–18972.

Macklin, K.D., Maus, A.D., Pereira, E.F., Albuquerque, E.X., and Conti-Fine, B.M. (1998). Human vascular endothelial cells express functional nicotinic acetylcholine receptors. J. Pharmacol. Exp. Ther. *287*, 435–439.

Madara, J.L., Moore, R., and Carlson, S. (1987). Alteration of intestinal tight junction structure and permeability by cytoskeletal contraction. Am. J. Physiol. *253*, C854-861.

Marchenko, S.M., and Sage, S.O. (1993). Electrical properties of resting and acetylcholine-stimulated endothelium in intact rat aorta. J Physiol *462*, 735–751.

Marie, I., and Bény, J.-L. (2002). Calcium imaging of murine thoracic aorta endothelium by confocal microscopy reveals inhomogeneous distribution of endothelial cells responding to vasodilator agents. J. Vasc. Res. *39*, 260–267.

Martins, B.M., and Locke, J.C. (2015). Microbial individuality: how single-cell heterogeneity enables population level strategies. Current Opinion in Microbiology *24*, 104–112.

McCarron, J.G., McGeown, J.G., Reardon, S., Ikebe, M., Fay, F.S., and Jr, J.V.W. (1992). Calcium-dependent enhancement of calcium current in smooth muscle by calmodulin-dependent protein kinase II. Nature *357*, 74–77.

McCarron, J.G., Chalmers, S., Bradley, K.N., MacMillan, D., and Muir, T.C. (2006). Ca^{2+} microdomains in smooth muscle. Cell Calcium *40*, 461–493.

McCarron, J.G., Chalmers, S., MacMillan, D., and Olson, M.L. (2010). Agonist-evoked Ca^{2+} wave progression requires Ca^{2+} and IP_3. J Cell Physiol *224*, 334–344.

McCarron, J.G., Lee, M.D., and Wilson, C. (2017). The Endothelium Solves Problems That Endothelial Cells Do Not Know Exist. Trends in Pharmacological Sciences *38*, 322–338.

McCarron, J.G., Wilson, C., Heathcote, H.R., Zhang, X., Buckley, C., and Lee, M.D. (2019). Heterogeneity and emergent behaviour in the vascular endothelium. Current Opinion in Pharmacology *45*, 23–32.

McDonald, T.F., Pelzer, S., Trautwein, W., and Pelzer, D.J. (1994). Regulation and modulation of calcium channels in cardiac, skeletal, and smooth muscle cells. Physiol. Rev. *74*, 365–507.

Mehta, D., and Malik, A.B. (2006). Signaling mechanisms regulating endothelial permeability. Physiol. Rev. *86*, 279–367.

Mehta, D., Rahman, A., and Malik, A.B. (2001). Protein kinase C-alpha signals rho-guanine nucleotide dissociation inhibitor phosphorylation and rho activation and regulates the endothelial cell barrier function. J. Biol. Chem. *276*, 22614–22620.

Michel, C. (2004). Fluid exchange in the microcirculation. J Physiol *557*, 701–702.

Michell, D.L., Andrews, K.L., Woollard, K.J., and Chin-Dusting, J.P.F. (2011). Imaging leukocyte adhesion to the vascular endothelium at high intraluminal pressure. J Vis Exp.

Mineta, K., Matsumoto, T., Osada, N., and Araki, H. (2015). Population genetics of non-genetic traits: evolutionary roles of stochasticity in gene expression. Gene *562*, 16–21.

Ming, X.-F., Barandier, C., Viswambharan, H., Kwak, B.R., Mach, F., Mazzolai, L., Hayoz, D., Ruffieux, J., Rusconi, S., Montani, J.-P., et al. (2004). Thrombin stimulates human endothelial arginase enzymatic activity via RhoA/ROCK pathway: implications for atherosclerotic endothelial dysfunction. Circulation *110*, 3708–3714.

Minshall, R.D., Tiruppathi, C., Vogel, S.M., and Malik, A.B. (2002). Vesicle formation and trafficking in endothelial cells and regulation of endothelial barrier function. Histochem. Cell Biol. *117*, 105–112.

Minta, A., Kao, J.P., and Tsien, R.Y. (1989). Fluorescent indicators for cytosolic calcium based on rhodamine and fluorescein chromophores. J. Biol. Chem. *264*, 8171–8178.

Moccia, F., Frost, C., Berra-Romani, R., Tanzi, F., and Adams, D.J. (2004). Expression and function of neuronal nicotinic ACh receptors in rat microvascular endothelial cells. American Journal of Physiology-Heart and Circulatory Physiology *286*, H486–H491.

Moccia, F., Berra-Romani, R., and Tanzi, F. (2012). Update on vascular endothelial Ca^{2+} signalling: A tale of ion channels, pumps and transporters. World J Biol Chem *3*, 127–158.

Moreira, A., and Santos, M.Y. (2019). CONCAVE HULL: A K-NEAREST NEIGHBOURS APPROACH FOR THE COMPUTATION OF THE REGION OCCUPIED BY A SET OF POINTS. pp. 61–68.

Mozhayeva, M.G., and Mozhayeva, G.N. (1996). Evidence for the existence of inositol (1,4,5)-trisphosphate- and ryanodine-sensitive pools in bovine endothelial cells. Ca^{2+} releases in cells with different basal level of intracellular Ca^{2+}. Pflugers Arch. *432*, 614–622.

Müller, A.M., Hermanns, M.I., Skrzynski, C., Nesslinger, M., Müller, K.-M., and Kirkpatrick, C.J. (2002). Expression of the Endothelial Markers PECAM-1, vWf, and CD34 in Vivo and in Vitro. Experimental and Molecular Pathology *72*, 221–229.

Mulvany, M.J., Hansen, O.K., and Aalkjaer, C. (1978). Direct evidence that the greater contractility of resistance vessels in spontaneously hypertensive rats is associated with a narrowed lumen, a thickened media, and an increased number of smooth muscle cell layers. Circ. Res. *43*, 854–864.

Mumtaz, S. (2013). Spatial and temporal characteristics of Ca^{2+} signaling in endothelial cells of intact rat tail artery. Artery Research *7*, 84–92.

Muñoz-Chápuli, R., Quesada, A.R., and Angel Medina, M. (2004). Angiogenesis and signal transduction in endothelial cells. Cell. Mol. Life Sci. *61*, 2224–2243.

Muoboghare, M.O., Drummond, R.M., and Kennedy, C. (2019). Characterisation of P2Y2 receptors in human vascular endothelial cells using AR-C118925XX, a competitive and selective P2Y2 antagonist. Br. J. Pharmacol. *176*, 2894–2904.

Nakamura, S., and Nishizuka, Y. (1994). Lipid mediators and protein kinase C activation for the intracellular signaling network. J. Biochem. *115*, 1029–1034.

Napoli, C., and Ignarro, L.J. (2001). Nitric oxide and atherosclerosis. Nitric Oxide *5*, 88–97.

Nausch, L.W.M., Bonev, A.D., Heppner, T.J., Tallini, Y., Kotlikoff, M.I., and Nelson, M.T. (2012). Sympathetic nerve stimulation induces local endothelial Ca^{2+} signals to oppose vasoconstriction of mouse mesenteric arteries. Am J Physiol Heart Circ Physiol *302*, H594–H602.

Navarro, S., Medina, P., Bonet, E., Corral, J., Martínez-Sales, V., Martos, L., Rivera, M., Roselló-Lletí, E., Alberca, I., Roldán, V., et al. (2013). Association of the thrombomodulin gene c.1418C>T polymorphism with thrombomodulin levels and with venous thrombosis risk. Arterioscler. Thromb. Vasc. Biol. *33*, 1435–1440.

Neher, E. (1998). Vesicle Pools and Ca^{2+} Microdomains: New Tools for Understanding Their Roles in Neurotransmitter Release. Neuron *20*, 389–399.

Noren, D.P., Chou, W.H., Lee, S.H., Qutub, A.A., Warmflash, A., Wagner, D.S., Popel, A.S., and Levchenko, A. (2016). Endothelial cells decode VEGF-mediated Ca^{2+} signaling patterns to produce distinct functional responses. Sci Signal *9*, ra20.

Oancea, E., and Meyer, T. (1996). Reversible desensitization of inositol trisphosphate-induced calcium release provides a mechanism for repetitive calcium spikes. J. Biol. Chem. *271*, 17253–17260.

Oliver James J., Webb David J., and Newby David E. (2005). Stimulated Tissue Plasminogen Activator Release as a Marker of Endothelial Function in Humans. Arteriosclerosis, Thrombosis, and Vascular Biology *25*, 2470–2479.

Orozco, A.S., Zhou, X., and Filler, S.G. (2000). Mechanisms of the proinflammatory response of endothelial cells to Candida albicans infection. Infect. Immun. *68*, 1134–1141.

Oshima, A. (2014). Structure and closure of connexin gap junction channels. FEBS Letters *588*, 1230–1237.

Otani, S., Nagaoka, T., Omae, T., Tanano, I., Kamiya, T., Ono, S., Hein, T.W., Kuo, L., and Yoshida, A. (2016). Histamine-Induced Dilation of Isolated Porcine Retinal Arterioles: Role of Endothelium-Derived Hyperpolarizing Factor. Invest. Ophthalmol. Vis. Sci. *57*, 4791–4798.

Oubaha, M., Lin, M.I., Margaron, Y., Filion, D., Price, E.N., Zon, L.I., Côté, J.-F., and Gratton, J.-P. (2012). Formation of a PKCζ/β-catenin complex in endothelial cells promotes angiopoietin-1–induced collective directional migration and angiogenic sprouting. Blood *120*, 3371–3381.

Palao, T., van Weert, A., de Leeuw, A., de Vos, J., Bakker, E.N.T.P., and van Bavel, E. (2018). Sustained conduction of vasomotor responses in rat mesenteric arteries in a two-compartment in vitro set-up. Acta Physiol (Oxf) *224*, e13099.

Palmer, R.M., Ferrige, A.G., and Moncada, S. (1987). Nitric oxide release accounts for the biological activity of endothelium-derived relaxing factor. Nature *327*, 524–526.

Palmer, R.M.J., Ashton, D.S., and Moncada, S. (1988). Vascular endothelial cells synthesize nitric oxide from L-arginine. Nature *333*, 664.

Pantazaka, E., Taylor, E.J.A., Bernard, W.G., and Taylor, C.W. (2013). Ca^{2+} signals evoked by histamine H_1 receptors are attenuated by activation of prostaglandin EP2 and EP4 receptors in human aortic smooth muscle cells. Br J Pharmacol *169*, 1624–1634.

Parekh, A.B. (2008). Ca^{2+} microdomains near plasma membrane Ca^{2+} channels: impact on cell function. J. Physiol. (Lond.) *586*, 3043–3054.

Parekh, A.B., and Penner, R. (1997). Store depletion and calcium influx. Physiological Reviews *77*, 901–930.

Parekh, A.B., and Putney, J.W. (2005). Store-operated calcium channels. Physiological Reviews *85*, 757–810.

Parker, I., and Smith, I.F. (2010). Recording single-channel activity of inositol trisphosphate receptors in intact cells with a microscope, not a patch clamp. J. Gen. Physiol. *136*, 119–127.

Parker, I., Choi, J., and Yao, Y. (1996). Elementary events of InsP3-induced Ca^{2+} liberation in Xenopus oocytes: hot spots, puffs and blips. Cell Calcium *20*, 105–121.

Parrish, J.K., Viscido, S.V., and Grünbaum, D. (2002). Self-Organized Fish Schools: An Examination of Emergent Properties. The Biological Bulletin *202*, 296–305.

Payne, G.W., Madri, J.A., Sessa, W.C., and Segal, S.S. (2004). Histamine inhibits conducted vasodilation through endothelium-derived NO production in arterioles of mouse skeletal muscle. The FASEB Journal *18*, 280–286.

Pesarin, F. (2016). Permutation Tests: Multivariate. In Wiley StatsRef: Statistics Reference Online, (American Cancer Society), pp. 1–15.

Peterson, W., Birdsall, T., and Fox, W. (1954). The theory of signal detectability. Transactions of the IRE Professional Group on Information Theory *4*, 171–212.

Pitrone, P.G., Schindelin, J., Stuyvenberg, L., Preibisch, S., Weber, M., Eliceiri, K.W., Huisken, J., and Tomancak, P. (2013). OpenSPIM: an open-access light-sheet microscopy platform. Nature Methods *10*, 598–599.

Pittman, R.N. (2011). The Circulatory System and Oxygen Transport (Morgan & Claypool Life Sciences).

Poduri, A., Chang, A.H., Raftrey, B., Rhee, S., Van, M., and Red-Horse, K. (2017). Endothelial cells respond to the direction of mechanical stimuli through SMAD signaling to regulate coronary artery size. Development *144*, 3241–3252.

Popel, A.S. (1980). Oxygen diffusion from capillary layers with concurrent flow. Mathematical Biosciences *50*, 171–193.

Prole, D.L., and Taylor, C.W. (2019). Structure and Function of IP_3 Receptors. Cold Spring Harb Perspect Biol a035063.

Pulvirenti, T.J., Yin, J.L., Chaufour, X., McLachlan, C., Hambly, B.D., Bennett, M.R., and Barden, J.A. (2000). P2X (purinergic) receptor redistribution in rabbit aorta following injury to endothelial cells and cholesterol feeding. J. Neurocytol. *29*, 623–631.

Qamar, M.I., Read, A.E., Skidmore, R., Evans, J.M., and Wells, P.N. (1986). Transcutaneous Doppler ultrasound measurement of superior mesenteric artery blood flow in man. Gut *27*, 100–105.

Radu, B.M., Osculati, A.M.M., Suku, E., Banciu, A., Tsenov, G., Merigo, F., Chio, M.D., Banciu, D.D., Tognoli, C., Kacer, P., et al. (2017). All muscarinic acetylcholine receptors (M 1 -M 5) are expressed in murine brain microvascular endothelium. Sci Rep *7*, 1–15.

Ramirez, A.N., and Kunze, D.L. (2002). P2X purinergic receptor channel expression and function in bovine aortic endothelium. Am. J. Physiol. Heart Circ. Physiol. *282*, H2106-2116.

Randell, D.A., Galton, A., Fouad, S., Mehanna, H., and Landini, G. (2017). Mereotopological Correction of Segmentation Errors in Histological Imaging. Journal of Imaging *3*, 63.

Ray, F.R., Huang, W., Slater, M., and Barden, J.A. (2002). Purinergic receptor distribution in endothelial cells in blood vessels: a basis for selection of coronary artery grafts. Atherosclerosis *162*, 55–61.

Regenmortel, M.H.V.V. (2004). Reductionism and complexity in molecular biology. EMBO Rep *5*, 1016–1020.

Reglin, B., and Pries, A.R. (2014). Metabolic Control of Microvascular Networks: Oxygen Sensing and Beyond. JVR *51*, 376–392.

Riddell, D.R., and Owen, J.S. (1999). Nitric oxide and platelet aggregation. Vitam. Horm. *57*, 25–48.

Ridgway, E.B., and Ashley, C.C. (1967). Calcium transients in single muscle fibers. Biochem. Biophys. Res. Commun. *29*, 229–234.

Rotrosen, D., and Gallin, J.I. (1986). Histamine type I receptor occupancy increases endothelial cytosolic calcium, reduces F-actin, and promotes albumin diffusion across cultured endothelial monolayers. The Journal of Cell Biology *103*, 2379–2387.

Rueden, C.T., Schindelin, J., Hiner, M.C., DeZonia, B.E., Walter, A.E., Arena, E.T., and Eliceiri, K.W. (2017). ImageJ2: ImageJ for the next generation of scientific image data. BMC Bioinformatics *18*, 529.

Rusko, J., Wang, X., and van Breemen, C. (1995). Regenerative caffeine-induced responses in native rabbit aortic endothelial cells. Br J Pharmacol *115*, 811–821.

Sadowski, J., and Badzynska, B. (2008). Intrarenal vasodilator systems: NO, prostaglandins and bradykinin. An integrative approach. J. Physiol. Pharmacol. *59 Suppl 9*, 105–119.

Sáez, J.C., Berthoud, V.M., Brañes, M.C., Martínez, A.D., and Beyer, E.C. (2003). Plasma Membrane Channels Formed by Connexins: Their Regulation and Functions. Physiological Reviews *83*, 1359–1400.

Safar, M.E., and Struijker-Boudier, H.A. (2010). Cross-talk between macro- and microcirculation. Acta Physiologica *198*, 417–430.

Saleem, H., Tovey, S.C., Rahman, T., Riley, A.M., Potter, B.V.L., and Taylor, C.W. (2013). Stimulation of Inositol 1,4,5-Trisphosphate (IP_3) Receptor Subtypes by Analogues of IP3. PLOS ONE *8*, e54877.

Samanta, K., and Parekh, A.B. (2017). Spatial Ca^{2+} profiling: decrypting the universal cytosolic Ca2+ oscillation. J Physiol *595*, 3053–3062.

Sambrook, J.F. (1990). The involvement of calcium in transport of secretory proteins from the endoplasmic reticulum. Cell *61*, 197–199.

Sanders, J.I., and Kepecs, A. (2014). A low-cost programmable pulse generator for physiology and behavior. Front Neuroeng *7*.

Satoh, H., and Inui, J. (1984). Endothelial cell-dependent relaxation and contraction induced by histamine in the isolated guinea-pig pulmonary artery. Eur. J. Pharmacol. *97*, 321–324.

Scheckenbach, K.E.L., Crespin, S., Kwak, B.R., and Chanson, M. (2011). Connexin Channel-Dependent Signaling Pathways in Inflammation. JVR *48*, 91–103.

Schindelin, J., Arganda-Carreras, I., Frise, E., Kaynig, V., Longair, M., Pietzsch, T., Preibisch, S., Rueden, C., Saalfeld, S., Schmid, B., et al. (2012). Fiji: an open-source platform for biological-image analysis. Nat Meth *9*, 676–682.

Senis, Y.A., Richardson, M., Tinlin, S., Maurice, D.H., and Giles, A.R. (1996). Changes in the pattern of distribution of von Willebrand factor in rat aortic endothelial cells following thrombin generation in vivo. Br. J. Haematol. *93*, 195–203.

Shen, and DiCorleto (2008). ADP Stimulates Human Endothelial Cell Migration via P2Y1 Nucleotide Receptor–Mediated Mitogen-Activated Protein Kinase Pathways. Circulation Research *102*, 448–456.

Shirwany, N.A., and Zou, M. (2010). Arterial stiffness: a brief review. Acta Pharmacol Sin *31*, 1267–1276.

Socha, M.J., and Segal, S.S. (2013). Isolation of Microvascular Endothelial Tubes from Mouse Resistance Arteries. J Vis Exp.

Socha, M.J., Domeier, T.L., Behringer, E.J., and Segal, S.S. (2012). Coordination of Intercellular Ca^{2+} Signaling in Endothelial Cell Tubes of Mouse Resistance Arteries. Microcirculation *19*, 757–770.

Sokoloff, L., and Kety, S.S. (1960). Regulation of cerebral circulation. Physiol Rev Suppl *4*, 38–44.

Sonkusare, S.K., Bonev, A.D., Ledoux, J., Liedtke, W., Kotlikoff, M.I., Heppner, T.J., Hill-Eubanks, D.C., and Nelson, M.T. (2012). Elementary Ca^{2+} Signals Through Endothelial TRPV4 Channels Regulate Vascular Function. Science *336*, 597–601.

Stojilković, S.S., Kukuljan, M., Iida, T., Rojas, E., and Catt, K.J. (1992). Integration of cytoplasmic calcium and membrane potential oscillations maintains calcium signaling in pituitary gonadotrophs. PNAS *89*, 4081–4085.

Stokes Leanne, Scurrah Katrina, Ellis Justine A., Cromer Brett A., Skarratt Kristen K., Gu Ben J., Harrap Stephen B., and Wiley James S. (2011). A Loss-of-Function Polymorphism in the Human $P2X_4$ Receptor Is Associated With Increased Pulse Pressure. Hypertension *58*, 1086–1092.

Stolwijk, J.A., Zhang, X., Gueguinou, M., Zhang, W., Matrougui, K., Renken, C., and Trebak, M. (2016). Calcium Signaling Is Dispensable for Receptor Regulation of Endothelial Barrier Function. J. Biol. Chem. *291*, 22894–22912.

Stuurman, N., Edelstein, A.D., Amodaj, N., Hoover, K.H., and Vale, R.D. (2010). Computer Control of Microscopes using μManager. Curr Protoc Mol Biol *CHAPTER*, Unit14.20.

Sukriti, S., Tauseef, M., Yazbeck, P., and Mehta, D. (2014). Mechanisms regulating endothelial permeability. Pulm Circ *4*, 535–551.

Sullivan, M.N., and Earley, S. (2013). TRP channel Ca^{2+} sparklets: fundamental signals underlying endothelium-dependent hyperpolarization. Am J Physiol Cell Physiol *305*, C999–C1008.

Swatton, J.E., Morris, S.A., Cardy, T.J., and Taylor, C.W. (1999). Type 3 inositol trisphosphate receptors in RINm5F cells are biphasically regulated by cytosolic Ca^{2+} and mediate quantal Ca^{2+} mobilization. Biochem. J. *344 Pt 1*, 55–60.

Szent-Györgyi, A.G., Szentkiralyi, E.M., and Kendrick-Jonas, J. (1973). The light chains of scallop myosin as regulatory subunits. J. Mol. Biol. *74*, 179–203.

Takano, H., Dora, K.A., Spitaler, M.M., and Garland, C.J. (2004). Spreading dilatation in rat mesenteric arteries associated with calcium-independent endothelial cell hyperpolarization. The Journal of Physiology *556*, 887–903.

Tanaka, N., Kawasaki, K., Nejime, N., Kubota, Y., Takahashi, K., Hashimoto, M., Kunitomo, M., and Shinozuka, K. (2003). P2Y receptor-mediated enhancement of permeation requires Ca^{2+} signalling in vascular endothelial cells. Clin. Exp. Pharmacol. Physiol. *30*, 649–652.

Tang, D.G., and Conti, C.J. (2004). Endothelial cell development, vasculogenesis, angiogenesis, and tumor neovascularization: an update. Semin. Thromb. Hemost. *30*, 109–117.

Taylor, C.W. (1998). Inositol trisphosphate receptors: Ca^{2+}-modulated intracellular Ca^{2+} channels. Biochim. Biophys. Acta *1436*, 19–33.

Taylor, C.W., and Laude, A.J. (2002). IP_3 receptors and their regulation by calmodulin and cytosolic Ca^{2+}. Cell Calcium *32*, 321–334.

Taylor, M.S., and Francis, M. (2014). Decoding dynamic Ca^{2+} signaling in the vascular endothelium. Front Physiol *5*.

Taylor, C.W., da Fonseca, P.C.A., and Morris, E.P. (2004). IP_3 receptors: the search for structure. Trends in Biochemical Sciences *29*, 210–219.

Tennant, M., and McGeachie, J.K. (1990). Blood vessel structure and function: a brief update on recent advances. Aust N Z J Surg *60*, 747–753.

Thillaiappan, N.B., Chavda, A.P., Tovey, S.C., Prole, D.L., and Taylor, C.W. (2017). Ca^{2+} signals initiate at immobile IP_3 receptors adjacent to ER-plasma membrane junctions. Nat Commun *8*, 1–16.

Tiruppathi, C., Minshall, R.D., Paria, B.C., Vogel, S.M., and Malik, A.B. (2002). Role of Ca^{2+} signaling in the regulation of endothelial permeability. Vascul. Pharmacol. *39*, 173–185.

Tomlinson, A., Van Vlijmen, H., Loesch, A., and Burnstock, G. (1991). An immunohistochemical study of endothelial cell heterogeneity in the rat: observations in “en face” Häutchen preparations. Cell Tissue Res. *263*, 173–181.

Toussaint, F., Charbel, C., Blanchette, A., and Ledoux, J. (2015). CaMKII regulates intracellular Ca^{2+} dynamics in native endothelial cells. Cell Calcium *58*, 275–285.

Touyz, R.M., Deng, L.Y., and Schiffrin, E.L. (1995). Ca^{2+} and contractile responses of resistance vessels of WKY rats and SHR to endothelin-1. J. Cardiovasc. Pharmacol. *26 Suppl 3*, S193-196.

Tran, Q.-K., Ohashi, K., and Watanabe, H. (2000). Calcium signalling in endothelial cells. Cardiovasc Res *48*, 13–22.

Tsien, R.Y. (1980). New calcium indicators and buffers with high selectivity against magnesium and protons: design, synthesis, and properties of prototype structures. Biochemistry *19*, 2396–2404.

Tsien, R.Y. (1981). A non-disruptive technique for loading calcium buffers and indicators into cells. Nature *290*, 527–528.

Tu, H., Wang, Z., Nosyreva, E., De Smedt, H., and Bezprozvanny, I. (2005). Functional characterization of mammalian inositol 1,4,5-trisphosphate receptor isoforms. Biophys. J. *88*, 1046–1055.

Tuma, P.L., and Hubbard, A.L. (2003). Transcytosis: Crossing Cellular Barriers. Physiological Reviews *83*, 871–932.

van Nieuw Amerongen, Draijer Richard, Vermeer Mario A., and van Hinsbergh Victor W. M. (1998). Transient and Prolonged Increase in Endothelial Permeability Induced by Histamine and Thrombin. Circulation Research *83*, 1115–1123.

VanBavel, E., Mooij, T., Giezeman, M.J., and Spaan, J.A. (1990). Cannulation and continuous cross-sectional area measurement of small blood vessels. J Pharmacol Methods *24*, 219–227.

Vanlandewijck, M., He, L., Mäe, M.A., Andrae, J., Ando, K., Del Gaudio, F., Nahar, K., Lebouvier, T., Laviña, B., Gouveia, L., et al. (2018). A molecular atlas of cell types and zonation in the brain vasculature. Nature *554*, 475–480.

Viana, F., De Smedt, H., Droogmans, G., and Nilius, B. (1998). Calcium signalling through nucleotide receptor $P2Y_2$ in cultured human vascular endothelium. Cell Calcium *24*, 117–127.

Wagner, A.J., Holstein-Rathlou, N.H., and Marsh, D.J. (1996). Endothelial Ca^{2+} in afferent arterioles during myogenic activity. Am. J. Physiol. *270*, F170-178.

Wang, G.-R., Zhu, Y., Halushka, P.V., Lincoln, T.M., and Mendelsohn, M.E. (1998). Mechanism of platelet inhibition by nitric oxide: In vivo phosphorylation of thromboxane receptor by cyclic GMP-dependent protein kinase. Proc Natl Acad Sci U S A *95*, 4888–4893.

Wang, X., Lau, F., Li, L., Yoshikawa, A., and van Breemen, C. (1995). Acetylcholine-sensitive intracellular Ca^{2+} store in fresh endothelial cells and evidence for ryanodine receptors. Circ. Res. *77*, 37–42.

Webb, R.C. (2003). Smooth Muscle Contraction and Relaxation. Advances in Physiology Education *27*, 201–206.

Wijnen, B., Hunt, E.J., Anzalone, G.C., and Pearce, J.M. (2014). Open-Source Syringe Pump Library. PLOS ONE *9*, e107216.

Williams, D.A., Fogarty, K.E., Tsien, R.Y., and Fay, F.S. (1985). Calcium gradients in single smooth muscle cells revealed by the digital imaging microscope using Fura-2. Nature *318*, 558–561.

Wilson, C., Saunter, C.D., Girkin, J.M., and McCarron, J.G. (2015). Pressure-dependent regulation of Ca^{2+} signalling in the vascular endothelium. J Physiol *593*, 5231–5253.

Wilson, C., Lee, M.D., and McCarron, J.G. (2016a). Acetylcholine released by endothelial cells facilitates flow-mediated dilatation. J Physiol *594*, 7267–7307.

Wilson, C., Saunter, C.D., Girkin, J.M., and McCarron, J.G. (2016b). Clusters of specialized detector cells provide sensitive and high fidelity receptor signaling in the intact endothelium. FASEB J fj.201500090.

Wilson, C., Lee, M.D., Heathcote, H., Zhang, X., Buckley, C., Girkin, J.M., Saunter, C.D., and McCarron, J.G. (2018). Mitochondrial ATP production provides long-range control of endothelial inositol trisphosphate–evoked calcium signaling. J. Biol. Chem. jbc.RA118.005913.

Wilson Calum, Zhang Xun, Buckley Charlotte, Heathcote Helen R., Lee Matthew D., and McCarron John G. (2019). Increased Vascular Contractility in Hypertension Results From Impaired Endothelial Calcium Signaling. Hypertension *74*, 1200–1214.

Wojciak-Stothard, B., and Ridley, A.J. (2002). Rho GTPases and the regulation of endothelial permeability. Vascul. Pharmacol. *39*, 187–199.

Worthen, L.M., and Nollert, M.U. (2000). Intracellular calcium response of endothelial cells exposed to flow in the presence of thrombin or histamine. Journal of Vascular Surgery *32*, 593–601.

Wu, D., Katz, A., and Simon, M.I. (1993). Activation of phospholipase C beta 2 by the alpha and beta gamma subunits of trimeric GTP-binding protein. PNAS *90*, 5297–5301.

Yakubu, M.A., and Leffler, C.W. (2002). L-type voltage-dependent Ca^{2+} channels in cerebral microvascular endothelial cells and ET-1 biosynthesis. American Journal of Physiology - Cell Physiology *283*, C1687–C1695.

Yamamoto, K., Korenaga, R., Kamiya, A., Qi, Z., Sokabe, M., and Ando, J. (2000). $P2X_4$ receptors mediate ATP-induced calcium influx in human vascular endothelial cells. Am. J. Physiol. Heart Circ. Physiol. *279*, H285-292.

Yamamoto, K., Sokabe, T., Matsumoto, T., Yoshimura, K., Shibata, M., Ohura, N., Fukuda, T., Sato, T., Sekine, K., Kato, S., et al. (2006). Impaired flow-dependent control of vascular tone and remodeling in P2X4-deficient mice. Nat Med *12*, 133–137.

Yamamoto, N., Watanabe, H., Kakizawa, H., Hirano, M., Kobayashi, A., and Ohno, R. (1995). A study on thapsigargin-induced calcium ion and cation influx pathways in vascular endothelial cells. Biochim. Biophys. Acta *1266*, 157–162.

Yamamoto, Y., Klemm, M.F., Edwards, F.R., and Suzuki, H. (2001). Intercellular electrical communication among smooth muscle and endothelial cells in guinea-pig mesenteric arterioles. J. Physiol. (Lond.) *535*, 181–195.

Yashiro, Y., and Duling, B.R. (2000). Integrated Ca^{2+} Signaling Between Smooth Muscle and Endothelium of Resistance Vessels. Circulation Research *87*, 1048–1054.

Yau, J.W., Teoh, H., and Verma, S. (2015). Endothelial cell control of thrombosis. BMC Cardiovasc Disord *15*.

Ying Xiaoyou, Minamiya Yoshihiro, Fu Chenzhong, and Bhattacharya Jahar (1996). Ca^{2+} Waves in Lung Capillary Endothelium. Circulation Research *79*, 898–908.

Yip, K.P., and Marsh, D.J. (1996). $[Ca^{2+}]i$ in rat afferent arteriole during constriction measured with confocal fluorescence microscopy. Am. J. Physiol. *271*, F1004-1011.

Yuan, L., Chan, G.C., Beeler, D., Janes, L., Spokes, K.C., Dharaneeswaran, H., Mojiri, A., Adams, W.J., Sciuto, T., Garcia-Cardeña, G., et al. (2016). A role of stochastic phenotype switching in generating mosaic endothelial cell heterogeneity. Nat Commun *7*, 10160.

Yuill, K.H., Yarova, P., Kemp-Harper, B.K., Garland, C.J., and Dora, K.A. (2011). A Novel Role for HNO in Local and Spreading Vasodilatation in Rat Mesenteric Resistance Arteries. Antioxid Redox Signal *14*, 1625–1635.

Zhou, M.-H., Zheng, H., Si, H., Jin, Y., Peng, J.M., He, L., Zhou, Y., Muñoz-Garay, C., Zawieja, D.C., Kuo, L., et al. (2014). Stromal Interaction Molecule 1 (STIM1) and Orai1 Mediate Histamine-evoked Calcium Entry and Nuclear Factor of Activated T-cells (NFAT) Signaling in Human Umbilical Vein Endothelial Cells. J. Biol. Chem. *289*, 29446–29456.

Zhu, L., Luo, Y., Chen, T., Chen, F., Wang, T., and Hu, Q. (2008). Ca^{2+} oscillation frequency regulates agonist-stimulated gene expression in vascular endothelial cells. Journal of Cell Science *121*, 2511–2518.

Ziegelstein, R.C., Spurgeon, H.A., Pili, R., Passaniti, A., Cheng, L., Corda, S., Lakatta, E.G., and Capogrossi, M.C. (1994). A functional ryanodine-sensitive intracellular Ca^{2+} store is present in vascular endothelial cells. Circulation Research *74*, 151–156.